ECF-300FF5-16-0091
Revision 0

Uranium Transport Modeling in Support of the Stage A Enhanced Attenuation Remedy at 300-FF-5 Operable Unit

Prepared for the U.S. Department of Energy
Assistant Secretary for Environmental Management

Contractor for the U.S. Department of Energy
under Contract DE-AC06-08RL14788

P.O. Box 1600
Richland, Washington 99352

Approved for Public Release;
Further Dissemination Unlimited

ECF-300FF5-16-0091
Revision 0

Uranium Transport Modeling in Support of the Stage A Enhanced Attenuation Remedy at 300-FF-5 Operable Unit

Document Type: ENV Program/Project: EP&SP

S. Mehta
CH2M HILL Plateau Remediation Company

A. Mayenna
INTERA, Inc.

Date Published
October 2016

Prepared for the U.S. Department of Energy
Assistant Secretary for Environmental Management

Contractor for the U.S. Department of Energy
under Contract DE-AC06-08RL14788

P.O. Box 1600
Richland, Washington 99352

APPROVED
By Julia Raymer at 9:24 am, Nov 01, 2016

Release Approval Date

Approved for Public Release;
Further Dissemination Unlimited

TRADEMARK DISCLAIMER

Reference herein to any specific commercial product, process, or service by tradename, trademark, manufacturer, or otherwise, does not necessarily constitute or imply its endorsement, recommendation, or favoring by the United States Government or any agency thereof or its contractors or subcontractors.

This report has been reproduced from the best available copy.

Printed in the United States of America

Contents

1 Purpose 1-1

2 Background 2-1

3 Methodology 3-1

4 Assumptions and Inputs 4-1

5 Software Applications 5-1

5.1 Software Details 5-1

5.2 Software Installation and Checkout 5-2

6 Observations and Conceptual Model Development 6-1

6.1 Stage A Phosphate Injection and Infiltration 6-1

6.2 Monitoring Results from Stage A Treatment 6-7

6.3 Comparison of Post-Treatment and Pretreatment Samples 6-13

6.3.1 Sequential Extraction 6-26

6.3.2 Flow-Through Column Leaching Tests 6-37

6.3.3 Labile Uranium Batch Test 6-41

6.3.4 Identification of Mineral Phases Using Surface Analysis 6-41

6.3.5 Observations of High Moisture Content 6-43

6.4 Determination of Desorption Parameters Using Post-Treatment Flow-Through Column Leach Tests 6-44

7 Three-Dimensional Flow and Transport Modeling Using STOMP 7-1

7.1 Background Information 7-1

7.2 Development of Hydrogeologic Model 7-2

7.3 Development of 3D STOMP Model Domain 7-5

7.4 Development of Flow Model 7-5

7.4.1 Recharge 7-5

7.4.2 Automated Water Level Network Data Usage 7-9

7.5 Model Calibration 7-10

7.6 Determination of Fate and Transport Parameters 7-12

7.6.1 Saturated Zone Hydraulic Conductivity 7-12

7.6.2 Macrodispersivity 7-15

7.6.3 Porosity 7-15

7.6.4 Particle Density and Bulk Density 7-17

7.6.5 Saturation-Pressure and Relative Permeability Relationships 7-17

7.6.6 Molecular Diffusion Coefficient 7-17

7.6.7 Specific Storativity 7-18

7.6.8 Uranium Sorption 7-18

7.7 Development of Initial Conditions 7-18
7.8 Modeling Uranium and Phosphate Transport 7-24
7.8.1 Modeling Uranium Transport Prior to Treatment (No Action Case) 7-24
7.8.2 Phosphate Transport Modeling During and Post-Treatment Time Periods 7-29
7.8.3 Uranium Transport Modeling During and Post-Treatment Period 7-36
8 Conclusions 8-1
9 References 9-1

Appendices

A Presentation of Sampling Data for Selected Wells ..... A-i
B Geochemical Evaluations and Reactive Transport Modeling ..... B-i
C Mathematical Model for Estimating Kinetic Sorption-Desorption Parameters ..... C-i
D MATLAB Files for Sample B347P4 Bulk Soil Kinetic Sorption Model Calculation ..... D-i
E Assessment of Effect of Polyphosphate Injection/Infiltration on Aquifer Properties ..... E-i
F Software Installation and Checkout Forms ..... F-i

Figures

Figure 6-1. Location of Injection Wells Along with Monitoring Wells and Soil Sampling Locations for Stage A Area 6-2
Figure 6-2. Infiltration System in the Stage A Treatment Area 6-4
Figure 6-3. Daily Sampled Concentrations at the Mixing Skid During (a) Injection Period and (b) Infiltration Period 6-5
Figure 6-4. Measured pH of the Solution Following Mixing at the Skids Prior to (a) Injection and (b) Infiltration 6-6
Figure 6-5. Uranium and Phosphate Trends from Daily Sampling of Wells 6-8
Figure 6-6. Electrical Conductivity in Selected Monitoring Wells Fitted with Data Loggers 6-10
Figure 6-7. Correlation between Electrical Conductivity and Phosphate Concentration in Monitoring Wells 6-11
Figure 6-8. Correlation between Electrical Conductivity and Phosphate Concentration at the Mixing Skids Prior to Injection and Infiltration 6-11
Figure 6-9. Location of ERT Sensors (Electrodes) Along Two Cross-Sections (A-A' and B-B') Relative to Stage A Treatment Area 6-12
Figure 6-10. Changes in Bulk Conductivity Observed Using ERT Imaging Along Two Lines for Selected Time Periods 6-14
Figure 6-11. Depth Averaged Phosphate Migration Rate Estimated from ERT Imaging Based on Breakthrough Magnitude Change in Bulk Conductivity of 0.002 S/m 6-14
Figure 6-12. Results from Monitoring Wells Located Away from the Stage A Treatment Area 6-15
Figure 6-13. Phosphate and Uranium Concentrations Observed in Wells 6-17
Figure 6-14. Borehole Locations to Evaluate Analyte Concentrations in Sediment 6-19

Figure 6-15. Total Uranium Concentration Profiles based on (a) Pre-Treatment Borehole Samples and (b) Collocated Post-Treatment Borehole Samples 6-22
Figure 6-16. Concentration of Phosphate (Total P as Phosphate) Based on 0.5 M Nitric Acid Extraction on (a) Pretreatment Samples and (b) Post-Treatment Samples 6-25
Figure 6-17. Phosphate Concentrations (total P as Phosphate) in Post-Treatment Samples Analyzed Using Water Extraction (Ion Chromatography [IC]) and Total Digestion (ICP-Atomic Emission Spectroscopy [ICP-AES; same as ICP-OES]) 6-26
Figure 6-18. Results from Sequential Extraction of Uranium Performed on Pretreatment Boreholes (Left) and Post-Treatment Boreholes (Right) 6-28
Figure 6-19. Results from Sequential Extraction of Calcium Performed on Pretreatment Boreholes (Left) and Post-Treatment Boreholes (Right) 6-30
Figure 6-20. Results from Sequential Extraction of Iron Performed on Pretreatment Boreholes (Left) and Post-Treatment Boreholes (Right) 6-32
Figure 6-21. Results from Sequential Extraction of Aluminum Performed on Pretreatment Boreholes (Left) and Post-Treatment Boreholes (Right) 6-33
Figure 6-22. Results from Sequential Extraction of Manganese Performed on Pretreatment Boreholes (Left) and Post-Treatment Boreholes (Right) 6-34
Figure 6-23. Eh-pH Diagram Presenting the Orthophosphate Aqueous Complex Stability Field for (a) Infiltrated Water Composition and (b) Hypothetical Water Where Orthophosphate, Bicarbonate, and Calcium Concentrations Are Approximately Equal 6-35
Figure 6-24. Conceptual Model of Probable Reactions Occurring in the Subsurface from Infiltration of Phosphate Bearing Solutions 6-36
Figure 6-25. Stability Field of Uranium Aqueous Complexes Under Varying Orthophosphate to Bicarbonate Ratio and pH 6-37
Figure 6-26. Results of Effluent Uranium Concentrations from Column Leach Tests Performed on Field-Textured Sediments from Post-Treatment Samples 6-39
Figure 6-27. Results of Effluent Uranium Concentrations from Column Leach Tests Performed on <2 mm Size Sediments from Post-Treatment Samples 6-39
Figure 6-28. Comparison of Effluent Uranium Concentrations Column Leach Tests Performed on Field-Textured Samples from Post-Treatment and Pretreatment Boreholes 6-40
Figure 6-29. Composite Uranium Concentrations Recovered During Labile Leach Testing 6-42
Figure 6-30. Spectral Analysis and Elemental Mapping Results of B347R7 Sample Collected from Borehole C9582 at Depth of 9 to 9.1 m (29.5 to 30 ft) 6-43
Figure 7-1. Columbia River Stage Fluctuations and Effect on Water Levels and Dissolved Uranium Concentration at Well 399-1-17A 7-2
Figure 7-2. View of the 300 Area Geologic Framework Model 7-3
Figure 7-3. Generalized Hydrostratigraphy at the 300 Area 7-3
Figure 7-4. 3D STOMP Model Domain to Evaluate the Stage A Remedy 7-6
Figure 7-5. Distribution of Hydrogeologic Units along a Cross-Section 7-7
Figure 7-6. Model Domain Showing the Grid Discretization along with Boundary Designations 7-7
Figure 7-7. Location of the River Gage (SWS-1) in the 300 Area 7-8

Figure 7-8. Comparison of Hourly and Daily Averaged Columbia River Stage Data at the 300 Area 7-9
Figure 7-9. Location of Automated Water Level Network in the Vicinity of Model Domain 7-9
Figure 7-10. Daily and Hourly Averaged Water Levels at (a) 399-1-12 and (b) 399-3-3 7-11
Figure 7-11. Comparison of Daily Averaged Hydraulic Heads for SWS-1 River Gage (East Boundary) and 399-1-12 (West Boundary) 7-12
Figure 7-12. Zones of Variable Hydraulic Conductivity for the Hanford Unit in the Unconfined Aquifer 7-14
Figure 7-13. Darcy Flux Distribution Along a 2D Cross-Section for Selected Times within a Year 7-16
Figure 7-14. Distribution of Initial Soil Labile Uranium Concentration Along an East-West-Trending Cross-Section Through the Stage A EAA 7-20
Figure 7-15. Comparison of Model Simulated Hydraulic Heads and Observed Heads at (a) 399-1-12 and (b) 399-2-2 7-22
Figure 7-16. Location Map of Monitoring Wells within the Model Domain 7-23
Figure 7-17. Measured and Simulated Groundwater Uranium Concentrations During the Calibration Period at Wells (a) 399-1-12, (b) 399-1-23, (c) 399-1-17A, (d) 399-1-2, (e) 399-1-7, and (f) 399-2-2 7-25
Figure 7-18. Simulated Uranium Plumes in Years 2015, 2022, and 2040 under No Action Scenario 7-27
Figure 7-19. Simulated Phosphate Concentration in Aquifers (a) 399-1-23, (b) 399-1-17A, and (c) 399-1-7 7-30
Figure 7-20. Simulated Phosphate Concentration Distribution in the Aquifer for (a) November 20, 2015; (b) November 30, 2015; (c) December 14, 2015; (d) December 20, 2015; (e) December 30, 2015; (f) January 15, 2016; and (g) December 31, 2016 7-31
Figure 7-21. Post-Injection Phosphate Concentrations (mg/L) Contours based on Observations on (a) November 20, 2015; (b) December 3, 2015; (c) December 10, 2015 7-33
Figure 7-22. Phosphate Concentration (mg/L) Comparison between Model Simulated and Interpolated Data Based on Observations 7-35
Figure 7-23. Simulated Uranium Concentrations for (a) 399-1-23 and (b) 399-1-17A Compared to Observed Data Before and Following Treatment 7-37
Figure 7-24. Post-Treatment Simulated Uranium Concentrations at End of December 2016 (a) 10 Times Reduction in Desorption Rate, (b) 5 Times Reduction in Desorption Rates, and (c) No Action Case 7-39
Figure 7-25. Long-Term Simulated Uranium Concentrations for (a) 399-1-23 and (b) 399-1-17A Comparing the Predicted Post-Treatment Results to the No Action Case 7-41

Tables

Table 6-1. Summary of Polyphosphate Solution Injection and Infiltration Schedule 6-1
Table 6-2. Pretreatment Sediment Analysis for Total Uranium by the GEL Laboratory and PNNL for Samples Located Greater Than 6 m (20 ft) in Depth Below Ground Surface 6-20
Table 6-3. Post-Treatment Sediment Analysis for Total Uranium by the ALS Lab and PNNL for Samples Located Greater Than 20 ft in Depth Below Ground Surface 6-23
Table 6-4. Flow-Through Column Test Parameters for Post-Treatment Samples 6-38
Table 6-5. Selected Samples and Flow-Through Column Test Parameters 6-44
Table 7-1. Model Parameters Used in the Simulations 7-21

This page intentionally left blank.

Terms

3D	three-dimensional
AWLN	automated water level network
bgs	below ground surface
CHPRC	CH2M HILL Plateau Remediation Company
COC	contaminant of concern
DOE	U.S. Department of Energy
EA	enhanced attenuation
EAA	Enhanced Attenuation Area
EC	electrical conductivity
ECF	environmental calculation file
EPA	U.S. Environmental Protection Agency
ERT	electrical resistivity tomography
GFM	geologic framework model
GWB	Geochemist's Workbench
HEIS	Hanford Environmental Information System
Hf	Hanford formation
IC	ion chromatography
ICP-AES	inductively coupled plasma-atomic emission spectroscopy
ICP-OES	inductively coupled plasma-optical emission spectroscopy
ID	identification
OU	operable unit
PNNL	Pacific Northwest National Laboratory
PRZ	periodically rewetted zone
RLM	Ringold Lower Mud
ROD	record of decision
SAP	sampling and analysis plan
SEM/EDX	scanning electron microscope/energy dispersive x-ray
STOMP	Subsurface Transport Over Multiple Phases

This page intentionally left blank.

1 Purpose

Completion of 300 Area cleanup on the Hanford Site is being accomplished under the 2013 U.S. Environmental Protection Agency (EPA) and U.S. Department of Energy (DOE) record of decision (ROD) and amendment (EPA and DOE, 2013, *Hanford Site 300 Area Record of Decision for 300-FF-2 and 300-FF-5, and Record of Decision Amendment for 300-FF-1* [hereafter referred to as the 300 Area ROD/ROD Amendment]), which identifies uranium as a contaminant of concern (COC). Part of the selected remedy for uranium contamination in groundwater is enhanced attenuation (EA) of uranium over a 12,140 m^2 (3 ac) area using phosphate solutions to reduce the uranium concentrations in the aquifer. The desired goal of injection and infiltration is to deliver phosphate in high concentrations to the vadose zone (and top of the aquifer), where uranium is present in the sediments, to precipitate phosphate bearing mineral phases that can bind labile uranium and sequester it. The EA remedy is being implemented in two sequential stages: Stage A and Stage B; Stage A covers an area of 3,035 m^2 (0.75 ac), and Stage B covers the remaining portion (9,105 m^2 [2.25 ac]).

The objectives of this report are two-fold: first, present monitoring data and observations on uranium and phosphate concentrations in the PRZ and aquifer following injections and infiltration; second, using numerical modeling, evaluate the fate and transport of uranium following the remedial action. During Stage A treatment, which occurred from November 6 through 18, 2015, high concentration polyphosphate amended solutions were injected into the aquifer and into the periodically rewetted zone (PRZ) along with surficial infiltration (below the root zone) into the vadose zone.

This report synthesizes relevant information for conducting fate and transport modeling to evaluate uranium concentrations in the aquifer in the vicinity of Stage A Enhanced Attenuation Area (EAA). Information gathered from geochemical evaluations of pretreatment and post-treatment soil samples, sequential extraction tests, batch desorption and flow-through column tests, mineral phase analysis, and observations made in the field regarding uranium and phosphate concentrations in groundwater are all used in developing parameters and conceptual models for conducting fate and transport calculations. For forward (predictive) modeling, an understanding of the processes governing uranium sequestration is needed so that proof-of-principle can be sufficiently justified. For this purpose, reactive transport modeling was conducted to understand the complex geochemical reactions. Based on that understanding, predictive fate and transport modeling was conducted to estimate uranium concentrations in the future.

This page intentionally left blank.

2 Background

The sampling and analysis plan (SAP) (DOE/RL-2014-42, *300-FF-5 Operable Unit Remedy Implementation Sampling and Analysis Plan*) presents the plans for the 300-FF-5 Groundwater Operable Unit (OU) remedy implementations, performance monitoring, and groundwater monitoring. The SAP is prepared in accordance with the groundwater remedial actions presented in the 300 Area ROD/ROD Amendment (EPA and DOE, 2013). The SAP supplements information provided in DOE/RL-2014-13, *Integrated Remedial Design Report/Remedial Action Work Plan for the 300 Area (300-FF-1, 300-FF-2 & 300-FF-5 Operable Units)*, and DOE/RL-2014-13-ADD2, *Remedial Design Report/Remedial Action Work Plan for the 300 Area Groundwater*. The 300-FF-5 OU comprises groundwater contaminated by releases from facilities and waste sites associated with past operation of uranium fuel production, research, and development in the 300 Area Industrial Complex. The 300 Area ROD/ROD Amendment identifies uranium, gross alpha, nitrate, tritium, trichloroethene, and *cis*-1,2-dichloroethene as groundwater COCs.

A key part of the groundwater remedy selected in the 300 Area ROD/ROD Amendment (EPA and DOE, 2013) was EA of uranium using sequestration by phosphate application in the vadose zone and PRZ. Uranium sequestration will be implemented using a staged approach. Stage A will consist of performing infiltration/injection in one section of the EAA, covering approximately 0.3 ha (0.75 ac). The treatment effectiveness of the Stage A phosphate application will be evaluated by comparing the overall decrease in uranium leachability in vadose zone and PRZ soil samples, taking into consideration a fate and transport model assumption that 50 percent of mobile uranium will be reduced from phosphate treatment. Treatment effectiveness will also be evaluated based on other factors from Stage A implementation, such as phosphate distribution efficiency, the degree of uranium mobilization to groundwater, and changes to hydraulic conductivity of the aquifer due to precipitation of phosphate minerals. The EA remedial action for the 300 Area is considered complete upon implementation of Stage A and Stage B infiltration and injection in the EAA unless otherwise agreed to by DOE and EPA following the Stage A delivery performance report. Stage B will be performed if a high likelihood of treatment effectiveness can be expected, based upon all the considerations from the Stage A evaluation. If Stage B is performed, Stage A results will be used to refine the Stage B approach for the remaining untreated portions of the EAA.

This report is structured in the following manner. Chapter 3 discusses the general methodology followed for evaluation of data towards building the fate and transport model for uranium, while Chapter 4 summarizes the approach regarding assumptions and inputs. Chapter 5 describes the software applications used, and Chapter 6 provides a discussion of key observations from monitoring along with development of a conceptual model. Chapter 7 discusses the development and results from the fate and transport model. Appendix A provides additional details based on monitoring of wells during treatment operations and post-treatment time period. Appendix B provides the details on reactive transport modeling that help in the development of parameter values for fate and transport modeling. Appendix C provide details on deriving kinetic sorption-desorption parameters based on leaching test results. Appendix D provides details regarding implementation of the numerical model described in Appendix C. Appendix E provides the results that help in the evaluation of any changes in hydraulic properties in the aquifer following treatment.

This page intentionally left blank.

3 Methodology

The following steps were undertaken to simulate post-treatment uranium concentrations in groundwater:

1. Obtain detailed information on the operational parameters and outcomes of the injections and infiltration conducted in Stage A.
    a. Evaluate concentrations of phosphate, sodium, and potassium in the amended solutions prior to injection and infiltration.
    b. Evaluate temporal changes in injection and infiltration rates, along with field sampled pH during the operations.
2. Evaluate data from 26 groundwater monitoring wells used in Stage A.
    a. Evaluate uranium and phosphate concentrations before, during, and after treatment in the seven wells monitored daily during treatment.
    b. Evaluate information collected from continuous electrical conductivity (EC) values from the six wells with data loggers in relation to the timing of injection/infiltration.
    c. Correlate specific conductance values and phosphate concentrations in the dilute solutions at the mixing skids.
    d. Evaluate the results available from electrical resistivity tomography (ERT) surveying regarding distribution of infiltrated phosphate bearing solutions. Review results related to breakthrough times and average velocity of the wetted front.
3. Evaluate data from sediment samples obtained from three pretreatment and three post-treatment boreholes.
    a. Compare pretreatment and post-treatment concentrations of uranium in the sediment.
    b. Evaluate the concentration of precipitated phosphate and compare data from water extracts, acid extracts, and total digestion of pretreatment and post-treatment samples and their concentrations relative to depth within the borehole and to the PRZ.
    c. Compare the data (phosphorous [P], calcium [Ca], aluminum [Al], iron [Fe], manganese [Mn], and uranium [U]) from sequential extraction tests conducted on pretreatment and post-treatment sediment samples, and interpret the data in terms of geochemical processes to explain the results.
    d. Compare the leaching behavior of the sediments subjected to flow-through column leach tests. Compare pretreatment and post-treatment leaching behavior of sediments in relation to uranium concentrations and proximity to the PRZ.
    e. Review the results from batch tests and surface analyses on post-treatment samples.
4. Develop conceptual model of possible geochemical reactions that occurred within the host rock as a result of treatment that led to sequestration of uranium. Perform detailed reactive transport modeling.
5. Simulate the fate and transport of uranium in the vadose zone and unconfined groundwater aquifer to evaluate the effectiveness of the Stage A remedy by predicting groundwater uranium concentrations in the near future.

This page intentionally left blank.

4 Assumptions and Inputs

Assumptions and inputs related to fate and transport modeling are discussed in Chapters 6 and 7, where details are presented. Appendix A provides additional information, based on monitoring data, to support fate and transport modeling.

Sections 6.3 and 6.4 provide assumptions and inputs information related to reactive transport modeling discussed in Appendix B; Chapter 7 provides information regarding development of three-dimensional (3D) flow and transport modeling for evaluating the uranium concentrations. Appendix C provides information on determination of desorption parameters based on column leach tests.

This page intentionally left blank.

5 Software Applications

The following software products were used in the development of this report:

- Subsurface Transport Over Multiple Phases (STOMP©[1]) was the primary software used for this environmental calculation file (ECF). Tecplot®, a commercial graphics software package, was used for graphical display of results.
- The Geochemist's Workbench® (GWB) software was used for performing reactive transport modeling.
- MATLAB® software was used for estimating kinetic sorption-desorption parameters, based on leaching test results.

5.1 Software Details

STOMP (PNNL-12030, *STOMP Subsurface Transport Over Multiple Phases Version 2.0 Theory Guide*; PNNL-15782, *STOMP Subsurface Transport Over Multiple Phases Version 4.0 User's Guide*; PNNL-11216, *STOMP Subsurface Transport Over Multiple Phases Application Guide*) was the software used for this calculation; as approved software, the information required is provided in this section.

The fate and transport calculations are performed using CH2M HILL Plateau Remediation Company (CHPRC) Build 4 of the STOMP software, registered in the Hanford Information System Inventory under identification (ID) number 2471. STOMP use by CHPRC is managed under the following software lifecycle documents: CHPRC-00222, *STOMP Functional Requirements Document*; CHPRC-00176, *STOMP Software Management Plan*; CHPRC-00211, *STOMP Software Test Plan*; CHPRC-00515, *STOMP Acceptance Test Report*; and CHPRC-00269, *STOMP Requirements Traceability Matrix*. STOMP was executed on the Green Linux cluster (owned and operated by INTERA, Inc. at its Richland, Washington office).

GWB (Version 11.0.3) is used for conducting geochemical evaluations and reactive transport modeling (presented in Appendix B). The GWB software is registered in the Hanford Information System Inventory under identification (ID) number 3845. Use of GWB by CHPRC is managed under CHPRC-01874, *The Geochemist's Workbench Integrated Software Management Plan Version 11.0.3*. The software was executed on the Blue Windows 2008 server (owned and operated by INTERA, Inc. at its Richland, Washington office).

Kinetic and equilibrium sorption models were solved using MATLAB R2011b 7.13.0.564 software. In this ECF, MATLAB was used analogously with a flat-file spreadsheet in which the calculation is wholly incorporated into this ECF and where the calculations, mathematical formulas, and input data were verified by the technical review of this ECF. Appendix D provides details regarding the calculations for one column using the single-site kinetic sorption model. The entire input file used in MATLAB is

[1] Battelle Memorial Institute (Battelle) retains copyright on all versions, revisions, and operational modes of the Subsurface Transport Over Multiple Phases (STOMP) software simulator, as permitted by the U.S. Department of Energy. STOMP is used here under a limited government use license.

® Tecplot is a registered trademark of TecPlot, Inc., Bellevue, Washington.

® Geochemist's Workbench is a registered trademark of Aqueous Solutions LLC, Champaign, Illinois.

® MATLAB is a registered trademark of The MathWorks, Inc., Natick, Massachusetts.

documented in Appendix D and verified by comparison to the mathematical formulation presented in Appendix C.

5.2 Software Installation and Checkout

A copy of the Software Installation and Checkout Form for STOMP and GWB installation used in this ECF is provided in Appendix F.

6 Observations and Conceptual Model Development

This chapter discusses observations made during Stage A treatment operations and the post-treatment time period that are relevant to fate and transport modeling. A conceptual model is also developed, based on evaluation of field-scale and lab-scale data.

6.1 Stage A Phosphate Injection and Infiltration

The operational period for Stage A infiltration and injections toward the goal of uranium sequestration was November 6 through 18, 2015. Treatment of the vadose zone, PRZ, and aquifer was conducted using a mixed effort of surface infiltration, direct injection to the PRZ, and chemical injection to the top of the aquifer. The polyphosphate solution injection and infiltration schedule for Stage A is summarized in Table 6-1. Beginning on November 6, 2015, application of the phosphate solutions mixed with river water was injected into the aquifer via groundwater wells configured with inflatable packers set at the interface point between the PRZ and the aquifer. The location of the injection wells within the Stage A area along with monitoring wells is shown in Figure 6-1. The rate of injection was approximately 189 L/min (50 gal/min) per well with simultaneous injections conducted in six wells, as shown in Table 6-1. The duration of various injections ranged from about 8 hours.

Table 6-1. Summary of Polyphosphate Solution Injection and Infiltration Schedule

Operation Day (Date)	Aquifer Injection Wells*	PRZ Injection Wells*	Average Infiltration Rate Achieved (L/min [gal/min])	Total Injection Rate Achieved (L/min [gal/min])
1 (Nov. 6)	1-89, 1-90, 1-91, 1-92, 1-93, 1-94	---	---	1,136 (300)
2 (Nov. 7)	---	---	212 (56)	---
3 (Nov. 8)	---	---	198 (52)	---
4 (Nov. 9)	1-92, 1-93, 1-94, 1-95, 1-96, 1-97	---	197 (52)	1,136 (300)
5 (Nov. 10)	---	---	202(53)	---
6 (Nov. 11)	---	---	254 (67)	---
7 (Nov. 12)	---	---	316 (84)	---
8 (Nov. 13)	---	---	311 (82)	---
9 (Nov. 14)	---	---	303 (80)	---
10 (Nov. 15)	---	---	298 (79)	---
11 (Nov. 16)	1-95, 1-96, 1-97, 1-89, 1-90, 1-91		---	1,136 (300)
	---	1-89, 1-90, 1-91, 1-92, 1-93, 1-94	---	1,136 (300)
12 (Nov. 17)	---	1-92, 1-93, 1-94, 1-95, 1-96, 1-97	---	1,136 (300)
13 (Nov. 18)	---	1-95, 1-96, 1-97, 1-89, 1-90, 1-91	---	1,136 (300)

* All well names begin with 399-.

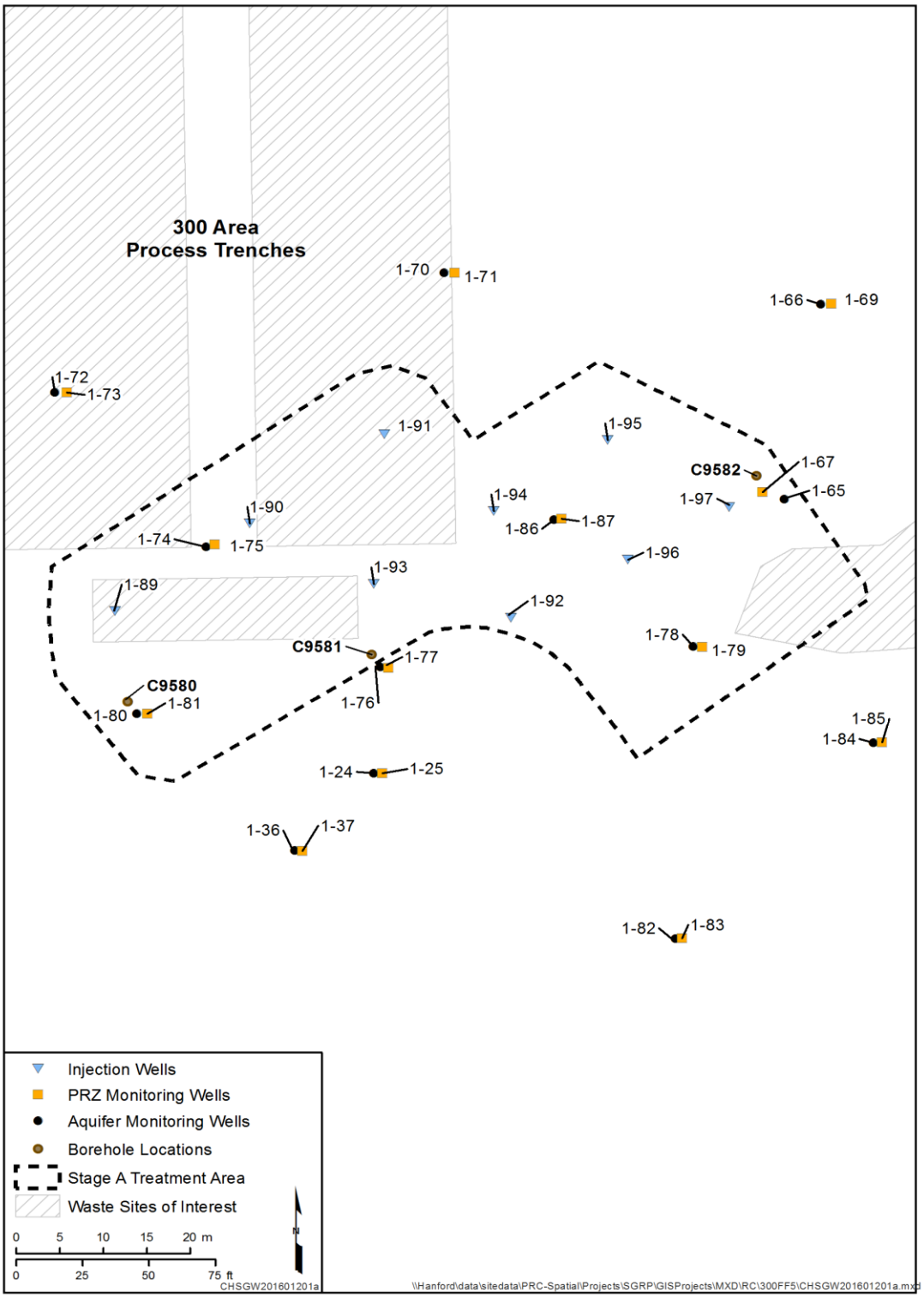

Figure 6-1. Location of Injection Wells Along with Monitoring Wells and Soil Sampling Locations for Stage A Area

Infiltration was initiated the following day (November 7, 2015) and concluded on November 15, 2015. A single mixing skid was used to mix concentrated phosphate solutions with Columbia River water and deliver it to a main distribution header and then through 44 buried drip lines (Figure 6-2). Once infiltration commenced, the system was operated continually (24 hr/day) for 9 days. During the first 4 days of infiltration, the mixed chemical solution was delivered at an approximate flow rate of about 212 L/min (56 gal/min). After the 15 psi pressure regulators connecting the header to the drip lines were replaced with 20 psi pressure regulators, flows increased to approximately 303 L/min (80 gal/min) for the remaining 5 days of infiltration. Some temporal variability in flow rates were observed during infiltration due to adjustments made to the mixing pumps during operations.

During the third day of infiltration, a second injection to the aquifer was conducted (Table 6-1). A final injection into the aquifer occurred on November 16, 2015 after infiltration had ended. The first of three injections to the PRZ also occurred on November 16, 2015 where phosphate solutions mixed with river water were injected into the same groundwater wells configured with packers, but only the solution was delivered to the top of the packer, which forced fluids out through a well interval screened in the PRZ.

Each injection well had two screened intervals: one in the aquifer, and the other in the PRZ. The screened intervals were about 3.1 m (10 ft) each, with approximate depths of 10.9 to 14 m (35.8 to 45.9 ft) below ground surface (bgs) for the aquifer and 6.2 to 9.3 m (20.3 to 30.5 ft) bgs for the PRZ. Minor depth variations occurred during construction; additional details are provided in SGW-59455, *300-FF-5 Operable Unit Stage A Uranium Sequestration System Installation Report*.

The objective of injection and infiltration was to deliver phosphate in high concentrations to the vadose zone (and top of the aquifer), where uranium is present in the sediments, to precipitate phosphate-bearing mineral phases that can bind labile uranium and sequester it. Based on a number of past experimental studies conducted with polyphosphate solutions to bind uranium, such as PNNL-17818, 300 *Area Treatability Test: Laboratory Development of Polyphosphate Remediation Technology for In Situ Treatment of Uranium Contamination in the Vadose Zone and Capillary Fringe*, and PNNL-21733, *Use of Polyphosphate to Decrease Uranium Leaching in Hanford 300 Area Smear Zone Sediment*, it was determined that polyphosphate solutions of high concentrations should be injected/infiltrated. Since most experiments were conducted using a phosphate concentration of about 50 mM, this concentration was initially selected as a target concentration with minor adjustment to account for polyphosphate solution (mixture of orthophosphate and pyrophosphate). However, to account for dilution within the PRZ and aquifer during injection, the target concentrations were raised higher for the injected solutions compared to the infiltrated solutions.

The polyphosphate solutions were composed of a mixture of 90 percent orthophosphate (mixture of NaH_2PO_4-Na_2HPO_4-KH_2PO_4-K_2HPO_4) and 10 percent pyrophosphate ($Na_4P_2O_7$). The orthophosphate solutions were prepared by mixing sodium hydroxide and potassium hydroxide with the phosphoric acid. The initial solutions were prepared at high concentrations, and then they were mixed with river water (using mixing skids) prior to injection and infiltration. The composition of the injected and infiltrated solutions for the three primary components (sodium, potassium, and phosphate) are shown in Figure 6-3 (a, b) based on daily samples collected following mixing in the skids. Concentrations are higher on the days when solutions were being injected, and lower when they were infiltrated, as per the design objectives. During injection, phosphate concentrations varied from about 8,000 mg/L to 9,000 mg/L (84 to 95 mM), reflecting variability in the manufacturing of the concentrated solution and mixing with the river water in the mixing skids. During infiltration, phosphate concentrations were generally maintained around 5,000 mg/L (53 mM) except for the first day of infiltration when the concentrations were around 12,000 mg/L (126 mM) due to operational issues related to mixing with river water. Sodium and potassium concentrations varied in proportion to the phosphate concentrations, with the sodium concentrations being slightly greater than potassium concentrations.

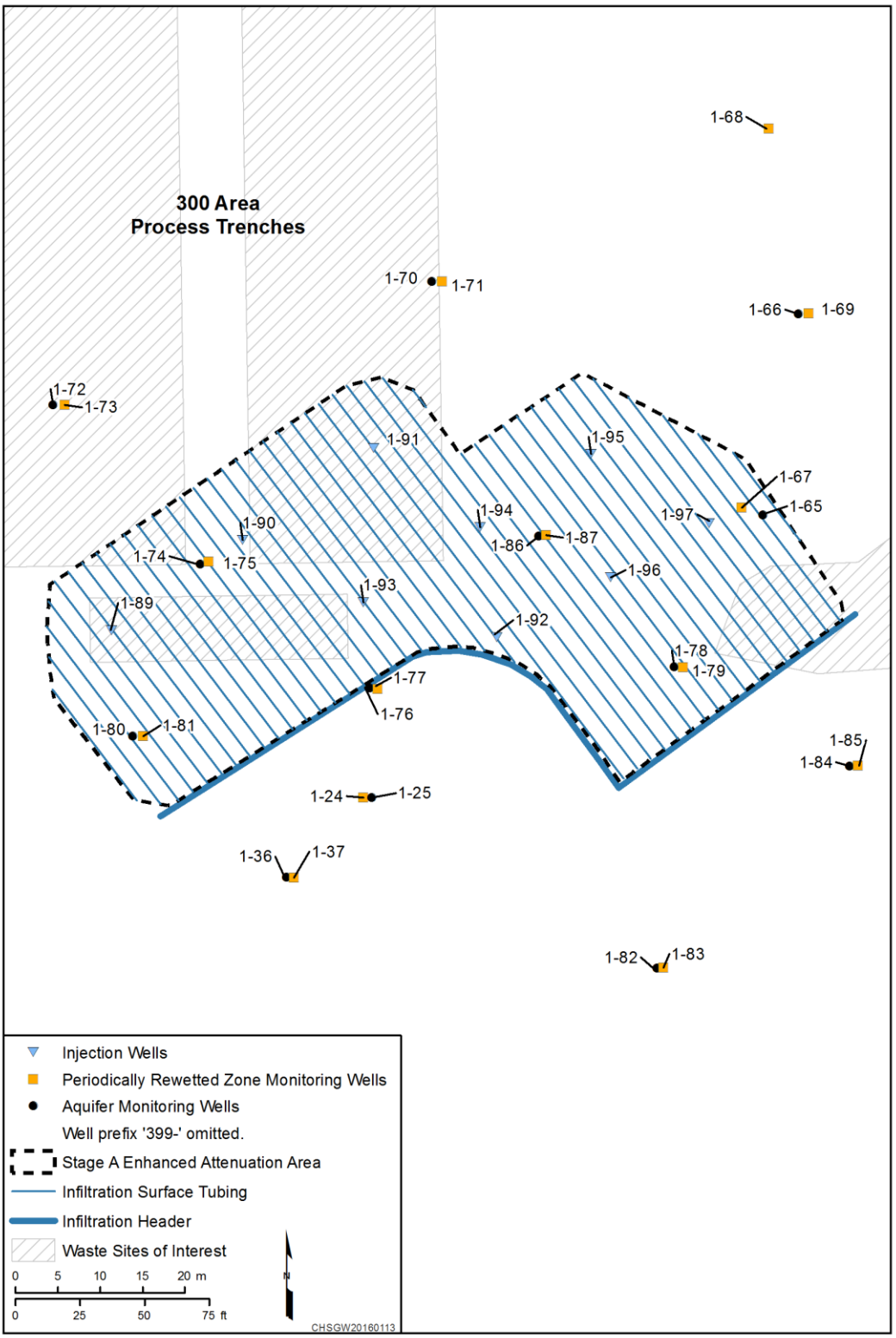

Figure 6-2. Infiltration System in the Stage A Treatment Area

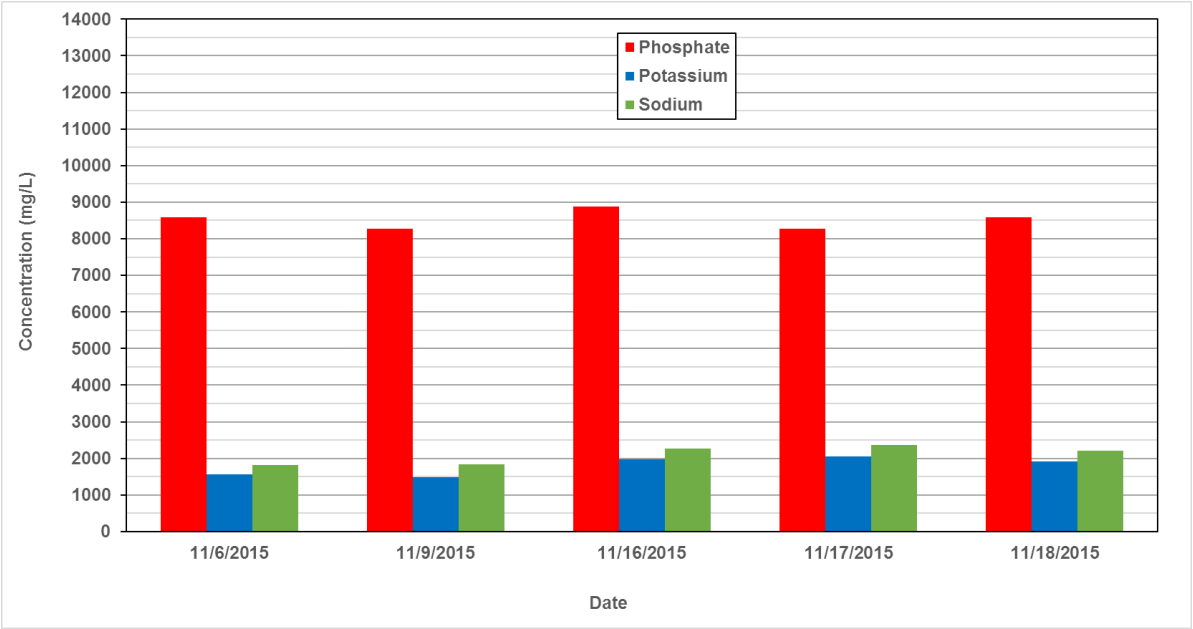

(a)

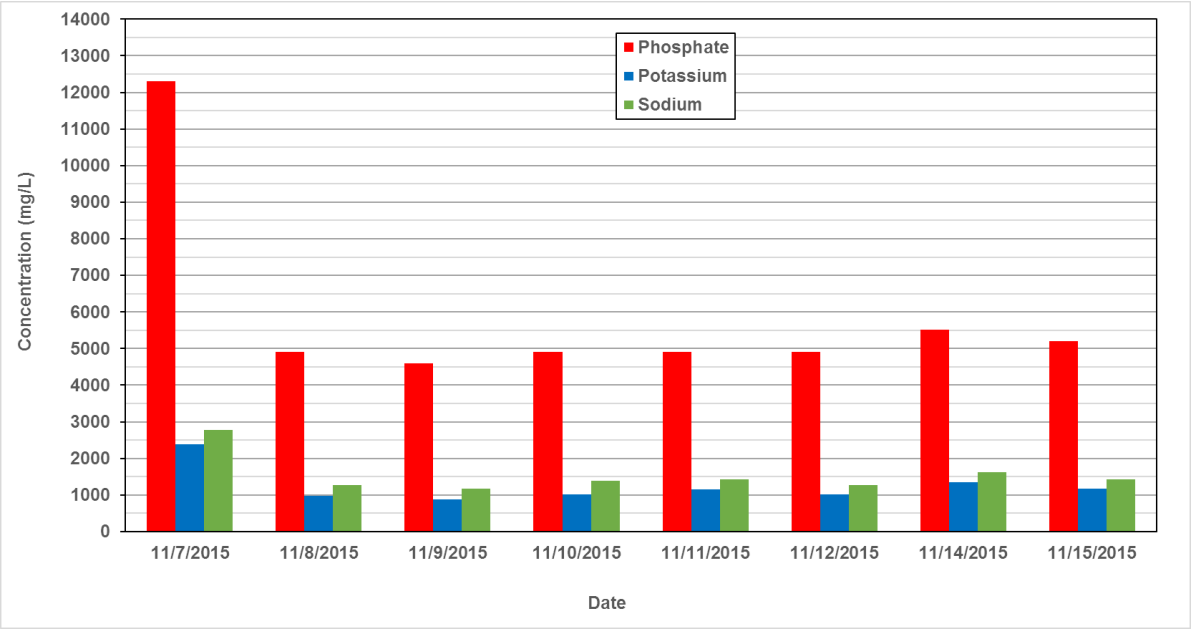

(b)

Note: No sample taken on November 13, 2015.

Figure 6-3. Daily Sampled Concentrations at the Mixing Skid During (a) Injection Period and (b) Infiltration Period

Figure 6-4 (a and b) shows the field sampled pH of the solution during the infiltration and injection period. The pH of the final mixed solution remained above 7 for most of the time period, typically in the range of 7 to 7.3, with short-term fluctuations outside this range. The intraday sharp declines in pH, followed by rises noticeable on November 9 and 10, 2015, likely reflect instrument error rather than changes in composition of the solution.

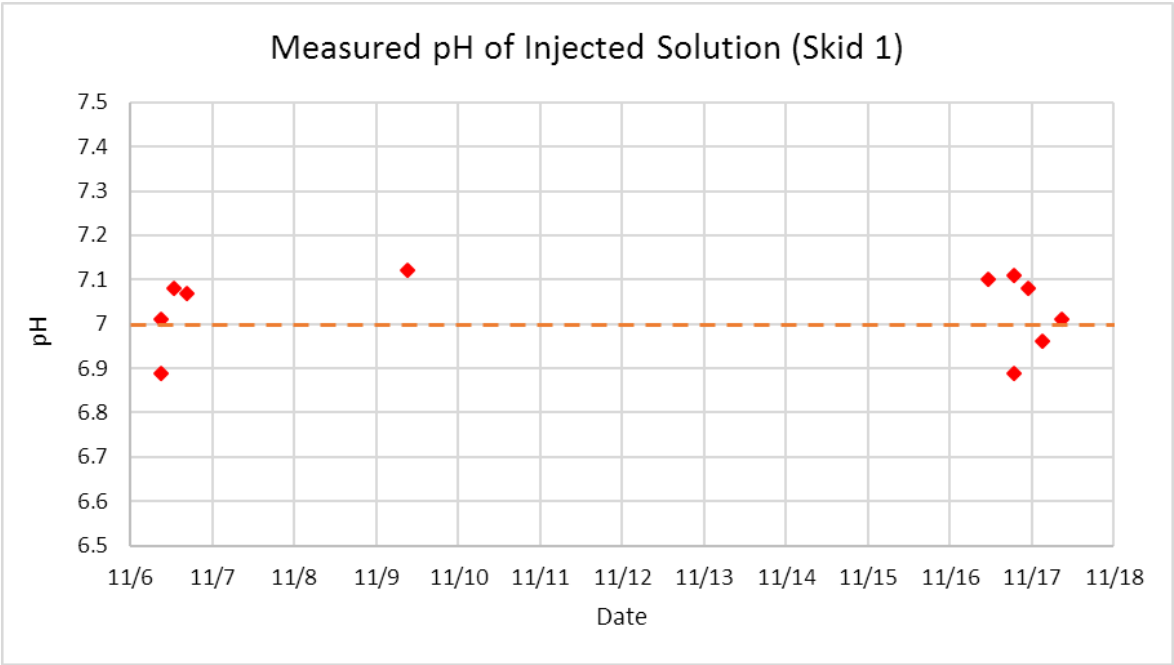

(a)

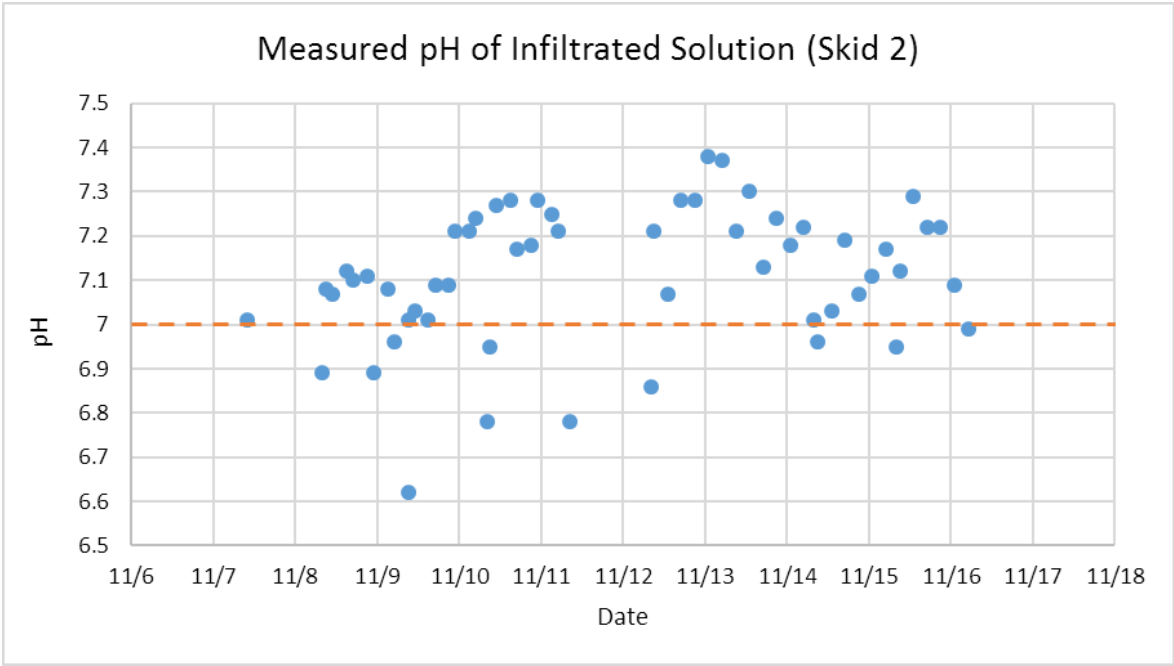

(b)

Figure 6-4. Measured pH of the Solution Following Mixing at the Skids Prior to (a) Injection and (b) Infiltration

6.2 Monitoring Results from Stage A Treatment

There are 26 individual monitoring wells, consisting of 13 collocated well pairs (including 2 existing well pairs and 1 well from the post-ROD investigation). For each well pair, one well is screened in the PRZ, and one well is screened in the aquifer to enable monitoring of each zone. As shown in Figure 6-1, the monitoring well system includes three monitoring well pairs upgradient (north and west) of the Stage A area, six monitoring well pairs within the Stage A area, and four monitoring well pairs downgradient (south and east) of the Stage A area (SGW-59455). The aquifer monitoring wells are generally screened from 10.9 m to 14 m (35.8 to 45.9 ft) bgs, while the PRZ monitoring wells are generally screened from 6.2 to 9.3 m (20.3 to 30.5 ft) bgs. Additional details are presented in SGW-59455.

Seven of these monitoring wells (a combination of PRZ and aquifer monitoring wells) were sampled daily, during and following Stage A, while other wells were sampled intermittently. Data loggers were also placed in six monitoring wells that were screened in the aquifer to provide continuous monitoring of water level fluctuations and EC. Details of the sampling plan are provided in SGW-58976, Field Instructions for Uranium Sequestration in the 300 Area. Data were also evaluated from groundwater monitoring wells being monitored by Pacific Northwest National Laboratory (PNNL) that were located away from the Stage A area.

The seven monitoring wells where daily sampling was conducted included two aquifer/PRZ well pairs (399-1-65/399-1-67 and 399-1-74/399-1-75) and three PRZ wells (399-1-77, 399-1-81, and 399-1-87). The uranium versus phosphate concentrations from the seven daily monitoring wells are presented in Figure 6-5. Uranium concentrations are shown in µg/L, while phosphate concentrations (total phosphorus as phosphate) are shown in mg/L. Results of the two aquifer/PRZ well pairs show that uranium and phosphate concentrations are higher in wells screened in the PRZ compared to wells screened in the aquifer. The observed peak in uranium concentrations precedes the peak in phosphate concentration because the labile fraction of uranium travels as an aqueous complex with the infiltrated water, while the phosphate undergoes chemical reactions with the sediment and is retarded in the vadose zone. The sharp increase in phosphate after November 16, 2015 occurs from PRZ injections that peak on November 18, 2015 (the last day of PRZ injection). A gradual decline in phosphate concentration is observed following the PRZ injection. While the phosphate concentrations are increasing, the uranium concentrations show a steep decline resulting likely from uranium-phosphate-calcium aqueous complexation and co-precipitation of amorphous monocalcium phosphate (PNNL-21733) with structural incorporation of uranium under circumneutral pH conditions (Mehta et al., 2016, “Effect of Reaction Pathway on the Extent and Mechanism of Uranium(VI) Immobilization with Calcium and Phosphate”). The uranium concentrations continue to remain low following treatment (ended on November 18, 2015), indicating that aqueous complexation, surface complexation, and mineral phase precipitation processes continue to sequester uranium from the phosphate that is still retained in the vadose zone. Other monitoring wells, within and around the Stage A area, that were sampled (usually on a weekly basis) also show similar trends. Additional monitoring results are presented in Appendix A.

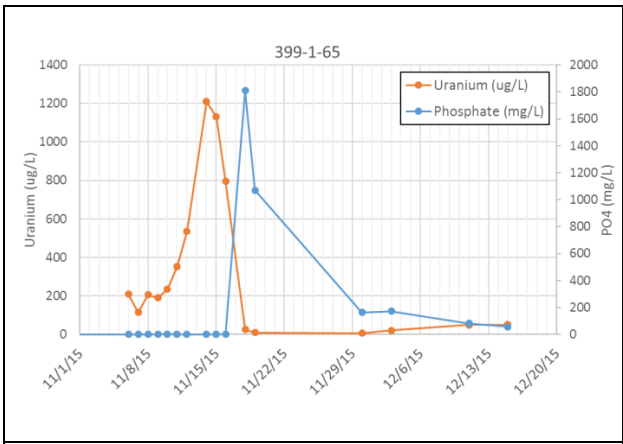

Aquifer Well

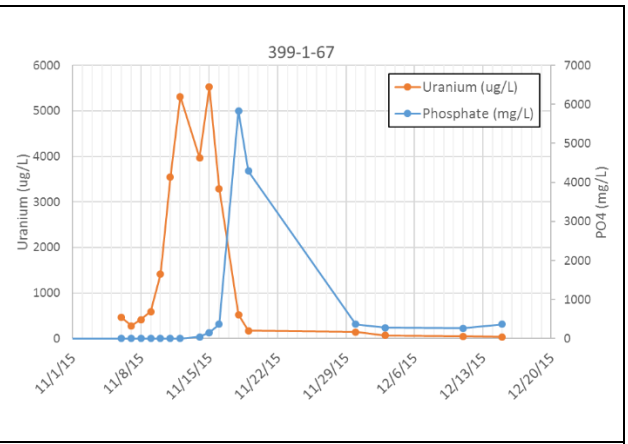

PRZ Well

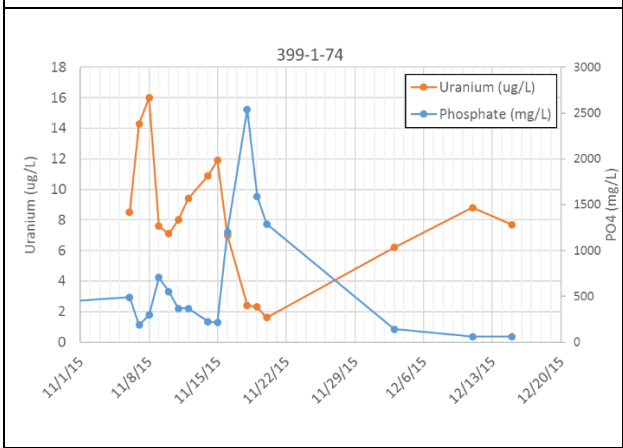

Aquifer Well

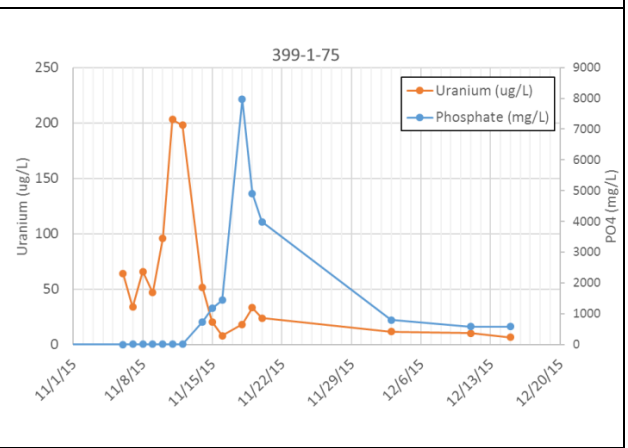

PRZ Well

Figure 6-5. Uranium and Phosphate Trends from Daily Sampling of Wells¶(page 1 of 2)

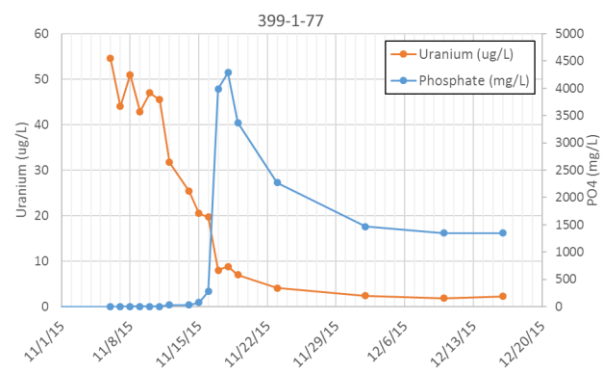

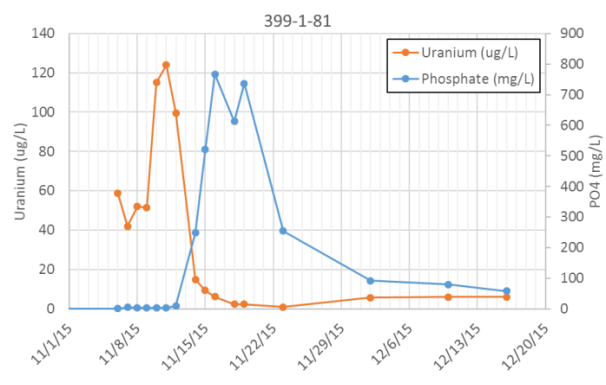

PRZ Well

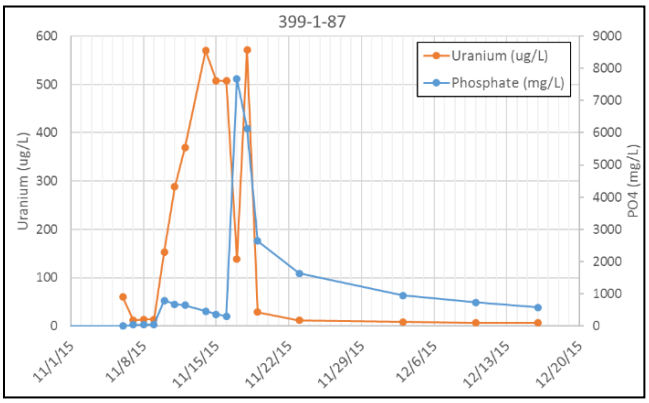

PRZ Well

Figure 6-5. Uranium and Phosphate Trends from Daily Sampling of Wells (page 2 of 2)

The six aquifer monitoring wells where data loggers were installed are 399-1-70, 399-1-76, 399-1-80, 399-1-82, 399-1-84, and 399-1-86. Of these, EC results are shown for wells 399-1-86 and 399-1-76 in Figure 6-6 because they are located close to the injection wells or just at the edge of the Stage A area (Figure 6-1). All others are located either outside the Stage A area or away from injection wells, leading to either negligible or no change in EC from injection/infiltration. The time periods of injections are indicated as vertical lines along with EC measurements. EC increases from background of about 500 µS/cm following injection events, but the increase is greatest from PRZ injections. EC results for 399-1-86 indicate that high concentrations (~3,000 µS/cm) were being maintained in the aquifer even after 2 weeks had passed since the injections ended. The sharp temporary decline in EC after November 22, 2015 is attributed to a data logger disturbance during post-treatment deactivation activities undertaken at the site. EC in 399-1-76 shows a gradual decline following injection after peaking at 9,000 µS/cm. Since this well is located at the downgradient edge of Stage A area, it received higher concentrations due to injections at multiple locations and mixing of waters; in comparison, 399-1-86 was probably only affected by one or two nearby injection wells.

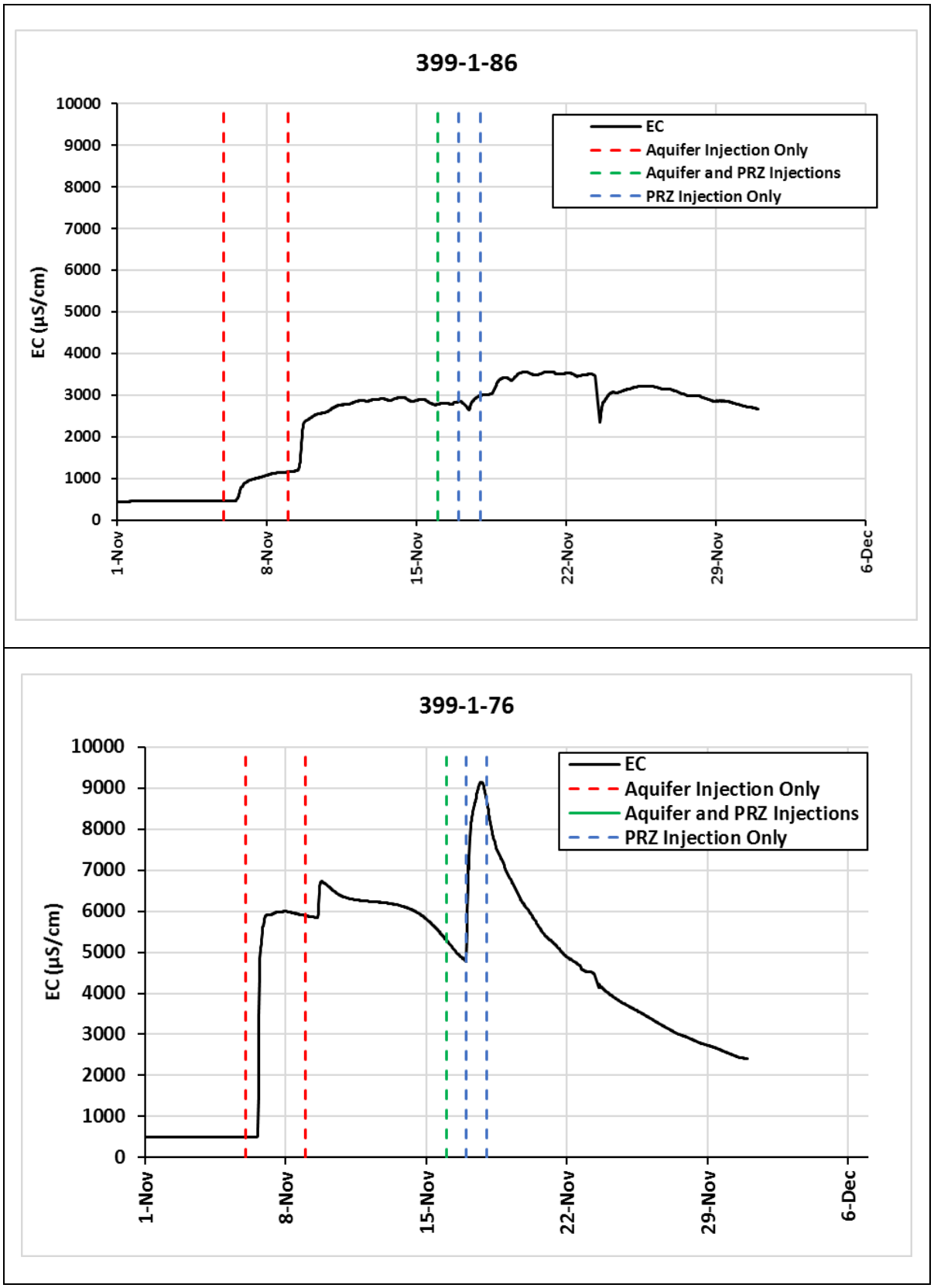

Figure 6-6. Electrical Conductivity in Selected Monitoring Wells Fitted with Data Loggers

Figure 6-7 presents the correlation between EC and measured phosphate concentrations (total phosphorus reported as phosphate). Based on this correlation, the EC value of 3,000 µS/cm approximates to about 2,190 mg/L of phosphate, while 9,000 µS/cm (peak value) is approximately equal to 7,400 mg/L of phosphate, which is close to the peak concentrations observed in the PRZ wells during injection (Figure 6-5). Figure 6-8 presents the correlation between EC and measured phosphate concentrations at the mixing skids prior to injection and infiltration. It indicates a similar strong correlation based on which 9,000 µS/cm is approximately equal to 6,800 mg/L phosphate. These results indicate that high phosphate concentrations were delivered to the PRZ (and aquifer), and the concentrations remained high in the aquifer for at least 2 weeks (duration of monitoring using data loggers) following injection.

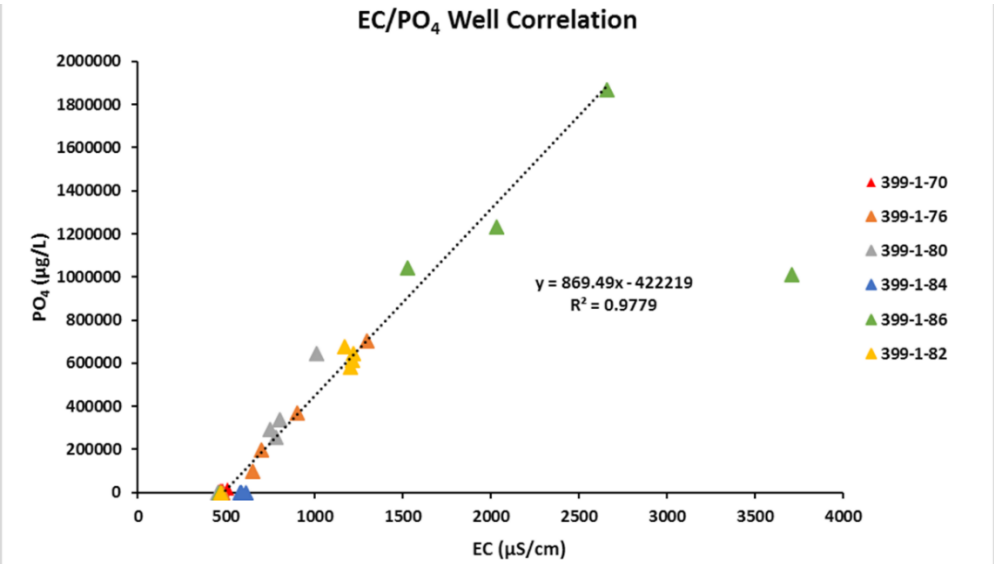

Note: Total P is reported as phosphate.

Figure 6-7. Correlation between Electrical Conductivity and Phosphate Concentration in Monitoring Wells

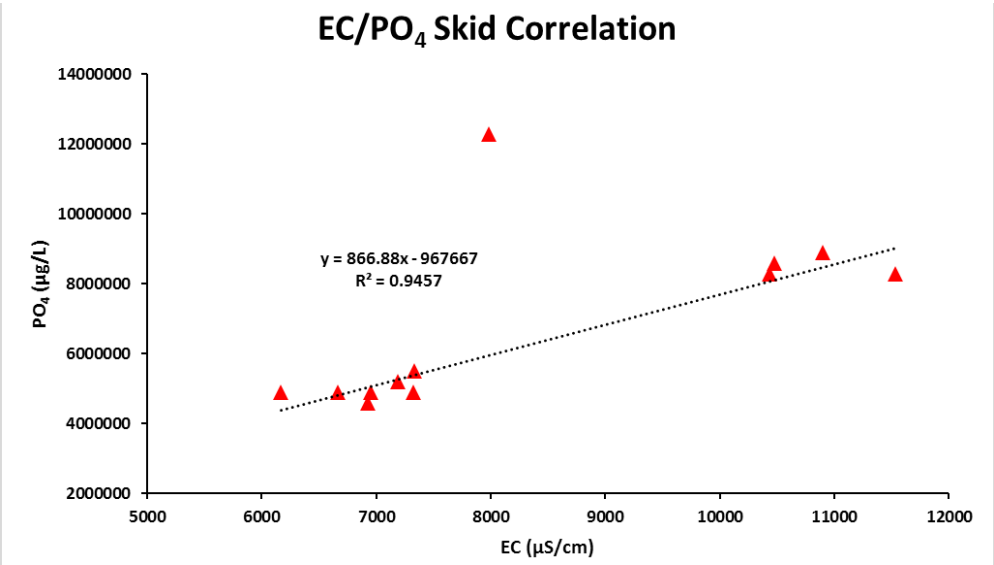

Note: Total P is reported as phosphate.

Figure 6-8. Correlation between Electrical Conductivity and Phosphate Concentration at the Mixing Skids Prior to Injection and Infiltration

During the injection and infiltration period, continuous imaging was performed in real time, using time-lapse ERT, to evaluate amendment delivery performance in the subsurface (PNNL-SA-25232, *Stage A Uranium Sequestration Amendment Delivery Monitoring Using Time-Lapse Electrical Resistivity Tomography*). ERT monitoring was conducted along two transects extending 89.9 m (295 ft) (transect A-A') and 70.1 m (230 ft) (transect B-B') within the treatment zone, as shown in Figure 6-9. A single ERT measurement is conducted by injecting current between a pair of electrodes and measuring the resulting voltage across several other electrode pairs. Using an array of electrodes, many such measurements are strategically collected to optimize imaging resolution. This set of measurements, termed ERT survey, is processed using a computationally intensive tomographic inversion algorithm that approximates the subsurface conductivity distribution that gave rise to the measurements.
When time-lapse imaging is conducted, surveys are continuously collected and processed to provide a chronological sequence of image frames that illustrate the change in bulk conductivity with time. Subtracting the baseline image (in this case, pretreatment image) from the time-lapse images reveals the change in bulk conductivity caused by the phosphate amendment, thereby revealing the distribution of amendment in space and time. Additional details are presented in PNNL-SA-25232.

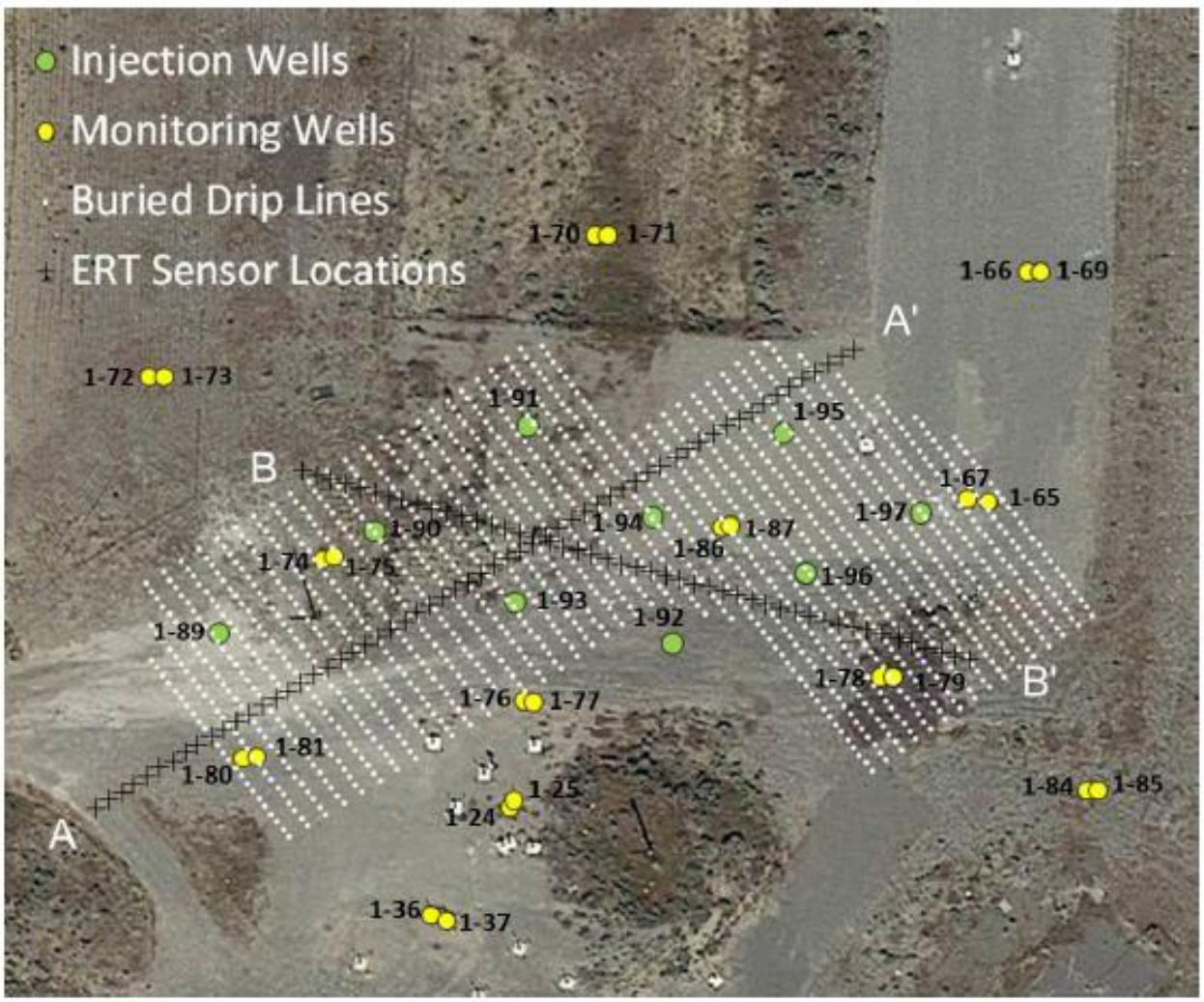

Note: White, gray, and black contour lines represent increases in bulk conductivity of 0.002, 0.003, and 0.004 S/m, respectively.

Figure 6-9. Location of ERT Sensors (Electrodes) Along Two Cross-Sections (A-A' and B-B') Relative to Stage A Treatment Area

Results of the ERT survey are presented in Figure 6-10 for 5 selected days of operations, from November 11 (sixth day of operation) through November 15, 2015 (tenth day of operation). The results show variable concentrations of phosphate solutions, with increased change in bulk conductivity correlating with higher concentration of phosphate (the primary ion in the solution). The variable concentrations indicate that the heterogeneities in the subsurface (variable permeability layers) lead to variable distribution of phosphate. The contour of 0.002 S/m and 0.003 S/m (white and gray contours) gets to the water table located at about 10 m depth by the tenth day of operation (November 15, 2015), while the contour of 0.004 S/m gets to a depth of about 6 m in most of the cross-section. Although earlier arrival is observed in cross-section A-A' for the location on the west side, most cross-section lengths of the contour lines are fairly uniform, indicating that the effect of heterogeneities leads to establishment of uniform distribution of infiltrated phosphate solution. Using the breakthrough times of 0.002 S/m contour at the water table, the average migration velocity is estimated in Figure 6-11. It ranges from about 0.5 m/day to 3 m/day, with most of the area experiencing migration velocity of about 1 to 1.5 m/day.

Results from monitoring wells located downgradient of the Stage A treatment area are presented in Figures 6-12 and 6-13. Figure 6-12(a) presents the location of monitoring wells downgradient of the Stage A treatment area, while Figure 6-12(b) shows EC measurements at 399-1-23. This well is located downgradient of Stage A and received injected and infiltrated solutions, as indicated by the changes in EC corresponding to various injections. Based on elevated EC values (greater than the background value that ranges from 450 to 500 µS/cm), it can be inferred that phosphate concentrations at 399-1-23 continued to remain high for 2 weeks after the treatment period. Figure 6-13 presents uranium and phosphate concentrations, based on sampling of wells 399-1-23, 399-1-17A, and 399-1-7, which are located approximately along the groundwater flow path downgradient of the Stage A treatment area. The decline in uranium concentrations correlates with the increase in phosphate concentrations, reflecting changes that have occurred in the Stage A treatment area. As the phosphate pulse moves downgradient, it gets retarded and dispersed. Uranium concentrations declined in all downgradient wells and have remained low over the 6 months of monitoring following treatment. A small rebound in uranium concentrations is noticeable in the wells, but concentrations have remained substantially lower than those prior to the treatment. This indicates that prior to treatment, uranium concentrations in this part of the aquifer were derived largely from the Stage A area.

6.3 Comparison of Post-Treatment and Pretreatment Samples

To evaluate performance of the remedy within the Stage A treatment area, three boreholes were drilled to collect post-treatment sediment samples for further analysis. Locations of the three boreholes (C9580, C9581, and C9582) are shown in bold red color (Figure 6-14). These boreholes were drilled adjacent to three boreholes where pretreatment samples were collected (shown in light red color in Figure 6-14), so a comparison can be made. Details of the analysis of post-treatment borehole samples are provided in PNNL-25420, *Analytical Data Report for Sediment Samples Collected from 300-FF-5: Boreholes C9580, C9581, and C9582*; results of similar analyses conducted on pretreatment samples are provided in PNNL-24911, *Analytical Data Report for Sediment Samples Collected From 300-FF-5 OU, Wells C8940 and C9451*, and SGW-58830, *300-FF-5 Supplemental Post-ROD Field Investigation Summary*.

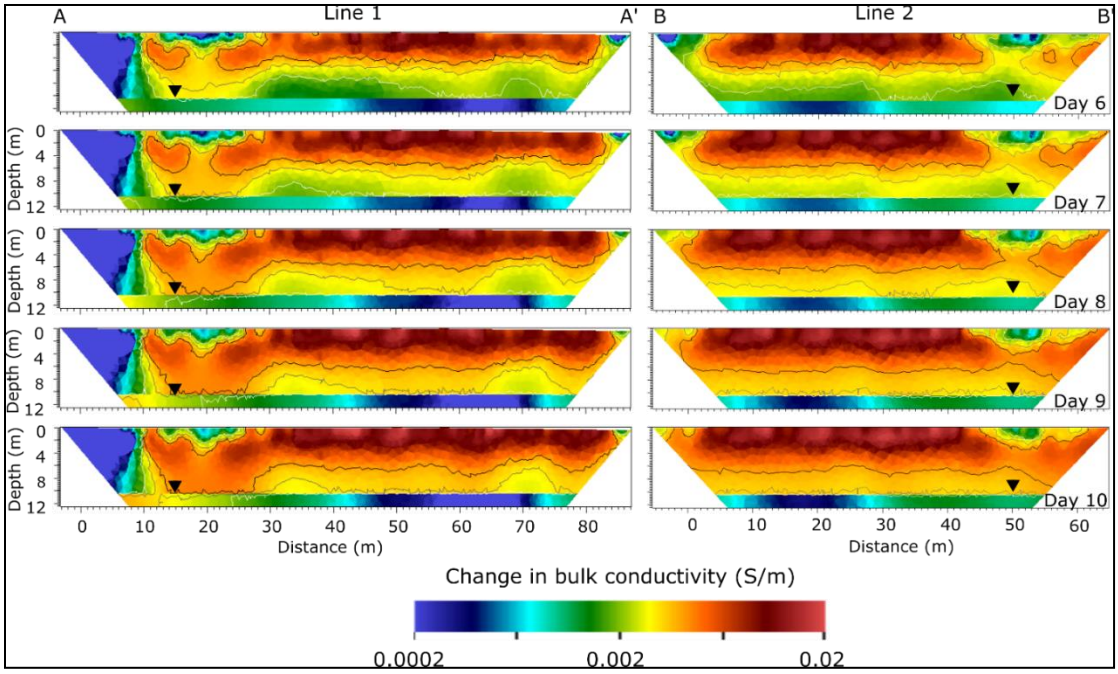

Figure 6-10. Changes in Bulk Conductivity Observed Using ERT Imaging Along Two Lines for Selected Time Periods

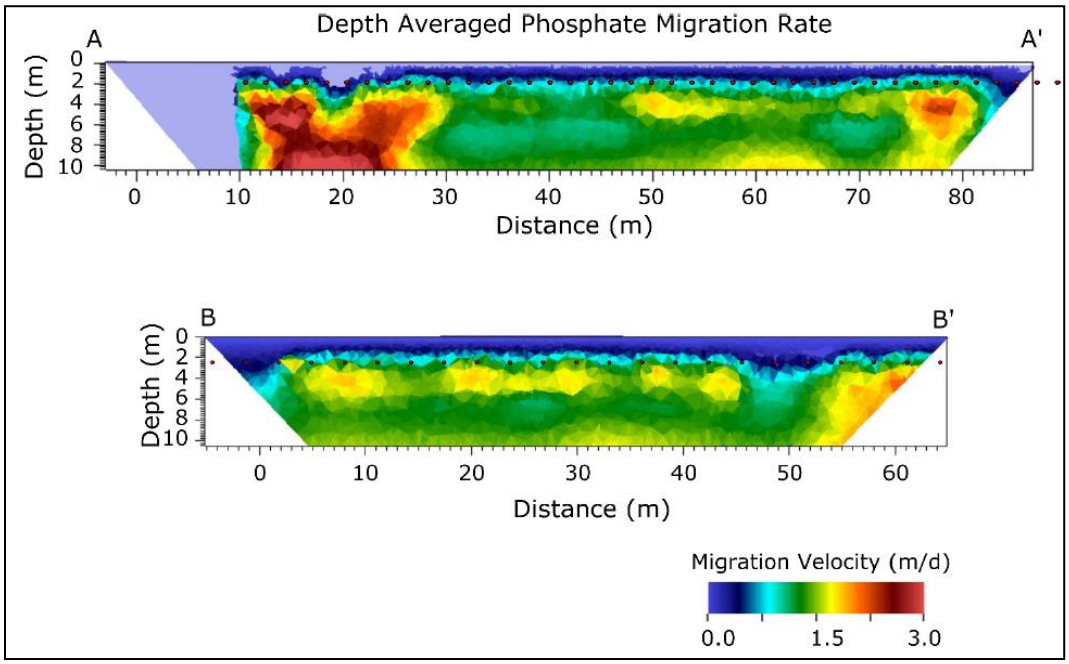

Figure 6-11. Depth Averaged Phosphate Migration Rate Estimated from ERT Imaging Based on Breakthrough Magnitude Change in Bulk Conductivity of 0.002 S/m

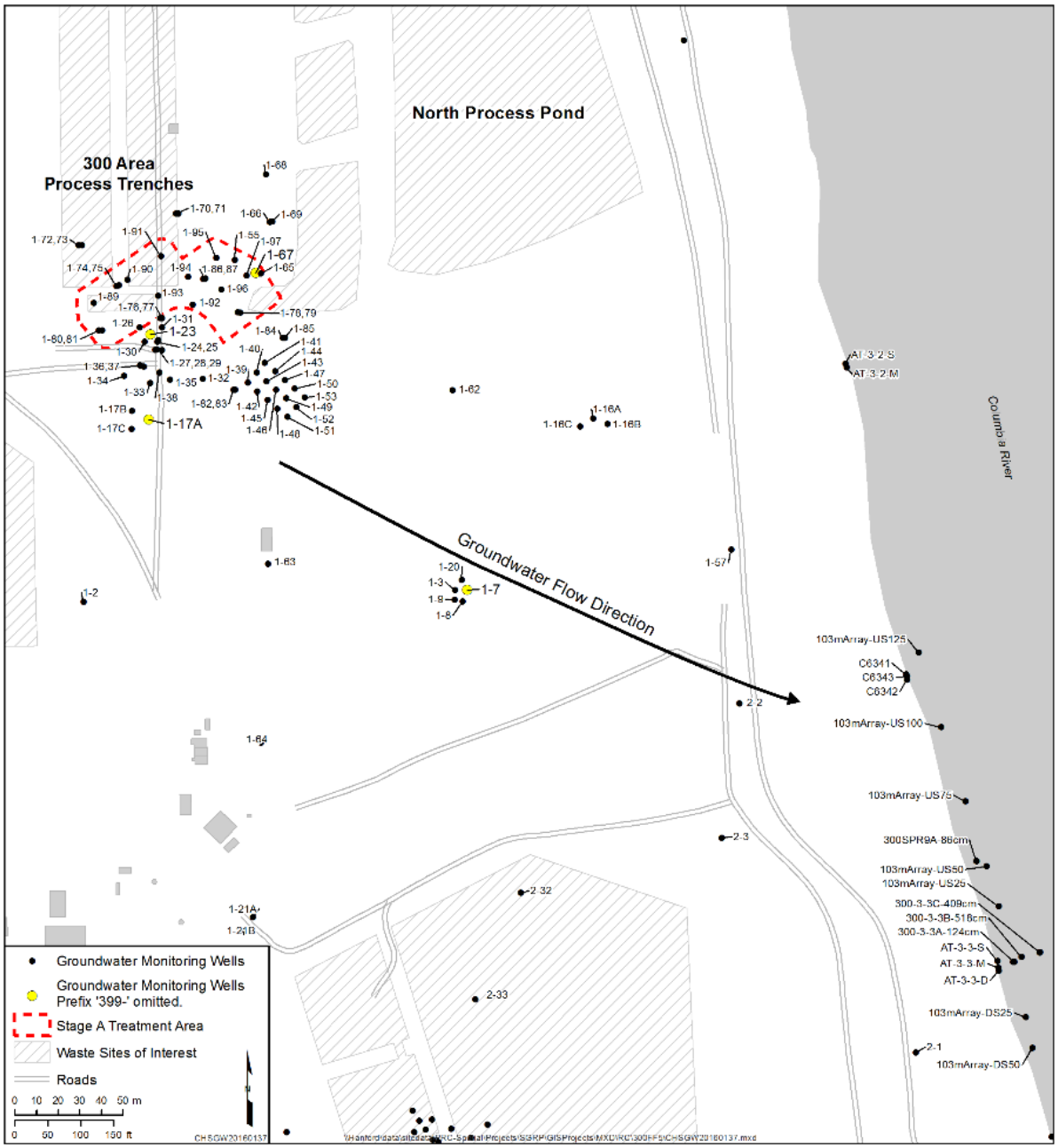

(a)

Figure 6-12. Results from Monitoring Wells Located Away from the Stage A Treatment Area¶(page 1 of 2)

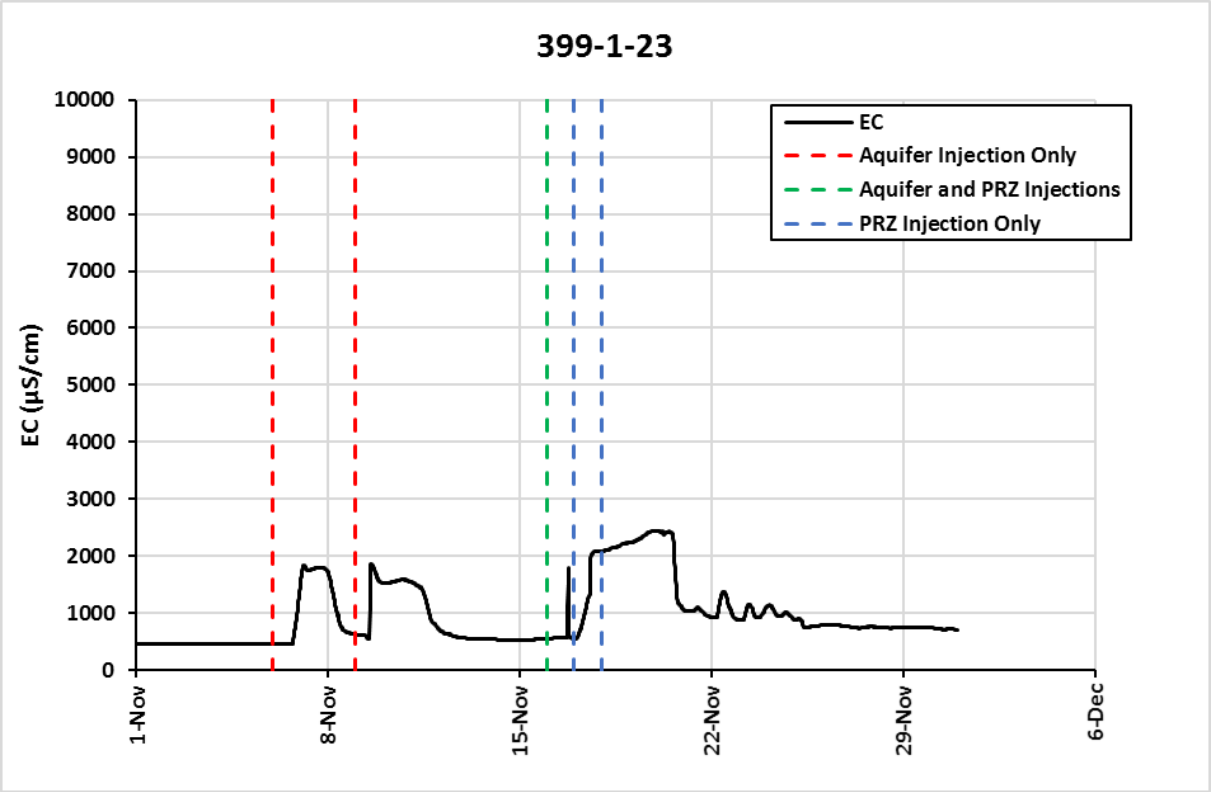

(b)

Note: The location map (a) and continuous EC measurements (b) are shown.

Figure 6-12. Results from Monitoring Wells Located Away from the Stage A Treatment Area (page 2 of 2)

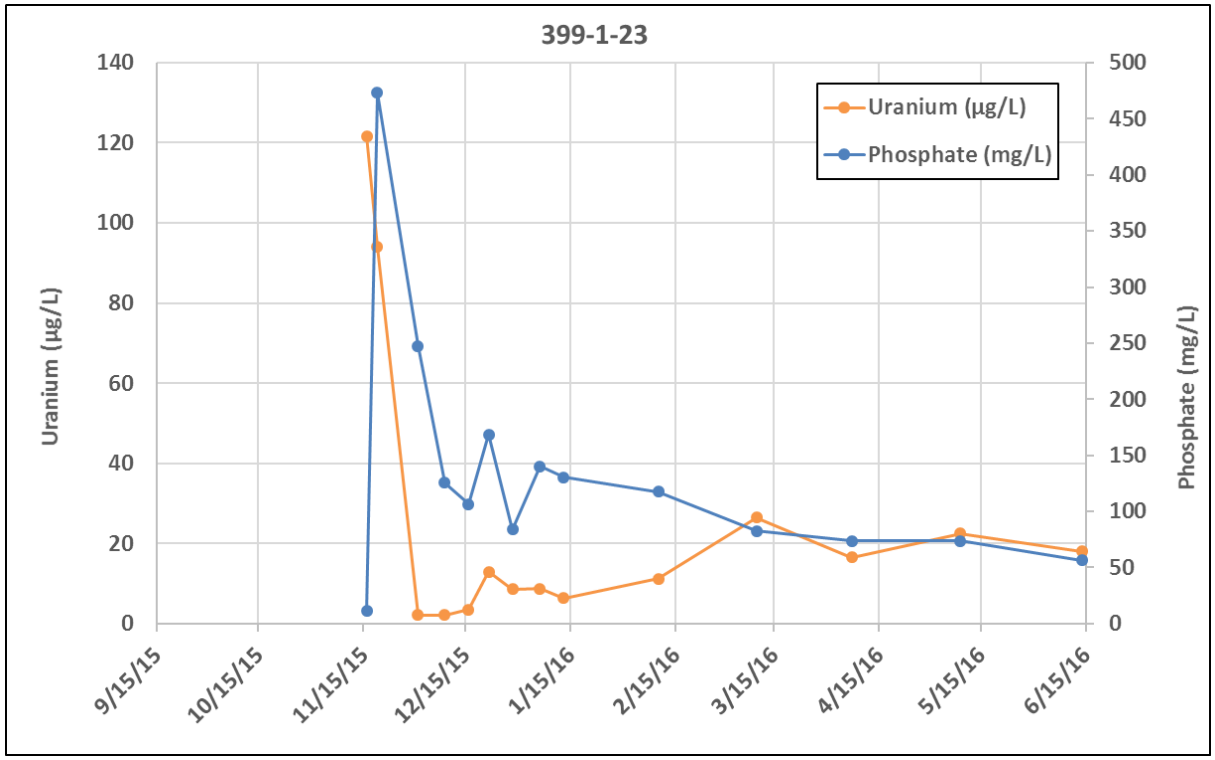

(a)

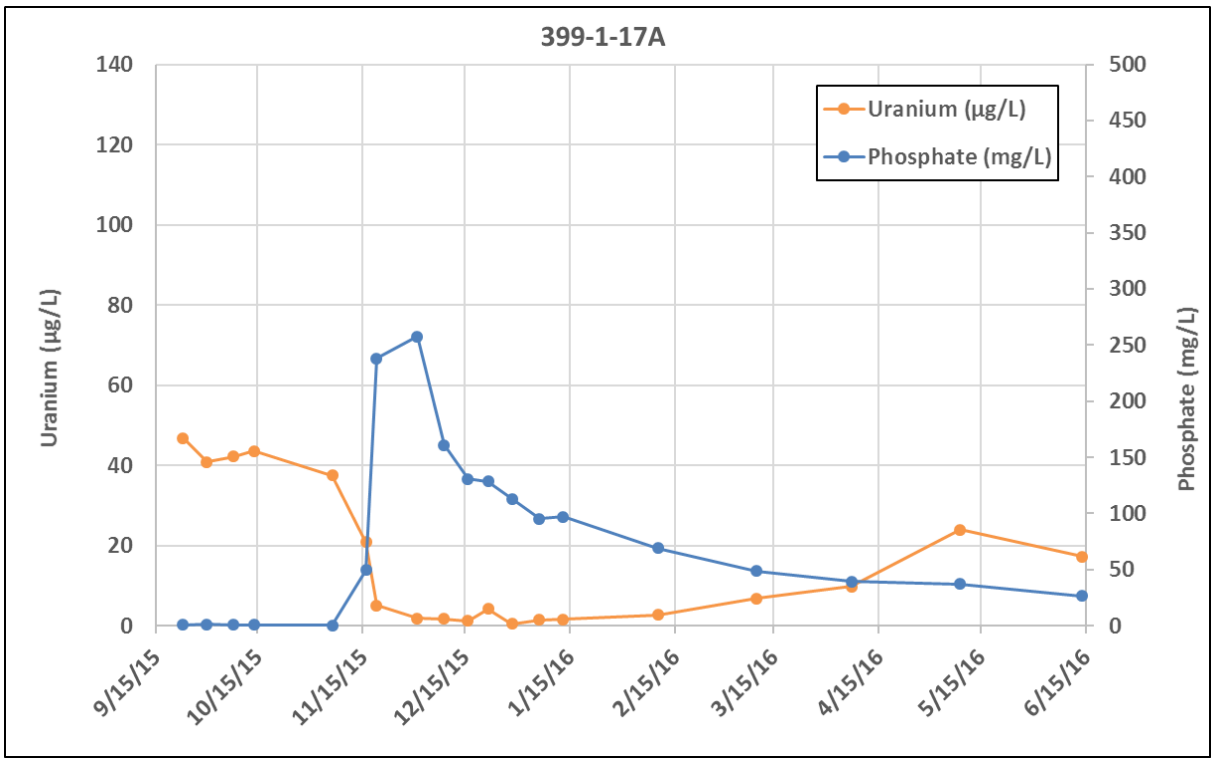

(b)

Figure 6-13. Phosphate and Uranium Concentrations Observed in Wells¶page 1 of 2)

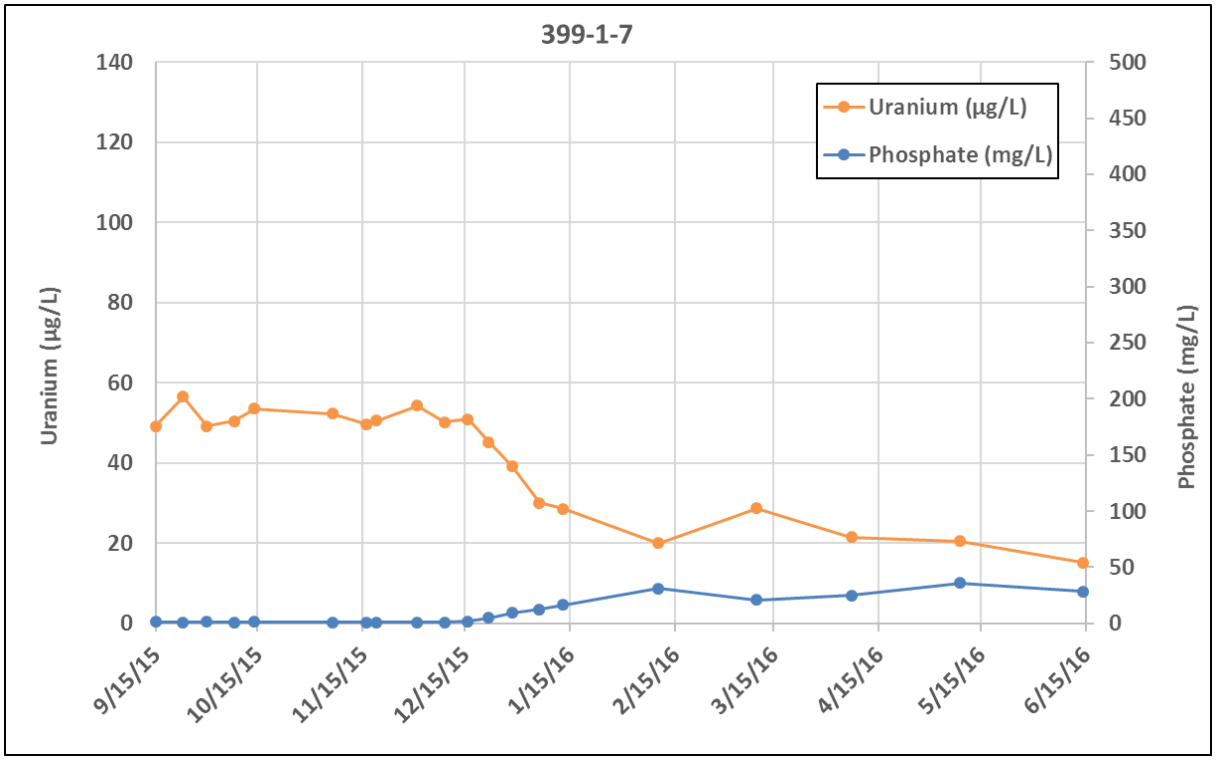

(c)

Note: 399-1-23 (a), 399-1-17A (b), and 399-1-7(c) are located downgradient of the Stage A treatment zone.

Figure 6-13. Phosphate and Uranium Concentrations Observed in Wells (page 2 of 2)

Three pretreatment boreholes of interest (Figure 6-14) are C8940 (399-1-76), C9451 (399-1-80), and C9451 (399-1-67). Sediment samples collected from various depths were analyzed for total uranium concentration using a contract (e.g., GEL or ALS) laboratory, and then specific sampling depths were selected for detailed laboratory evaluations performed at PNNL. The detailed laboratory tests consisted of sequential uranium extraction tests, labile uranium leach tests, flow-through column tests on both intact (field-texture) split-spoon liner samples and <2-mm repacked columns, and identification of uranium mineral phase(s) and surface coating(s). Total uranium analysis results for the pretreatment samples are presented in Table 6-2. GEL was the contract laboratory used for this evaluation. Later, when selected samples were sent to PNNL for detailed analyses, total uranium concentrations were recalculated based on the results of sequential extraction. These are also presented in Table 6-2 for comparison purposes. The results indicate that where total uranium concentrations were low, the GEL and PNNL results matched but, where total uranium concentrations were high, the GEL analysis consistently resulted in lower concentrations compared to PNNL results. Since detailed laboratory evaluations were conducted by PNNL, to be internally consistent, the total uranium concentrations from PNNL are used in further analysis. Figure 6-15 (part a) shows the vertical profiles of total uranium concentrations based on sampled depth intervals from the pretreatment boreholes.

Total uranium analyses results for post-treatment samples collected from C9580, C9581, and C9582 are presented in Table 6-3. Samples from various depth intervals were sent to the contract laboratory (ALS). Based on uranium concentrations, a subset of samples was selected for detailed laboratory analyses conducted at PNNL. Total uranium results from both labs, presented in Table 6-3, indicate reasonable comparisons between the two labs. Figure 6-15 (part b) shows the vertical profiles of total uranium concentrations based on sampled depth intervals from the post-treatment boreholes.

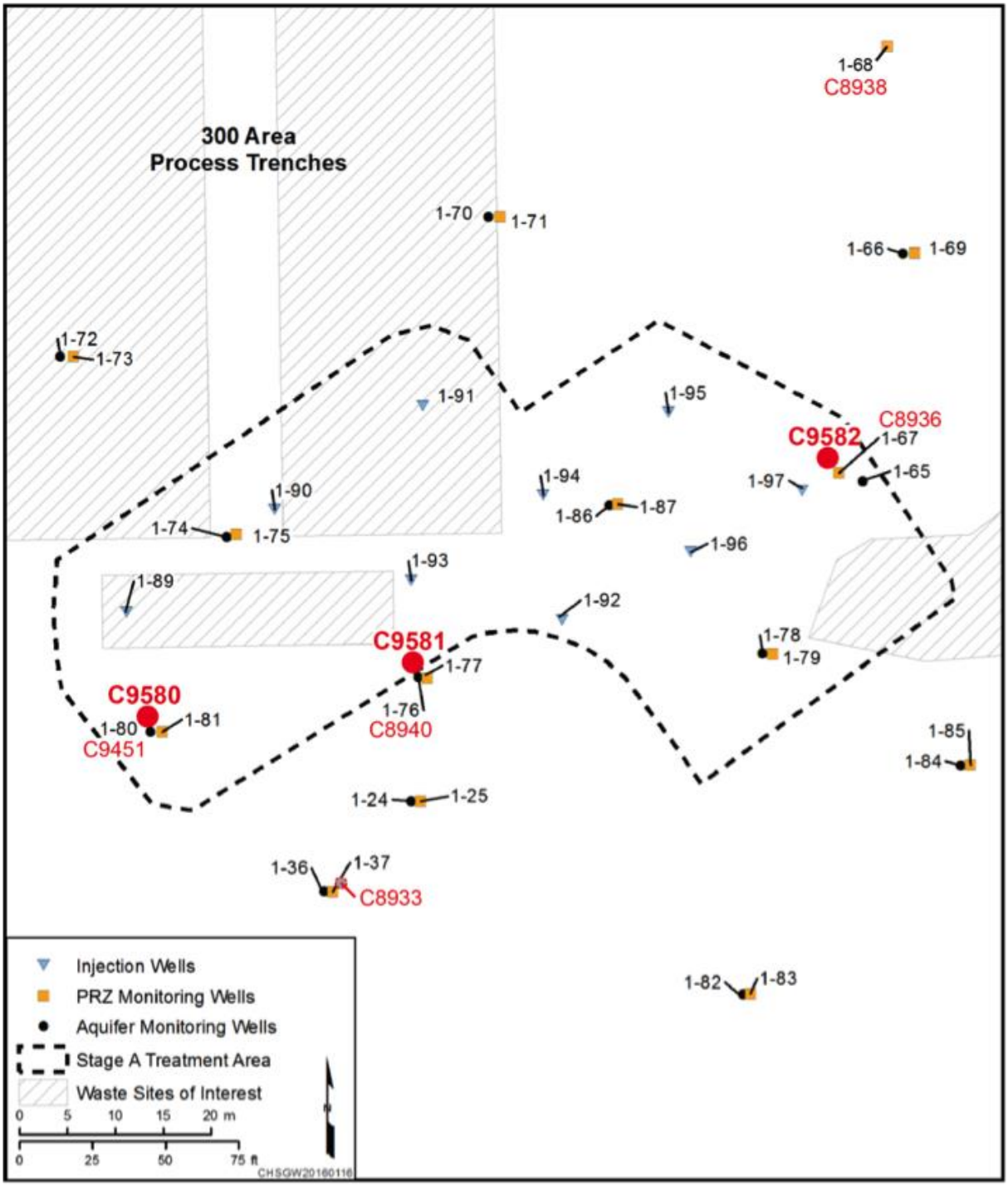

Note: Bold red represents post-treatment boreholes, while pretreatment sampling locations are shown in light red.

Figure 6-14. Borehole Locations to Evaluate Analyte Concentrations in Sediment

Table 6-2. Pretreatment Sediment Analysis for Total Uranium by the GEL Laboratory and PNNL for Samples Located Greater Than 6 m (20 ft) in Depth Below Ground Surface

Well ID	Sample ID (GEL Lab)	Borehole, Sampling Interval	Depth Below Ground in m (ft)	GEL Lab Based Total Uranium in Sediment Sample (µg/g)	PNNL Lab Based Total Uranium (µg/g) (Total from Sequential Extraction)	Sample ID (PNNL Leach)
C8940 (399-1-76)	B31N14	I-005B	6.6 to 6.7 (21.5 to 22)	2.54	--	--
	B31N15	I-005B (Duplicate)	6.6 to 6.7 (21.5 to 22)	2.14	--	--
	B31N20	I-006B	7.3 to 7.5 (24 to 24.5)	2.50	--	--
	B31N25	I-007B	7.9 to 8.1 (26 to 26.5)	5.90	--	--
	B31N30	I-008B	8.7 to 8.8 (28.5 to 29)	11.50	14.4	B31N29
	B31N35	I-009B	9.4 to 9.6 (31 to 31.5)	4.49	--	--
C9451 (399-1-80)	B31N86	I-005B	6.4 to 6.6 (21 to 21.5)	12.0	12.72	B31N85
	B31N91	I-006B	7.3 to 7.5 (24 to 24.5)	5.44	--	--
	B31N97	I-007B	8.1 to 8.2 (26.5 to 27)	10.6	13.02	B31N96
	B31NB2	I-008B	8.7 to 8.8 (28.5 to 29)	9.29	14.96	B31NB1
	B31NB7	I-009B	9.6 to 9.8 (31.5 to 32)	6.5	--	--
C8936 (399-1-67)	B30524	I-004B	5.3 to 6.1 (17.5 to 20)	34.8	57.66	B30525
	B30529	I-005B	6.4 to 7 (21 to 23)	26.1	--	--
	B30534	I-006B	7.2 to 7.8 (23.5 to 25.5)	16.9	--	--
	B30535	I-006B (Duplicate)	7.2 to 7.8 (23.5 to 25.5)	20.6	--	--
	B30540	I-007B	7.9 to 8.7 (26-28.5)	41.4	125.79	B30538
	B30545	I-008B	8.7 to 9.4 (28.5 to 31)	20.8	31.0	B30546

Table 6-2. Pretreatment Sediment Analysis for Total Uranium by the GEL Laboratory and PNNL for Samples Located Greater Than 6 m (20 ft) in Depth Below Ground Surface

Well ID	Sample ID (GEL Lab)	Borehole, Sampling Interval	Depth Below Ground in m (ft)	GEL Lab Based Total Uranium in Sediment Sample (µg/g)	PNNL Lab Based Total Uranium (µg/g) (Total from Sequential Extraction)	Sample ID (PNNL Leach)
	B30550	I-009B	9.8 to 10.5 (32 to 34.5)	25.8	--	--
	B309C9	(Contingency)	10.5 to 11.1 (34.5 to 36.5)	12.3	--	--
	B30552	I-0010	10.7 (35)	19.9	--	--

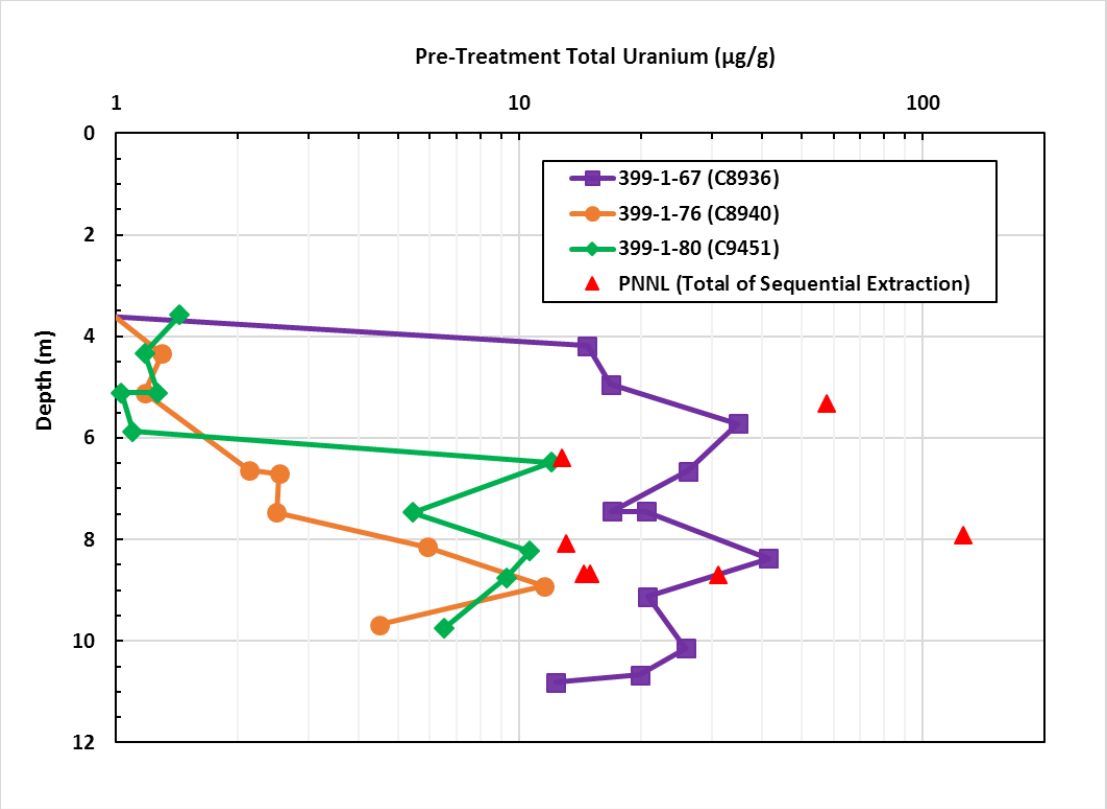

(a)

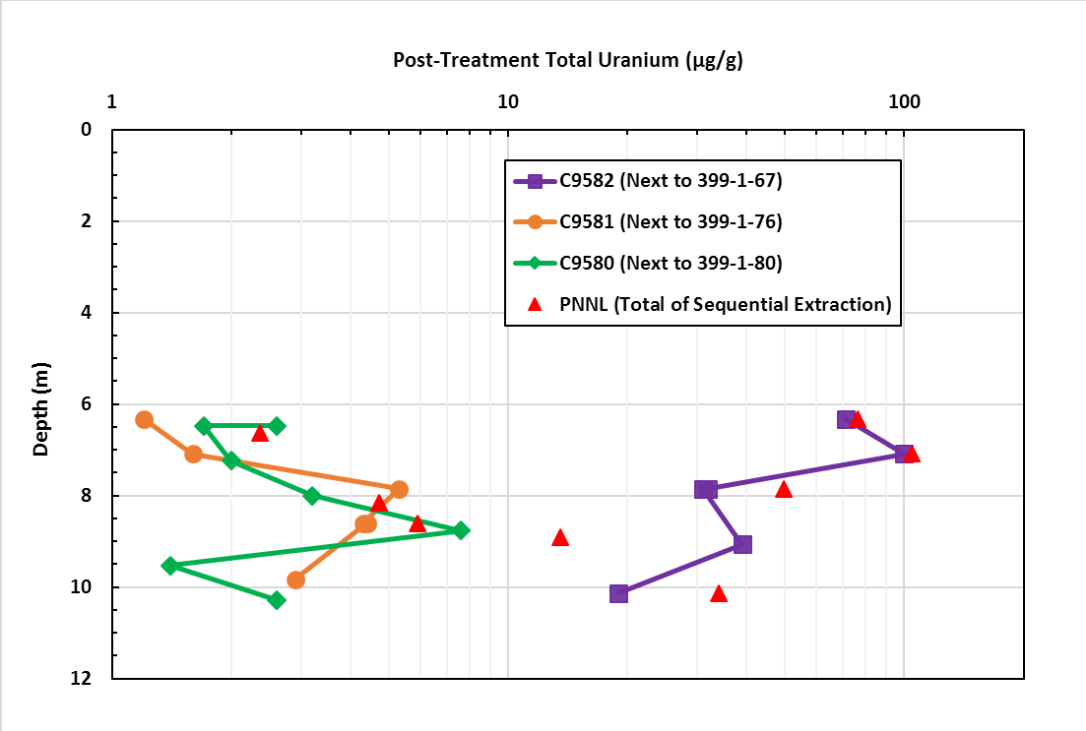

(b)

Figure 6-15. Total Uranium Concentration Profiles based on (a) Pre-Treatment Borehole Samples and (b) Collocated Post-Treatment Borehole Samples

Table 6-3. Post-Treatment Sediment Analysis for Total Uranium by the ALS Lab and PNNL for Samples Located Greater Than 20 ft in Depth Below Ground Surface

Well ID	Sample ID (GEL Lab)	Borehole, Sampling Interval	Depth (ft below ground surface)	ALS Lab Based Total Uranium in Sediment Sample (µg/g)	PNNL Lab Based Total Uranium (µg/g) (Total from Sequential Extraction)	Sample ID (PNNL Leach)
C9581	B347J9	I-001	6.1 to 6.9 (20 to 22.5)	1.2	--	--
	B347K5	I-002	6.9 to 7.6 (22.5 to 25)	1.6	--	--
	B347L0	I-003	7.6 to 8.4 (25 to 27.5)	5.3	--	--
	B347L5	I-004	8.4 to 9.1 (27.5 to 30)	4.3	5.8	B347L4
	B347L6	--	--	4.4	--	--
	B347M1	I-005	9.1 to 9.9 (30 to 32.5)	2.9	--	--
C9580	B347C7	I-001	6.1 to 6.9 (20 to 22.5)	2.6	2.3	B347C6
	B3347C9	--	--	1.7	--	--
	B347D3	I-002	6.9 to 7.6 (22.5 to 25)	2.0	--	--
	B347D9	I-003	7.6 to 8.4 (25 to 27.5)	3.2	4.7	B347D8
	B347F4	I-004	8.4 to 9.1 (27.5 to 30)	7.6	13.3	B347F1, B347F3
	B347F9	I-005	9.1 to 9.9 (30 to 32.5)	1.4	--	--
	B347H4	I-006	9.9 to 10.7 (32.5 to 35)	2.6	--	--
C9582	B347P1	I-001	6.1 to 6.9 (20 to 22.5)	71.0	74.8	B347P0
	B347P6	I-002	6.9 to 7.6 (22.5 to 25)	100.0	102.3	B347P4, B347P5, B347P8
	B347R2	I-003	7.6 to 8.4 (25 to 27.5)	32.0	48.1	B347R0, B347R1
	B347R3	--	--	31.0	--	--
	B347R8	I-004	8.4 to 9.1 (27.5 to 30)	39.0	--	--
	B347T8	I-006	9.9 to 10.7 (32.5 to 35)	19.0	33.4	B347T6, B347T7

Comparing total uranium concentrations between the collocated pretreatment and post-treatment boreholes (Figure 6-15) indicates that uranium concentrations remained largely unchanged in the sediment following treatment. (NOTE: For the purpose of comparison, the pretreatment borehole profile for 399-1-67 [C8936] has been used based on PNNL data instead of GEL data.) This shows that most of the uranium present in the sediment remained in place, and only a limited amount was displaced during injection and infiltration.

Acid extractions using 0.5 M nitric acid were conducted on selected post-treatment samples (boreholes C9580, C9581, and C9582) as well as pretreatment samples from boreholes C8940 (399-1-76) and C9451 (399-1-80) to evaluate the precipitated phosphate concentration by etching the sediments without digesting the sample (PNNL-25420). For each sample, 0.5 M nitric acid was added at a solid-to-solution ratio of 1 g/2 mL. The sample was then agitated on an orbital shaker for 15 minutes, centrifuged, decanted, and filtered. The results in terms of phosphate concentration (total P as phosphate) are presented in Figure 6-16 (pretreatment samples are shown in part a, and post-treatment samples [prior to any leaching] are shown in part b). Results from pretreatment samples provide an average phosphate concentration of 1,750 mg/kg, indicating that some residual phosphate existed prior to injection/infiltration from past discharge activities in this area. Results from post-treatment samples (Figure 6-16, b) show that phosphate concentrations are typically higher than 2,000 mg/kg for C9580 and for deeper samples at C9582, indicating that these resulted from Stage A treatment. Borehole C9580 shows high phosphate concentrations throughout its depth profile, consistent with the ERT data, where faster migration of infiltrated solutions was observed resulting in higher bulk conductance (Figures 6-10 and 6-11). Higher phosphate concentrations observed at a deeper depth at C9582 indicate that injections conducted in the PRZ were instrumental in precipitating phosphate. Higher phosphate concentration is also observed for the deeper sample collected at C9581, which confirms the effect of injection in delivering high concentrations of phosphate.

Sediment samples collected from post-treatment boreholes were also analyzed for phosphate concentration (at the ALS laboratory) by performing water extraction (analyzed using ion chromatography) and total digestion (analyzed using inductively coupled plasma-optical emission spectroscopy [ICP-OES]; SW6010B). Vertical profiles, based on water extraction and total digestion of the sample, are shown in Figure 6-17. Phosphate concentrations derived from total digestion performed in the ALS laboratory are compared to the total phosphate, based on sequential extraction performed by PNNL. They show values of similar magnitude with depth. The concentration shows a marked increase in the PRZ, indicating that injections performed in the PRZ led to formation of phosphate precipitate, and they are considerably greater than the background phosphate concentration of about 3,600 mg/kg, which is inferred for the 300 Area samples (for total digestion) based on evaluation of results. A similar increase in phosphate concentration is also noticeable for the water extracted profiles within the PRZ. Above the PRZ, phosphate concentrations are controlled by the infiltrated solutions. Concentrations above the PRZ vary by location indicating variable depths to which highly concentrated phosphate solutions reached. The infiltrated solutions at C9580 appear to have influenced phosphate precipitation throughout the vadose zone (down to PRZ), while only high concentrations are noticeable in the shallow portion (<4 m depth) above the PRZ at C9581. The sharp increase in phosphate concentration at about 5 m depth at C9580 is due to presence of a silt lens indicating enhanced reaction with phosphate. At C9582, the amount of phosphate precipitation above the PRZ does not appear to be appreciable, and they may be impacted by local heterogeneities in permeability that could have precluded uniform distribution of phosphate in the upper vadose zone.

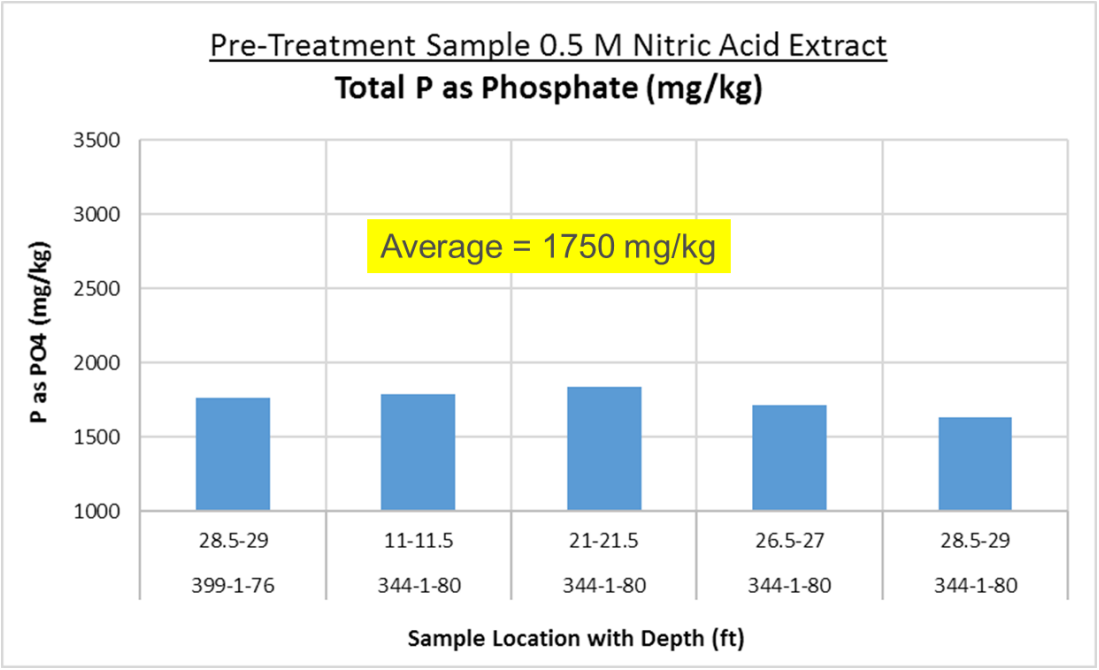

(a)

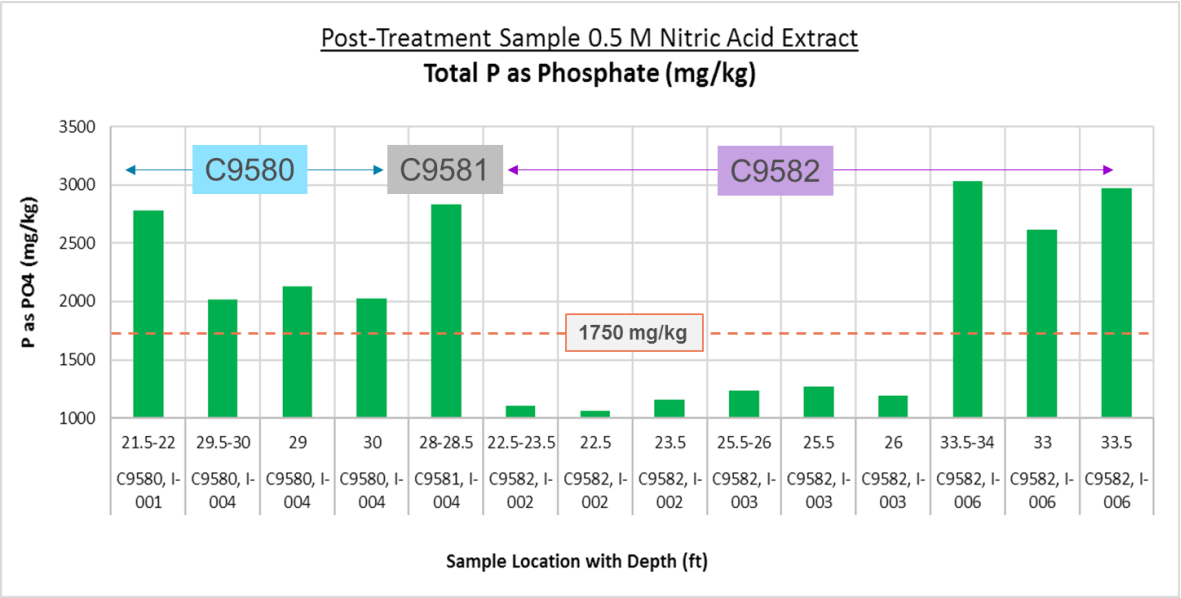

(b)

Figure 6-16. Concentration of Phosphate (Total P as Phosphate) Based on 0.5 M Nitric Acid Extraction on (a) Pretreatment Samples and (b) Post-Treatment Samples

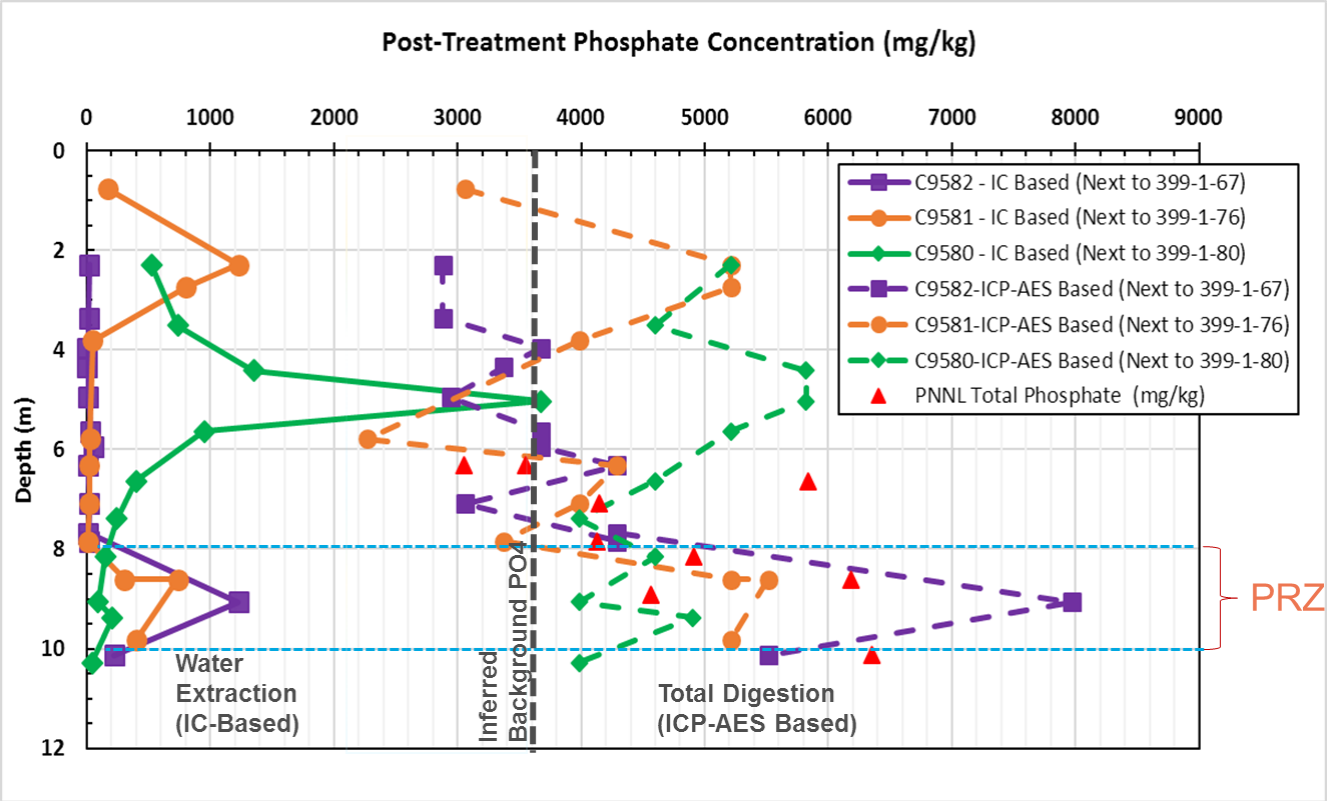

Note: Vertical line of background phosphate concentration is inferred for the samples undergoing total digestion.

Figure 6-17. Phosphate Concentrations (total P as Phosphate) in Post-Treatment Samples Analyzed Using Water Extraction (Ion Chromatography [IC]) and Total Digestion (ICP-Atomic Emission Spectroscopy [ICP-AES; same as ICP-OES])

6.3.1 Sequential Extraction

Sequential extraction tests were performed on both the pretreatment and post-treatment samples. Aliquots of air dried <2 mm size fraction are used in the analysis. These tests use a sequential chemical extraction technique described in PNNL-14022, *300 Area Uranium Leach and Adsorption Project*, and PNNL-21733. The tests can provide information on the relative amount of uranium (or other elements) present in extractable phases of carbonate coatings, carbonate solid-bearing compounds, amorphous hydrous oxides, crystalline iron oxides, and strong acid leachable compounds. The following extractions were undertaken in sequence:

1. Weak Acetic Acid Extraction: This involved contacting the sediment with a weak acetic acid consisting of 1 mol/L sodium acetate with a final pH of ~5. The solid-to-solution ratio is kept at 1 g/2 mL, and the sample is agitated in an orbital shaker for 1 hour. The solution is removed, decanted, and filtered. Target uranium phases for this extraction are the adsorbed (weakly bound) uranium and some of the uranium associated with carbonate minerals.

2. Strong Acetic Acid Extraction: The sample from the previous extraction is contacted with a strong acetic acid (concentrated glacial acetic acid) at a pH of 2.3 for 5 days. The sample is centrifuged, and the solution is decanted and filtered. The target phase for the strong acetic acid is the strongly bound uranium associated with carbonate minerals.

3. Ammonium Oxalate Extraction: The third extraction used a solution consisting of 0.1 mol/L ammonium oxalate with 0.1 mol/L oxalic acid. After 1 hour of contact time, the samples are centrifuged, decanted, and filtered. Target phases for the oxalate solution are the amorphous Fe, Al, Mn, and Si oxides.

4. Nitric Acid Extraction: The final extraction involved contacting the sample from the previous step with 8 mol/L of nitric acid and heating at 95°C for 2 hours on a hot plate. Target phases for the nitric acid extraction included clays and crystalline oxides of Fe, Al, and Mn.

Each extractant solution was collected and analyzed for P, Ca, Al, Fe, Mn via ICP-OES, and uranium content via inductively coupled plasma-mass spectroscopy. Results are presented in Figures 6-18 through 6-22 for each analyzed element by comparing pretreatment borehole samples with post-treatment borehole samples (same colors used for collocated boreholes). The following observations are based on the results presented for uranium (Figure 6-18):

1. In the pretreatment samples, uranium is associated primarily with two different mineral phases: the majority of the uranium is associated with crystalline oxides of Fe (including Al and Mn) and with clay minerals (based on extraction using nitric acid), while a significant yet somewhat lower amount is weakly adsorbed on sediment surface or weakly complexed with carbonate minerals (based on extraction using weak acetic acid).

2. In the post-treatment samples, uranium is primarily present as strongly bound with carbonate minerals (based on extraction using strong acetic acid) and as weakly complexed with carbonate mineral phases (based on weak acetic acid extraction). According to PNNL-20004, *Remediation of Uranium in the Hanford Vadose Zone Using Ammonia Gas: FY 2010 Laboratory-Scale Experiments*, Na-boltwoodite (uranium bearing silicate) is also predominantly dissolved (85 percent) in the acetic acid extraction. Therefore, it is possible that some of the uranium fraction is present as silicate in addition to being associated with carbonates.

3. In the post-treatment samples, an appreciable reduction of nitric acid extracted uranium fraction is noticeable, indicating that the uranium present with iron oxides and clay minerals prior to treatment has been remobilized (underwent dissolution), that later complexed with carbonate phases in the solution (along with surface adsorption and reprecipitation). The increased association of uranium with carbonate phases following phosphate treatment of uranium contaminated sediments has also been observed by Shi et al., 2009, "Inhibition Effect of Secondary Phosphate Mineral Precipitation on Uranium Release from Contaminated Sediments."

4. No appreciable change in uranium association with amorphous oxides (Fe, Mn, and Al) occurred based on extraction using ammonium oxalate. This does not mean that amorphous oxides were not impacted, but rather similar concentrations of uranium are associated with these phases prior to and following the treatment. It is possible that dissolution and precipitation also occurred, but the net effect is small.

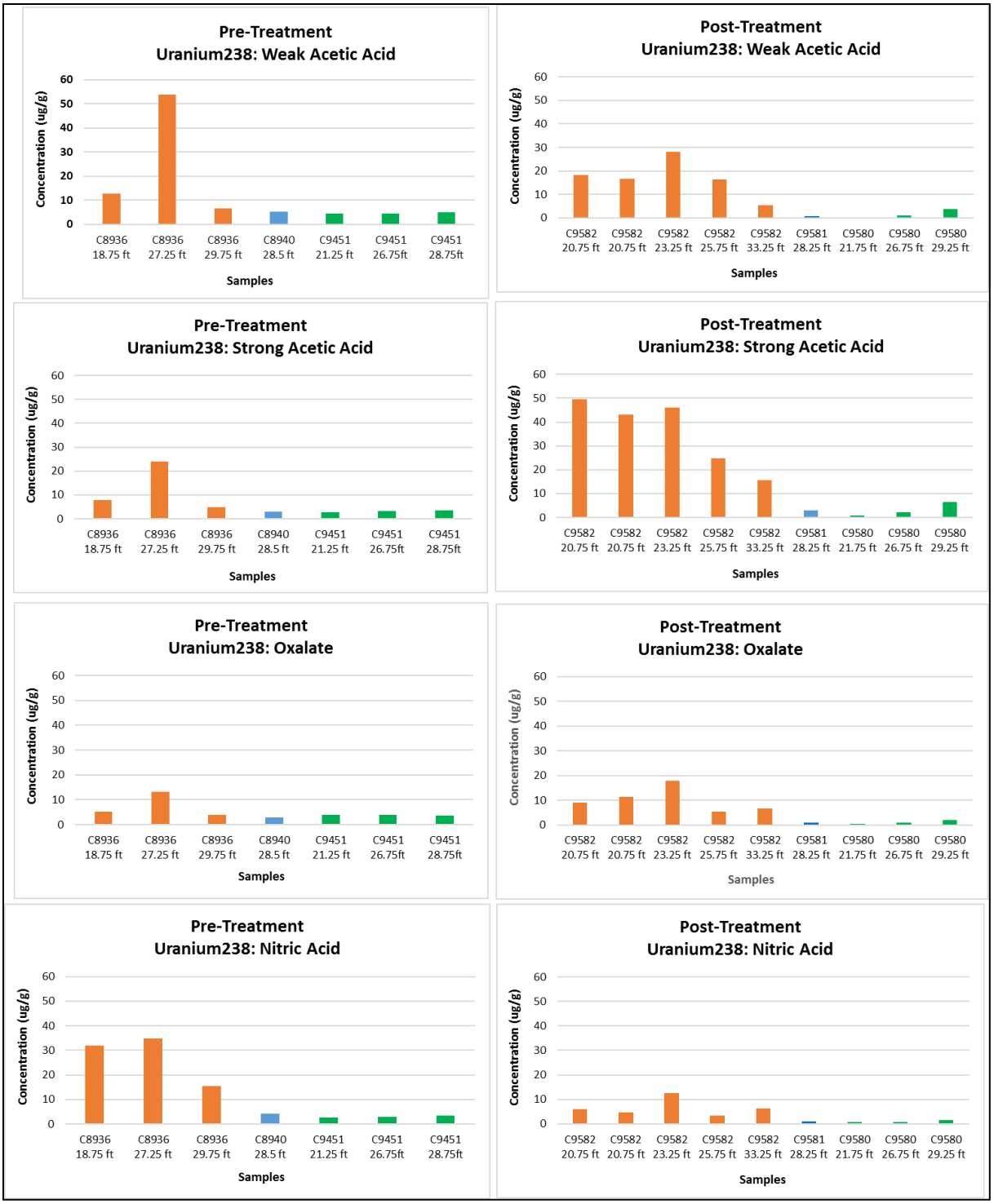

Note: Collocated boreholes are shown using the same color scheme.

Figure 6-18. Results from Sequential Extraction of Uranium Performed on Pretreatment Boreholes (Left) and Post-Treatment Boreholes (Right)

Figure 6-19 compares the pretreatment and post-treatment sequential extraction results for calcium. In the post-treatment samples, the nitric acid extracted calcium fraction decreased while fraction associated with weak and strong acetic acid extraction increased (along with the fraction extracted with oxalic acid). This indicates that calcium bearing clay and oxide mineral phases may have dissolved and reprecipitated with other components present in the solution, including phosphate and uranium. Calcium also undergoes ion exchange reactions once sodium (and potassium) contacts the sediments. It is the primary exchanger with sodium and potassium in the injected/infiltrated solution. The remedy depends on calcium being made available in solution via ion exchange, to complex with phosphate, leading to precipitation of amorphous monocalcium phosphate that slowly over several weeks recrystallizes to dicalcium to octacalcium phosphate and eventually forms hydroxyapatite over a period of months to years (PNNL-21733; Sumner, 2000, "Soil Fertility and Plant Nutrition"). The average ion exchange capacity of sediments is reported to be 1.2 to 2 meq/100 g, with 77 percent of ion exchange sites occupied with Ca^{2+}, and the total calcium available is 0.9 to 1.5 mmol/100 g (PNNL-18303, *Sequestration of Sr-90 Subsurface Contamination in the Hanford 100-N Area by Surface Infiltration of a Ca-Citrate-Phosphate Solution*). It is expected that some fraction of this calcium would exchange in the high Na-bearing phosphate solutions.

A separate study reported that 300 Area North Process Pond sediments contain 49 mg/L of water extractable calcium (PNNL-14022). Experiments conducted on these sediments (Wellman et al., 2007, "Efficacy of soluble sodium tripolyphosphate amendments for the in-situ immobilisation of uranium") indicate that aqueous phosphate in the mobile phase tends to increase the dissolution rate of calcite. The reaction of phosphate with calcite involves surface adsorption followed by dissolution of calcite to facilitate precipitation of the more thermodynamically favored calcium-phosphate solid phases. About 30 percent of the uranium was found to be associated initially with carbonate solids within these sediments and, therefore, would undergo some type of mobilization due to dissolution followed by reprecipitation. Brown, 1980, "Calcium Phosphate Precipitation in Aqueous Calcitic Limestone Suspensions," illustrated rapid sorption of phosphorus on calcareous sediments followed by rapid precipitation of hydroxyapatite under pH conditions similar to the ones existing for Stage A treatment.

Results from the sequential extraction of calcium indicate that calcium has been mobilized in the solution as a result of both dissolution of the carbonate bearing mineral phases (primarily calcite) and ion exchange reactions with sodium and potassium ions. The available calcium in solution then reacted with phosphate and carbonate in the pore water (along with available uranium complexes) and formed amorphous precipitates.

Note: Collocated boreholes are shown using the same color scheme.

Figure 6-19. Results from Sequential Extraction of Calcium Performed on Pretreatment Boreholes (Left) and Post-Treatment Boreholes (Right)

Figure 6-20 shows the comparison for iron between pretreatment and post-treatment samples. Iron concentrations in the post-treatment sediment samples show a significant decrease in the nitric acid extractable fraction and a significant increase in the strong acetic acid extractable fraction. This reflects that iron initially associated with crystalline oxides and clay minerals has been dissolved and reprecipitated with carbonates. This is consistent with the changes observed for uranium and calcium. Sequential extraction results presented for aluminum (Figure 6-21) and manganese (Figure 6-22) show behavior similar to that observed for iron, indicating that crystalline oxides and clay mineral phases containing Fe, Mn, and Al have undergone dissolution and have reprecipitated with predominantly calcium phosphate and calcium carbonate bearing mineral phases. Uranium is also associated with these mineral phases either as part of the mineral phase (by incorporation) or by surface adsorption (forming both weak and strong surface complexes).

In the strong acetic acid extraction step, the iron concentration of the post-treatment samples is the highest among the elements analyzed. This indicates that iron played an important role in the reactions that occurred from injecting/infiltrating phosphate solutions at high concentrations. Almost half of the total iron in the pretreatment sample (C8936) has been dissolved away, based on results from collocated post-treatment borehole (C9582) sample, with an appreciable amount now co-precipitated with calcium carbonates and calcium phosphate (and some silicates). Surface complexation of phosphate ions with iron oxyhydroxide mineral phases (such as ferrihydrite and goethite) is an important process that occurs due to excess availability of orthophosphate that exceeds the buffering capacity of sediments.

The addition of concentrated sodium-potassium bearing phosphate solutions to the subsurface leads to release of Ca^{2+} from cation-exchange reactions with the sediment and dissolution of calcite. Based on the pH of the system, the predominant aqueous phosphate species in solution is either dihydrogen phosphate ($H_2PO_4^-$) or hydrogen phosphate (HPO_4^{2-}); both species are present in equal amounts around pH of 7.2 (Figure 6-23, part a), which is the second dissociation constant of phosphoric acid. If pH reduces from 7.2, then dihydrogen phosphate ($H_2PO_4^-$) becomes dominant; if it increases, then hydrogen phosphate (HPO_4^{2-}) would become the dominant species. As more Ca^{2+} becomes available in the solution, the aqueous complexation with phosphate species will likely lead to $CaHPO_4$ for the range of chemical conditions that are relevant to the subsurface at the 300 Area. The aqueous complex stability field is shown in part b of Figure 6-23.

With continued addition of phosphate and reaction with Ca^{2+}, the aqueous concentrations would increase, leading to precipitation of amorphous calcium phosphate that thermodynamically favors formation of mineral phases, such as hydroxyapatite and whitlockite, as conceptualized below. In this process, hydrogen ions, which could get consumed in the surface complexation reactions between existing iron oxyhydroxide minerals (e.g., present as surface coatings) and monohydrogen and dihydrogen phosphate anions, are released.

Reaction from Injection/Infiltration	$5\ Ca^{2+} + 3\ HPO_4^{2-} + H_2O \rightarrow Ca_5(PO_4)_3OH + 4\ H^+$ *(Hydroxyapatite)*
	$3\ Ca^{2+} + 2\ HPO_4^{2-} \rightarrow Ca_3(PO_4)_2 + 2\ H^+$ *(Whitlockite)*
Resulting Surface Complexes	$\equiv FeOH + H_2PO_4^- + H^+ \leftrightarrow \equiv FeH_2PO_4 + H_2O$
	$\equiv FeOH + HPO_4^{2-} + H^+ \leftrightarrow \equiv FeHPO_4^- + H_2O$
Aqueous Speciation	$HPO_4^{2-} + H^+ \leftrightarrow H_2PO_4^-$

Note: Collocated boreholes are shown using the same color scheme.

Figure 6-20. Results from Sequential Extraction of Iron Performed on Pretreatment Boreholes (Left) and Post-Treatment Boreholes (Right)

Notes: Weak acetic acid extractions for pretreatment samples from boreholes C8940 and C9451 were not conducted. Collocated boreholes are shown using the same color scheme.

Figure 6-21. Results from Sequential Extraction of Aluminum Performed on Pretreatment Boreholes (Left) and Post-Treatment Boreholes (Right)

Note: Collocated boreholes are shown using the same color scheme.

Figure 6-22. Results from Sequential Extraction of Manganese Performed on Pretreatment Boreholes (Left) and Post-Treatment Boreholes (Right)

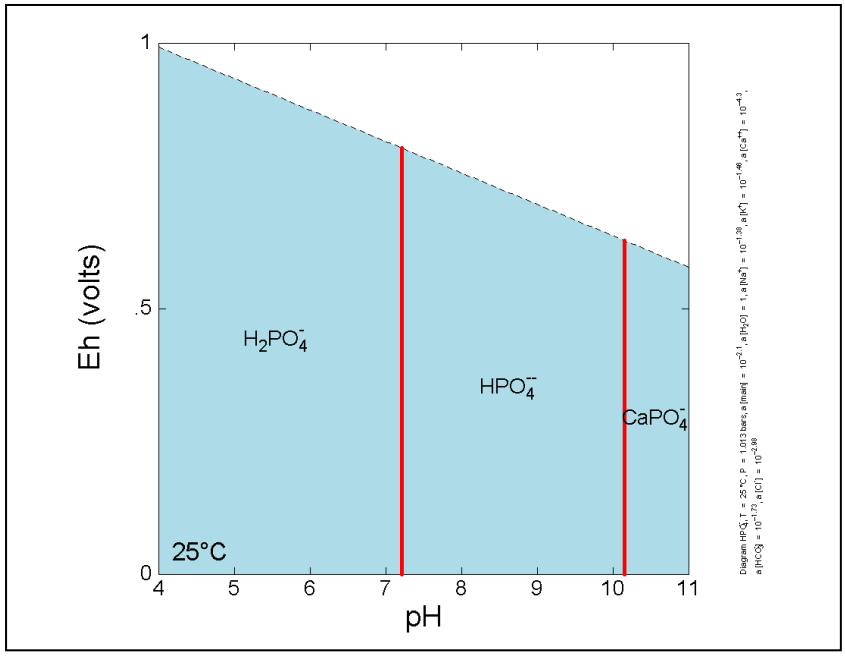

(a)

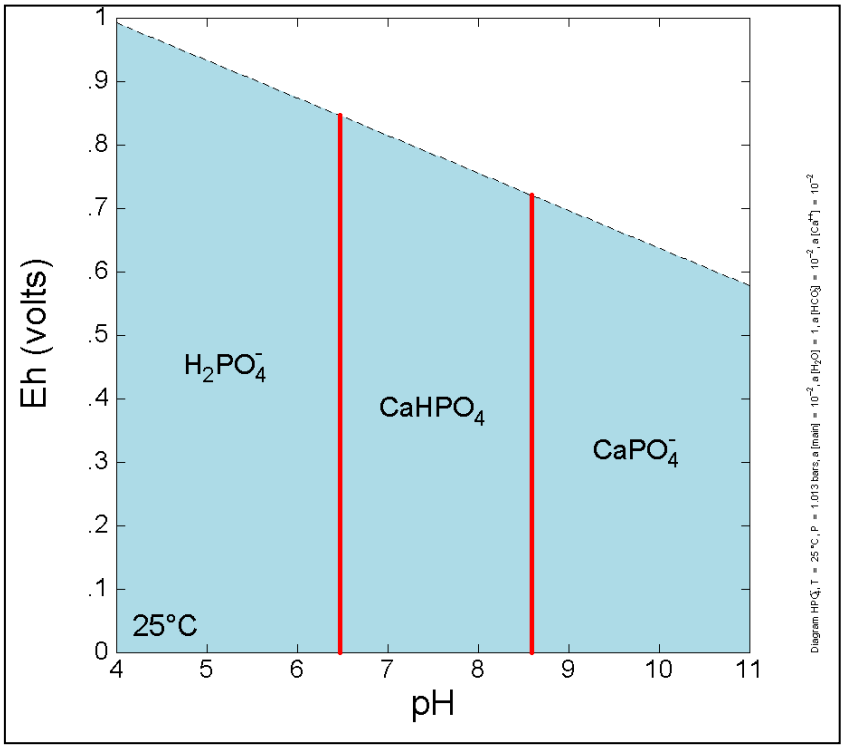

(b)

Note: Figure is based on activity of HPO_4^{2-}, HCO_3^-, and Ca^{2+} set at 10^{-2} in the solution.

Figure 6-23. Eh-pH Diagram Presenting the Orthophosphate Aqueous Complex Stability Field for (a) Infiltrated Water Composition and (b) Hypothetical Water Where Orthophosphate, Bicarbonate, and Calcium Concentrations Are Approximately Equal

With continued supply of phosphate and reactions leading to formation of calcium phosphate bearing mineral phases, the supply of hydrogen ions released to the solution could exceed the buffering capacity in the pore volume, leading to reduction in pH. The degree of pH reduction will be dependent upon the amount of reactive carbonate minerals (primarily calcite); clay minerals; oxides of Fe, Mn, and Al; and uranium bearing minerals. Small reductions in pH (even by half a pH unit) can lead to large changes in the activity of total dissolved iron and, therefore, favor dissolution of iron containing mineral phases, such as present in clay minerals (e.g., chlorite group) and hydrous ferric oxide bearing cement coatings around the grains. The chlorite group of phyllosilicate (clay) minerals contains Fe, Mg, Al, Mn, which would be released into the solution upon partial or complete dissolution of clay minerals. The released Fe (along with other metal ions such as Al and Mn) could get mobilized and react with dissolved species in the solution (predominantly Ca^{2+}, Na^{+}, $H_2PO_4^{-}$, HPO_4^{2-}, and HCO_3^{-}) leading to co-precipitation. These and related reactions are conceptualized in Figure 6-24 as phosphate bearing solutions infiltrate through the vadose zone.

The aqueous complexes formed by uranium will depend on the ratio of HPO_4^{2-}/HCO_3^{-} in the solution and pH. The stability field for such uranium complexes is presented in Figure 6-25. As long as the activity ratio of HPO_4^{2-}/HCO_3^{-} remains greater than 10^{-5} and pH is below 8, the primary aqueous complexes formed will be $UO_2(H_2PO_4)_2$ (a neutral species). Under these conditions, formation of uranyl orthophosphate mineral phase, $(UO_2)_3(PO_4)_2(H_2O)_4$, is favored assuming no other reactants are in the solution. Mehta et al. (2016) determined that when dissolved uranium, calcium, and phosphate are present together, uranium is structurally incorporated into a newly formed amorphous calcium phosphate solid. But when uranium is contacted with preformed amorphous calcium phosphate solids adsorption is the dominant removal mechanism for uranium. Both mechanisms are likely during Stage A treatment.

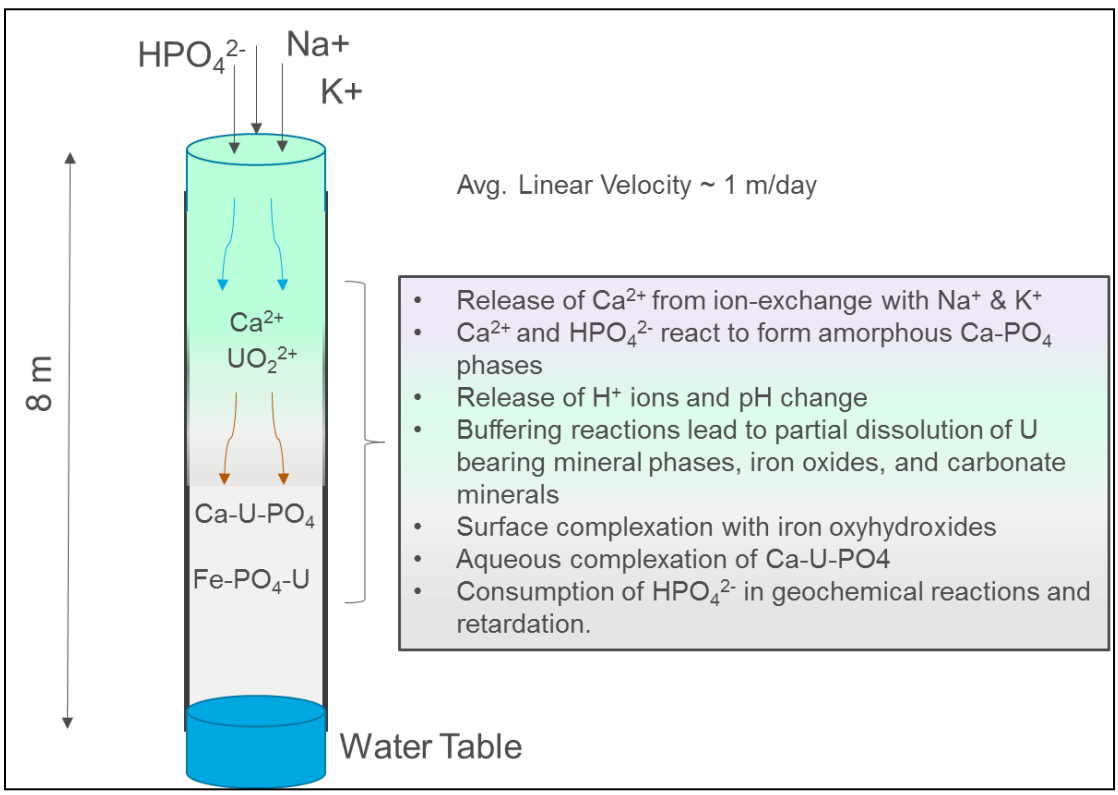

Figure 6-24. Conceptual Model of Probable Reactions Occurring in the Subsurface from Infiltration of Phosphate Bearing Solutions

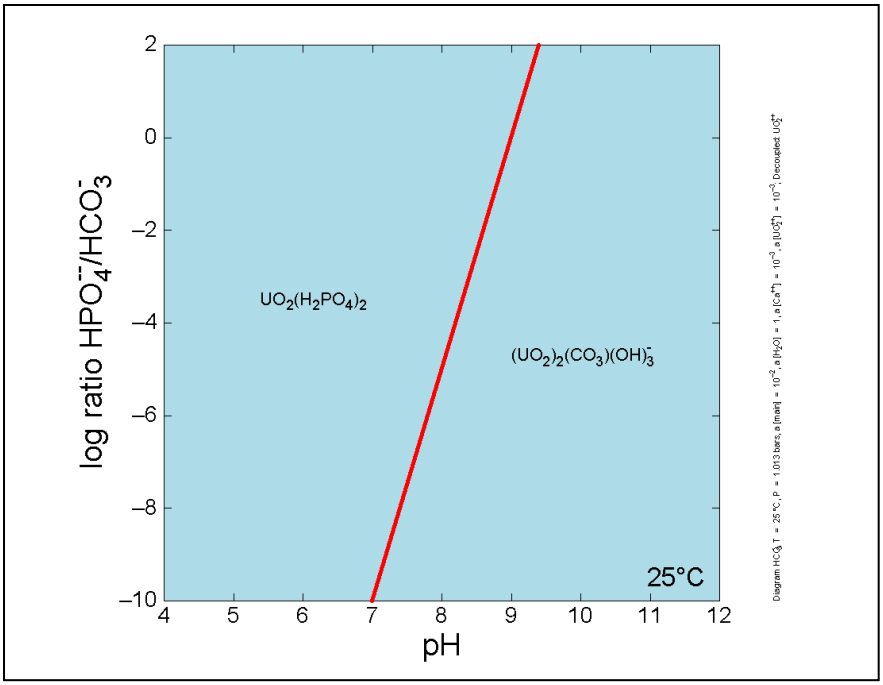

Figure 6-25. Stability Field of Uranium Aqueous Complexes Under Varying Orthophosphate to Bicarbonate Ratio and pH

6.3.2 Flow-Through Column Leaching Tests

Flow-through column leach experiments were conducted on three intact (field-textured) samples and four repacked columns containing <2 mm size material from post-treatment boreholes. The sampling depth intervals selected on post-treatment boreholes is shown in Table 6-4. These depth intervals were selected, based on the uranium soil distribution and depth of the pretreatment samples.

The column experiments were performed using 15.2 cm (6 in.) long and 2.5 cm (1 in.) diameter glass columns. The influent water was a synthetic groundwater that is based on the groundwater composition at the 300 Area (average of 42 wells [Ma et al., 2010, "A field-scale reactive transport model for U(VI) migration influenced by coupled multirate mass transfer and surface complexation reactions"]). The synthetic groundwater is a calcium-bicarbonate type water that is adjusted to pH of 7.3 and does not include phosphate, as documented in PNNL-25420.

The flow rate through the columns containing <2 mm size sediments was maintained at approximately 0.1 cm^3/min or 0.25 pore volumes per hour, yielding pore water velocities of about 70 to 90 cm/day. For the columns containing field-textured sediment, the flow rate was approximately 1.5 cm^3/min or 0.25 pore volumes per hour yielding pore water velocities of about 110 cm to 180 cm/day. The column experiments were run for approximately 10 pore volumes, with two stop flow events: one approximately after 4 pore volumes for about 48 hours, and one at approximately 7 pore volumes for about 72 hours. At the end of the tests, sodium bromide was injected to evaluate the breakthrough times for a conservative tracer. Additional details are provided in PNNL-25420.

Table 6-4. Flow-Through Column Test Parameters for Post-Treatment Samples

Borehole	HEIS Sample ID	Sample/Depth Interval (ft)	Preparation	Bulk Density (g/cm^3)	Porosity	Average Flow Rate (cm^3/min)	Average Pore Water Velocity (cm/day)[a]	Total Pore Volumes[b]
C9580	B347F1 F347F3	I-004 / 29.0-29.5 I-004 / 29.5-30.0	<2-mm composite	1.66	0.37	0.092	72.2	9.1
C9582	B347P4	I-002 / 23.5-24.0	Field texture	2.05	0.23	1.2	110	16.9
	B347P5 B347P8	I-002 / 23.0-23.5 I-002 / 23.5-24.0	<2-mm composite	1.72	0.35	0.092	77.1	10.7
	B347R0	I-003 / 26.0-26.5	Field texture	2.18	0.18	1.2	141	12.5
	B347R1	I-003 / 25.5-26.0	<2 mm	1.79	0.32	0.095	85.7	12.4
	B347T6	I-006 / 33.5-34.0	Field texture	2.26	0.15	1.2	167	16.2
	B347T7	I-006 / 33.0-33.5	<2 mm	1.78	0.33	0.093	83.7	11.9

(a) Average linear velocity
(b) Prior to bromide elution

HEIS = Hanford Environmental Information System

Uranium concentrations in the effluent as a function of pore volumes flushed are presented for the field-textured (intact) samples in Figure 6-26 and for the <2 mm size sediment samples in Figure 6-27. For the field-textured and <2 mm size sediments taken from adjacent depths same color scheme is used in the two figures for direct comparison. There is one extra sample analyzed for the <2 mm size sediment (from borehole C9580); all of the rest of the samples are taken from borehole C9582.

Results for field-textured sediments (Figure 6-26) show high initial uranium concentrations for two samples (B347P4/P5 and B347R0) of about 3,000 to 4,000 µg/L. The concentrations decline within the first two pore volumes, following which the rate of decline is slower. The intermittent increase in concentrations and gradual decline results from resumption of flow following the stop-flow event. Concentrations remain above 200 µg/L throughout the experiment duration for these two samples, indicating that uranium continues to leach out from dissolution of uranium bearing mineral phases. The leaching behavior of the third sample (B347T6), however, shows a remarkable difference, where the concentrations start low (< 30 µg/L) and remain low throughout the duration of the experiment (~10 µg/L). The total uranium soil concentration in all three samples is high (ranging from 33 to 102 µg/g), and the effluent concentrations are sustained, indicating that uranium mass has not been depleted. In fact, for the two samples that show high dissolved uranium concentrations, the total uranium soil concentration is different by a factor of two, which indicates that above a certain threshold soil concentration, there is enough uranium to sustain high concentrations in the effluent. The third sample that shows low dissolved uranium concentration seems to be affected by the phosphate concentrations. This sample is located at depth (10.2 to 10.4 m [33.5 to 34 ft]) and is, therefore, most likely impacted by injection in the PRZ. Figure 6-17 shows higher concentrations of phosphate distribution for borehole C9582 at depth, and it may have sequestered uranium through formation of calcium-uranium-phosphate bearing amorphous or mineral phases. Since all three post-treatment boreholes show similar high phosphate concentrations at depth (Figure 6-17), similar leaching behavior of uranium is expected in all three locations as indicated by B347T6. The higher uranium concentrations observed in the leaching tests for the other two samples indicate that perhaps at these depths (7 to 8 m [23.5 to 26.5 ft] bgs) high concentration of phosphate could not be delivered, since these depths are above the PRZ screened interval and are deep enough for the infiltrated solutions to deliver high concentrations of phosphate. It is possible that most of the phosphate reacted above, within the 4 to 6 m (13.1 to 19.7 ft) depth range during infiltration. The ERT image shown in Figure 6-10 indicates that 0.0004 S/m contour (and higher values) are restricted to a depth of 6 m (19.7 ft), indicating that high concentration phosphate bearing solutions are present at shallow depths.

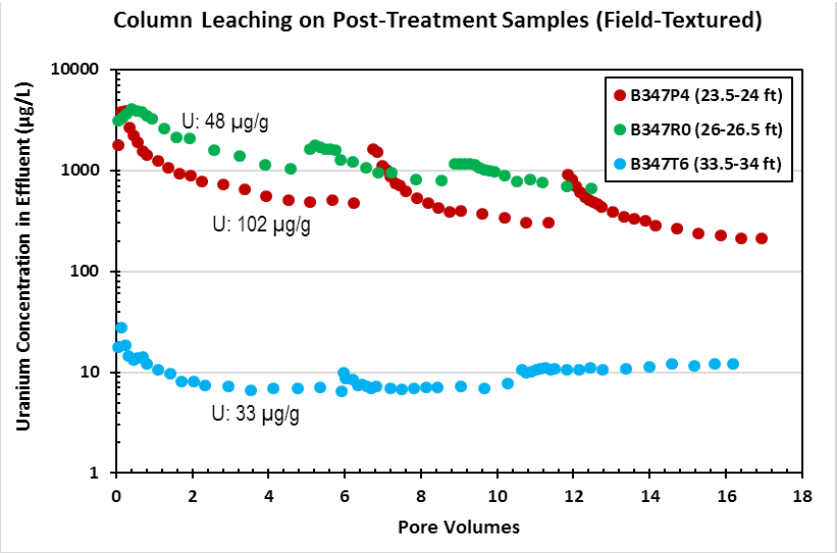

Note: Total uranium soil concentrations based on sequential leach tests are shown next to the column test results.

Figure 6-26. Results of Effluent Uranium Concentrations from Column Leach Tests Performed on Field-Textured Sediments from Post-Treatment Samples

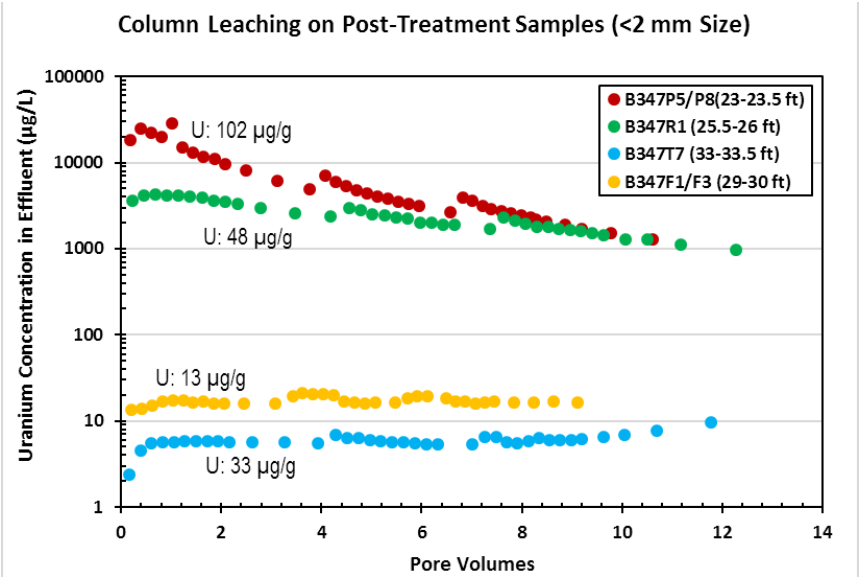

Note: Total uranium soil concentrations based on sequential leach tests are shown next to the column test results.

Figure 6-27. Results of Effluent Uranium Concentrations from Column Leach Tests Performed on <2 mm Size Sediments from Post-Treatment Samples

Figure 6-27 compares the results for the <2 mm size sediment samples. High effluent uranium concentrations from two samples (B347P5/P8 and B347R1) correspond to the two samples from field-textured samples. The concentrations from the other two samples are much lower. Sample B347T7 shows leaching behavior that is similar to the paired field-textured sample (B347T6) from deeper depths corresponding to the PRZ. Effluent concentrations remain at or below 10 µg/L, indicating that phosphate

bearing mineral phases have sequestered uranium as per the remedy. Results from sample B347F1 (from borehole C9580), which is also from deeper depth that is representative of the PRZ, also show lower sustained concentrations where high phosphate concentrations are observed (Figure 6-17 for borehole C9580). Both deep samples where observed phosphate concentrations appear to be higher than background show lower leachable concentrations of uranium that are orders of magnitude smaller than other samples.

Results from flow-through column leach tests performed on pretreatment borehole samples are compared to the post-treatment borehole samples for the collocated boreholes. The pretreatment samples were collected from borehole C8936 (399-1-67), and column tests were performed on two samples from the lower vadose zone. Results of the column tests are discussed in SGW-58830. Tests were performed on both field-textured and <2 mm size sediments, but only results from field-textured samples are discussed here because the <2 mm size sediments showed similar results. The pretreatment field-textured sample B30541 was collected from a depth of 8.4 to 8.6 m (27.7-28.2 ft), while B30543 was collected from 8.9 to 9.1 m (29.2 to 29.7 ft). This pretreatment borehole (C8936 [399-1-67]) is collocated with borehole C9582. Flow-through column test results are compared in Figure 6-28, with the open circles indicating results from the two pretreatment samples. The flow-through column leaching behavior of pretreatment samples is similar to the leaching behavior observed for the two post-treatment samples that are located above the PRZ. In the pretreatment samples, initial high concentrations (>1,000 and >500 µg/L) of uranium are observed that decline over the first few pore volumes; however, after about five pore volumes, concentrations do not appear to vary much until after the stop flow events and remain high (above 100 µg/L). These results indicate that the leaching behavior of post-treatment samples located above the PRZ (but below 6 m [19.7 ft] depth) is similar to pretreatment samples. Perhaps the high phosphate concentrations from infiltration were not available to sequester the uranium at deeper depths because most of the phosphate may have reacted in the upper vadose zone. As discussed earlier, leaching characteristics of the samples collected from the PRZ show much lower leachability, indicating the effects of sequestration from phosphate injections.

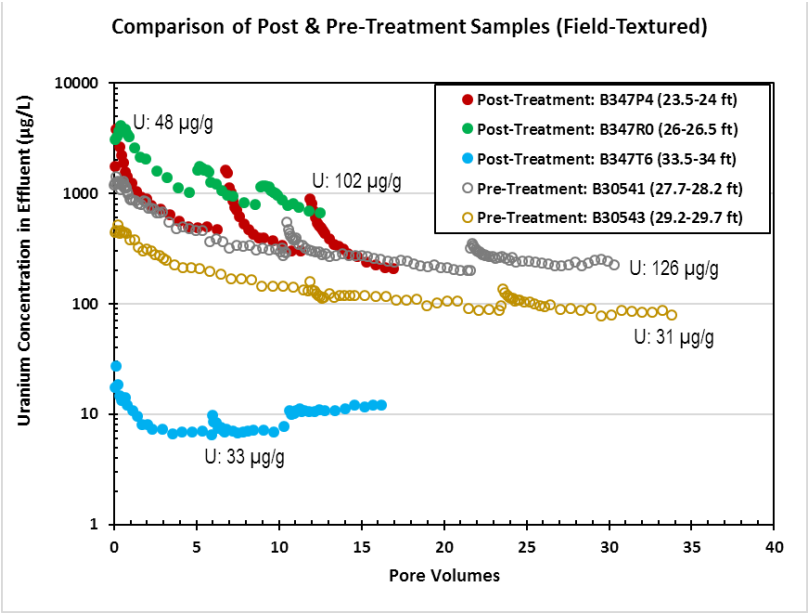

Note: Total uranium soil concentrations based on sequential leach tests are shown next to the column test results.

Figure 6-28. Comparison of Effluent Uranium Concentrations Column Leach Tests Performed on Field-Textured Samples from Post-Treatment and Pretreatment Boreholes

6.3.3 Labile Uranium Batch Test

Aliquots of the air-dried <2-mm size fraction from the nine selected sample intervals were subjected to labile uranium leach testing (PNNL-25420). The labile uranium leach test measures the readily leachable uranium to estimate the relative proportion of total uranium that is leachable when contacted with sodium carbonate-bicarbonate solution. In this approach (Kohler et al., 2004, "Methods for Estimating Adsorbed Uranium(VI) and Distribution Coefficients of Contaminated Sediments"), a solution containing 0.0144 mol/L of sodium bicarbonate (NaHCO3) and 0.0028 mol/L of sodium carbonate (Na_2CO_3) with a pH of approximately 9.45 was added to the sediment at a solid-to solution ratio of 1 g/2 mL and was allowed to agitate on an orbital shaker for 1,000 hours (~42 days).

Results of the labile uranium testing are presented in Figure 6-29 for five different times. The results indicate that even after 66 days, the equilibrium had not been attained, and the uranium concentrations continued to increase. These results further indicate that uranium-containing carbonates are present in sufficient amount and continue to dissolve. This type of nonequilibrium, kinetically controlled leaching in contact with a bicarbonate water solution could be expected to continue under field conditions.

The amount of uranium leached is low for three samples taken at post-treatment borehole C9580, one sample taken at post-treatment borehole C9581, and two samples located at depth for the post-treatment borehole C9582 (B347R7 and B347T7). Based on vertical phosphate profiles shown in Figure 6-17, phosphate appears to have been delivered at high concentration at C9580. This is also supported by the high concentrations observed in the ERT survey resulting from faster migration rates of phosphate solution through the vadose zone (Figures 6-10 and 6-11). The sample taken at C9581 is from PRZ depth (8.5 to 8.7 m [28 to 28.5 ft]) where phosphate was delivered through PRZ injection. Based on these results, it is inferred that the labile uranium concentration remains relatively low in samples where phosphate concentration is observed to be above background due to possible reactions with calcium-phosphate.

6.3.4 Identification of Mineral Phases Using Surface Analysis

Selected samples from post-treatment boreholes were evaluated to identify uranium-bearing mineral phases and calcium phosphate precipitates using sequential application of surface analysis techniques, including cryogenic laser fluorescence spectroscopy, electron microprobe, and/or scanning electron microscope/energy dispersive x-ray (SEM/EDX) spectroscopy (PNNL-25420).

Analysis of samples from borehole C9580 with higher uranium concentrations indicated that U(VI) (uranium in hexavalent state) is adsorbed on quartz, and U(VI)-phosphate surface complexes are adsorbed on montmorillonite. Because quartz is the dominant mineral phase in Hanford vadose zone sediments and phyllosilicates often exist as fine surface coatings on soil and mineral grains, surface uranium complexes adsorbed to the mineral hosts are expected.

Analysis of fluorescence spectra from C9582 samples that were located above the PRZ (but deeper than 6 m [19.7 ft]), where soil uranium concentrations were found to be the highest but where appreciable phosphate was not observed, indicated the presence of uranyl-tricarbonate and noticeable levels of calcium carbonate minerals with adsorbed U(VI). None of the samples analyzed showed characteristic features of crystalline uranyl-phosphate precipitates. This was somewhat expected as amorphous monocalcium phosphate phases are predicted to form primarily with uranium incorporated in the solids instead of crystalline uranyl-phosphate under the prevailing chemical conditions (Mehta et al., 2016). Furthermore, uranium is nonuniformly dispersed in the sediment and present at concentrations below the detection limits of instrument. The EDX detection limit is > 500 ppm, which is greater than uranium concentration in all samples analyzed.

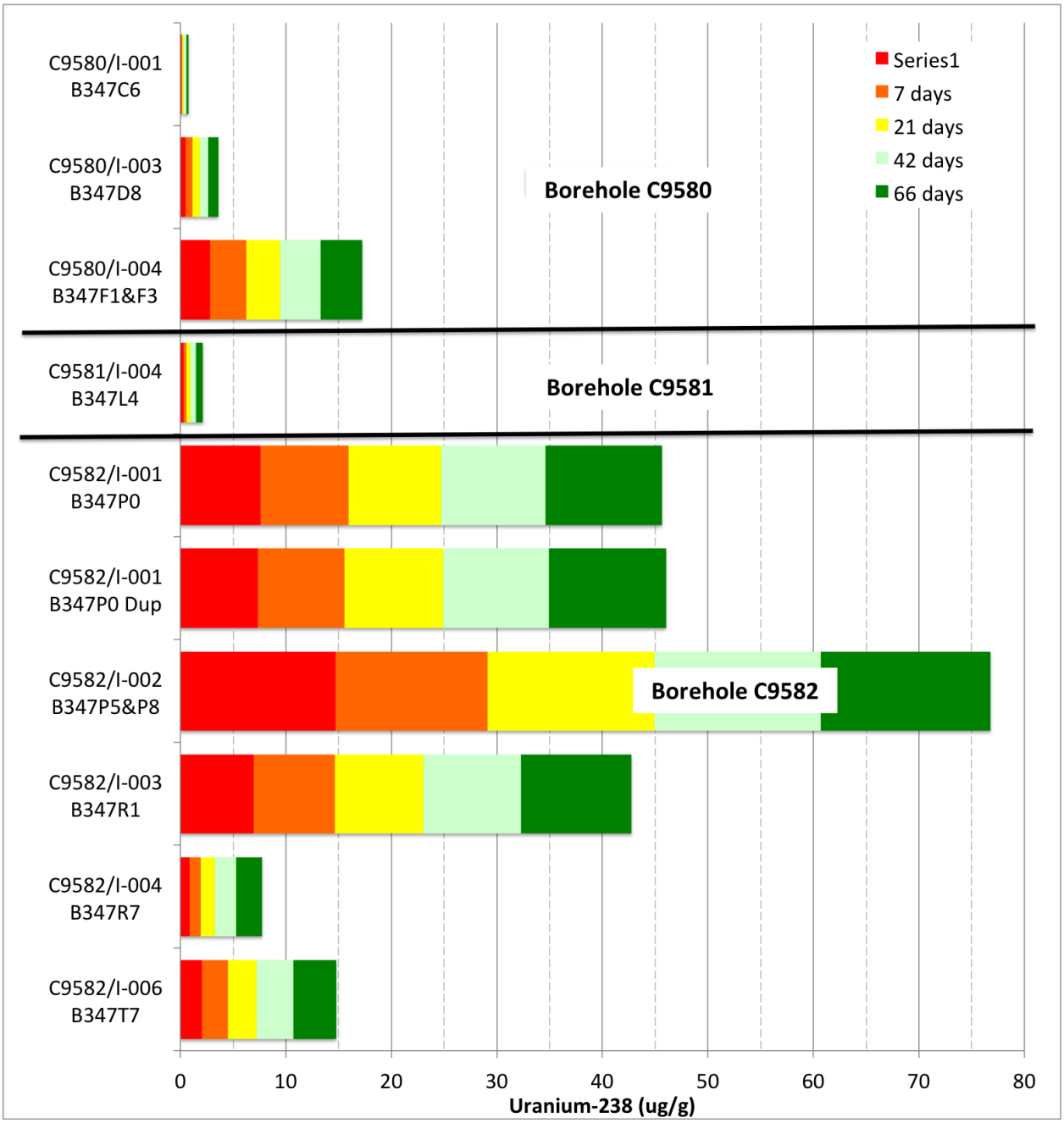

Figure 6-29. Composite Uranium Concentrations Recovered During Labile Leach Testing

Results from SEM/EDX spectroscopy and electron microprobe analysis of C9580 samples indicate that calcium and phosphorus are distributed uniformly, while iron is variably distributed. For the C9582 borehole sample (B347R7) collected in the PRZ at a depth of 9 to 9.1 m (29.5 to 30 ft), results indicate the presence of calcium, phosphorus, iron, and manganese (Figure 6-30). Results of the surface elemental analysis indicated about 18 percent of phosphorus and 23 percent of calcium by weight. The total uranium concentration in this sample was 31 µg/g.

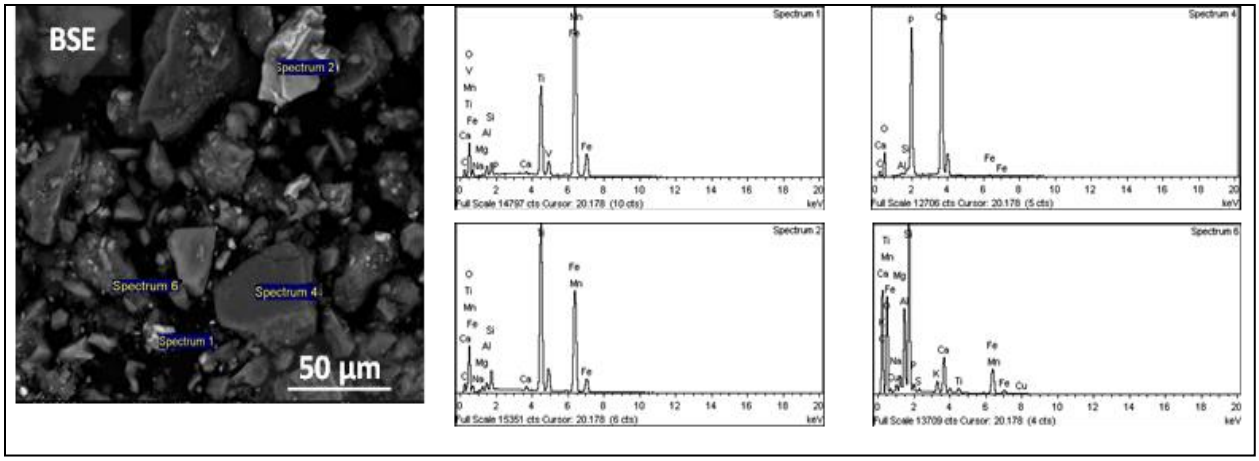

EDS for Sample B347R7 the spectrum 4

Element	Weight%	Atomic%
C	15.41	24.94
O	43.05	52.30
Al	0.22	0.16
Si	0.31	0.22
P	17.71	11.12
Ca	23.11	11.21
Fe	0.19	0.06

Figure 6-30. Spectral Analysis and Elemental Mapping Results of B347R7 Sample Collected from Borehole C9582 at Depth of 9 to 9.1 m (29.5 to 30 ft)

6.3.5 Observations of High Moisture Content

All post-treatment borehole samples appeared to be much wetter than pretreatment borehole samples. All sampled intervals in the vadose zone were visibly very wet, even though the sediments were mostly gravel dominated and easily drainable. Post-treatment drilling was conducted about 2 months after completion of injection/infiltration.

Wellman et al. (2007) reported a steady increase in moisture content during the unsaturated column experiments using sodium tripolyphosphate solutions and attributed it to change in water retention characteristics as a result of reactions with phosphorus. Lutz et al., 1966, “Effect of Phosphorus on Some Physical Properties of Soils: II. Water Retention,” studied the effect of adding phosphorus on physical properties of soils and concluded that phosphate bearing solutions increased the water holding properties of soils. They found it to be directly related to increase in the negative charge of the soil particles. This surface charge was closely related to the Al-phosphate to Fe-phosphate ratio. In some instances, even 50 parts per million of phosphorus concentrations in solution led to increased water holding capacity. They hypothesized that the negative charge of the particle might be increased by the phosphate ion replacing a hydroxyl ion on the octahedral layer of the clay crystal leading to increased negative charge that may attract polar water molecules.

6.4 Determination of Desorption Parameters Using Post-Treatment Flow-Through Column Leach Tests

Uranium sorption-desorption parameters are determined by matching the transport model based results with laboratory leaching test results conducted on post-treatment samples. A single-site kinetic sorption model is developed that evaluates the forward and reverse rates. A single-site sorption model is deemed adequate, based on the level of knowledge on uranium desorption characteristics from sediments following treatment with phosphate. The objective is to develop uranium desorption parameters that can be upscaled for usage in a 3D fate and transport model at the scale of the 300 Area.

Some of the column leaching characteristics and experimental setup details were presented in Section 3.2. Uranium leaching experiments were run with field-textured (intact bulk) sediment and with fine grain soil (<2 mm grain) for which the larger gravel was removed. Water is injected at the top of the column at a measured rate. During the time history of the experiment, effluent samples are collected from the end of the column, and the dissolved concentrations of uranium are measured. The experiments have two stop-flow events in order to demonstrate the impact of nonequilibrium sorption. The first stop flow event has a duration of 48 hours, while the second stop flow event has a duration of 72 hours.

Flow-through experiments also included injection of nonsorbing species (bromide). For the bromide experiments, the initial concentration within the column is zero, and the injection stream contains a known bromide concentration. The transport model without the sorption kinetics is used to match the nonsorbing bromide data, which provides a verification of the transport parameters.

Vadose zone soil samples representative of contamination during remediation activity were collected from multiple borehole locations within the 300 Area. The soil samples of interest for the experimental study (PNNL-25420) are shown in Table 6-5, which provides the borehole location, borehole interval and depth, sample preparation, column geometry, bulk density, water content, and injection rate.

Table 6-5. Selected Samples and Flow-Through Column Test Parameters

Borehole Identification	Sample Number	Sample Interval	Interval Depth (ft)	Sample Preparation	Length (cm)	Diameter (cm)	Bulk Density (gm/cm^3)	Water Content	Injection Rate (mL/hr)
C9580	B347F1F3	I-004	29.5 to 30	<2 mm size	15	2.5	1.66	0.372	5.53
C9582	B347P5P8	I-002	23.5 to 24	<2 mm size	15	2.5	1.72	0.380	5.54
	B347P4	I-002	23.5 to 24	Field-Textured	13.2	9.53	2.05	0.228	74.2
	B347R1	I-003	25.5 to 26	<2 mm size	15	2.5	1.79	0.338	5.69
	B347R0	I-003	26 to 26.5	Field-Textured	14.0	9.53	2.18	0.177	74.5
	B347T7	I-006	33 to 33.5	<2 mm size	15	2.5	1.78	0.347	5.61
	B347T6	I-006	33.5 to 34	Field-Textured	13.7	2.93	2.26	0.146	72.7

Boundary conditions matching the uranium leach column experimental conditions are applied. For each sample, estimates of the kinetic sorption reaction rates and partition coefficient are obtained by history matching the model results with the existing experimental data. The flow-through column initial uranium concentration is assigned to match the early time experimental results.

The mathematical model used for fitting the uranium leaching results is described in Appendix C. Results of the model fit are presented in Appendix C as estimated well and kinetic sorption-desorption parameter values. An alternative method for determining the kinetic sorption parameters is also discussed that assigns an estimated value of the reverse reaction rate for all samples. The estimated kinetic sorption-desorption parameters are used in the fate and transport modeling.

This page intentionally left blank.

7 Three-Dimensional Flow and Transport Modeling Using STOMP

The purpose of this chapter is to simulate the fate and transport of uranium in the vadose zone and unconfined groundwater aquifer to evaluate effectiveness of Stage A remedy. The modeling results will be used to predict possible changes in groundwater uranium concentrations in the near future.

This effort includes the simulation of uranium concentrations in the aquifer prior to the Stage A remedy along with a series of simulations, which will describe the impact of the remedial actions (phosphate injection and infiltration) on the uranium groundwater concentrations.

7.1 Background Information

The approach to the uranium fate and transport modeling within the 300-FF-5 OU uses a mathematical hydrogeological construct to represent the physical conditions within the vadose zone and unconfined aquifer. It also involves developing a conceptual model by incorporating some of the following important features, events, and processes that control the uranium transport:

- Seasonal fluctuations of flow in the Columbia River at the 300 Area can result in more than 3 m (9.8 ft) of change in river stage between the high discharge period (May to June) and the low discharge period (December to January) (Figure 7-1). These seasonal fluctuations are the driving mechanism for the rise and fall of the water table beneath the 300 Area for extended periods of time and for creating the dynamic hydraulic and geochemical environment found in the unconfined aquifer of the 300 Area. The seasonal fluctuations in river stage also lead to remobilization of the sorbed uranium mass from the lower part of the vadose zone as shown for 399-1-17A (Figure 7-1) due to rise in water table elevations.

- Seasonal river stage fluctuations lead to changes in the flow direction within the aquifer. Considerable variability in the flow direction also exists spatially as well within the same season. Changing flow directions can cause redistribution of uranium in the aquifer as well as in the PRZ above the water table.

- Effect of variably saturated conditions need to be considered in the modeling. The river stage fluctuations can temporally and spatially increase the water saturation and vary the chemical conditions that can lead to variable transport of uranium. Therefore, a coupled vadose zone and saturated-zone flow and transport need to be considered.

- The change in groundwater chemistry (i.e., alkalinity) within the unconfined aquifer due to mixing of groundwater with river water needs to be considered in the context of adsorption/desorption of uranium.

- Due to variable flow and chemical conditions, the sorption/desorption of uranium may be kinetically limited, and full equilibrium may not be established between dissolved and sorbed mass of uranium. The modeling will evaluate both equilibrium and nonequilibrium (kinetic) sorption.

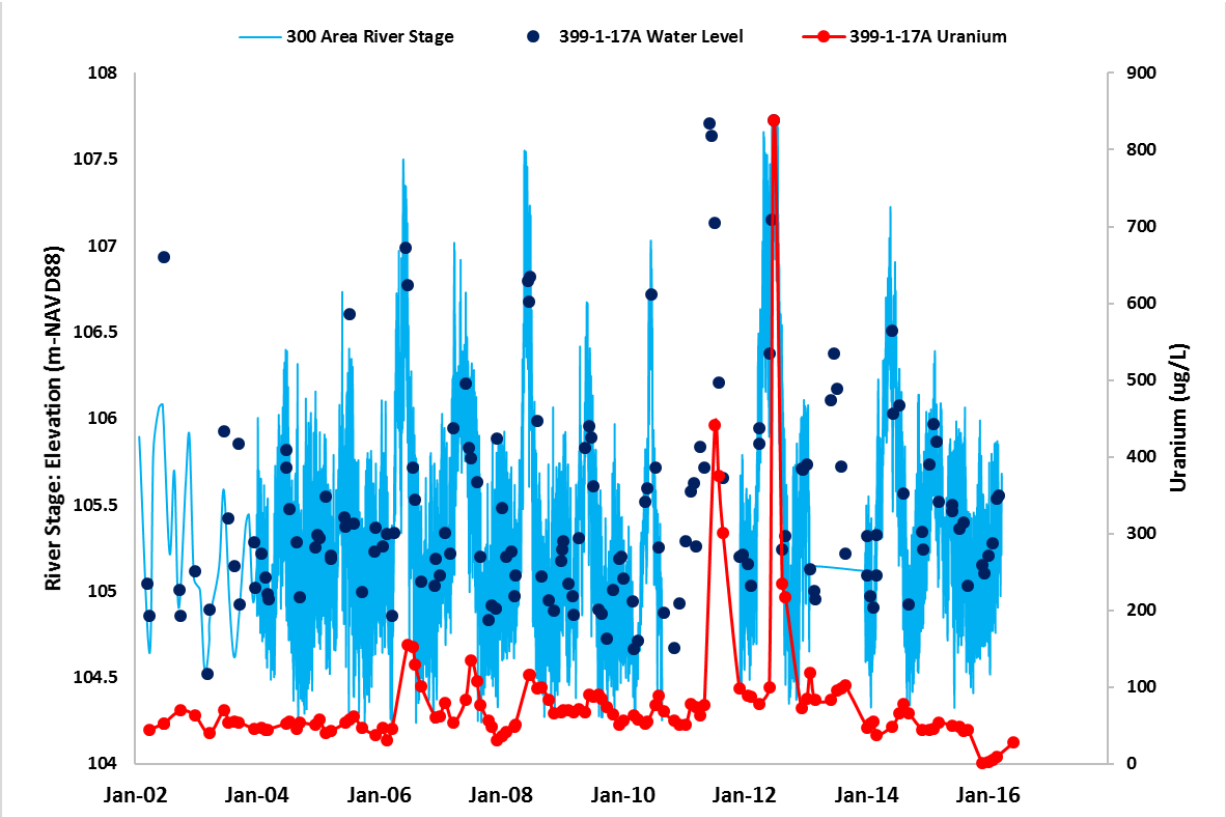

Figure 7-1. Columbia River Stage Fluctuations and Effect on Water Levels and Dissolved Uranium Concentration at Well 399-1-17A

7.2 Development of Hydrogeologic Model

Leapfrog® Geo software (version 3.0.0) was used to create a 3D solid hydrogeologic model within the 300 Area (Figure 7-2). The geologic framework beneath the 300 Area consists of a Hanford formation (Hf) vadose zone made up of unconsolidated sandy gravels containing spatially (horizontally and vertically) variable amounts of silts and clays and a saturated zone of the same material underlain by more consolidated materials of the Ringold formation unit E (ECF-300FF5-16-0087, *Determination of Vadose Zone Uranium Concentration Distribution Extents and Development of a Three-Dimensional Geologic Framework Model for the 300-FF-5 Operable Unit, Hanford, Washington*). Underlying Ringold unit E is the Ringold Lower Mud (RLM) unit consisting of predominantly silts and clays, and underlying the RLM is the Columbia River Basalt Group bedrock. A generalized hydrostratigraphic column for the 300 Area is presented in Figure 7-3.

® Leapfrog is a registered trademark of ARANZ Geo Limited, Christchurch, New Zealand.

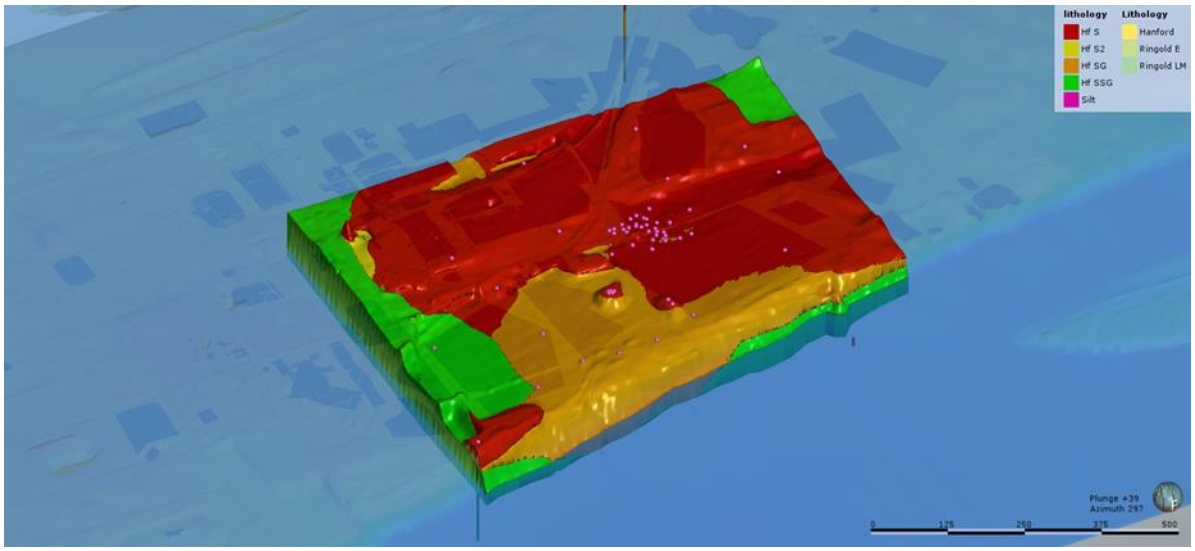

Note: Geologic units: red = Hf sand unit 1, orange = Hf sandy gravel, yellow = Hf sand unit 2, and green = Hf silty sandy gravel. Pink dots represent detailed vadose zone model well locations. Blue semitransparent shading represents the water table surface.

Figure 7-2. View of the 300 Area Geologic Framework Model

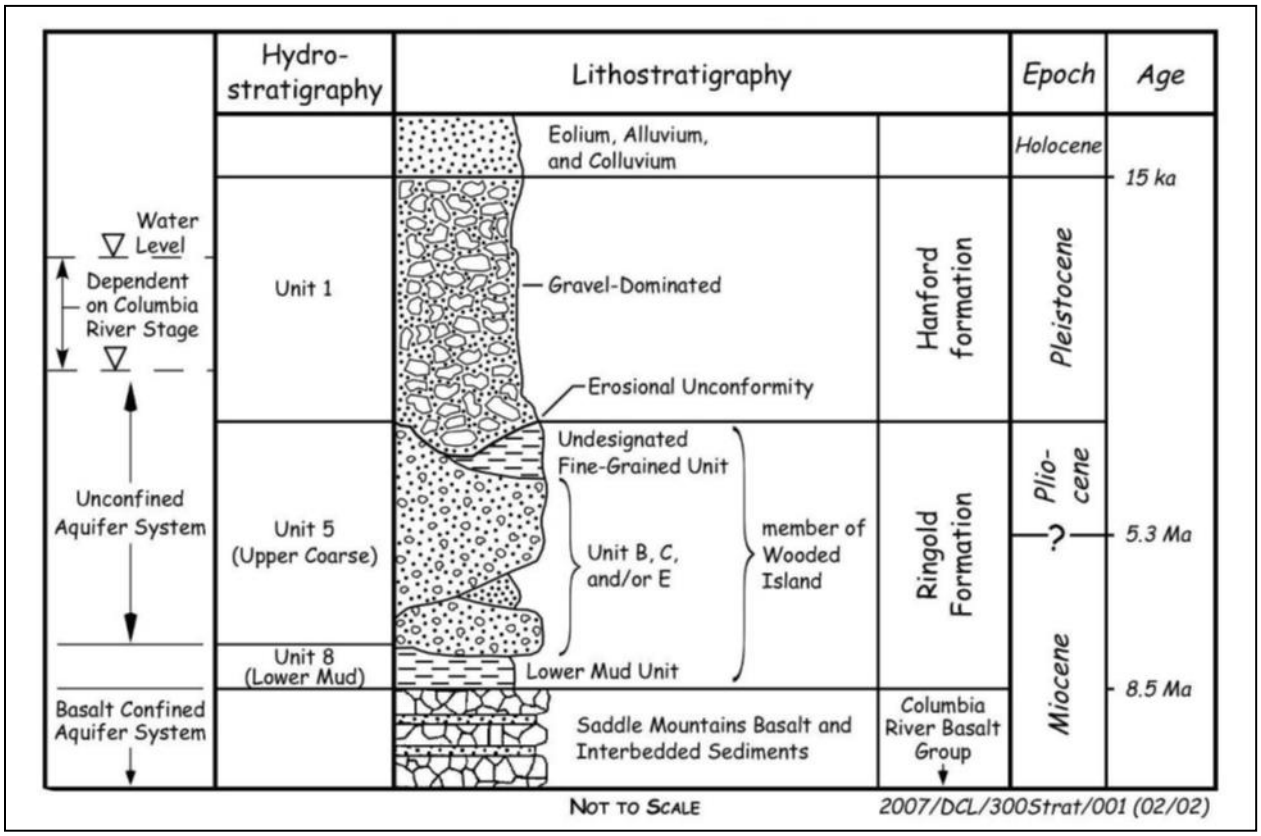

Note: Figure is from DOE/RL-2009-30, *300 Area Decision Unit Remedial Investigation/Feasibility Study Work Plan for the 300-FF-1, 300-FF-2, and 300-FF-5 Operable Units* (Figure 2-17).

Figure 7-3. Generalized Hydrostratigraphy at the 300 Area

The primary geologic unit of concern is the Hf because of the location of uranium contamination within the deep vadose and PRZ. In the existing Hanford South geologic framework model (GFM; ECF-HANFORD-13-0029, *Development of the Hanford South Geologic Framework Model, Hanford Site, Washington*), the Hf is undifferentiated. Because the vertical and lateral distribution of fine materials in the vadose zone could affect the uranium contamination plume extents, it was necessary to construct a GFM specific to the 300 Area complete with detailed, differentiated Hf subunits. The subunits were defined by interpreting borehole geologic and geophysical logs obtained by accessing the Hanford Site Well Information and Document Lookup and from CHPRC for newly drilled boreholes as part of the Stage A EAA (ECF-300FF5-15-0014, *Determination of Vadose Zone Uranium Concentration Distribution Extents and Establishment of the Stage A Enhanced Attenuation Area for 300-FF-5*). The following specific Hf geologic subunits comprise the upper portion of the 300 Area GFM:

- Hf is categorized into five sub-units from land surface downward based on the observed sequence of deposition in the study area:
  - Hf sand unit 1 – fine to coarse sand of mixed basaltic and felsic composition
  - Hf sandy gravel – unconsolidated mostly pebble to cobble gravels with sand
  - Hf sand unit 2 – unconsolidated, fine to coarse sand (mostly basalt) with some silt
  - Hf Silt – 100 percent silt unit identified in several wells drilled as part of the Stage A EAA uranium sequestration by polyphosphate remedy
  - Hf silty sandy gravel – unconsolidated mostly basalt pebble to cobble gravel with silt and sand
  - Hf gravel – unconsolidated predominantly basaltic pebble to cobble gravel with some sand and/or silt

The Hf subunits listed were interpreted, based on the following criteria:

- Hf Sand unit 1 – ≥90 percent sand of mostly basaltic composition
- Hf Sandy Gravel – between 50 percent and 60 percent gravel with sand fraction ranging 50 percent to 40 percent. Gravels are predominantly basaltic
- Hf Sand Unit 2 – 80 percent to 90 percent sand with silt, sand, or gravel fraction ranging from 20 percent to 10 percent
- Hf Silt – 100 percent silt described in borehole geologic logs as being moderately plastic and grayish-brown in color
- Hf Silty Sandy Gravel – 50 percent to 70 percent gravels to cobbles, 20 percent to 10 percent sands, and 20 percent to 10 percent silt (gravel to cobble fraction is mostly basaltic; sand is moderately to poorly sorted)
- Hf Gravel – 85 percent to 90 percent gravels with 15 percent to 10 percent sand and/or silt fractions (gravels are at least 50 percent basaltic)

The lower portion of the 300 Area GFM was constructed using interpolated unit-top surfaces for Ringold unit E and RLM. The surfaces were extracted from the Hanford south GFM (ECF-HANFORD-13-0029).

The information gained from the described GFM efforts and Stage A EAA drilling and sampling activities laid the backdrop for the EAA determination. Previous geological and characterization studies

were instrumental in providing information used in the geologic and uranium contamination distribution modeling discussed herein.

7.3 Development of 3D STOMP Model Domain

The 3D STOMP model domain has been selected in a way that adequately covers the Stage A EAA, and it has some monitoring wells close to the boundary. Figure 7-4 shows the model domain location in the 300 Area.

The total dimension of the model domain is 600 m (1,968 ft) in the X direction (east-west) and 600 m (1,968 ft) in the Y direction (north-south). Vertically (Z direction), the model extends from ground surface to Ringold unit E. The vertical grid spacing was chosen to be 0.5 m (1.6 ft). Figure 7-5 shows the vertical discretization and the distribution of hydrogeologic units along the model cross-section. In the X and Y directions, grid spacing varies from 50 m to 6.25 m (164 to 20.5 ft). A finer grid spacing of 6.25 m (20.5 ft) was assigned in the EAA. The model has the following hydrogeologic zonations split between unsaturated (or variably saturated) and saturated zones:

<u>Unsaturated Zone</u>

- Hf silty sandy gravel (Hf SSG)
- Hf sand (Hf S; sand units 1 and 2 given the same hydraulic property)
- Hf sandy gravel (Hf SG)
- Hf gravel (Hf G)
- Hf silt (S)

<u>Saturated Zone</u>

- Saturated Ringold unit E
- Saturated Hf
- Saturated Hanford 2 zone (a higher hydraulic conductivity zone)
- Saturated Hanford 3 zone (a lower hydraulic conductivity zone)
- Saturated silt
- River alluvium

7.4 Development of Flow Model

Development of the flow model involved deriving and applying appropriate flow boundary conditions and calibrating the hydraulic properties to match the field observations. The model grid is presented in Figure 7-6.

7.4.1 Recharge

The aerially applied recharge rate was based on the analysis (PNL-10285, *Estimated Recharge Rates at the Hanford Site*) of lysimeter drainage at the south caisson located in the Buried Waste Test Facility of the north 300 Area from July 1985 to June 1993. Over the 8-year period of record, recharge ranged from 2.4 to 11.1 cm/yr with an average of 5.54 cm/yr. Drainage data from the lysimeter reflect a nonvegetated cover and medium to coarse sand. The recharge boundary condition in the model was specified as a Neumann (specified flux) boundary condition with a flux rate of 5.54 cm/yr.

Note: The model grid is shown in orange, while the Stage A EAA is shown in green.

Figure 7-4. 3D STOMP Model Domain to Evaluate the Stage A Remedy

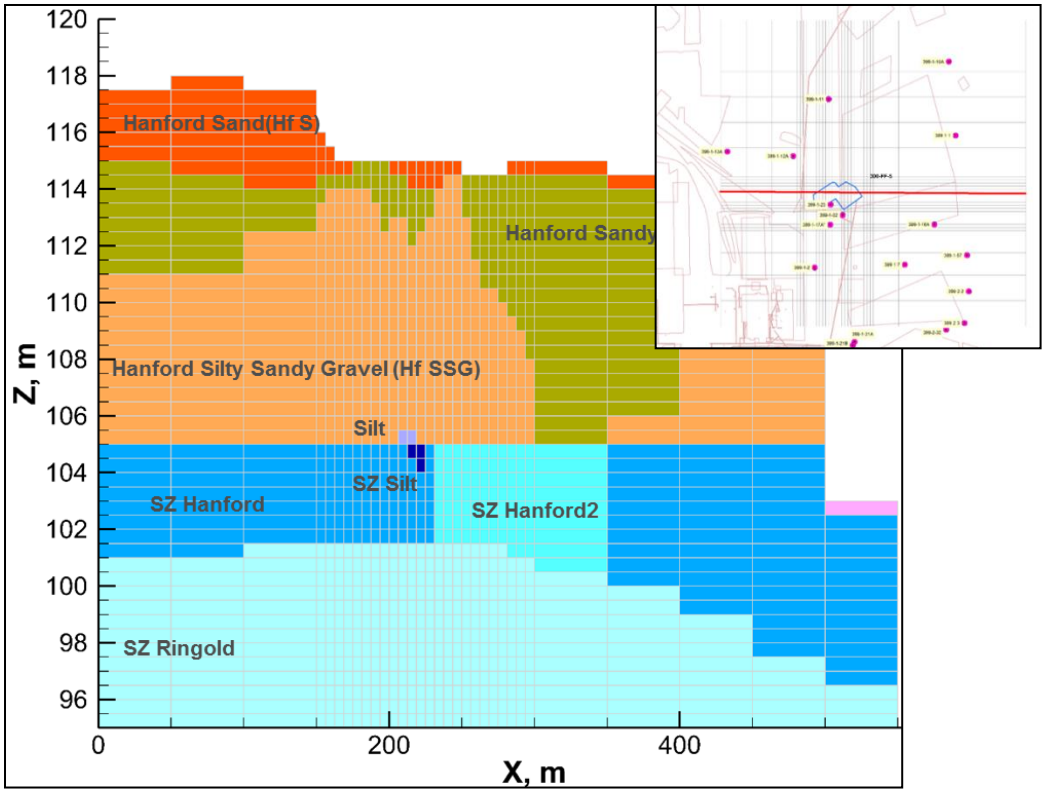

Figure 7-5. Distribution of Hydrogeologic Units along a Cross-Section

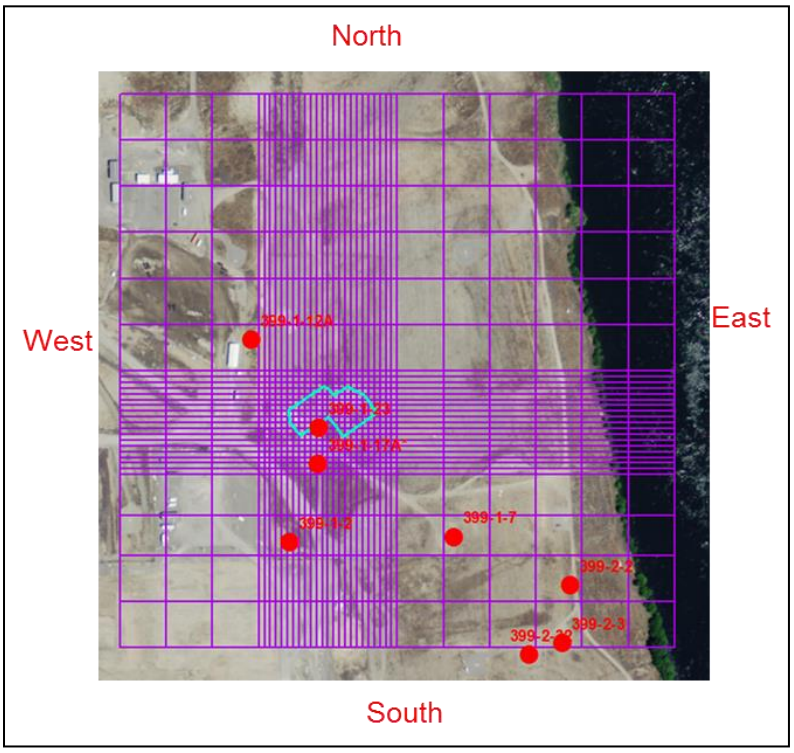

Note: The outline of Stage A EAA is shown in blue line.

Figure 7-6. Model Domain Showing the Grid Discretization along with Boundary Designations

Columbia River stage is a major driver in the hydrologic system in the 300 Area. Changes in Columbia River stage reflect the release of water upstream at Priest Rapids Dam to meet electric power demand. The seasonal cycle in river stage is related to the timing and volume of snowpack and snowmelt in the watershed with lower river stages typically occurring during fall and winter. The average range of diurnal fluctuations is ~0.5 m. Weekly, daily, and subdaily cycles are also evident from the river stage data.

Hourly Columbia River stage data from the river stage recorder in the 300 Area (river gauge station SWS-1) were used to set a time varying hydrostatic pressure at the river boundary. The SWS-1 river gage is located on the west bank of the Columbia River slightly south of the transect lines and is part of the monitoring network (Figure 7-7). The river stage data was collected manually beginning in 1991 at approximately monthly intervals until collection of automated hourly measurements began in January 2004. The river stage data were implemented in the model by averaging the hourly data over a daily cycle for the period starting from January 1, 2014, through December 31, 2015 (Figure 7-8). Over this period, the minimum and maximum river stages were 104.4 m and 107.1 m (342.5 and 351.3 ft), respectively. The median stage over this time period was 105.3 m (345.4 ft).

The east boundary of the model has been set up from the daily averaged SWS-1 river gage data. The gradient along the river has been interpolated from two stations (319 and 321), based on a computational fluid dynamic model of the Columbia river (PNNL-22886, *System-Scale Model of Aquifer, Vadose Zone, and River Interactions for the Hanford 300 Area – Application to Uranium Reactive Transport*). The interpolated value is 3.19E-04 m/m, which is used in applying flow boundary conditions at the river boundary of the model.

Figure 7-7. Location of the River Gage (SWS-1) in the 300 Area

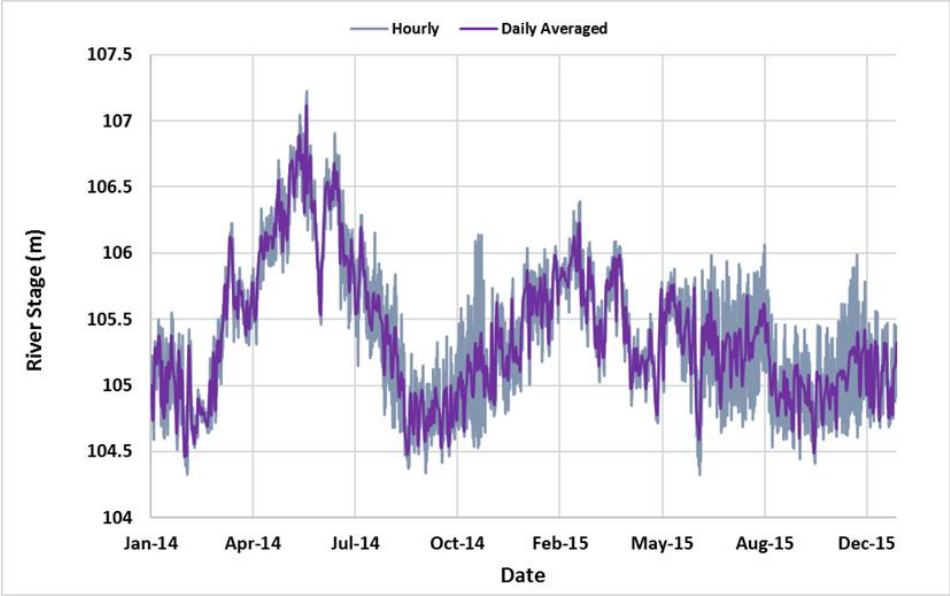

Figure 7-8. Comparison of Hourly and Daily Averaged Columbia River Stage Data at the 300 Area

7.4.2 Automated Water Level Network Data Usage

Hourly water level measurements from the automated water level network (AWLN) were used to assign flow boundary conditions on the inland edge of the model grid. A number of wells are part of the AWLN in the 300 Area, as shown in Figure 7-7. Subset of wells used for determining fate and transport model boundary conditions and for model calibration are presented in Figure 7-9.

Figure 7-9. Location of Automated Water Level Network in the Vicinity of Model Domain

The water level data at AWLN gage 399-1-12, the well located closest to the boundary of the model grid (Figure 7-6), were used to set time varying hydrostatic pressures at west and north boundaries. The south boundary was based on the water level data from nearby well 399-2-3. Because this well is slightly inland and upgradient of the south boundary, water levels from well 399-2-3 were modified by a constant -0.05 m (-0.16 ft) for the south boundary. This method resulted in better water level and tracer concentration matches.

The hourly water levels were averaged daily from 2014 through 2015, and daily varying boundary conditions were applied. The hourly and daily averaged water levels for 399-1-12 and 399-2-3 are shown in Figure 7-10 (a and b). Over the 2014 through 2015 simulation time period, the minimum, maximum, and median water levels at 399-1-12 were 104.8 m, 106.8 m, and 105.3 m, respectively; for well 399-2-3, the minimum, maximum, and median water levels were 104.7 m, 106.7 m, and 105.2 m, respectively. The period of sustained high water levels generally occurs during the months of May through August. Figure 7-11 presents the daily averaged hydraulic head of SWS-1 river gage and well 399-1-12 that are used for setting the east and west hydraulic boundaries, respectively.

7.5 Model Calibration

Calibration of flow and transport parameters in the 3D STOMP model was undertaken to match the following measurements:

- Water levels in the selected monitoring wells where AWLN data were available
- Extent of river water and groundwater mixing, based on EC measurements from selected monitoring wells where AWLN data were available (EC of end-member waters [upgradient groundwater and river water] were estimated, and simple mixing was performed)
- Uranium concentrations and trends at selected monitoring wells over the past 20 years

In order to match the observed water levels and extent of river-groundwater mixing, adjustments were made to the spatial distribution of hydraulic conductivity in the saturated Hanford unit. Minor adjustments were also made to the boundary conditions. For matching uranium concentrations, the initial uranium soil concentrations were adjusted based on the gravel fraction. Details regarding specific choice of parameters is provided in the following sections.

The calibrations were performed manually. Since the focus of the work is on evaluating uranium concentrations prior to and following remedy treatment in Stage A, particular focus was placed on matching the uranium concentrations in nearby wells that have long-term monitoring records.

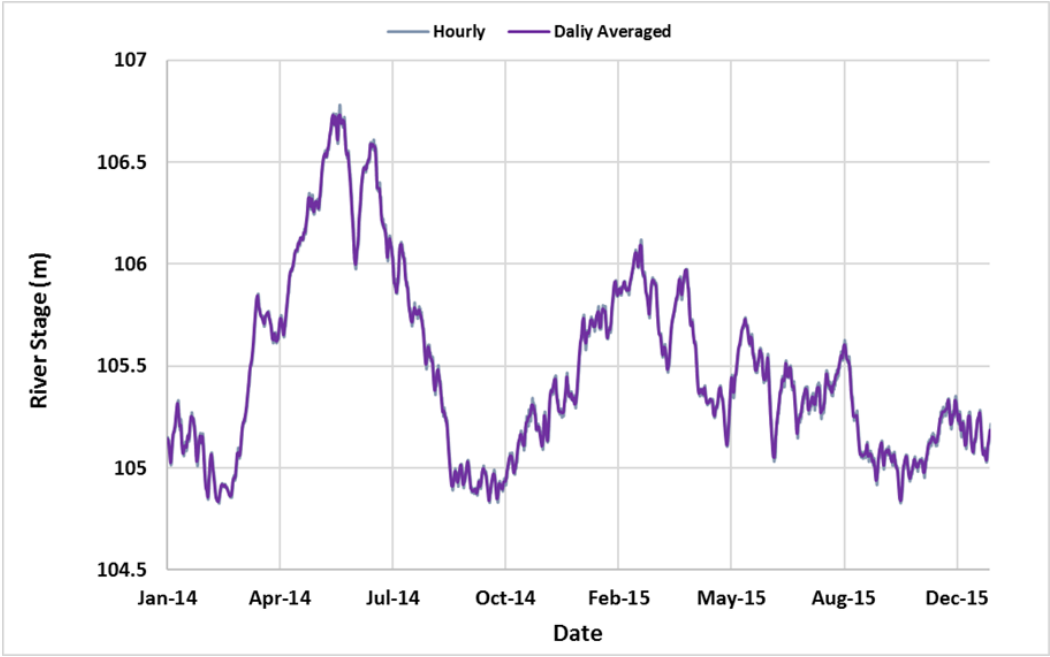

(a)

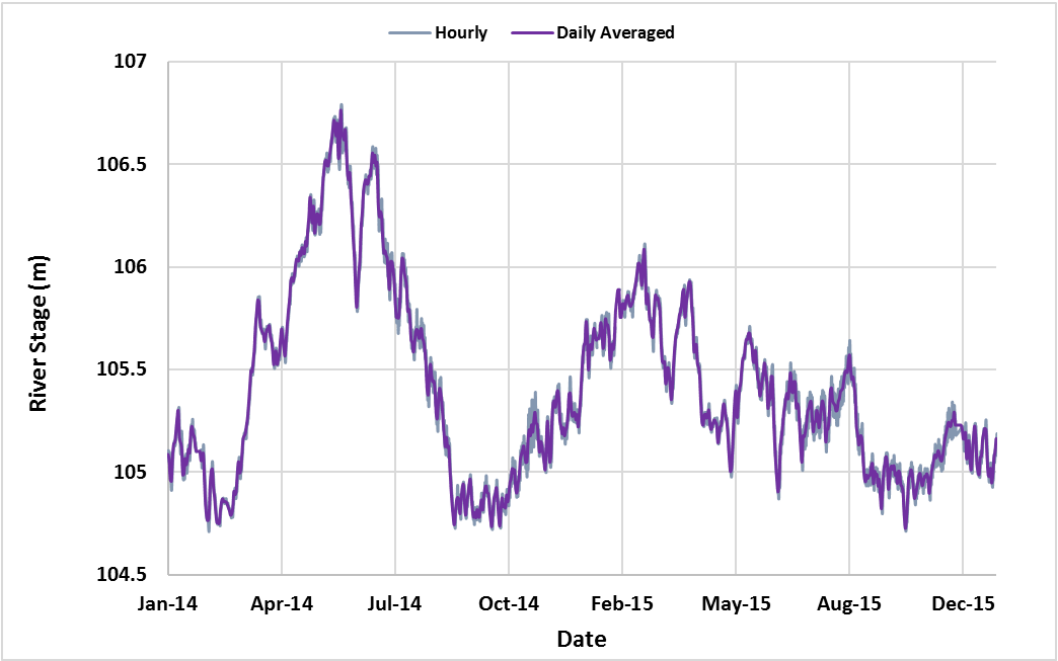

(b)

Figure 7-10. Daily and Hourly Averaged Water Levels at (a) 399-1-12 and (b) 399-3-3

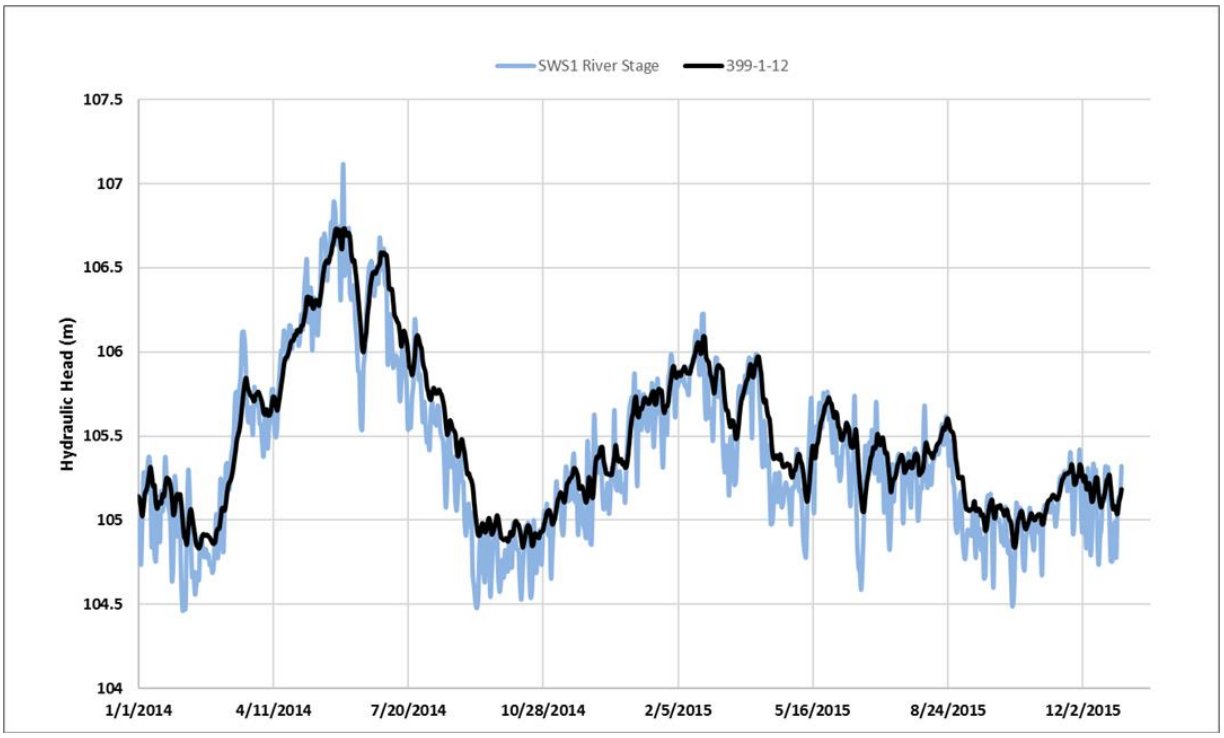

Figure 7-11. Comparison of Daily Averaged Hydraulic Heads for SWS-1 River Gage (East Boundary) and 399-1-12 (West Boundary)

7.6 Determination of Fate and Transport Parameters

The following fate and transport parameters were used in the model:

- Saturated zone hydraulic conductivity
- Macrodispersivity
- Porosity
- Particle density and bulk density
- Saturation pressure and relative permeability relationships
- Molecular diffusion coefficient
- Specific storativity
- Uranium sorption

7.6.1 Saturated Zone Hydraulic Conductivity

The saturated hydraulic conductivity of the Hanford formation has reportedly been difficult to determine from aquifer testing due to its highly transmissive nature. Constant rate aquifer tests conducted at wells screened in the saturated Hanford formation within the 300 Area resulted in values of horizontal hydraulic conductivity ranging from approximately 980 m/d to 15,000 m/d (PNL-6716, *Interim Characterization Report for the 300 Area Process Trenches*). Re-evaluation of these tests (PNNL-17708, *Three-Dimensional Groundwater Models of the 300 Area at the Hanford Site, Washington State*) identified recharge boundary effects in some cases leading to unreliable results. Aquifer test results with hydraulic conductivities >5,000 m/d were considered uncertain due to the low drawdown obtained during the tests (<0.1 m), making accurate analysis difficult. Horizontal hydraulic conductivity of the Hf is reported for previous two-dimensional (2D) and 3D numerical modeling studies: 2,000 to 10,000 m/d

(PNNL-17708), 1,500 m/d (Yabusaki et al., 2008, "Building conceptual models of field-scale uranium reactive transport in a dynamic vadose zone-aquifer-river system"), and 7,000 m/d (Ma et al., 2010). Average value of hydraulic conductivity determined from short-duration constant rate injection tests performed at the Integrated Field Research Challenge project site located within the 300 Area was about 7000 m/d with a range of ~4,600 to 11,000 m/d (PNNL-22886).

A spatially variable depth-averaged hydraulic conductivity field was determined for the Hanford formation in PNNL-22886 using a parameter estimation methodology. It resulted in a spatially variable permeability field that varied over an order of magnitude for the Hanford formation. Lower values of depth averaged permeability (1×10^{-10} m^2) were estimated close to the river that typically increased inland (4×10^{-9} m^2) when moving westwards. This information was used qualitatively during the model calibration exercise. The model calibration was primarily based on evaluation of (1) spatial and temporal trends in uranium concentrations, (2) changes in specific conductance due to river and groundwater mixing at monitoring wells, and (3) geologic information on preferential pathways within the surficial aquifer (e.g., a paleochannel). Based on this information, the saturated zone of the Hanford formation (Hf unit) was divided into the following three different hydraulic conductivity zones (Figure 7-12):

- Saturated Hanford 1 zone covers most of the model domain and was assigned a saturated hydraulic conductivity of 4,000 m/d, based on evaluation of past modeling studies.
- Saturated Hanford 2 zone covers an area of higher hydraulic conductivity (paleochannel) where preferential movement of uranium (and phosphate) has been observed. The saturated hydraulic conductivity of 6,000 m/d was assigned to this zone that resulted in a better match to uranium concentrations.
- Saturated Hanford 3 zone, a lower hydraulic conductivity zone of 1,000 m/d near the river, was assigned to dampen the effect of river stage fluctuations at the river-aquifer interface due to the presence of lower permeability lithologic unit near the base of the river channel. Hydraulic conductivities were shown to be smaller near the water-sediment interface and increasing exponentially with depth (Fritz and Arntzen, 2007, "Effect of Rapidly Changing River Stage on Uranium Flux through the Hyporheic Zone"). This lowering is also consistent with parameter estimation in other modeling studies (PNNL-22886; PNNL-17708).

Hydraulic testing of the Ringold formation gave reliable horizontal hydraulic conductivity estimates between 2 and 51 m/d (PNNL-17708). Of these estimates, horizontal hydraulic conductivity of 42 m/d was reported in PNL-6716 for pumping tests conducted at well 399-1-16A, while an averaged result of 43.25 m/d was reported in WHC-SD-EN-TI-052, *Phase I Hydrogeologic Summary of the 300-FF-5 Operable Unit, 300 Area*, for pumping tests conducted further from the current study but within the 300 Area (PNNL-17708). In previous 2D and 3D numerical modeling studies, the assigned Ringold unit E hydraulic conductivity value ranges from 15 m/d (Yabusaki et al., 2008) to 40 m/d (PNNL-17708; Ma et al., 2010). A horizontal hydraulic conductivity of 40 m/d was assigned to Ringold unit E and was not adjusted during model calibration since most of the flow occurs through the saturated Hanford formation.

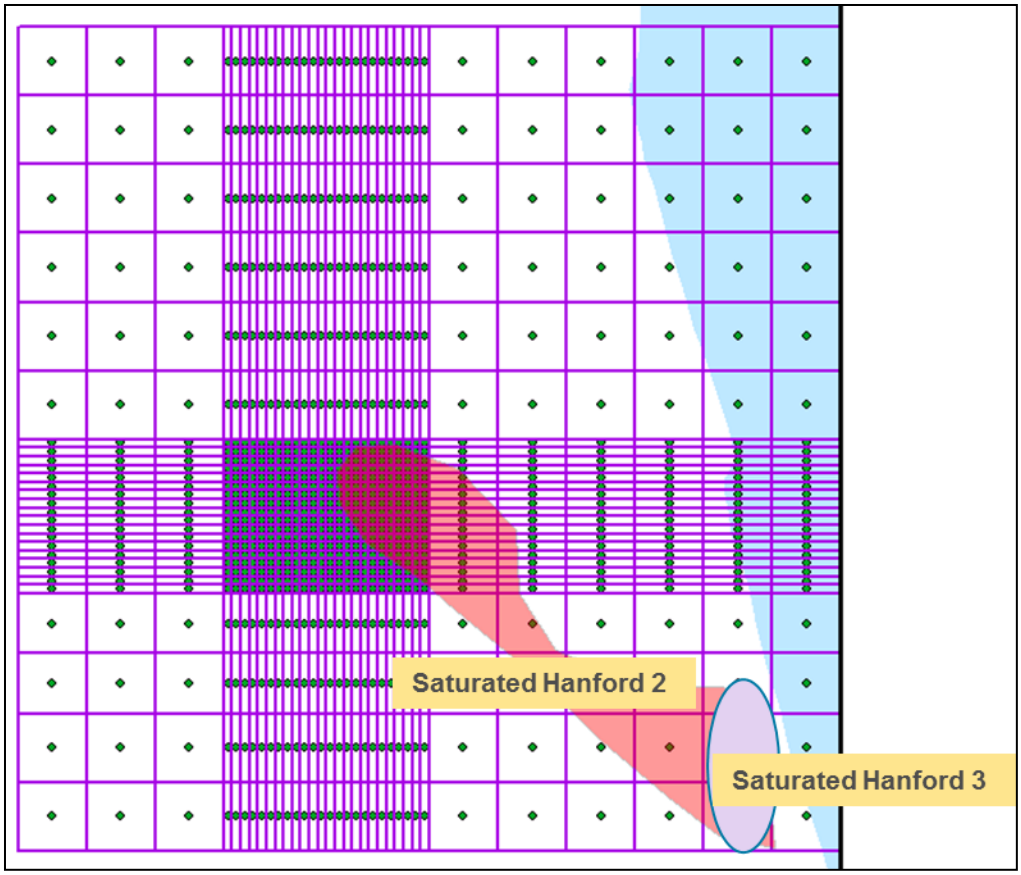

Note: Saturated Hanford 1 is the portion that is not colored

Figure 7-12. Zones of Variable Hydraulic Conductivity for the Hanford Unit in the Unconfined Aquifer

The hydraulic conductivity of alluvium in the hyporheic zone of the Columbia River adjacent to the 300 Area has been estimated between 0.63 and 103.68 m/d (Fritz and Arntzen, 2007), based on slug tests conducted in nine piezometers with depths to top of screen ranging from 19 to 180 cm. Hydraulic conductivities were shown to be smaller near the water-sediment interface and increasing exponentially with depth. An effective vertical hydraulic conductivity was determined for three of the piezometers and ranged from 0.37 to 7.0 m/d. Hydraulic conductivity of the river alluvium was adjusted as part of model calibration.

The vertical hydraulic conductivity of the Hanford and Ringold units were set to 0.1 times the horizontal conductivity which is consistent with previous groundwater modeling studies that assume the vertical hydraulic conductivity of the Hanford and Ringold units range from 0.01 to 0.1 times the horizontal conductivity (NUREG/CR-6940, *Combined Estimation of Hydrogeologic Conceptual Model, Parameter, and Scenario Uncertainty with Application to Uranium Transport at the Hanford Site 300 Area*; PNNL-17708; Yabusaki et al., 2008). The river alluvium was simulated as isotropic. The previous study (PNNL-17708) that explicitly simulated river sediments also used an isotropic hydraulic conductivity.

The calibration involved running the model for the 2014-2015 2-year period and evaluating the fit between the simulated and observed heads at wells 399-1-12 and 399-2-2. At the location of each monitoring well, the model nodes that fell within the top and bottom screen elevation for each well were flagged for output of saturation, hydraulic head, and concentration. For each time step, the well nodes that registered a water saturation of 1.0 were used in the calculation of the average concentration at each well.

The arithmetic mean was used for the average where concentrations for all nodes were weighted equally. Determination of goodness of fit was done by visual inspection. Adjustments to parameters governing flow and transport were made and the simulation run again. This process was repeated until a suitable match was obtained between measured and simulated water levels.

Figure 7-13 shows the quarterly changes in the magnitude of Darcy flux and flow direction in the aquifer for selected times in Year 2014 due to the changes in the river stage. In the first quarter of the year, from January to April, the flow direction is from river to groundwater due to the high river stage. During the month of August, the flow direction reversal occurs because of the higher water level in the upgradient location than the river stage. The flow direction changes again during the month of December due to the high river stage. The calculated horizontal linear velocity in the saturated Hanford unit near the Stage A area is approximately 10 m/d and the Darcy flux is ~1.3 m/d and the hydraulic gradient is ~3.25E-4 m/m. The hydraulic gradient value is consistent with the observed gradient (3.0E-4 m/m) value in the field and the velocity estimates are consistent with the average tracer drift velocity of about 11 m/day reported by PNNL-22048, *Updated Conceptual Model for the 300 Area Uranium Groundwater Plume*.

7.6.2 Macrodispersivity

The initial longitudinal macrodispersivity used in the models was 8.75 m for the saturated Hanford unit and Ringold unit E. A macrodispersivity of 8.75 m reflects the value derived using the weighted least squares method of Xu and Eckstein, 1995, "Use of Weighted Least-Squares Method in Evaluation of the Relationship Between Dispersivity and Field Scale," based on the approximate plume length.
The longitudinal macrodispersivity was set to 1.0 m for the river alluvium units. These values are comparable to previous modeling studies that assigned values of 1 m to 3 m for the Hanford unit and values of 0.5 to 3.0 m for Ringold unit E (PNNL-17708; Ma et al., 2010; NUREG/CR-6940).

For all material property zones, except the Hanford vadose zone, the vertical transverse-to-longitudinal dispersivity ratio was set to 0.01 during calibration of the model. Previous modeling studies at Hanford have set the transverse-to-longitudinal dispersivity ratio from 0.01 to 1.0 (NUREG/CR-6940; PNNL-17708; Ma et al., 2010). Longitudinal macrodispersivity for the Hanford vadose zone (above the PRZ) was set at one-tenth of Hf longitudinal macrodispersivity, while the transverse dispersivity remained unchanged, because macrodispersivity in the unsaturated media is typically less than that in the saturated zone.

7.6.3 Porosity

Total porosity refers to both isolated and connected pore space. Diffusive porosity refers to the connected pore space and is the porosity through which flow and transport occurs in the model. For purposes of assigning values of diffusive porosity in the model, the diffusive porosity was assumed equal to values of total porosity listed in the literature. Total and diffusive porosity was specified as 0.177 cm^3/cm^3 for the Ringold Formation and river alluvium (PNNL-14702, *Vadose Zone Hydrogeology Data Package for Hanford Assessment* [Table 4.5]). Porosity for the Hf was specified as 0.167 cm^3/cm^3 (PNNL-14702, Table 4.5, Soil Class Hg). For all other units, the values are taken from PNNL-18564, *Selection and Traceability of Parameters to Support Hanford-Specific RESRAD Analyses: Fiscal Year 2008 Status Report*. For the silt unit, the value is 0.419 cm^3/cm^3; for all of the Hanford sand units, the value is 0.379 cm^3/cm^3. For Hanford gravel, the value is 0.102 cm^3/cm^3, and the rest are the same as the Hanford unit (0.167 cm^3/cm^3).

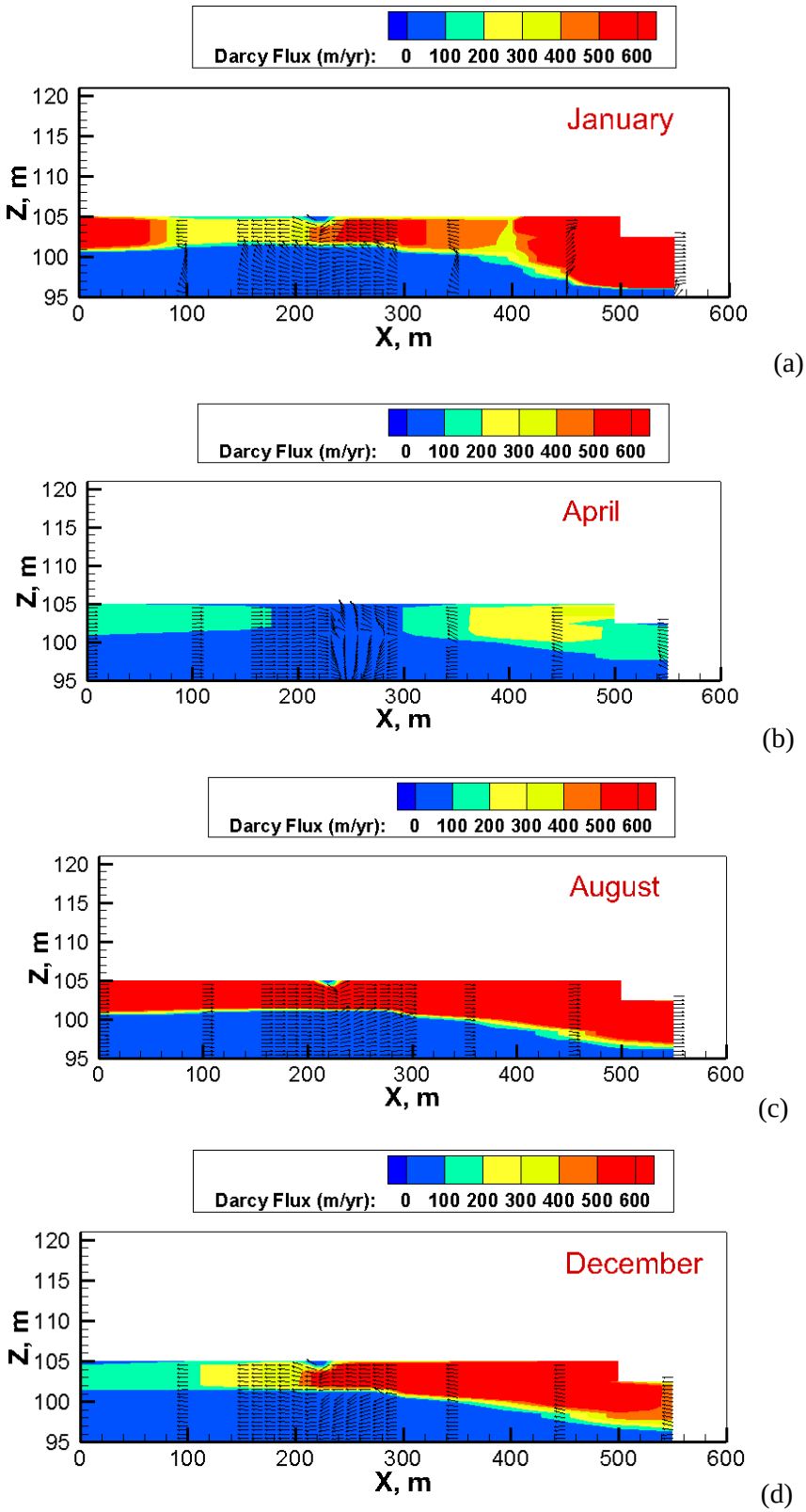

The line of the cross-section passes in an east-west direction through Stage A EAA as shown in previous figure.

Figure 7-13. Darcy Flux Distribution Along a 2D Cross-Section for Selected Times within a Year

7.6.4 Particle Density and Bulk Density

Bulk density for the Hf, taken as 2.23 g/cm^3, reflects the modal value of measurements for sandy gravel at the 300 Area (PNNL-17708, Table A.3). A bulk density of 2.23 g/cm^3 is also reasonable, given the range of bulk densities for Hanford coarse gravel of 1.56 to 2.42 g/cm^3 for a gravel content ranging from 50 to 85 percent, respectively (PNNL-14702, Table B-21). The particle density for the Hf was 2.68 g/cm^3, based on porosity of 0.167 cm^3/cm^3 and bulk density of 2.23 g/cm^3.

A particle density of 2.63 g/cm^3 and 2.66 g/cm^3 was reported (PNNL-17708, Appendix A) for Ringold unit E for the 300 Area with an average value of 2.65 g/cm^3 assigned in the model. Using a porosity of 0.177 for the Ringold unit gives a bulk density of 2.18 g/cm^3 and is nearly identical to the value of 2.17 g/cm^3 for Ringold sandy gravel for 82 percent gravel (PNNL-14702, Table B-27). Particle density of 2.76 g/cm^3 was used to represent the river alluvium (PNNL-17708). Using a diffusive porosity of 0.177 gives a bulk density of 2.27 g/cm^3.

The particle density value of 2.89 g/cm^3 was used to represent the silt unit (PNNL-18564); using a diffusive porosity of 0.419 gives a bulk density of 1.67 g/cm^3.

For all of the sand units, the particle density value of 2.57 g/cm^3 (PNNL-18564) was used; using a diffusive porosity of 0.379 gives a bulk density of 1.6 g/cm^3. For Hanford silty sandy gravel and sand gravel units, 2.31 g/cm^3 (PNNL-18564) was used; using a diffusive porosity of 0.167 gives a bulk density of 1.92 g/cm^3. For the Hanford gravel unit, the particle density value of 2.19 g/cm^3 (PNNL-18564) was used; using a diffusive porosity of 0.102 gives a bulk density of 1.97 g/cm^3.

7.6.5 Saturation-Pressure and Relative Permeability Relationships

The relationship between capillary pressure and saturation was characterized using the van Genuchten function (van Genuchten, 1980, "A Closed-form Equation for Predicting the Hydraulic Conductivity of Unsaturated Soils") and the Mualem pore distribution model (Mualem, 1976, "A New Model for Predicting the Hydraulic Conductivity of Unsaturated Porous Media"). In the models developed for the 300 Area, only Hf has the potential to be variably saturated. The parameters needed to describe the van Genuchten moisture retention constitutive relation and the Mualem relative permeability constitutive relation include the parameters such as α (proportional to the inverse of the air-entry matric potential), saturated and residual volumetric water contents, θ_s and θ_r, dimensionless fitting parameters *n*, and *m*, and saturated hydraulic conductivity, K_{sat}. The horizontal K_{sat} for the vadose zone units is taken to be 10 times the vertical K_{sat}. These parameters are presented in Table 7-1 and are based on statistical average of laboratory measurements summarized in PNNL-14702 (Table 4.5). The default option was used for the *m* parameter where $m = 1 - 1/n$.

Same hydraulic property set is used for the silty sandy gravel and sandy gravel unit due to lack of information. For the silt unit the hydraulic properties listed in PNNL-14702 (Table 4-5) for the Cold Creek Silt dominated unit were chosen. The α parameter of 0.017 1/cm for sandy gravel listed in PNNL-14702 (Table 4-5) was thought to represent too large of an air entry potential near the capillary fringe. As a result, α was assigned a value of 0.1 1/cm.

7.6.6 Molecular Diffusion Coefficient

The molecular diffusion option used in the model was conventional with a molecular diffusion coefficient of 2.5×10^{-9} m^2/s and solute partition option of continuous. The molecular diffusion coefficient, held constant during all simulations, was not included as a calibration parameter in the model. The uranium aqueous species effective molecular diffusion coefficient is set at 1×10^{-9} m^2/s.

7.6.7 Specific Storativity

Specific storativity, used in the model, was taken as the default value where it is equal to $1 \times 10^{-7} \times$ diffusive porosity. Specific storativity was held constant during all simulations and not included as a calibration parameter in the model.

7.6.8 Uranium Sorption

Uranium sorption-desorption parameters for simulating the pretreatment conditions are taken from ECF-300FF5-11-0151, *Groundwater Flow and Uranium Transport Modeling in Support of the 300 Area FF-5 RI/FS*. These were developed based on the desorption experiments conducted by PNNL-SA-58541, *Uranium(VI) Release from Contaminated Vadose Zone Sediments: Estimation of Potential Contributions from Dissolution and Desorption*, and Liu et al., 2008, "Scale-dependent desorption of uranium from contaminated subsurface sediments." The results presented in these papers are internally consistent and comprehensive and, therefore, are used exclusively for developing the sorption parameters before phosphate treatment. The sorption/desorption parameters presented here apply specifically to uranyl ion, which has the chemical formula of $(UO_2)^{2+}$, resulting in an oxidation state of +6. For simplicity, it is referred to in this report as U(VI). The uranyl ion forms from hydrolysis of uranium mineral during water-mineral interaction.

Based on information presented in ECF-300FF5-11-0151, the uranium K_d value of 3.17 mL/g was chosen for the aquifer (based on groundwater alkalinity), while a K_d value of 2.18 mL/g was chosen for the vadose zone. Both an equilibrium sorption and a kinetic sorption model was developed to cover the range of uncertainty expected in the uranium leaching characteristics. For the equilibrium sorption model the above mentioned K_d values are used. For the kinetic sorption-desorption model, the forward reaction rate constant was calculated to be 9.31×10^{-3} hr^{-1} based on a representative backward (desorption) rate constant of 5×10^{-4} hr^{-1} derived for field-textured samples (ECF-300FF5-11-0151). The kinetic model is implemented using the *Valocchi Sorption* option within the Kinetic Reactions card of STOMP input file.

7.7 Development of Initial Conditions

Simulations were initially conducted over a 2-year period (January 1, 2014 through December 31, 2015). This period coincides with complete water level data sets available for the inland and river model boundaries from well 399-1-12, and well 399-2-3 and the river gage, respectively. Additional wells within the model domain also had complete or nearly complete data sets for the same 2-year period that were useful in the calibration process. For the 2014 to 2015 period, 2014 exhibits the highest river stage and corresponding aquifer water levels, while the maximum river stage and aquifer water levels measured in 2015 are lower. High water levels are thought to be largely responsible for rewetting of the PRZ and increased influx of labile uranium from the top of the PRZ. This, in turn, is surmised to be responsible for generating periodic pulses to the uranium groundwater plumes with concentrations exceeding 60 to 90 µg/L. The high river stage during the summer of 2015 is lower than that observed in 2014 such that groundwater does not intersect sediments near the top of the PRZ that potentially contain higher soil uranium concentrations. Thus, the use of data from the 2014 to 2015 period provides a sampling of different flow behaviors and resulting uranium transport in the aquifer.

Boundary conditions are established by setting boundary pressures from observed data, as discussed earlier, and were based on a hydrostatic head distribution. The 3D flow and transport model was initially run for 15 cycles (30 years), starting from Year 1992, to establish the uranium concentrations in the aquifer under a "No Action" scenario. The hydraulic heads in the model rapidly equilibrated to the boundary conditions, and initial conditions were seen to diminish within the first 2-year cycle. The 3D transport modeling of phosphate injection/infiltration, along with uranium transport, was

performed by exercising the model starting from Year 2015 and running it over the 2-year period (Year 2015 and 2016). Initial heads for the start of the model cycle were taken from the restart file, which was accessed by STOMP using the Restart option in the Solution Control Card of the STOMP input file.

Details of the data compilation and development of 3D uranium soil distribution can be found in ECF-300FF5-15-0087. Since the uranium soil concentrations were determined on <2 mm size sediment, soil concentrations were corrected for gravel content for the purpose of applying uranium mass on the bulk volume basis. This correction is necessary because almost all of the uranium mass is associated with the <2 mm size fraction, and a negligibly small amount is associated with the gravel fraction.

The gravel correction factor was derived by determining the fraction of <2 mm grain size in the 300 Area soils. The gravel content varies within the Stage A area due to varying lithologies. However, because most of the vadose zone and upper part of the unconfined aquifer is dominated by sandy gravel unit, a 60 percent gravel fraction was deemed reasonable. Uranium soil concentrations determined from the <2 mm size fraction were adjusted (multiplied by 0.4 for bulk volume), which is indicative of 40 percent of the sediment being <2 mm size that contains majority of uranium mass.

Prior to setting initial concentrations, the data were further adjusted for the component of uranium that would be exchangeable or labile (Figure 7-14). This was considered to be 60 percent based on evaluations presented in ECF-300FF5-11-0151. The gravel corrected bulk soil concentrations were multiplied by 0.6 to adjust for the labile fraction and the soil uranium plumes were reinterpolated.

Table 7-1 summarizes the model parameters following calibration. Figure 7-15 presents the hydraulic head comparisons among the observed and simulated heads for wells 399-1-12 and 399-2-2 that are located far from each other (Figure 7-16). Simulated hydraulic heads for all other wells within the model domain also show excellent matches with observations.

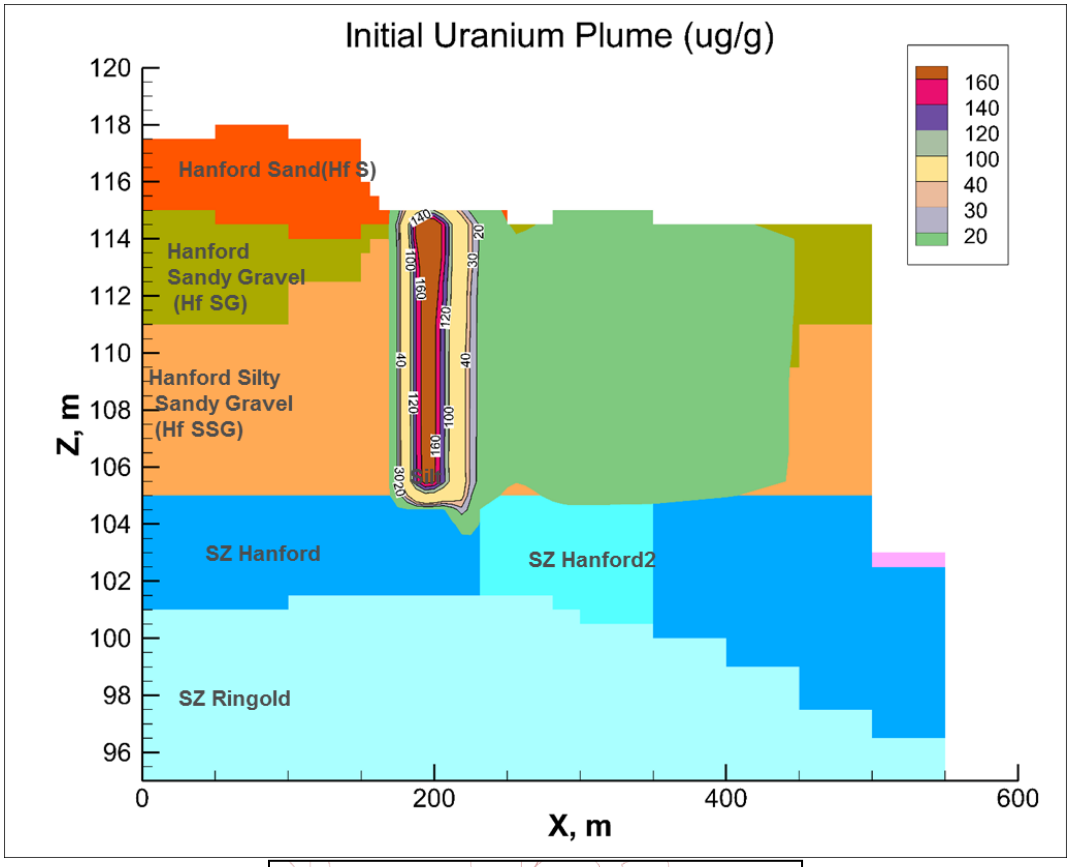

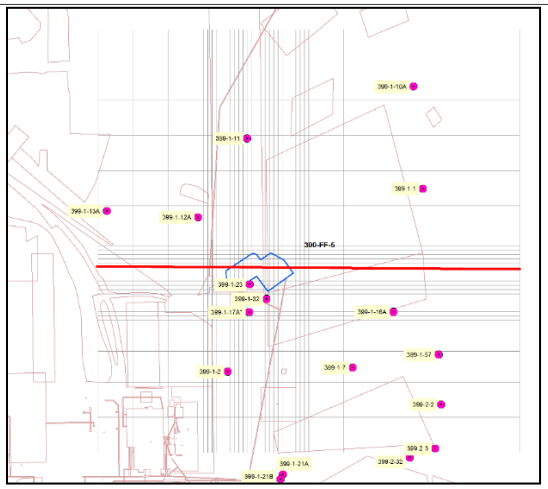

Note: The location of cross-section line is shown in the lower figure

Figure 7-14. Distribution of Initial Soil Labile Uranium Concentration Along an East-West-Trending Cross-Section Through the Stage A EAA

Table 7-1. Model Parameters Used in the Simulations

	Hanford Gravel (Hf G)	Hanford Sand (Hf S)	Hanford Sandy Gravel (Hf SG)	Hanford Silty Sandy Gravel (Hf SSG)	Hanford Silt (S)	Saturated Silt (Saturated S)	Hanford (Saturated)	Hanford2 (Saturated)	Hanford 3 (Saturated)	Ringold Unit E (Saturated)	River Alluvium
Horizontal K_{sat} (m/d)	12.6	3.2	2.85	2.85	0.5	0.5	4,000*	6,000*	1,000*	40	10*
K Anisotropy (K_z/K_x)	0.1	0.1	0.1	0.1	0.1	0.1	0.1	0.1	0.1	0.1	1.0
Diffusive Porosity (cm^3/cm^3)	0.102	0.379	0.167	0.167	0.419	0.419	0.167	0.167	0.167	0.177	0.177
Longitudinal Dispersivity, α_L (m)	0.875	0.875	0.875	0.875	0.875	8.75	8.75	8.75	8.75	8.75	1
Dispersivity Anisotropy, α_T/α_L	0.1	0.1	0.1	0.1	0.1	0.01	0.01	0.01	0.01	0.01	0.01
van Genuchten α (1/cm)	0.007	0.027	0.017	0.017	0.005	0.005	0.082	0.082	0.082	0.008	0.008
van Genuchten *n* (-)	1.831	2.168	1.725	1.725	2.249	2.249	2.093	2.093	2.093	1.66	1.66
Residual Saturation (cm^3/cm^3)	0.196	0.0844	0.132	0.132	0.0954	0.0954	0.152	0.152	0.152	0.147	0.147
Particle Density, ρ_P (g/cm^3)	2.19	2.57	2.31	2.31	2.89	2.89	2.63	2.63	2.63	2.68	2.76
Bulk Density, ρ_B (g/cm^3)	1.97	1.6	1.92	1.92	1.68	1.68	2.19	2.19	2.19	2.21	2.27

* Based on model calibration.

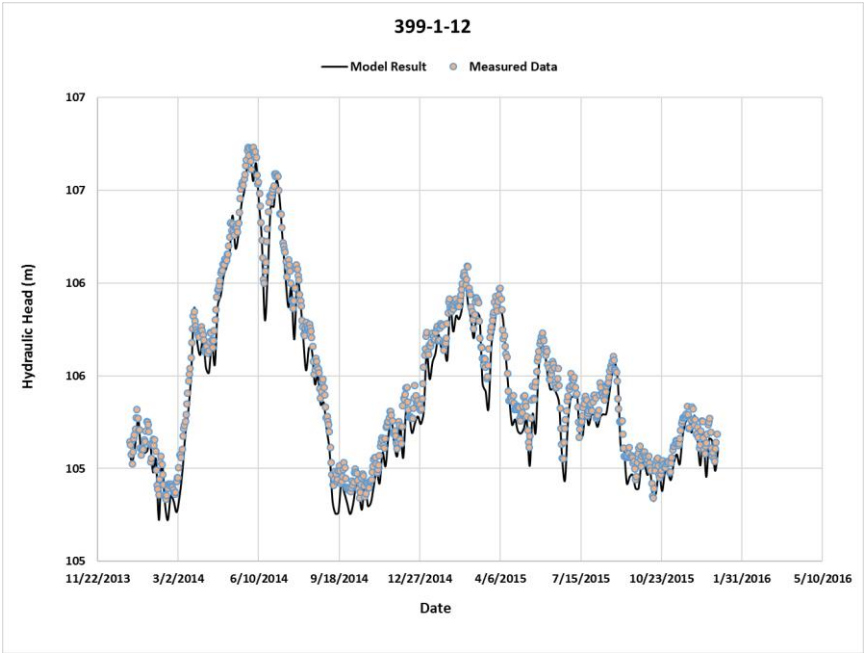

(a)

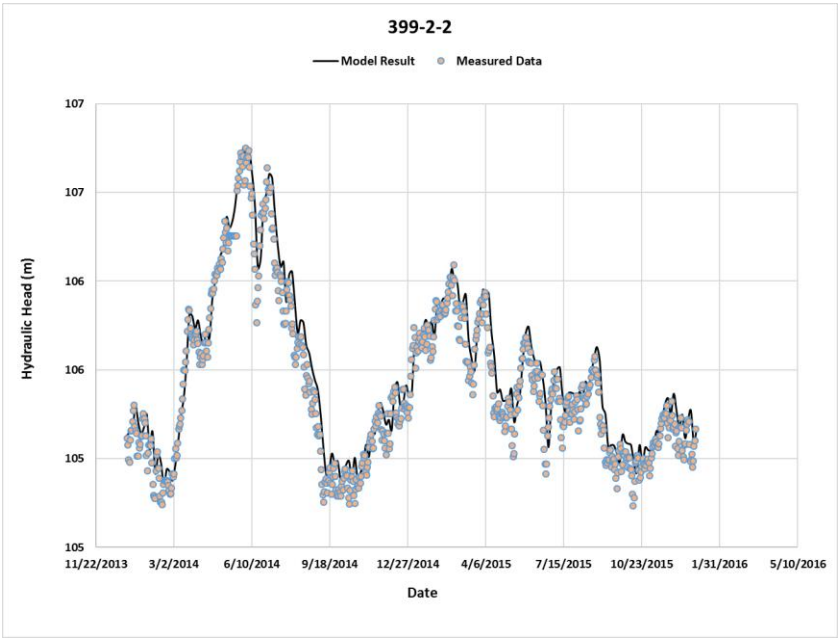

(b)

Figure 7-15. Comparison of Model Simulated Hydraulic Heads and Observed Heads at (a) 399-1-12 and (b) 399-2-2

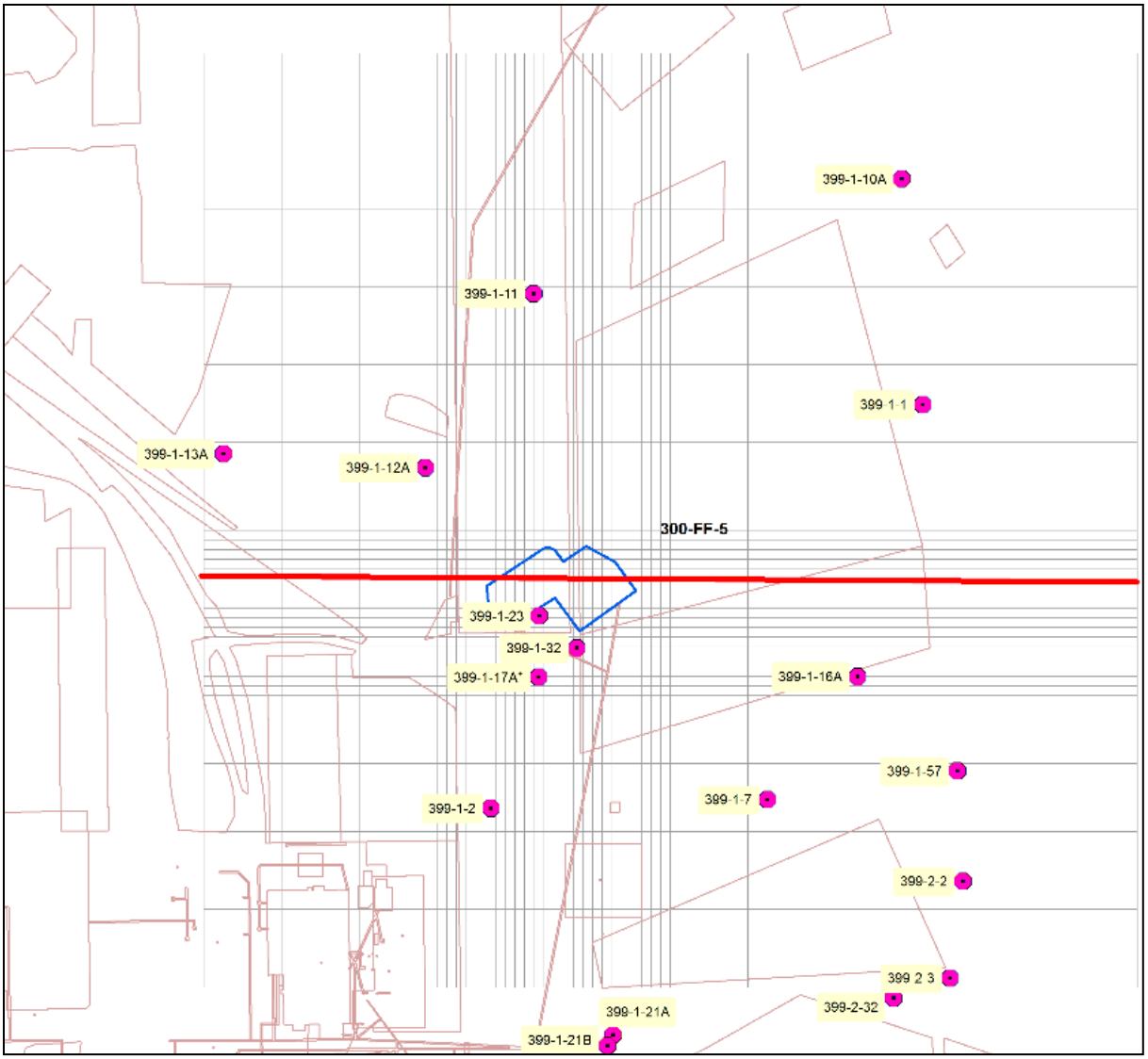

Notes: The cross-section line (red line) is used for presenting Darcy flux distribution.

Well 399-1-12 is located in the northwest portion of the model domain, while 399-2-2 is located in the southeast portion of the model domain.

Figure 7-16. Location Map of Monitoring Wells within the Model Domain

7.8 Modeling Uranium and Phosphate Transport

This section provides details on uranium and phosphate transport modeling conducted using STOMP. 3D fate and transport modeling using STOMP was performed in three stages:

1. Modeling uranium transport prior to Stage A treatment
2. Modeling phosphate transport during treatment and post-treatment time periods
3. Modeling uranium transport during post-treatment times

7.8.1 Modeling Uranium Transport Prior to Treatment (No Action Case)

A fate and transport model was developed to estimate the uranium soil and groundwater concentrations prior to Stage A treatment. The emphasis of this model was to match the uranium concentrations in the aquifer observed over the past 20 years (approximately). Since some simplifications are inherent in modeling complex uranium leaching and transport characteristics within a dynamic aquifer, the focus was on matching the trend in uranium concentrations in selected wells where long-term monitoring records exist and to be reasonably close to the magnitude of uranium concentrations observed in the aquifer. The exact reconstruction of the past was not the objective of the model due to limited information on the uranium soil distribution and various past remediation activities. The hydraulic properties and boundary conditions developed for this model were used in the later models with minor changes where necessary.

Calibration of the uranium model included adjusting the maximum initial uranium concentrations (labile fraction) to better match with measured uranium concentrations from 1997 through 2015. Initial concentrations were adjusted by setting all saturated zone Hanford and Ringold unit soil concentrations to zero and all concentrations below background value to background, based on the understanding that the labile fraction would have been removed over many decades of pore volume flushing prior to start of the model.

The simulated uranium groundwater concentrations are compared to the observed concentration for selected monitoring wells in Figure 7-17 using both an equilibrium and kinetic sorption model. These simulations are performed assuming no remedial action has occurred (no action scenario) using hydraulic boundary conditions based on 2-year data from 2014-2015. These plots show how the transport model mimics the observed increases in the uranium groundwater concentrations during the typically high water month of June. Well 399-1-17A has the best long-term monitoring record of uranium concentrations. The simulation results (Figure 7-17) show that the kinetic model mimics the observed uranium groundwater concentrations more accurately than the equilibrium model. The model results show that during the typical high water month of June, uranium groundwater concentrations increase at the inland wells (Figure 7-17 a, b, c, and d), and decrease at the wells near the river (Figure 7-17 e and f). This behavior in the inland wells is a result of the rising water levels coming in contact with uranium mass within the upper portions of the PRZ, and capillary fringe, near the southern end of the 300 Area Process Trench, thereby increasing desorption from the soil to the aqueous phase and increasing concentrations in the groundwater. As water levels decline, uranium groundwater concentrations decrease due to reduced leaching from the PRZ. The decrease in uranium groundwater concentrations for the wells near the river is due to a combination of dilution and mixing from the influx of river water. Figure 7-18 shows the simulated uranium plume maps for equilibrium and kinetic sorption models for Years 2015, 2022, and 2040. The results presented herein demonstrate adequacy of the modeling methodology and choice of parameters at the scale of the model domain.

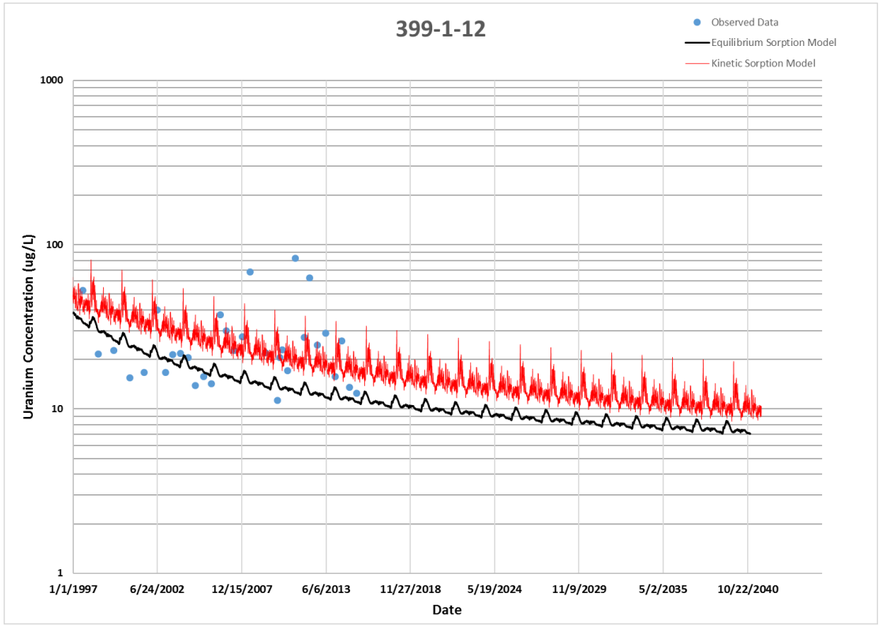

(a)

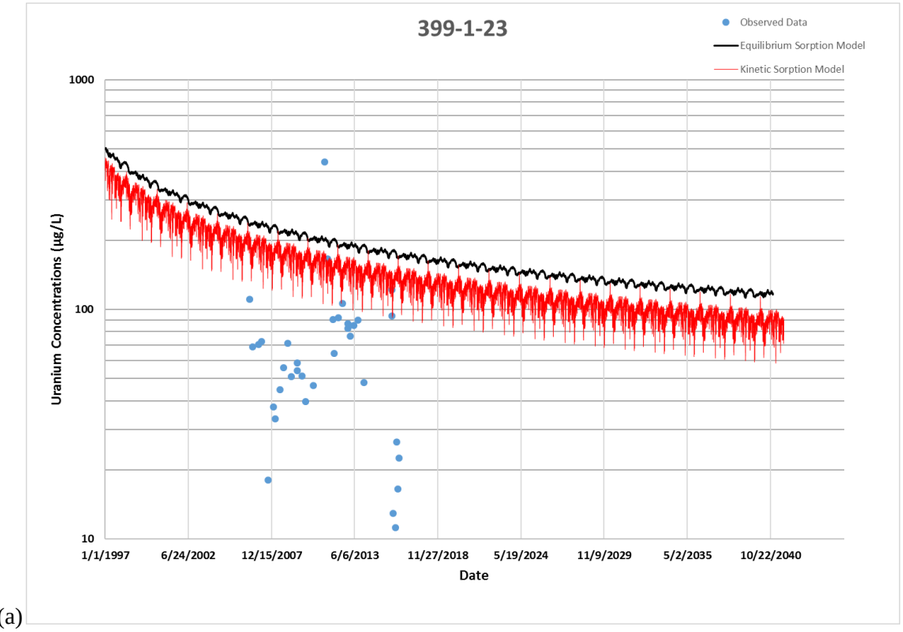

(b)

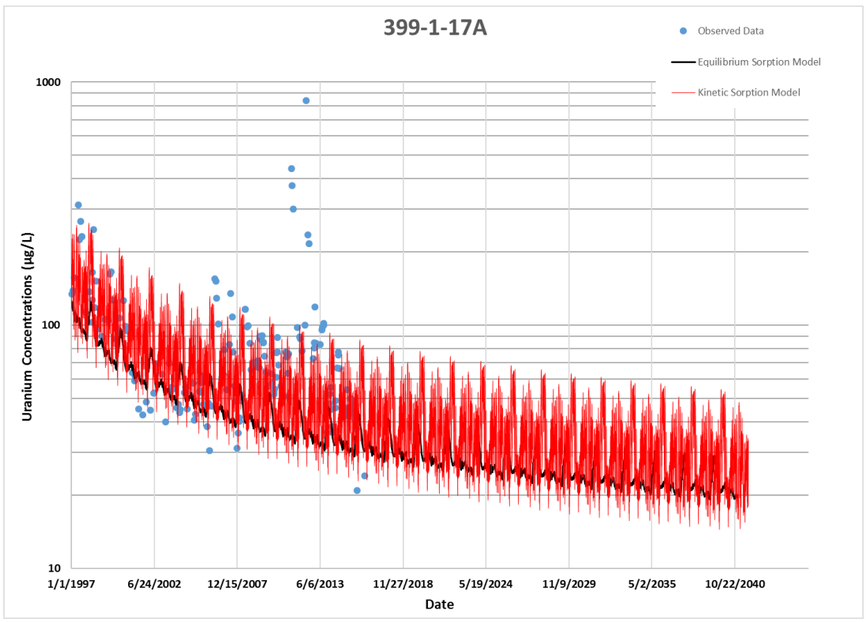

(c)

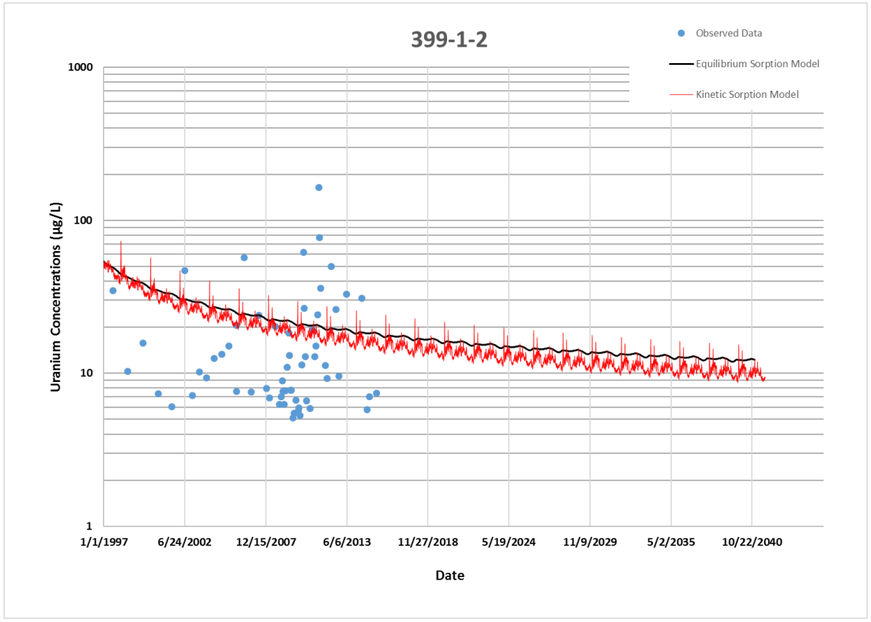

(d)

Figure 7-17. Measured and Simulated Groundwater Uranium Concentrations During the Calibration Period at Wells (a) 399-1-12, (b) 399-1-23, (c) 399-1-17A, (d) 399-1-2, (e) 399-1-7, and (f) 399-2-2¶(page 1 of 2)

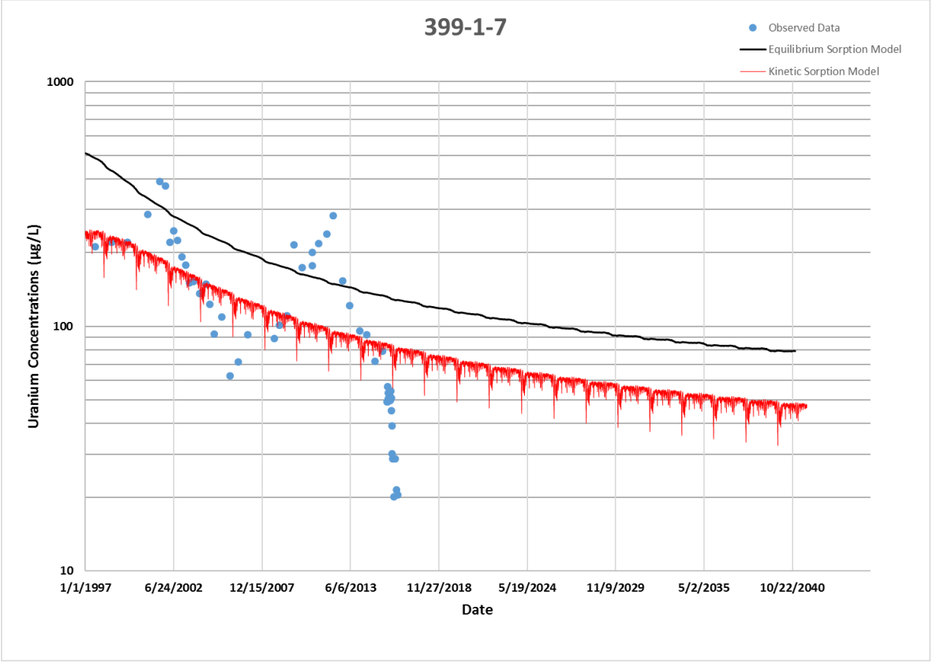

€

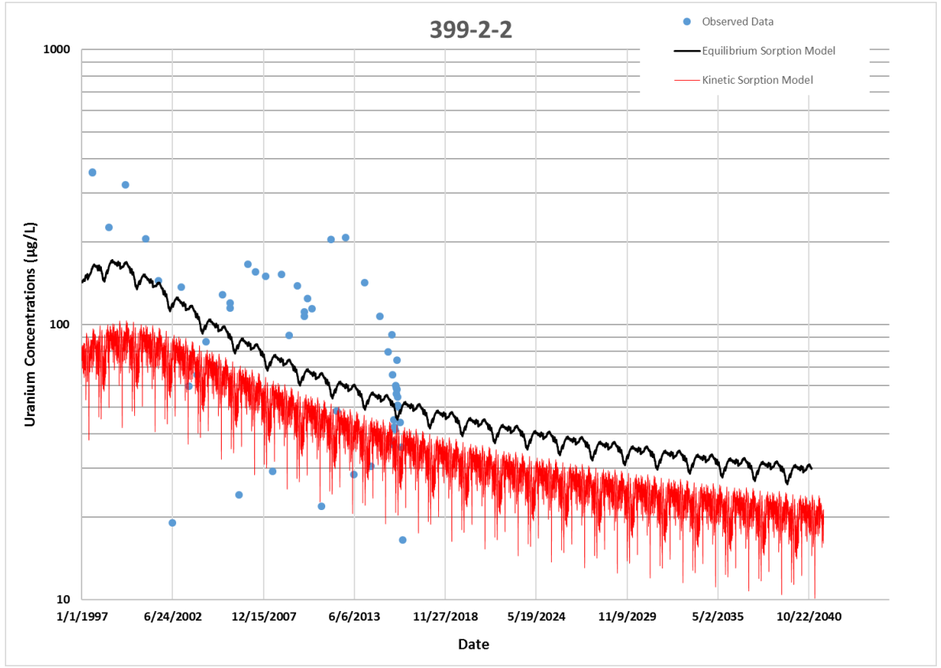

(f)

Figure 7-17. Measured and Simulated Groundwater Uranium Concentrations During the Calibration Period at Wells (a) 399-1-12, (b) 399-1-23, (c) 399-1-17A, (d) 399-1-2, (e) 399-1-7, and (f) 399-2-2 (page 2 of 2)

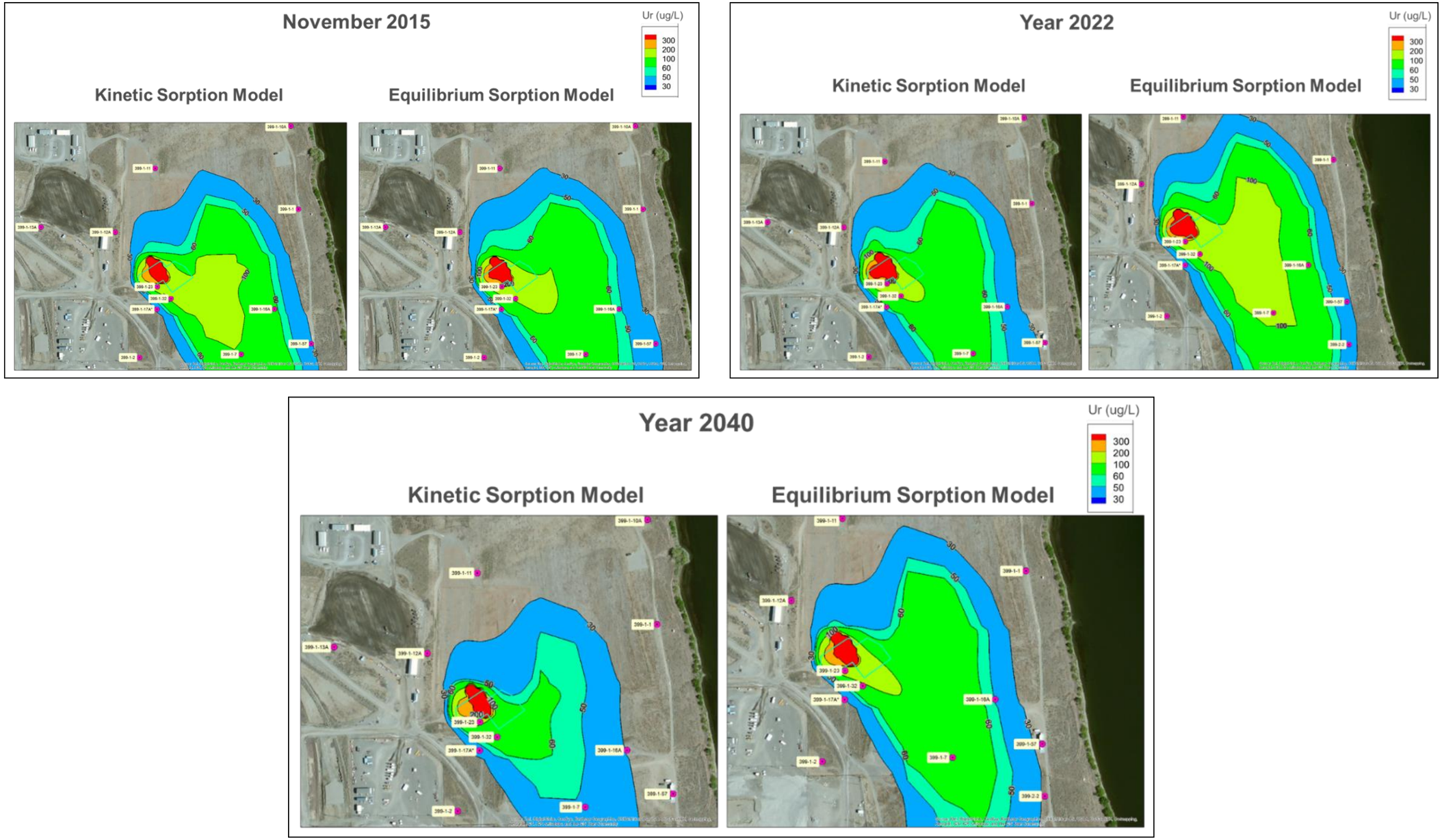

Figure 7-18. Simulated Uranium Plumes in Years 2015, 2022, and 2040 under No Action Scenario

This page intentionally left blank.

7.8.2 Phosphate Transport Modeling During and Post-Treatment Time Periods

Based on information derived from experimental data on phosphate migration and retardation and from observations of phosphate concentrations made during the treatment and post-treatment time periods, modeling of phosphate transport was undertaken. Phosphate injections and infiltration operations were simulated, and phosphate concentrations were compared to the observations made in the PRZ and aquifer wells. The results were used to demonstrate adequacy of parameters for modeling phosphate transport in the vadose zone and aquifer and for projecting concentrations in the aquifer.

Phosphate injection and infiltration were simulated, based on the operational records for Stage A. The rate of injection and infiltration along with timings and locations were consistent with the Stage A operation schedule (Table 6-1). To simulate the infiltration, as a modeling simplification, a constant rate of 212 L/min (56 gal/min) was applied over the first four days of infiltration and 303 L/min (80 gal/min) for the remaining 5 days.

For modeling transport of phosphate, the K_d value within the vadose zone was chosen to be 0.02 mL/g, based on experimental evaluations reported in PNNL-17818, Table 4.2. A 10 times higher value of 0.2 mL/g is applied to the saturated zone based on evaluation of monitoring data on phosphate migration in the aquifer. All other transport parameters (e.g., dispersivity and molecular diffusion) were left unchanged. The simulated phosphate concentrations are compared with the observed data for selected groundwater monitoring wells (Figure 7-19). The simulated plume maps of phosphate in the aquifer are presented in Figure 7-20 for times during the treatment and for the post-treatment time period. For comparison, spatial plume maps are drawn based on available information from monitoring wells at selected times (Figure 7-21), which indicate that high phosphate concentrations persisted in the aquifer even after three weeks following injection. The simulated plume map for November 20, 2015 is compared with the interpolated map, based on the observed data from monitoring wells (Figure 7-22). The black contours in the figure show the simulated results, while other color contours are drawn from the measured phosphate concentration data. The simulated concentration contour of 250 mg/L is spatially located approximately where such concentrations are interpolated based on observations.

An assessment of any changes in aquifer hydraulic properties from phosphate injection/infiltration is provided in Appendix E. Evaluation of observed changes in water levels before and after treatment indicates that no or negligible changes have occurred in the aquifer properties within the Stage A EAA.

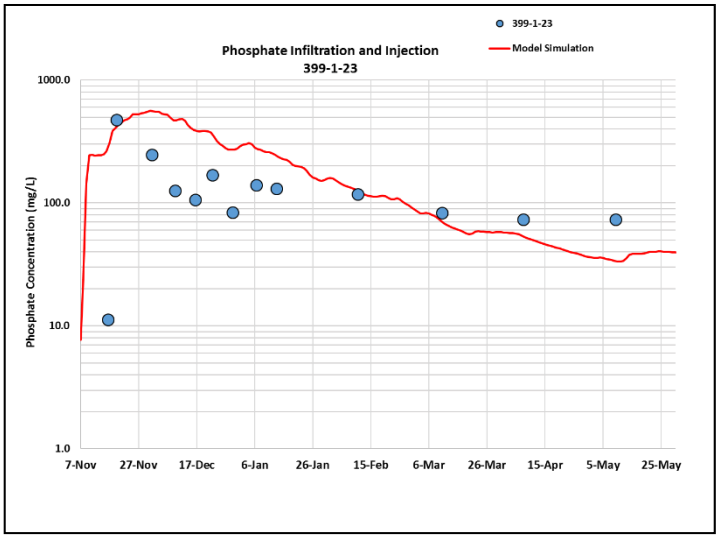

(a)

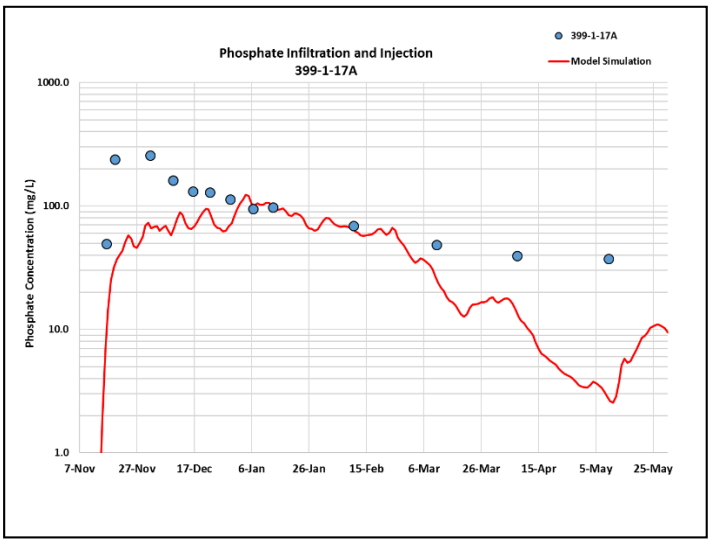

(b)

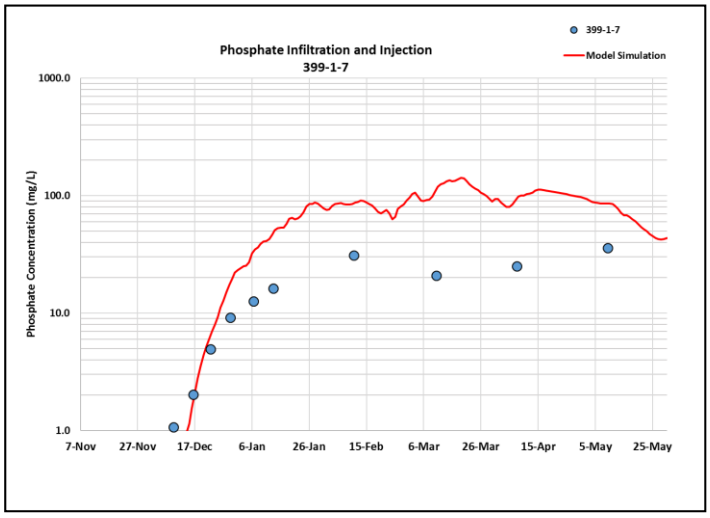

(c)

Figure 7-19. Simulated Phosphate Concentration in Aquifers (a) 399-1-23, (b) 399-1-17A, and (c) 399-1-7

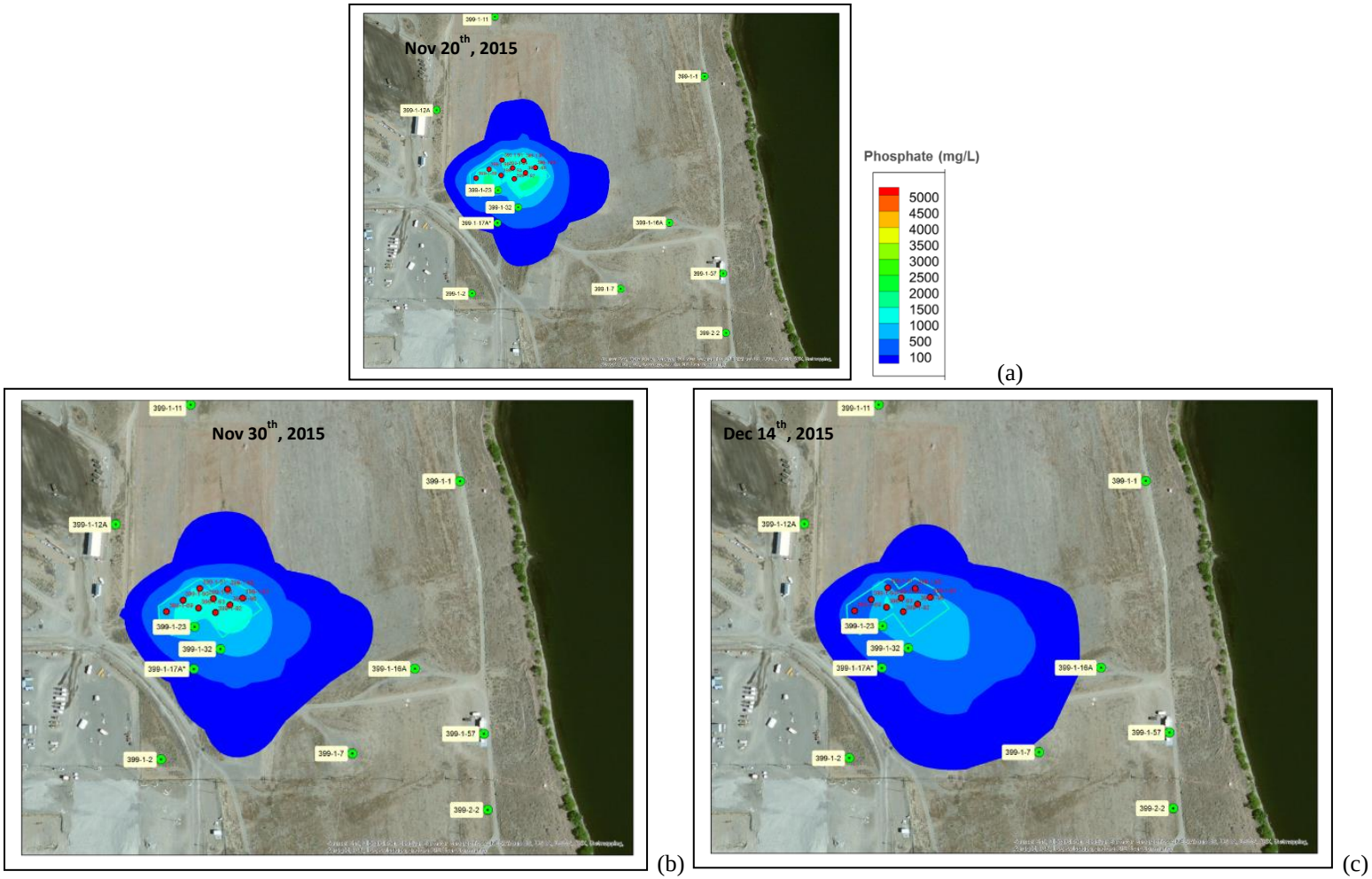

Figure 7-20. Simulated Phosphate Concentration Distribution in the Aquifer for (a) November 20, 2015; (b) November 30, 2015; (c) December 14, 2015; (d) December 20, 2015; (e) December 30, 2015; (f) January 15, 2016; and (g) December 31, 2016¶(page 1 of 2)

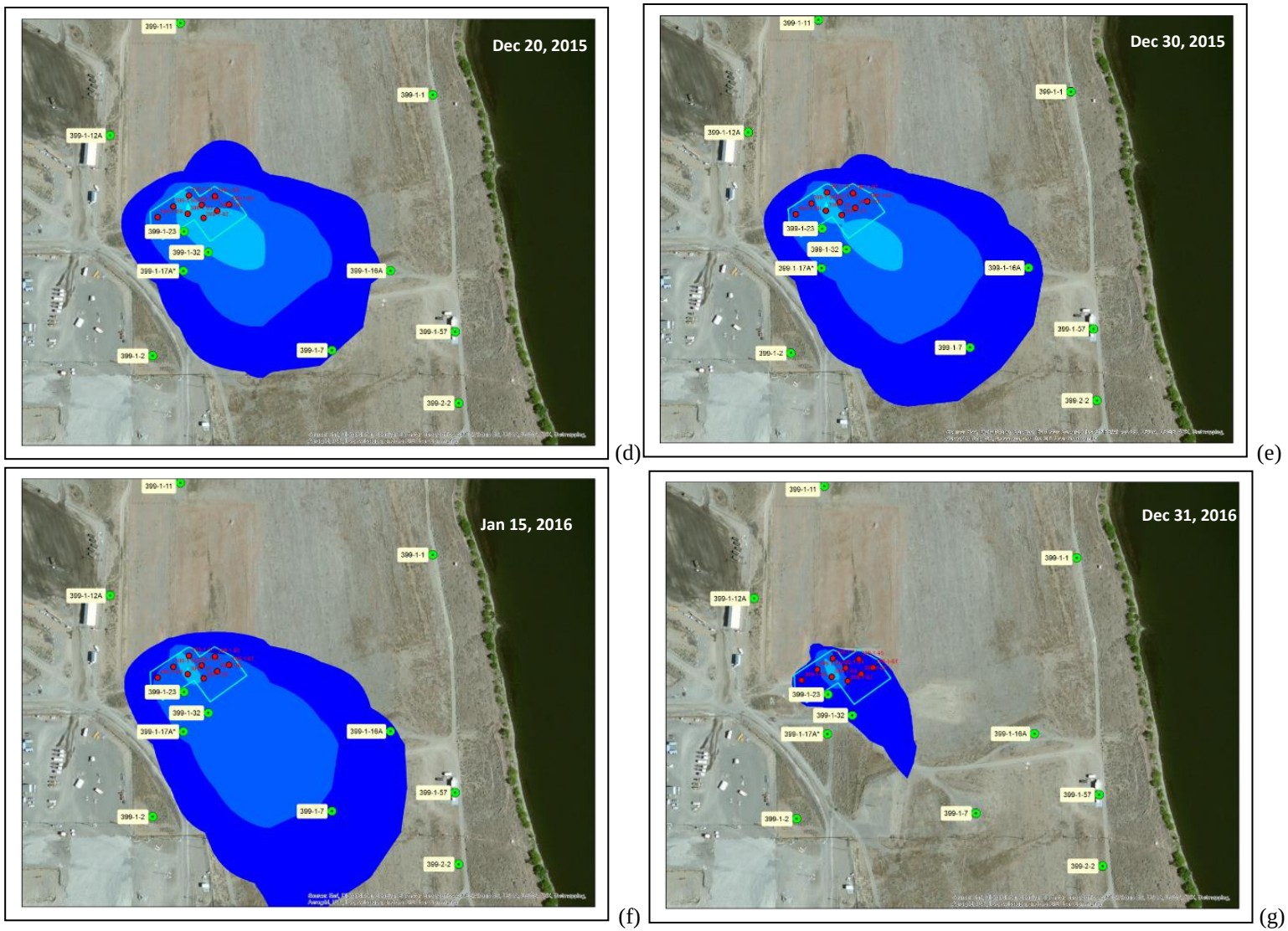

Figure 7-20. Simulated Phosphate Concentration Distribution in the Aquifer for (a) November 20, 2015; (b) November 30, 2015; (c) December 14, 2015; (d) December 20, 2015; (e) December 30, 2015; (f) January 15, 2016; and (g) December 31, 2016 (page 2 of 2)

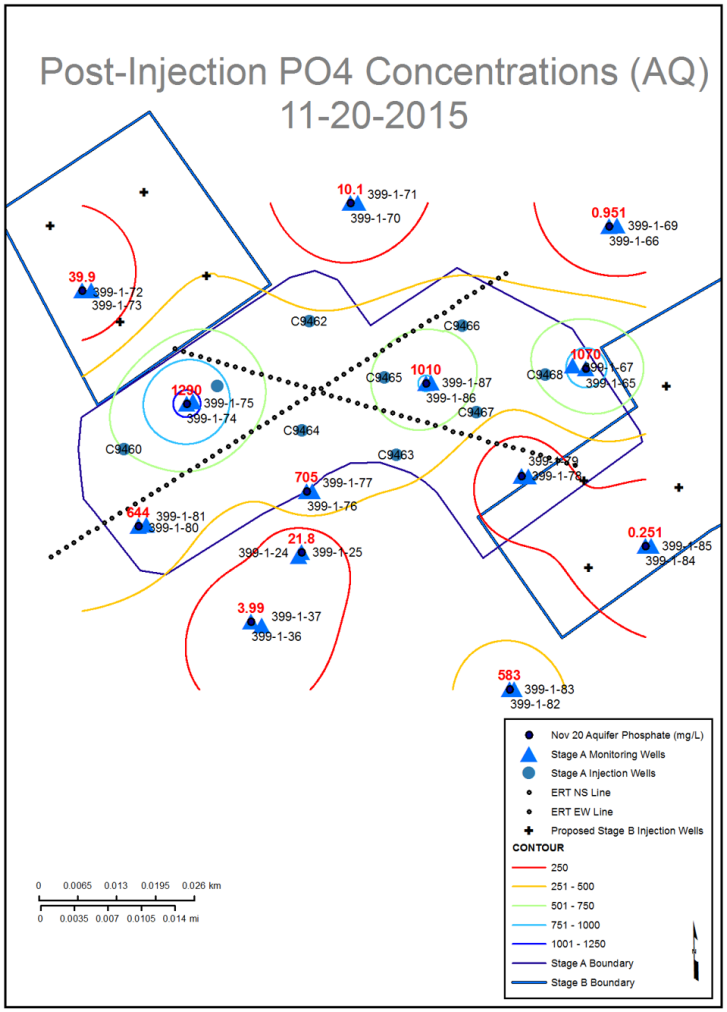

(a)

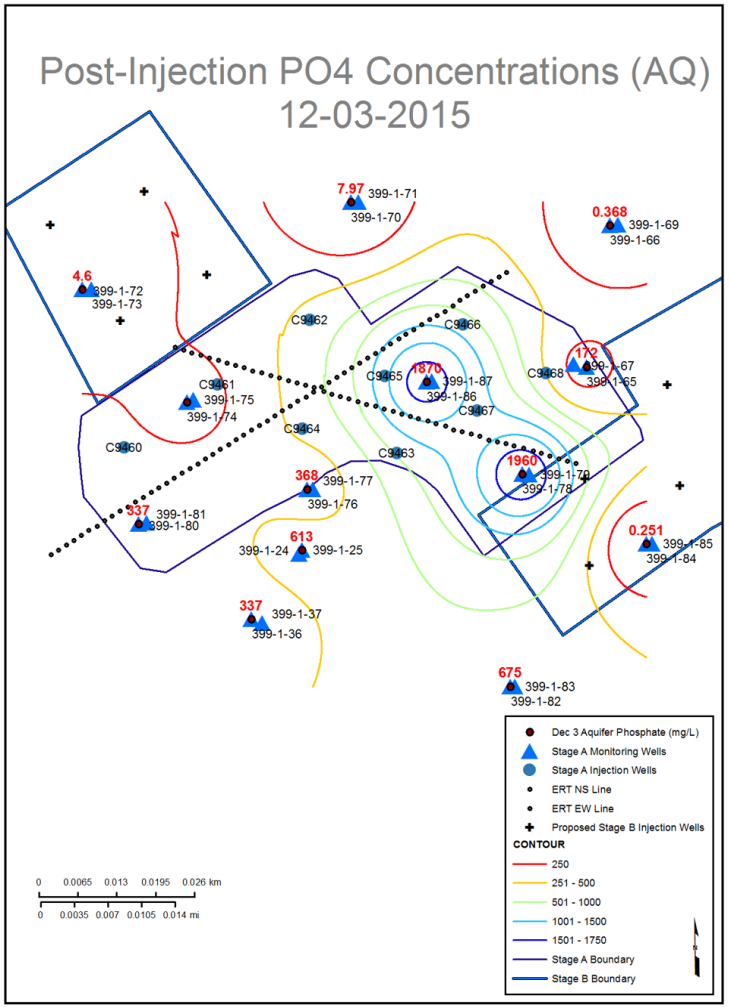

(b)

Figure 7-21. Post-Injection Phosphate Concentrations (mg/L) Contours based on Observations on (a) November 20, 2015; (b) December 3, 2015; (c) December 10, 2015¶(page 1 of 2)

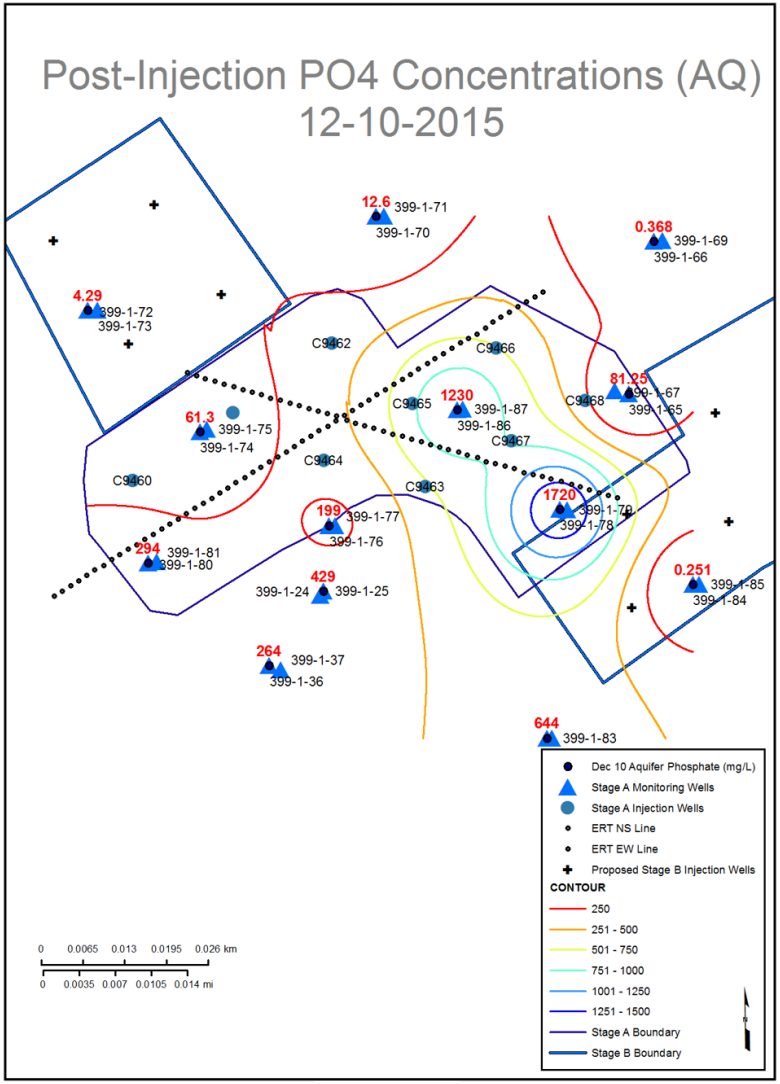

(c)

Figure 7-21. Post-Injection Phosphate Concentrations (mg/L) Contours based on Observations on (a) November 20, 2015; (b) December 3, 2015; (c) December 10, 2015 (page 2 of 2)

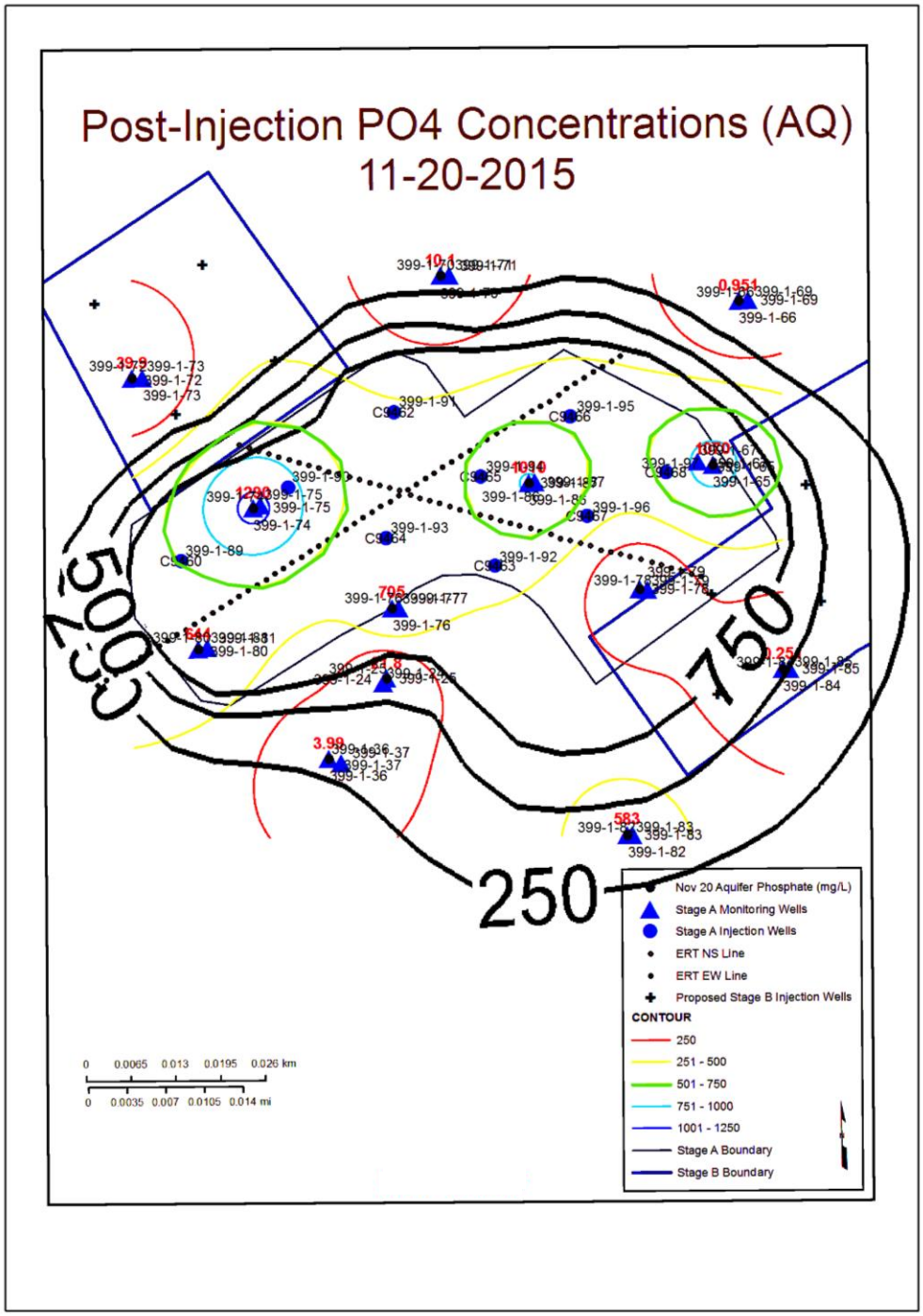

Figure 7-22. Phosphate Concentration (mg/L) Comparison between Model Simulated and Interpolated Data Based on Observations

7.8.3 Uranium Transport Modeling During and Post-Treatment Period

Fate and transport modeling of uranium during and following the phosphate treatment is conducted by simulating the effects of injection and infiltration during the operation period. For this purpose, the kinetic sorption-desorption model was used. Prior to that time, the uranium distribution within the vadose zone and aquifer was based on the pretreatment model results using the kinetic sorption model. During and following the treatment, the backward (desorption) rate constant[2] for kinetic sorption is reduced by factors of 5 and 10 within the Stage A EAA. The choice of reduction factor was based on the following considerations:

1. Flow-through column tests conducted on sediment samples collected from the PRZ, where higher phosphate concentrations were observed, indicated much lower uranium concentrations in the effluent compared to other samples that did not have high phosphate concentrations (see Section 6.3.1.2). A concentration reduction factor of 10 to 100 is noticeable during the leaching tests presented in Figures 6-26 and 6-27.

2. Based on fitting kinetic rate model to the flow-through column experiments (Appendix C) it was observed that the desorption rates are appreciably lower for the samples where phosphate concentrations are higher. In Appendix C.1.3, it is noted that <2 mm size sediment samples B347F1F3 and B347T7 have K_d values that are about factor of 5 to 10 greater than B347P5P8 and B247R1. For the field-textured (bulk) sediment samples, the K_d value for B347T6 is twice that of other two bulk sediment samples (B347R0 and B347P4). The samples showing higher K_d values are located at PRZ depths (Table 6-5) and have higher phosphate concentrations resulting from PRZ injections (and infiltration) as shown in Figure 6-17.

3. PNNL-17818 provides an estimate of the dissolution rate of uranium-rich calcite in the presence and absence of polyphosphate amended solution. Under varying phosphate concentration, the rate of uranium release is maintained at, or below, the minimum rate observed in the absence of aqueous phosphate, regardless of pH. The release rate within the pH range of 6 to 8 for solutions where phosphate is not present is about 10^{-8} mol/m^2/sec but under low to moderate phosphate concentrations (PO_4^{3-} of 10^{-2} mol/L) is typically a factor of 3 to 5 smaller.

4. Concentrations of uranium in the groundwater monitoring wells (e.g., 399-1-23 and 399-1-17A) in the vicinity of Stage A EAA have shown a sharp drop following the treatment (Figure 6-13) and have stayed low for the 6-month monitoring period for which the record currently exists.

The modeling results related to uranium concentrations prior to and following the treatment are shown in the Figure 7-23 and compared to the observed concentrations at wells 399-1-23 and 399-1-17A. The results are presented for model cases where the backward (desorption) kinetic rate constant has been reduced by a factor of 5 and 10 to cover the probable range of uncertainty. The observed concentrations show a sharp decline in uranium concentration immediately following the Stage A treatment but then increase over time. The last three monthly observations indicate establishment of newly equilibrated concentrations that vary within a narrow range. The focus of the modeling is to match these concentrations as they are expected to persist in the aquifer over the near future.

[2] The forward reaction rate constant for kinetic sorption is calculated as the product of K_d, the backward (desorption) rate constant, and the ratio of bulk density to porosity. Increasing the value of K_d by a factor of 5 (or 10), while holding all other parameters constant, has the effect of reducing the backward (desorption) rate constant by a factor of 5 (or 10) compared to the pretreatment value.

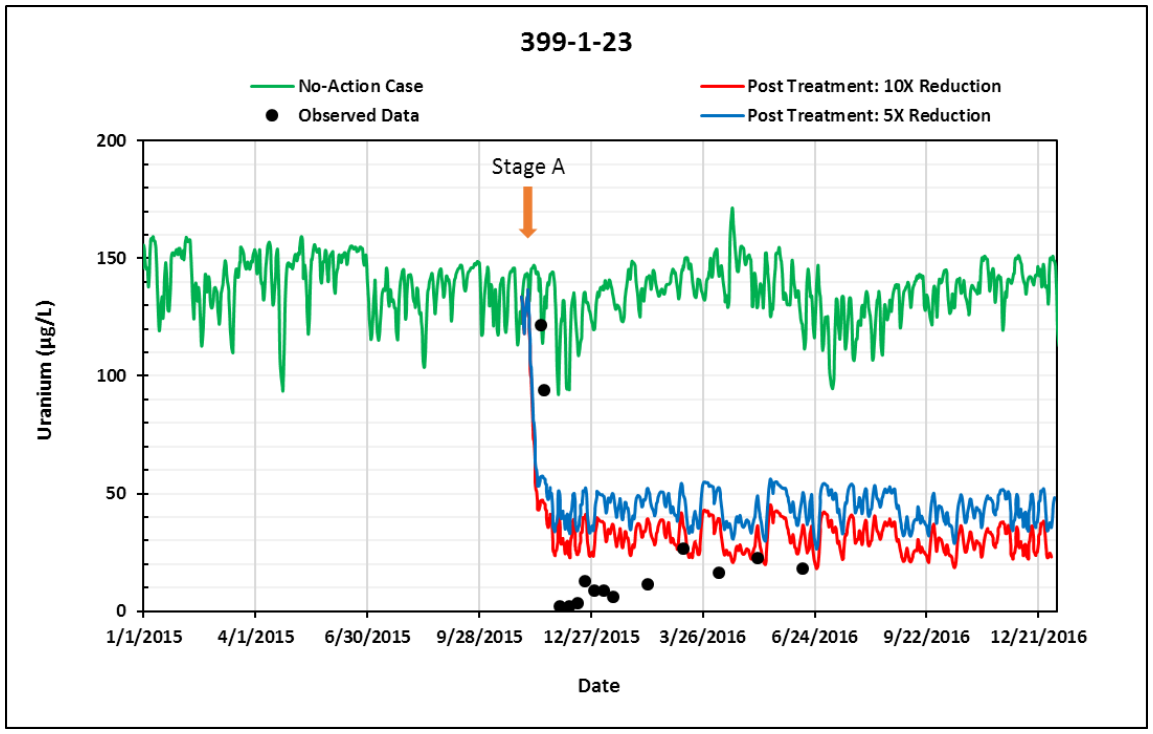

(a)

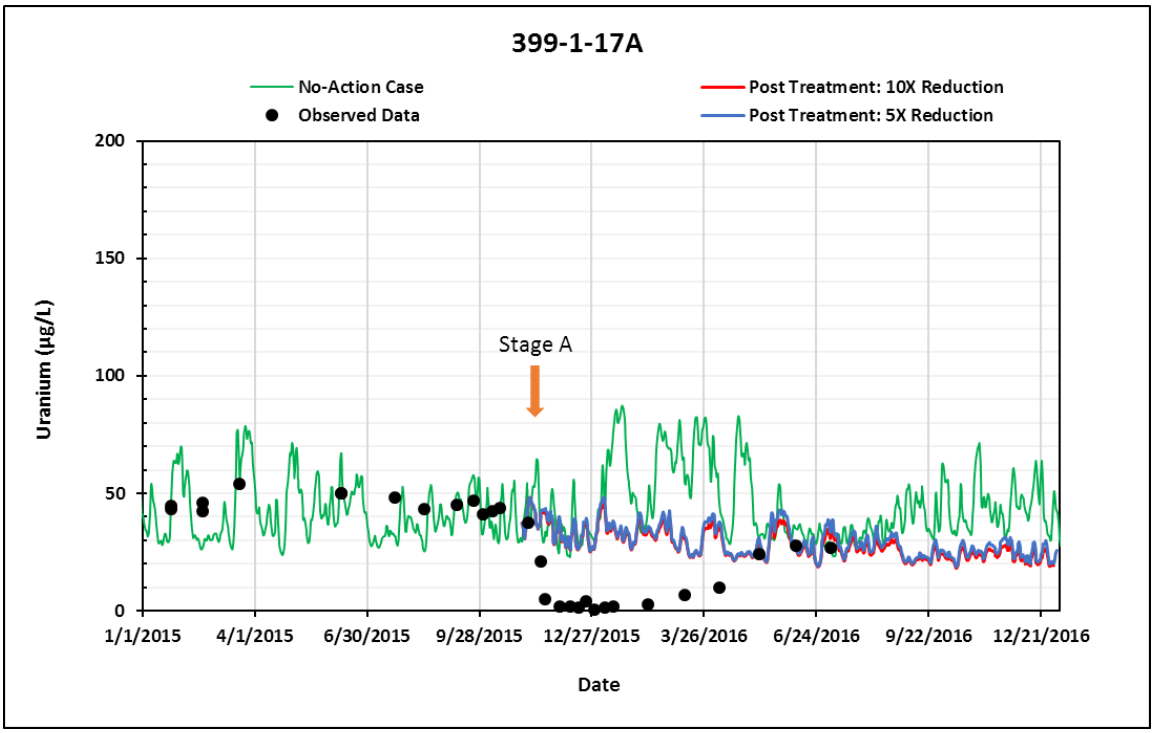

(b)

Figure 7-23. Simulated Uranium Concentrations for (a) 399-1-23 and (b) 399-1-17A Compared to Observed Data Before and Following Treatment

The model predicted results match reasonably well with observed post-treatment uranium concentration trends in the field indicating that the desorption rates have indeed declined within the Stage A area as a result of phosphate injection and infiltration. A factor of 4 to 6 reduction in uranium concentrations is observed between the pretreatment and the post-treatment concentrations at well 399-1-23. This indicates that the remedy implemented for Stage A has been successful. The simulated concentrations in well 399-1-17A following treatment decline less steeply than at wells 399-1-23 because 399-1-17A is located further downgradient of Stage A EAA and, therefore, is influenced by uranium mass from areas outside the Stage A EAA. Nevertheless, some lowering of concentration (up to a factor of 2) along with the change in long-term trend is noticeable.

Figure 7-24 presents the footprint of predicted uranium plume at the end of Year 2016. The model predicts that due to the treatment, the extent of the high concentration uranium plume area in the aquifer has reduced considerably in the Stage A EAA area and remains reduced. This can be seen by comparing and contrasting the plume map under the no action scenario shown in part c of Figure 7-24.

The model setup used for short-term predictions (Figure 7-23) is extended to evaluate long-term uranium concentrations. For this purpose, the post-treatment model parameters are kept unchanged, and the model is exercised to run up to Year 2040. The results are presented in Figure 7-25 for the cases where the backward (desorption) kinetic rate constants are reduced by factors of 5 and 10. These results are compared to the no action case in order to compare the change predicted from phosphate treatment in Stage A EAA. The predictive cases are presented assuming that desorption rates are not going to change over the simulated time period. Due to these assumptions, the uncertainty in these estimates is high and need to be considered when making any decisions based on the model predictions. The long-term simulated concentrations for 399-1-23 show a gradual rise but remain below the no action case. The gradual rise reflects the combined effect of slow continued desorption of uranium into the aquifer from Stage A EAA and contribution to the aquifer from areas outside Stage A. The long-term simulated concentrations for 399-1-17A also continue to remain below the no action case.

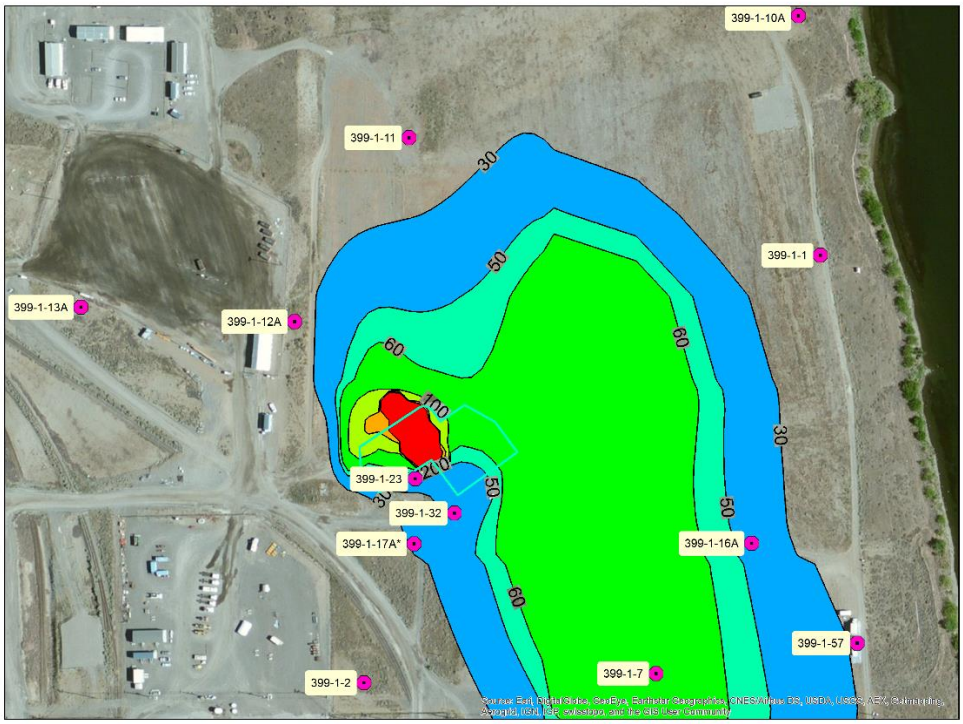

(a)

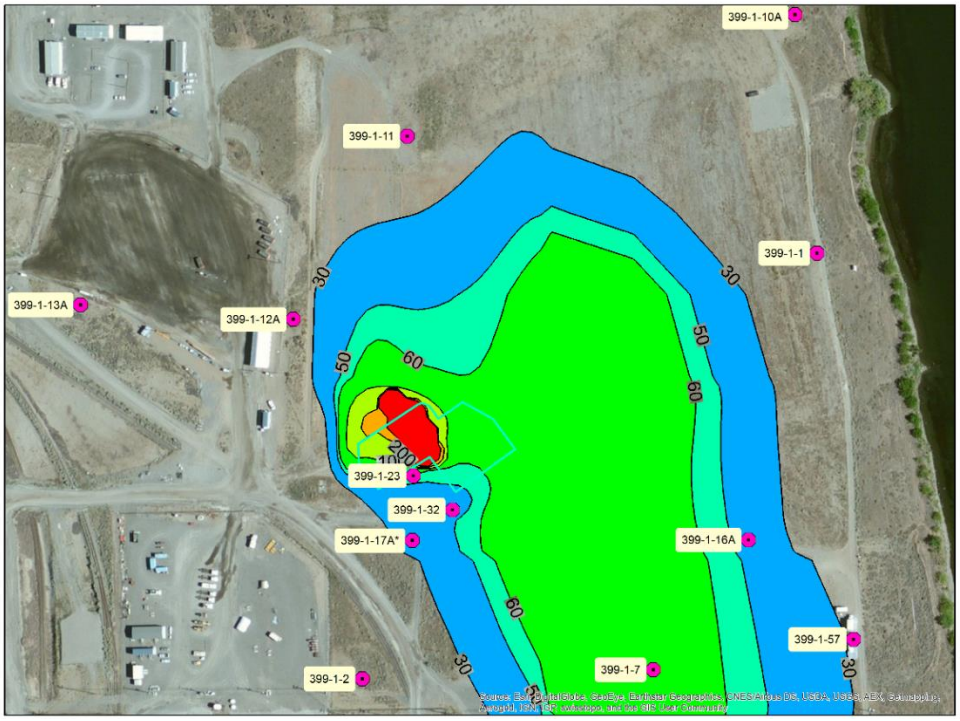

(b)

Figure 7-24. Post-Treatment Simulated Uranium Concentrations at End of December 2016 (a) 10 Times Reduction in Desorption Rate, (b) 5 Times Reduction in Desorption Rates, and (c) No Action Case¶page 1 of 2)

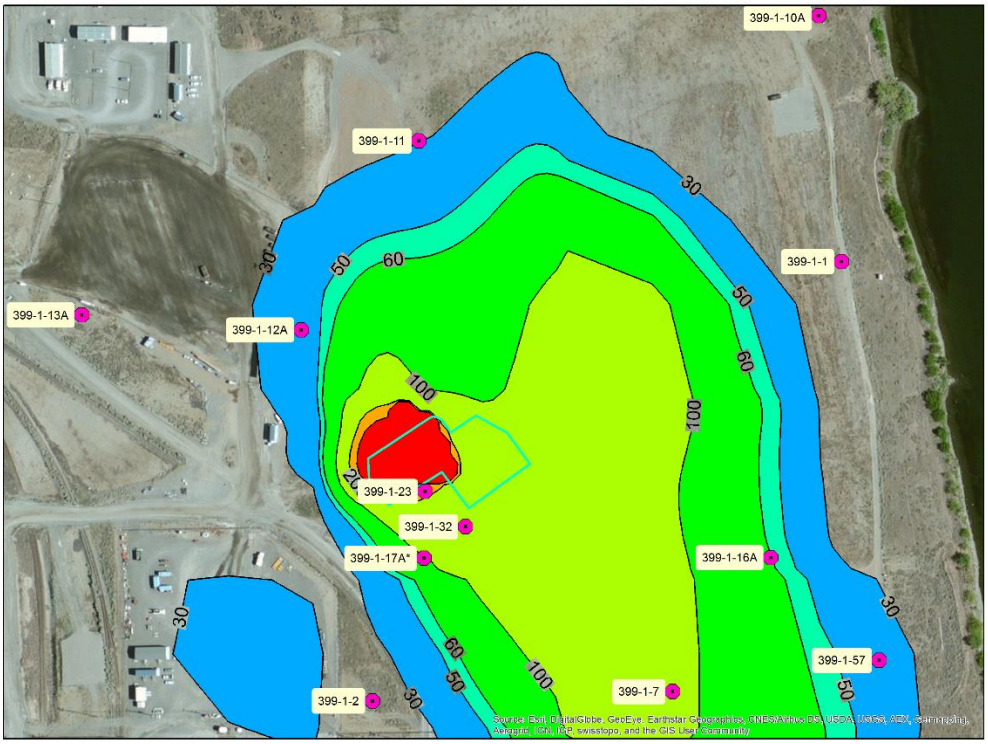

(c)

Figure 7-24. Post-Treatment Simulated Uranium Concentrations at End of December 2016 (a) 10 Times Reduction in Desorption Rate, (b) 5 Times Reduction in Desorption Rates, and (c) No Action Case (page 2 of 2)

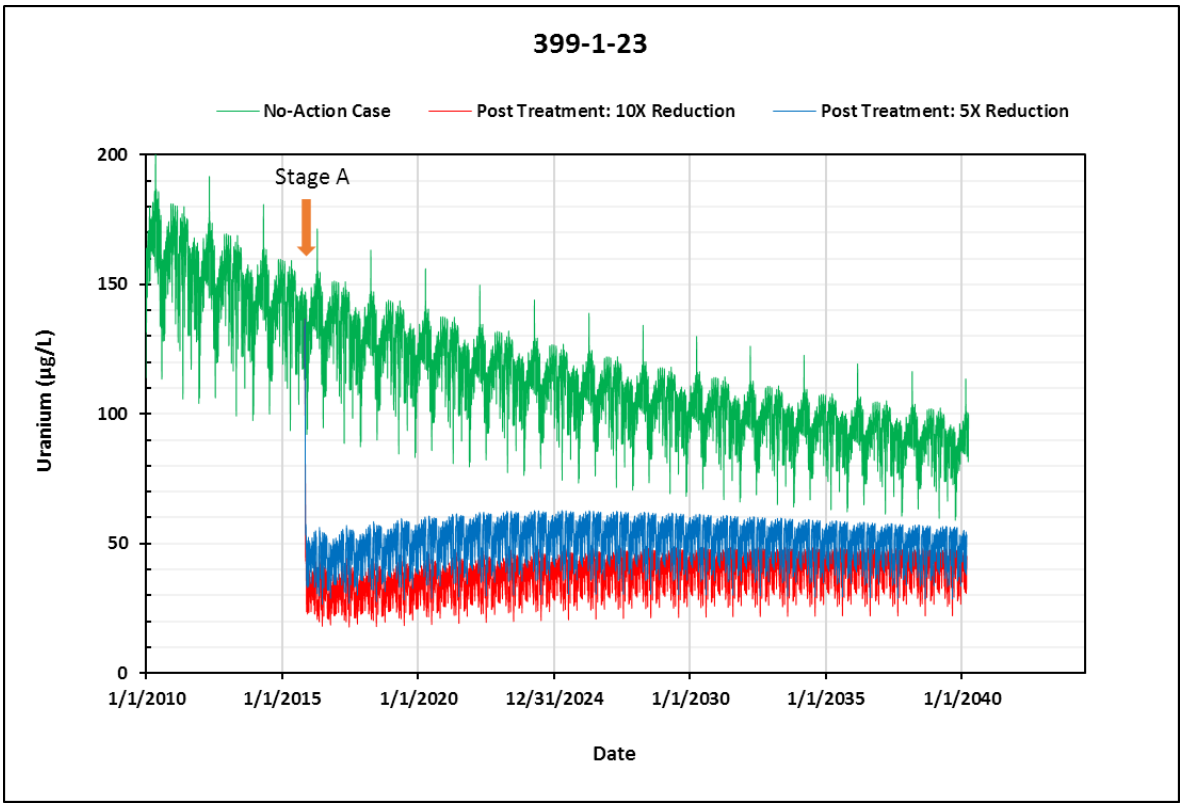

(a)

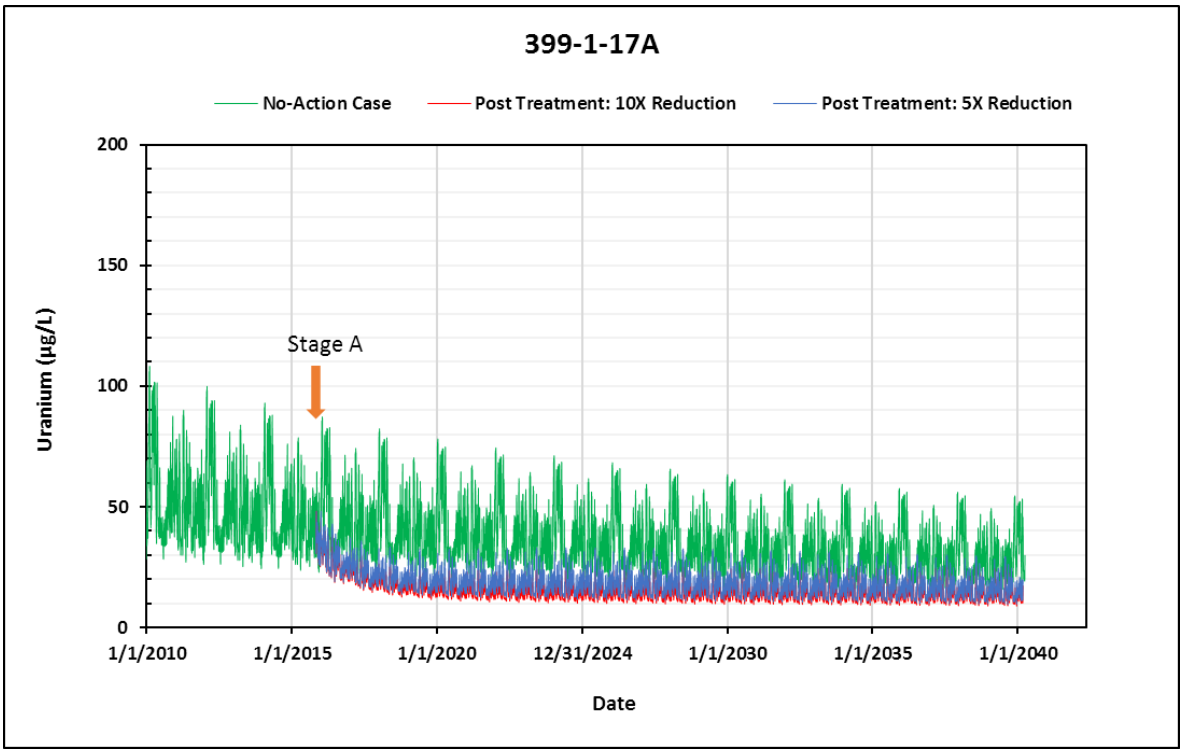

(b)

Figure 7-25. Long-Term Simulated Uranium Concentrations for (a) 399-1-23 and (b) 399-1-17A Comparing the Predicted Post-Treatment Results to the No Action Case

This page intentionally left blank.

8 Conclusions

The desired goal of injection and infiltration in Stage A EAA is to deliver phosphate at high concentrations to the vadose zone and top of the aquifer where uranium is present in the sediments in order to precipitate phosphate bearing mineral phases that can bind labile uranium and sequester it. This report summarizes the information gathered before, during, and post-treatment time periods and synthesizes all of the relevant information for developing a conceptual understanding of the phosphate solution-sediment interactions during and following the treatment.

Reactive-transport modeling was conducted to develop an understanding of the various reactions in the subsurface that lead to sequestration of uranium. For development of predictive fate and transport model, an understanding of the processes governing uranium sequestration is needed, so the proof-of-principle can be sufficiently justified. Geochemical and reactive transport modeling was performed to match the experiments and observations to justify the proof-of-principle. Information gathered from geochemical evaluations of pretreatment and post-treatment soil samples, sequential extraction tests, batch desorption and flow-through column tests, mineral phase analysis, and observations made in the field regarding uranium and phosphate concentrations in groundwater, are all used in developing parameters and conceptual models for conducting fate and transport calculations. A factor of 4 to 6 reduction in uranium concentrations is observed between the pretreatment concentrations and the post-treatment concentrations in the groundwater monitoring wells. This indicates that the remedy implemented for Stage A was successful in sequestering uranium in situ. The longer term predictive calculations indicate that the uranium concentrations will continue to remain below the pre-treatment levels; however, some small gradual increase in concentration over time may occur. However, due to a variety of modeling assumptions (e.g., in situ uranium mass distribution and sorption-desorption characteristics), the longer term predictive uncertainty is high and needs to be considered when making any decisions for Stage B design and implementation.

This page intentionally left blank.

9 References

Brown, James L., 1980, "Calcium Phosphate Precipitation in Aqueous Calcitic Limestone Suspensions," *Journal of Environmental Quality* 9(4):641-644.

CHPRC-00176, 2016, *STOMP Software Management Plan*, Rev. 4, CH2M HILL Plateau Remediation Company, Richland, Washington.

CHPRC-00211, 2016, *STOMP Software Test Plan*, Rev. 3, CH2M HILL Plateau Remediation Company, Richland, Washington.

CHPRC-00222, 2016, *STOMP Functional Requirements Document*, Rev. 2, CH2M HILL Plateau Remediation Company, Richland, Washington.

CHPRC-00269, 2016, *STOMP Requirements Traceability Matrix*, CHPRC Build 5, Rev. 4, CH2M HILL Plateau Remediation Company, Richland, Washington.

CHPRC-00515, 2016, *STOMP Acceptance Test Report*, CHPRC Build 5, Rev. 4, CH2M HILL Plateau Remediation Company, Richland, Washington.

CHPRC-01874, 2016, *The Geochemist's Workbench Integrated Software Management Plan Version 11.0.3*, Rev. 2, CH2M HILL Plateau Remediation Company, Richland, Washington.

DOE/RL-2009-30, 2010, *300 Area Decision Unit Remedial Investigation/Feasibility Study Work Plan for the 300-FF-1, 300-FF-2, and 300-FF-5 Operable Units*, Rev. 0, U.S. Department of Energy, Richland Operations Office, Richland, Washington. Available at: http://pdw.hanford.gov/arpir/index.cfm/viewDoc?accession=0084376.

DOE/RL-2011-50, 2012, *Regulatory Basis and Implementation of a Graded Approach to Evaluation of Groundwater Protection*, Rev. 1, U.S. Department of Energy, Richland Operations Office, Richland, Washington. Available at: http://pdw.hanford.gov/arpir/index.cfm/viewDoc?accession=0093361.

DOE/RL-2014-13, 2015, *Integrated Remedial Design Report/Remedial Action Work Plan for the 300 Area (300-FF-1, 300-FF-2 & 300-FF-5 Operable Units)*, Rev. 0, U.S. Department of Energy, Richland Operations Office, Richland, Washington. Available at: http://pdw.hanford.gov/arpir/index.cfm/viewDoc?accession=0081153H.

DOE/RL-2014-13-ADD2, 2015, *Remedial Design Report/Remedial Action Work Plan Addendum for the 300 Area Groundwater*, Rev. 0, U.S. Department of Energy, Richland Operations Office, Richland, Washington. Available at: http://pdw.hanford.gov/arpir/index.cfm/viewDoc?accession=0081151H.

DOE/RL-2014-42, 2015, *300-FF-5 Operable Unit Remedy Implementation Sampling and Analysis Plan*, Rev. 0, U.S. Department of Energy, Richland Operations Office, Richland, Washington. Available at: http://pdw.hanford.gov/arpir/index.cfm/viewDoc?accession=0079669H.

ECF-300FF5-11-0151, 2012, *Groundwater Flow and Uranium Transport Modeling in Support of the 300 Area FF-5 RI/FS*, Rev. 3, CH2M HILL Plateau Remediation Company, Richland, Washington. Available at: http://pdw.hanford.gov/arpir/index.cfm/viewDoc?accession=0078650H.

ECF-300FF5-15-0014, 2015, *Determination of Vadose Zone Uranium Concentration Distribution Extents and Establishment of the Stage A Enhanced Attenuation Area for 300-FF-5*, Rev. 0, CH2M HILL Plateau Remediation Company, Richland, Washington.

ECF-300FF5-16-0087, 2016, *Determination of Vadose Zone Uranium Concentration Distribution Extents and Development of a Three-Dimensional Geologic Framework Model for the 300-FF-5 Operable Unit, Hanford, Washington*, Rev. 0, CH2M HILL Plateau Remediation Company, Richland, Washington.

ECF-HANFORD-13-0029, 2015, *Development of the Hanford South Geologic Framework Model, Hanford Site Washington*, Rev. 2, CH2M HILL Plateau Remediation Company, Richland, Washington.

EPA and DOE, 2013, *Hanford Site 300 Area Record of Decision for 300-FF-2 and 300-FF-5, and Record of Decision Amendment for 300-FF-1*, U.S. Environmental Protection Agency and U.S. Department of Energy, Richland, Washington, Richland, Washington. Available at: http://pdw.hanford.gov/arpir/index.cfm/viewDoc?accession=0087180.

Fritz, Brad G. and Evan V. Arntzen, 2007, "Effect of Rapidly Changing River Stage on Uranium Flux through the Hyporheic Zone," *Ground Water* 45(6):753-760. Available at: http://info.ngwa.org/GWOL/pdf/072682493.pdf.

Kohler, M., G.P. Curtis, D.E. Meece, and J.A. Davis, 2004, "Methods for Estimating Adsorbed Uranium(VI) and Distribution Coefficients of Contaminated Sediments," *Environ. Sci. Technol*. 38(1):240-247. Available at: http://pubs.acs.org/doi/pdf/10.1021/es0341236.

Liu, Chongxuan, John M. Zachara, Nikolla P. Qafoku, and Zheming Wang, 2008, "Scale-dependent desorption of uranium from contaminated subsurface sediments," *Water Resources Research* 44:13 pp. Available at: http://digitalcommons.unl.edu/cgi/viewcontent.cgi?article=1304&context=usdoepub.

Lutz, J.F., R.A. Pinto, R. Garcia-Lagos, and H.G. Hilton, 1966, "Effect of Phosphorus on Some Physical Properties of Soils: II. Water Retention," *Soil Sci. Soc. Amer. Proc*. 30(4):433-437.

Ma, R., C. Zheng, H. Prommer, J. Greskowiak, C. Liu, J. Zachara, and M. Rockhold, 2010, "A field-scale reactive transport model for U(VI) migration influenced by coupled multirate mass transfer and surface complexation reactions," *Water Resources Research* 46(5):1-17

Mehta, V. S., F. Maillot, Z. Wang, J.G. Catalano, and D.E. Giammar, 2016, "Effect of Reaction Pathway on the Extent and Mechanism of Uranium(VI) Immobilization with Calcium and Phosphate," *Environmental Science & Technology* 50:3128-3136.

Mualem, Yechezkel, 1976, "A New Model for Predicting the Hydraulic Conductivity of Unsaturated Porous Media," *Water Resources Research* 12(3):513-522. Available at: https://hwbdocuments.env.nm.gov/Los%20Alamos%20National%20Labs/TA%2054/11570.pdf.

NUREG/CR-6940, 2007, *Combined Estimation of Hydrogeologic Conceptual Model, Parameter, and Scenario Uncertainty with Application to Uranium Transport at the Hanford Site 300 Area*, PNNL-16396, U.S. Nuclear Regulatory Commission, Washington, D.C. Available at: http://www.pnl.gov/main/publications/external/technical_reports/PNNL-16396.pdf.

PNL-6716, 1988, *Interim Characterization Report for the 300 Area Process Trenches*, Pacific Northwest Laboratory, Richland, Washington. Available at: http://www.osti.gov/energycitations/servlets/purl/6676561-CQApoo/.

PNL-10285, 1995, *Estimated Recharge Rates at the Hanford Site*, Pacific Northwest Laboratory, Richland, Washington. Available at: http://www.osti.gov/scitech/servlets/purl/10122247.

PNNL-11216, 1997, *STOMP Subsurface Transport Over Multiple Phases Application Guide*, Pacific Northwest National Laboratory, Richland, Washington. Available at: http://stomp.pnl.gov/documentation/application.pdf.

PNNL-12030, 2000, *STOMP Subsurface Transport Over Multiple Phases Version 2.0 Theory Guide*, Pacific Northwest National Laboratory, Richland, Washington. Available at: http://stomp.pnl.gov/documentation/theory.pdf.

PNNL-14022, 2002, *300 Area Uranium Leach and Absorption Project*, Pacific Northwest National Laboratory, Richland, Washington. Available at: http://www.pnl.gov/main/publications/external/technical_reports/PNNL-14022.pdf.

PNNL-14702, 2006, *Vadose Zone Hydrogeology Data Package for Hanford Assessments*, Rev. 1, Pacific Northwest National Laboratory, Richland, Washington. Available at: http://www.pnl.gov/main/publications/external/technical_reports/PNNL-14702rev1.pdf

PNNL-15782, 2006, *STOMP Subsurface Transport Over Multiple Phases Version 4.0 User's Guide*, Pacific Northwest National Laboratory, Richland, Washington. Available at: http://stomp.pnl.gov/documentation/userguide.pdf.

PNNL-17708, 2008, *Three-Dimensional Groundwater Models of the 300 Area at the Hanford Site, Washington State*, Pacific Northwest National Laboratory, Richland, Washington. Available at: http://www.pnl.gov/main/publications/external/technical_reports/PNNL-17708.pdf.

PNNL-17818, 2008, *300 Area Treatability Test: Laboratory Development of Polyphosphate Remediation Technology for In Situ Treatment of Uranium Contamination in the Vadose Zone and Capillary Fringe*, Pacific Northwest National Laboratory, Richland, Washington. Available at: http://www.pnl.gov/main/publications/external/technical_reports/PNNL-17818.pdf.

PNNL-18303, 2009, *Sequestration of Sr-90 Subsurface Contamination in the Hanford 100-N Area by Surface Infiltration of a Ca-Citrate-Phosphate Solution*, Pacific Northwest National Laboratory, Richland, Washington. Available at: http://www.pnl.gov/main/publications/external/technical_reports/PNNL-18303.pdf.

PNNL-18564, 2009, *Selection and Traceability of Parameters to Support Hanford-Specific RESRAD Analyses: Fiscal Year 2008 Status Report*, Pacific Northwest National Laboratory, Richland, Washington. Available at: http://www.pnl.gov/main/publications/external/technical_reports/PNNL-18564.pdf.

PNNL-20004, 2010, *Remediation of Uranium in the Hanford Vadose Zone Using Ammonia Gas: FY 2010 Laboratory-Scale Experiments*, Pacific Northwest National Laboratory, Richland, Washington. Available at: http://www.pnl.gov/main/publications/external/technical_reports/PNNL-20004.pdf.

PNNL-21733, 2012, *Use of Polyphosphate to Decrease Uranium Leaching in Hanford 300 Area Smear Zone Sediment*, Pacific Northwest National Laboratory, Richland, Washington. Available at: http://www.pnnl.gov/main/publications/external/technical_reports/PNNL-21733.pdf.

PNNL-22048, 2012, *Updated Conceptual Model for the 300 Area Uranium Groundwater Plume*, Pacific Northwest National Laboratory, Richland, Washington. Available at: http://www.pnnl.gov/main/publications/external/technical_reports/PNNL-22048.pdf.

PNNL-22886, 2013, *System-Scale Model of Aquifer, Vadose Zone, and River Interactions for the Hanford 300 Area –Application to Uranium Reactive Transport*, Pacific Northwest National Laboratory, Richland, Washington. Available at: http://www.pnnl.gov/main/publications/external/technical_reports/PNNL-22886.pdf.

PNNL-24911, 2015, *Analytical Data Report for Sediment Samples Collected From 300-FF-5 OU, Wells C8940 and C9451*, Pacific Northwest National Laboratory, Richland, Washington.

PNNL-25420, 2016, *Analytical Data Report for Sediment Samples Collected from 300-FF-5: Boreholes C9580, C9581, and C9582*, Pacific Northwest National Laboratory, Richland, Washington.

PNNL-SA-25232, 2016, *Stage A Uranium Sequestration Amendment Delivery Monitoring Using Time-Lapse Electrical Resistivity Tomography*, Pacific Northwest National Laboratory, Richland, Washington.

PNNL-SA-58541, 2007, *Uranium(VI) Release from Contaminated Vadose Zone Sediments: Estimation of Potential Contributions from Dissolution and Desorption*, U.S. Geological Survey, Menlo Park, California and Pacific Northwest National Laboratory, Richland, Washington. Available at: http://ifchanford.pnnl.gov/pdfs/bond_zachara_58541.pdf.

SGW-58830, 2015, *300-FF-5 Supplemental Post-ROD Field Investigation Summary*, Rev. 0, CH2M HILL Plateau Remediation Company, Richland, Washington. Available at: http://pdw.hanford.gov/arpir/index.cfm/viewDoc?accession=0079681H.

SGW-58976, 2015, *Field Instructions for Uranium Sequestration in the 300 Area*, Rev. 0, CH2M HILL Plateau Remediation Company, Richland, Washington. Available at: http://pdw.hanford.gov/arpir/index.cfm/viewDoc?accession=0078185H.

SGW-59455, 2016, *300-FF-5 Operable Unit Stage A Uranium Sequestration System Installation Report*, Rev. 0, CH2M HILL Plateau Remediation Company, Richland, Washington. Available at: http://pdw.hanford.gov/arpir/index.cfm/viewDoc?accession=0077730H.

Shi, Z., C. Liu, J. M. Zachara, Z. Wang, and B. Deng, 2009, "Inhibition Effect of Secondary Phosphate Mineral Precipitation on Uranium Release from Contaminated Sediments," *Environmental Science & Technology* 43:8344-8349.

Sumner, M.E., 2000, "Soil Fertility and Plant Nutrition," *Handbook of Soil Science*, CRC Press, Boca Raton, Florida.

van Genuchten, M.Th., 1980, "A Closed-form Equation for Predicting the Hydraulic Conductivity of Unsaturated Soils," *Soil Sci. Soc. Am. J.* 44(5):892-898. Available at: http://people.ucalgary.ca/~hayashi/glgy607/reading/van_Genuchten1980.pdf.

Wellman, Dawn M., Eric M. Pierce, and Michelle M. Valenta, 2007, "Efficacy of soluble sodium tripolyphosphate amendments for the in-situ immobilisation of uranium," *Environ. Chem.* 4(5):293-300.

WHC-SD-EN-TI-052, 1992, *Phase I Hydrogeologic Summary of the 300-FF-5 Operable Unit, 300 Area*, Rev. 0, Westinghouse Hanford Company, Richland, Washington. Available at: http://pdw.hanford.gov/arpir/index.cfm/viewDoc?accession=D196121502.

Xu, Moujin and Yoram Eckstein, 1995, "Use of Weighted Least-Squares Method in Evaluation of the Relationship Between Dispersivity and Field Scale," *Ground Water* 33(6):905-908. Available at: http://info.ngwa.org/gwol/pdf/952964066.PDF.

Yabusaki, Steven B., Yilin Fang, and Scott R. Waichler, 2008, "Building conceptual models of field-scale uranium reactive transport in a dynamic vadose zone-aquifer-river system," *Water Resources Research* 44(12):24 pp. Available at: http://onlinelibrary.wiley.com/doi/10.1029/2007WR006617/pdf.

This page intentionally left blank.

Appendix A

Presentation of Sampling Data for Selected Wells

This page intentionally left blank.

Terms

EAA	Enhanced Attenuation Area
PRZ	periodically rewetted zone

This page intentionally left blank.

A1 Presentation of Sampling Data for Selected Wells

In this appendix, several indicators are examined to provide information about how dissolved uranium concentrations have been affected by phosphate injection and infiltration. The following results are presented for selected well pairs:

- Phosphate to bicarbonate molar ratio compared to pH
- Concentration of uranium compared to the concentration of calcium
- Concentration of uranium compared to the concentration of phosphate
- Concentration of calcium compared to the concentration of phosphate
- Calcium/sodium ratio in milliequivalents per liter compared to pH

These comparisons are examined at three pairs of wells (399-1-65 and 399-1-67; 399-1-74 and 399-1-75; and 399-1-80 and 399-1-81); each pair consists of a well screened in the periodically rewetted zone (PRZ) and a well screened in the aquifer (Figure A-1). Two wells that are not part of a vadose zone/aquifer pairing but are just in the aquifer are also considered. The unpaired wells (399-1-23 and 399-1-17A) are located outside the Stage A Enhanced Attenuation Area (EAA) (see Chapter 6 [Figure 6-12a] in the main text of this calculation for location).

Most wells were measured once, at the beginning of September, but these samples have been omitted for ease of viewing. However, they do offer some insight into the background values. The data from these wells show that for all the sites, the background ratio of PO_4:HCO_3 is fairly low—typically on the order of ~0.001. At the time sampling of these wells ceased (after treatment), all of the wells had much higher PO_4:HCO_3 values, even if the values were declining.

A1.1 Phosphate to Bicarbonate Ratio Compared to pH

Figures A-2 through A-5 show a comparison of the phosphate to bicarbonate ratio to pH. The higher the ratio, the more phosphate there is relative to bicarbonate in the PRZ and groundwater. The greater the ratio of phosphate to bicarbonate, conditions for uranium bonding to phosphate are more favorable.

A1.2 Uranium Concentration Compared to Calcium Concentration

Figures A-6 through A-8 show a comparison of the uranium concentrations against the calcium concentrations for selected wells. The calcium concentrations in the PRZ wells show an increase as the uranium is being released indicating simultaneous ion exchange reactions. This indicates that favorable conditions are being created for reaction of calcium with incoming phosphate.

A1.3 Uranium Concentration Compared to Phosphate Concentration

Figures A-10 through A-13 show the concentrations of uranium and phosphate for the selected wells. Uranium breakthrough resulting from infiltration occurs earlier while phosphate concentrations remain low throughout that period. Phosphate concentrations increase following injections in the PRZ and aquifer. In the aquifer wells located outside the Stage A EAA (Figure A-13), the uranium concentrations show a steep drop, followed by a slow rebound which ends at a lower concentration than it began. The decline in uranium concentrations correspond with the increasing phosphate concentrations. Well 1-23 is missing the preinjection baseline data, but Well 1-17A starts out with a fairly high baseline uranium value before the rapid dropoff and gradual rebound. The phosphate data show a definite peak during uranium's lowest point.

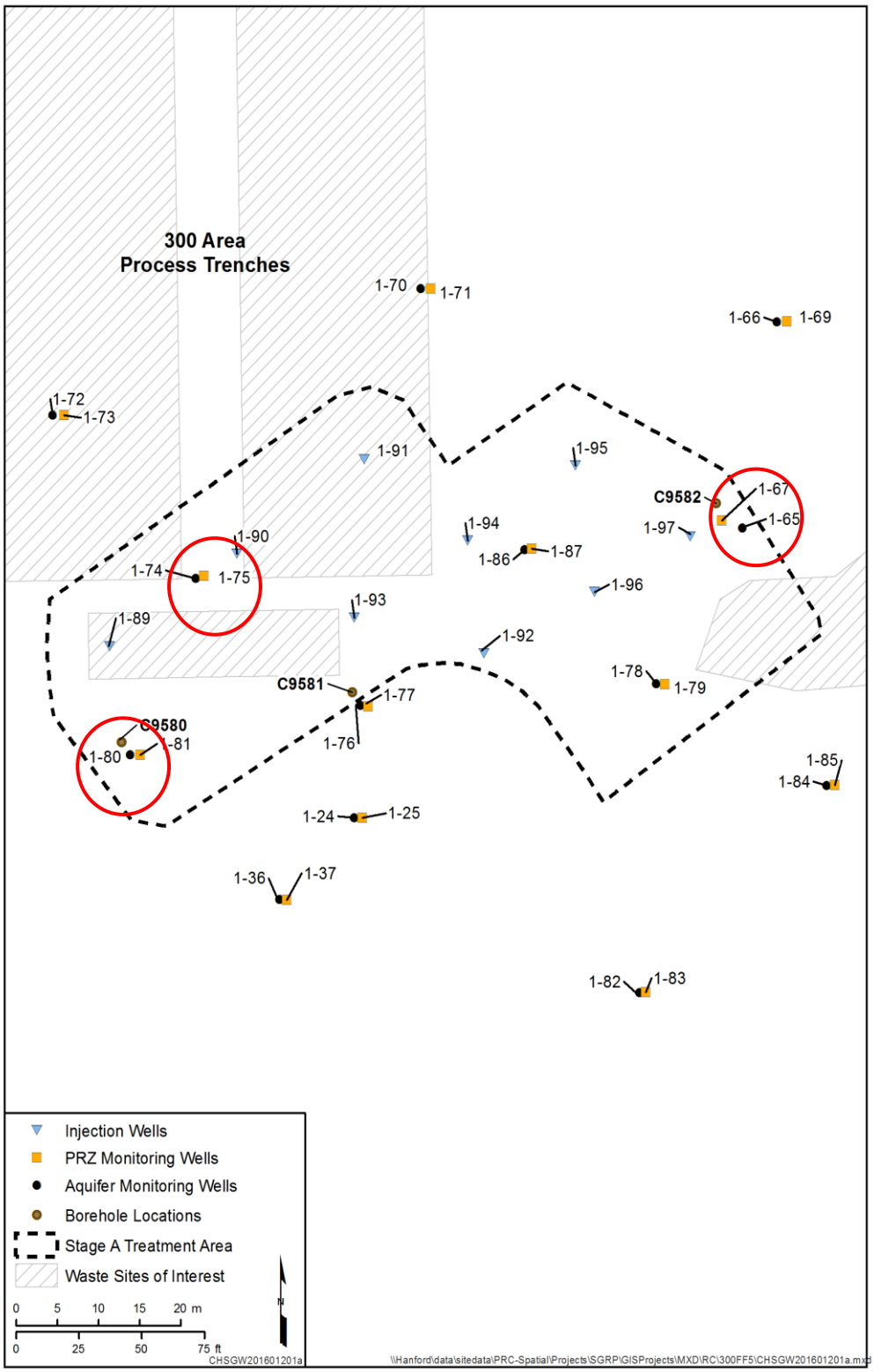

Figure A-1. Locations of Paired Vadose Zone Wells (PRZ Monitoring Wells) and Aquifer Monitoring Wells

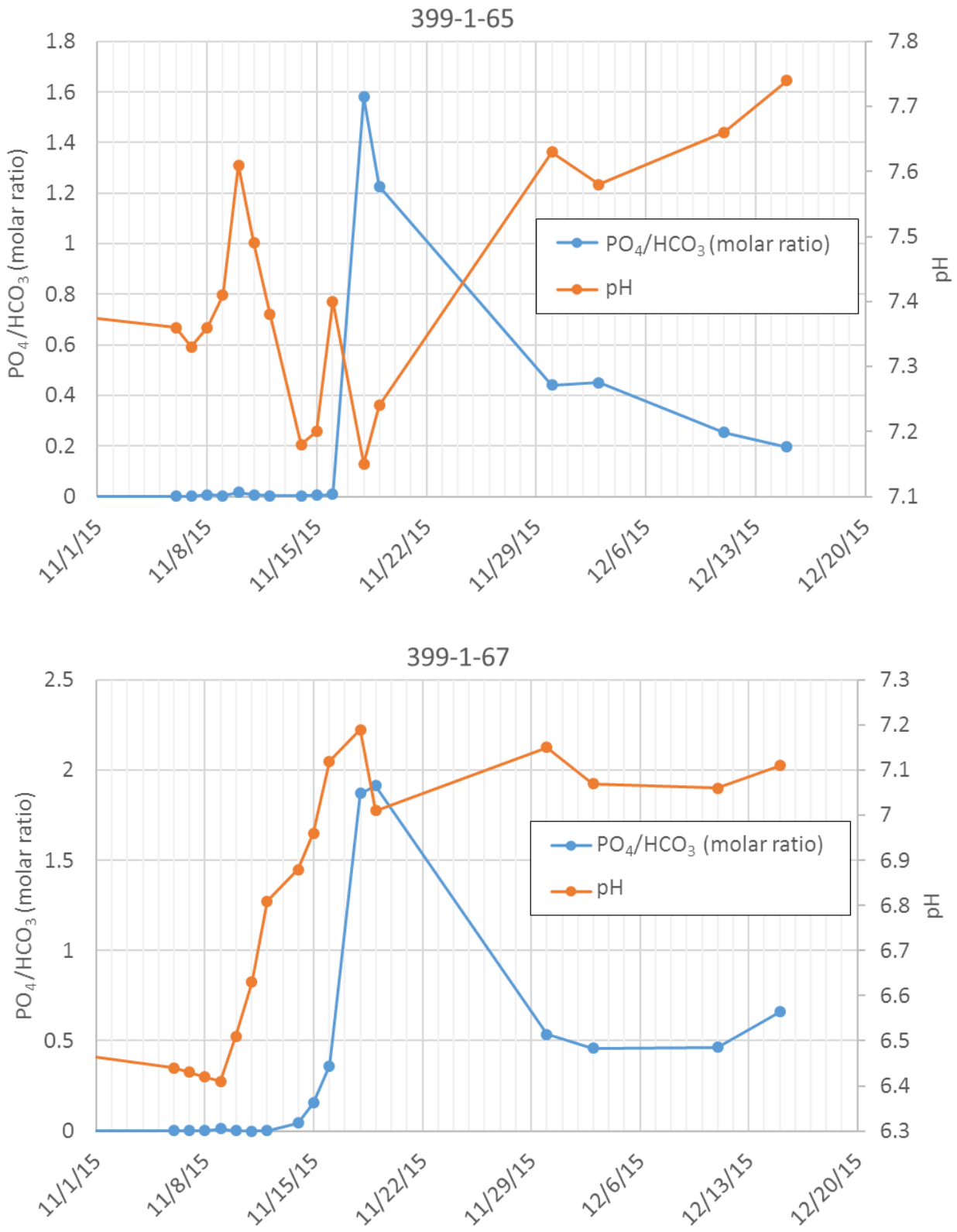

Figure A-2. Comparison of Phosphate to Bicarbonate Ratios to pH for Wells 399-1-65 and 399-1-67

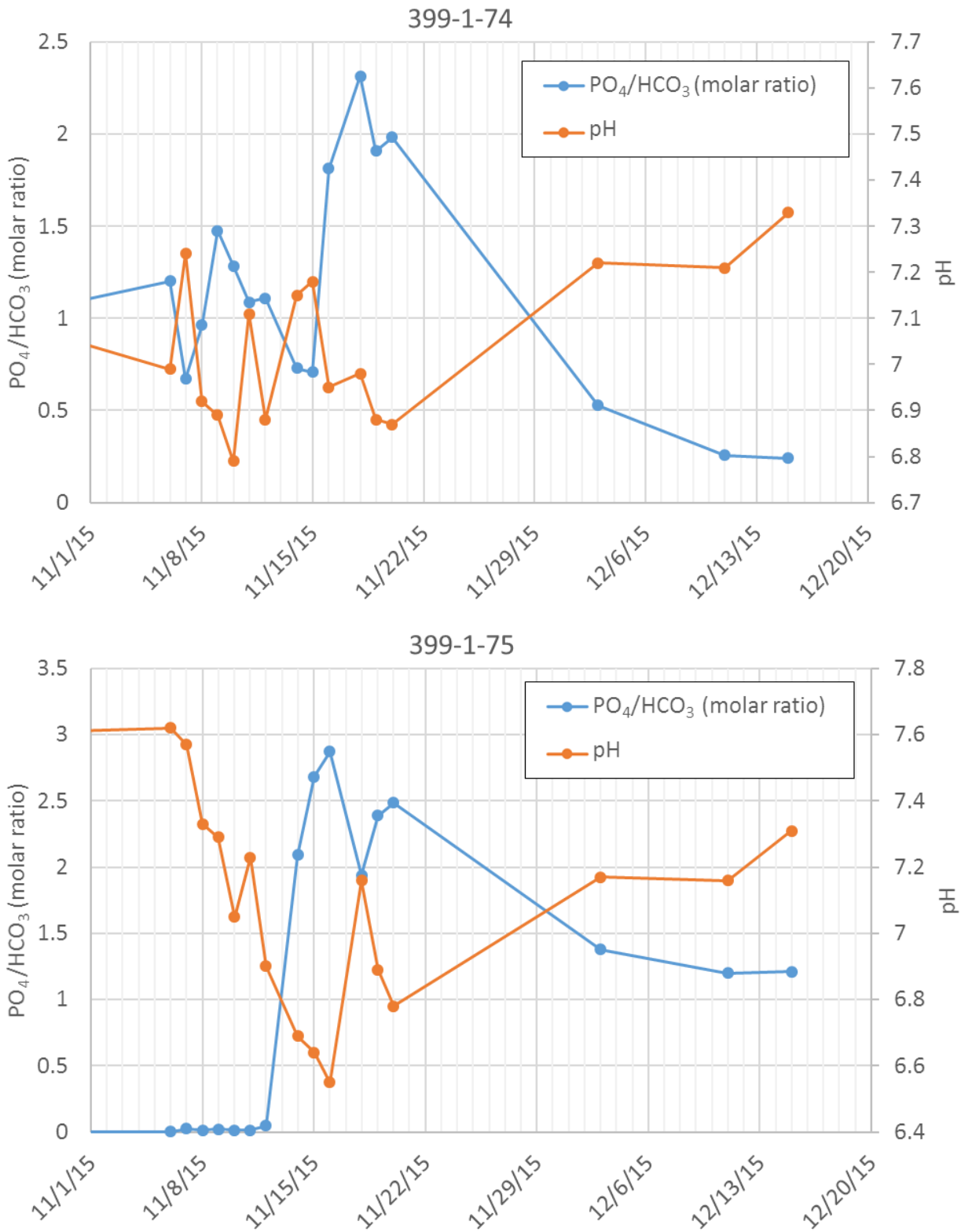

Figure A-3. Comparison of Phosphate to Bicarbonate Ratios to pH for Wells 399-1-74 and 399-1-75

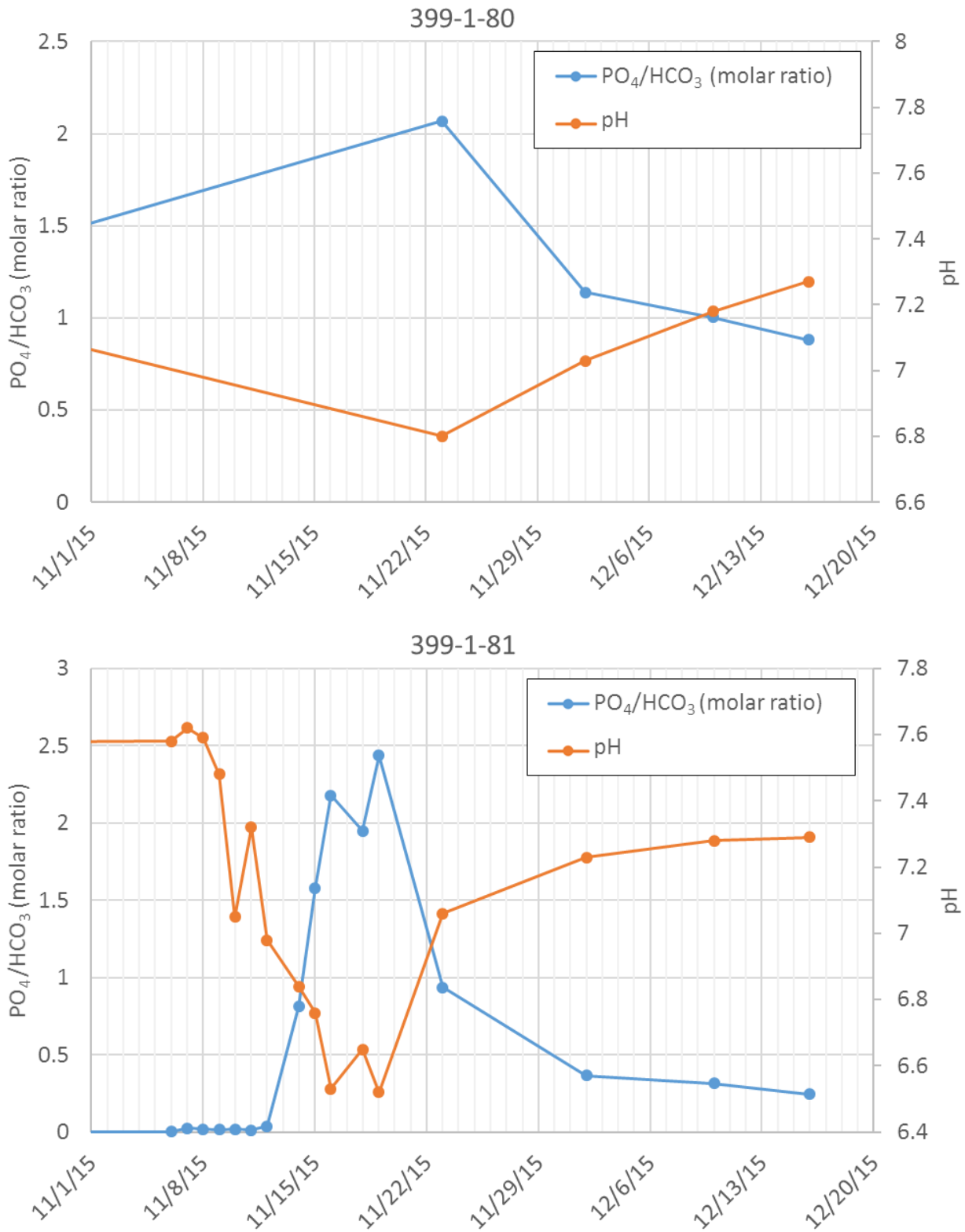

Figure A-4. Comparison of Phosphate to Bicarbonate Ratios to pH for Wells 399-1-80 and 399-1-81

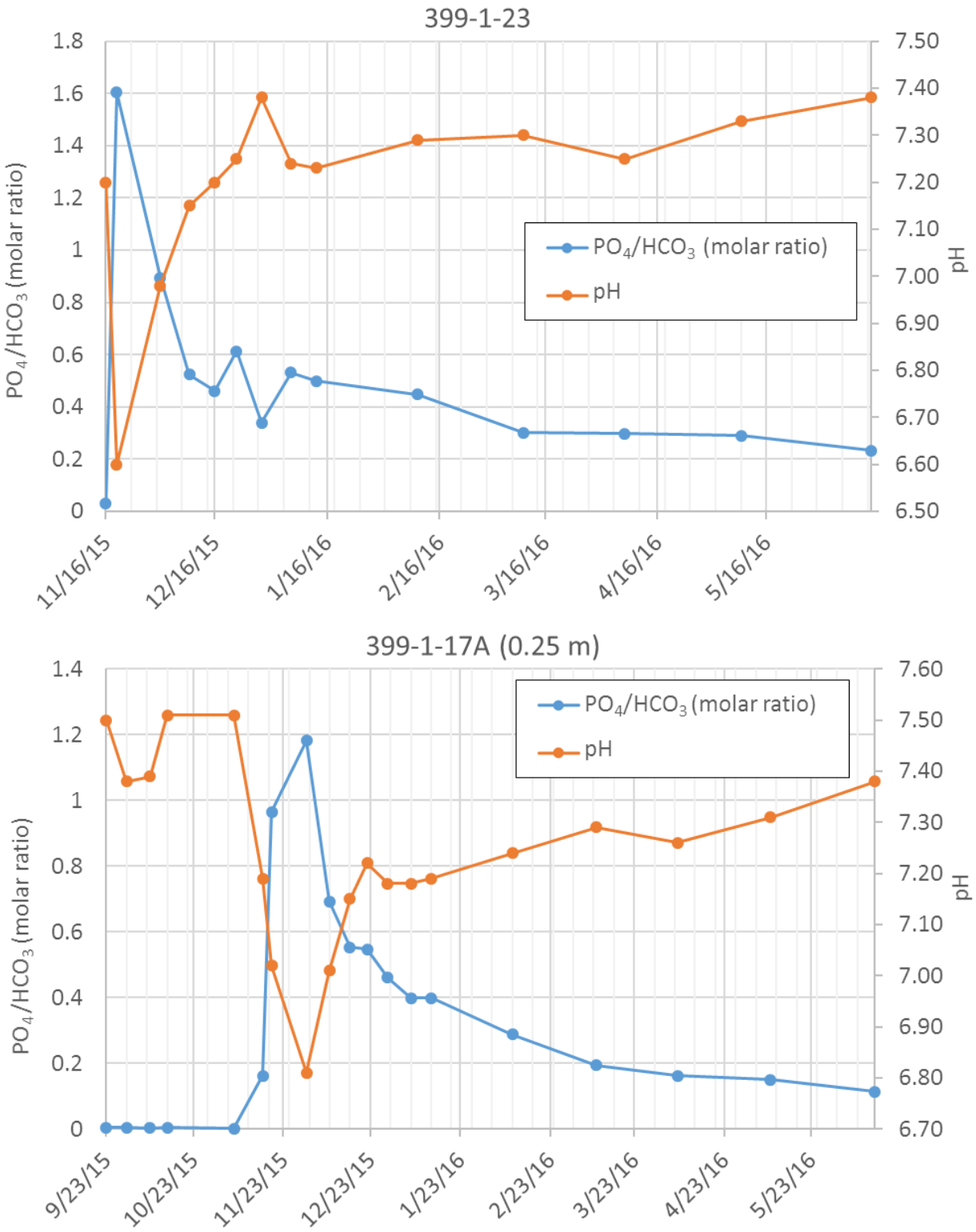

Figure A-5. Comparison of Phosphate to Bicarbonate Ratios to pH for Wells 399-1-23 and 399-1-17A

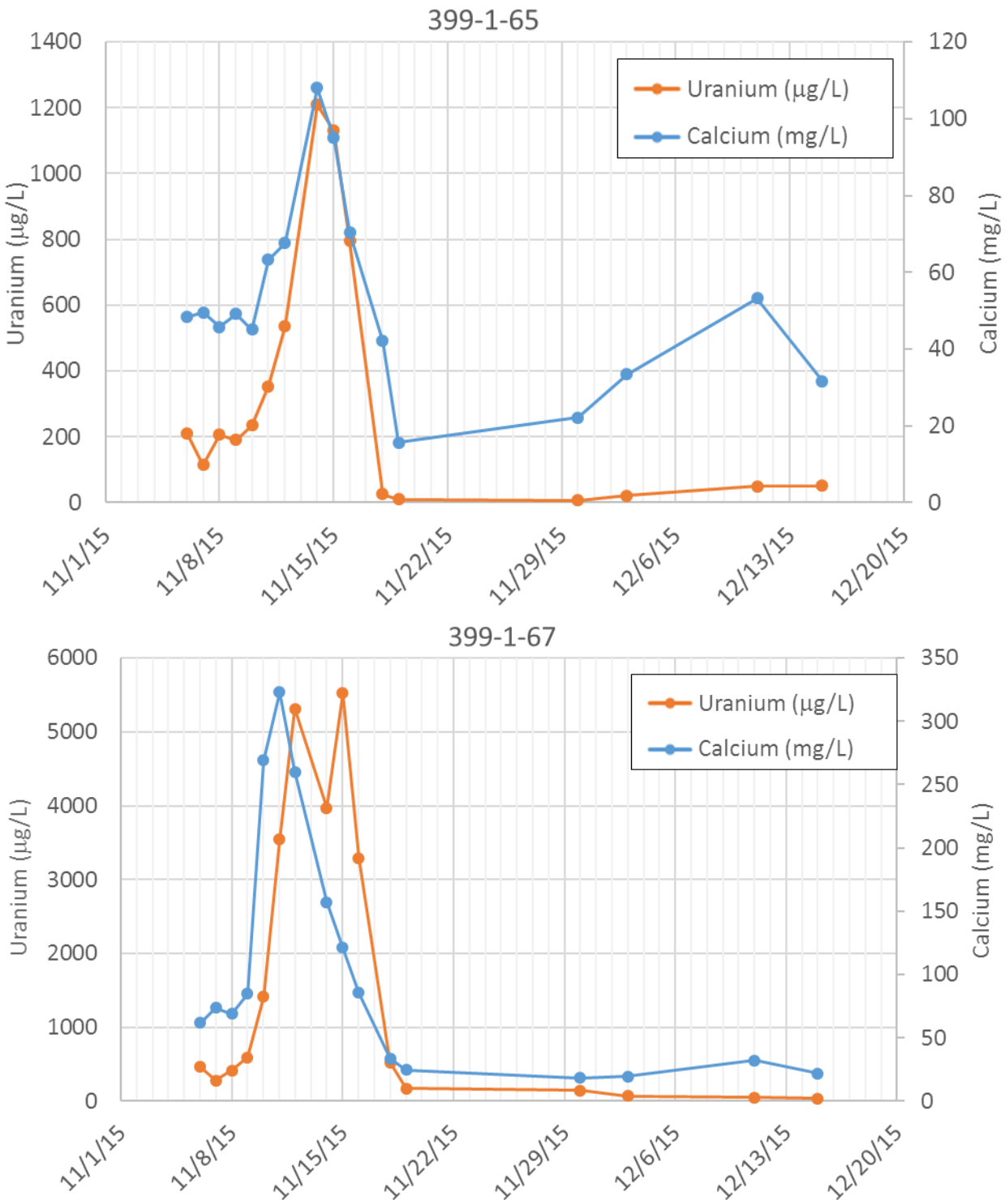

Figure A-6. Comparison of Uranium to Calcium Concentrations for Wells 399-1-65 and 399-1-67

Figure A-7. Comparison of Uranium to Calcium Concentrations for Wells 399-1-74 and 399-1-75

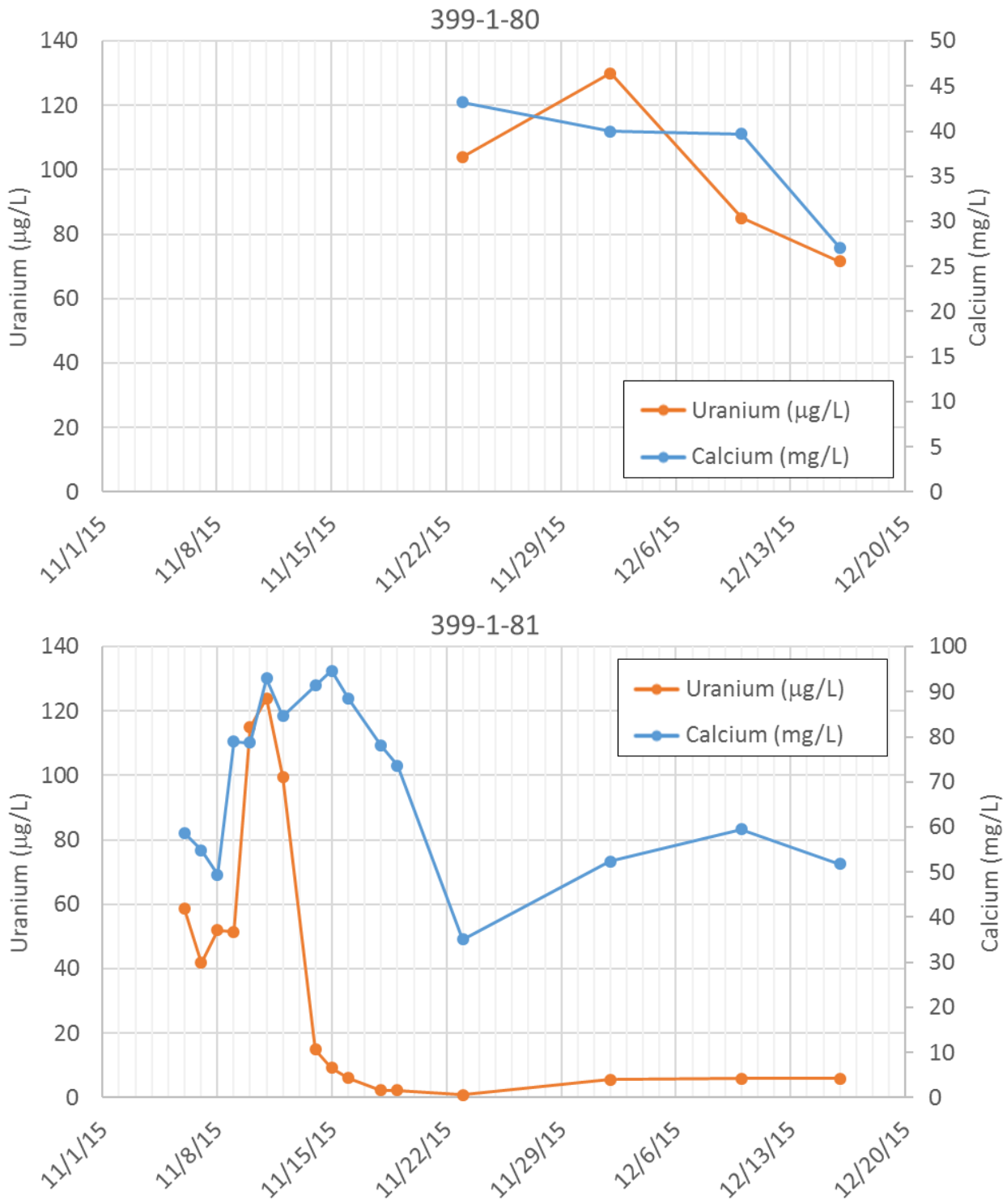

Figure A-8. Comparison of Uranium to Calcium Concentrations for Wells 399-1-80 and 399-1-81

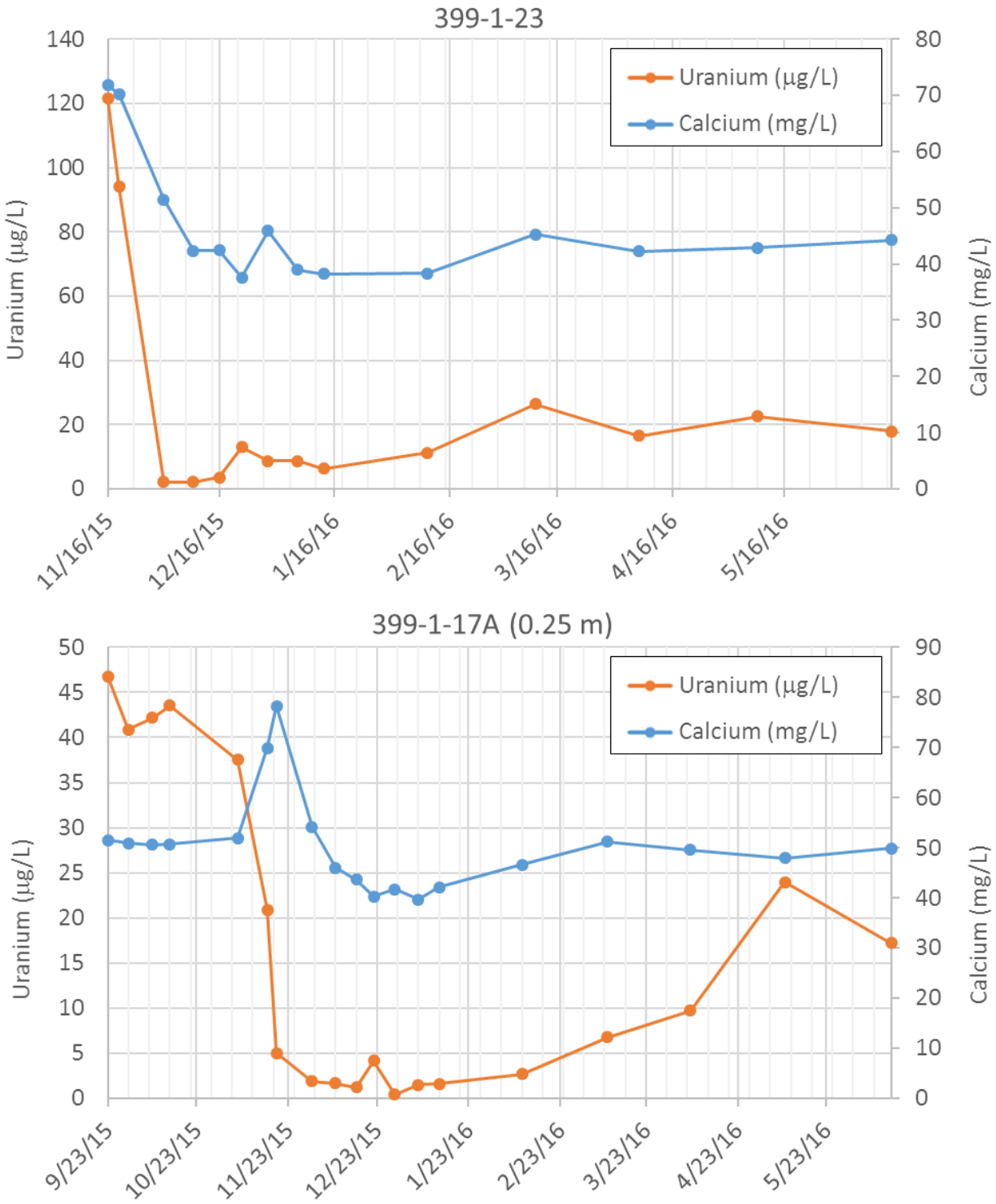

Figure A-9. Comparison of Uranium to Calcium Concentrations for Wells 399-1-23 and 399-1-17A

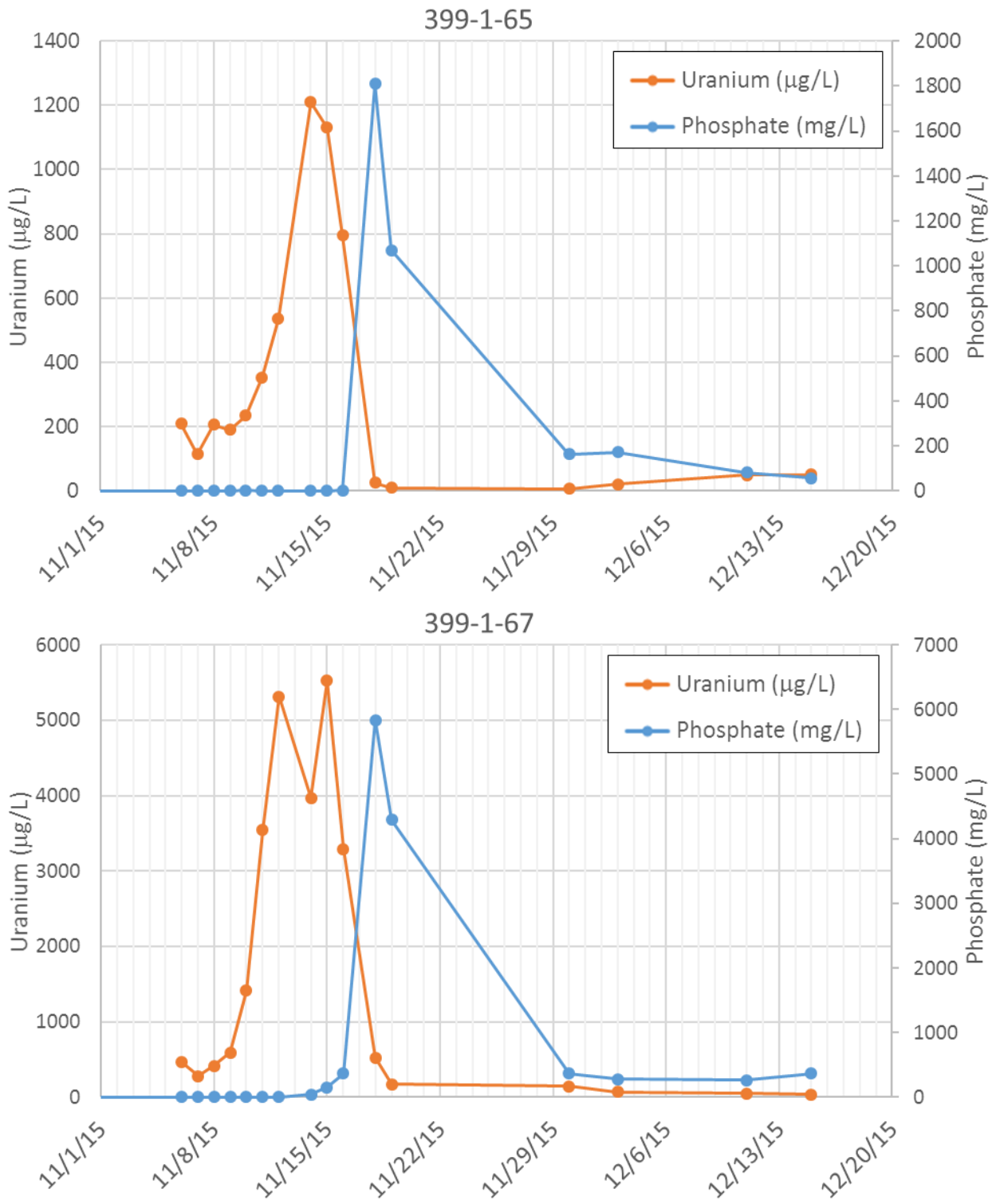

Figure A-10. Comparison of Uranium to Phosphate Concentrations for Wells 399-1-65 and 399-1-67

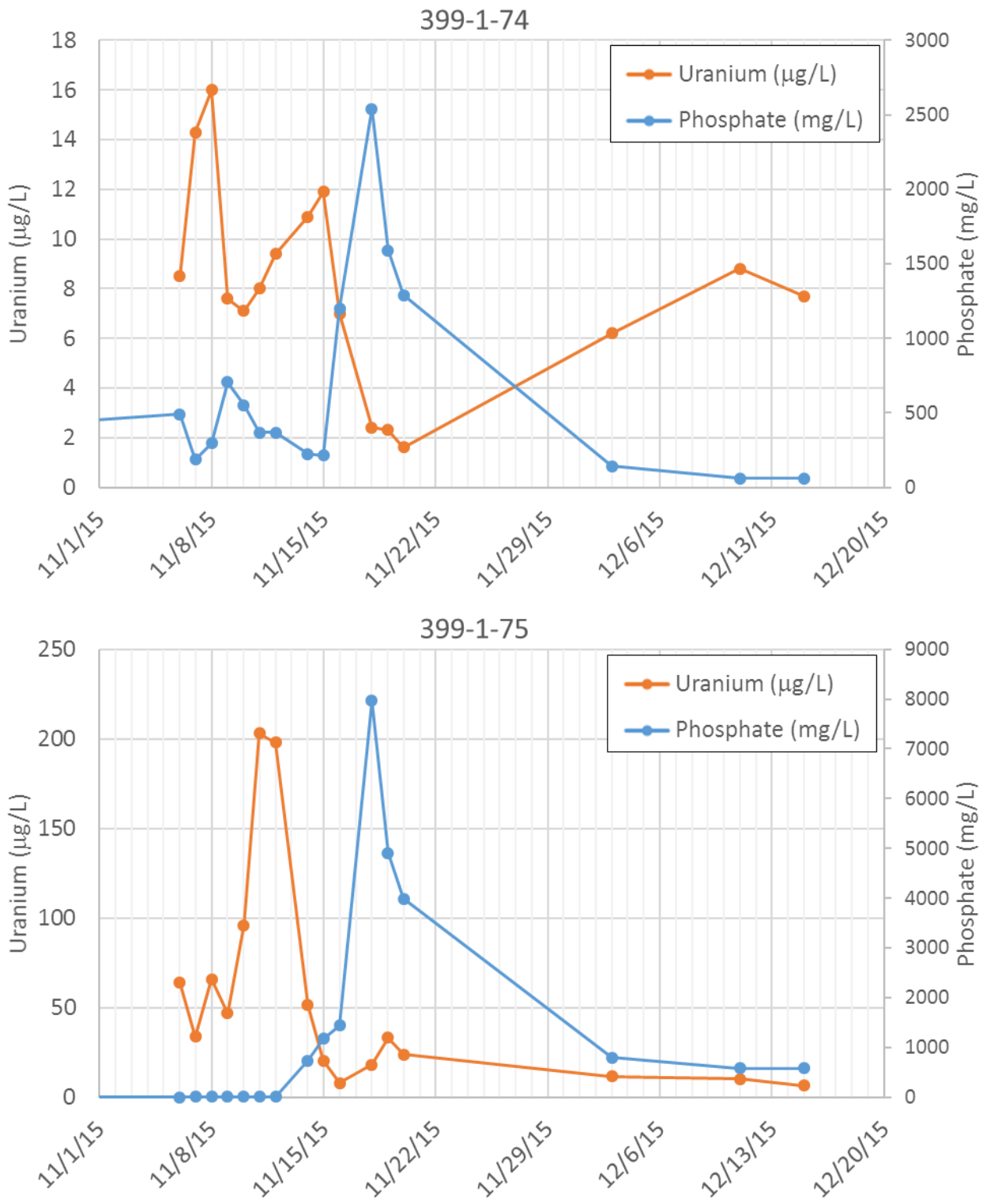

Figure A-11. Comparison of Uranium to Phosphate Concentrations for Wells 399-1-74 and 399-1-75

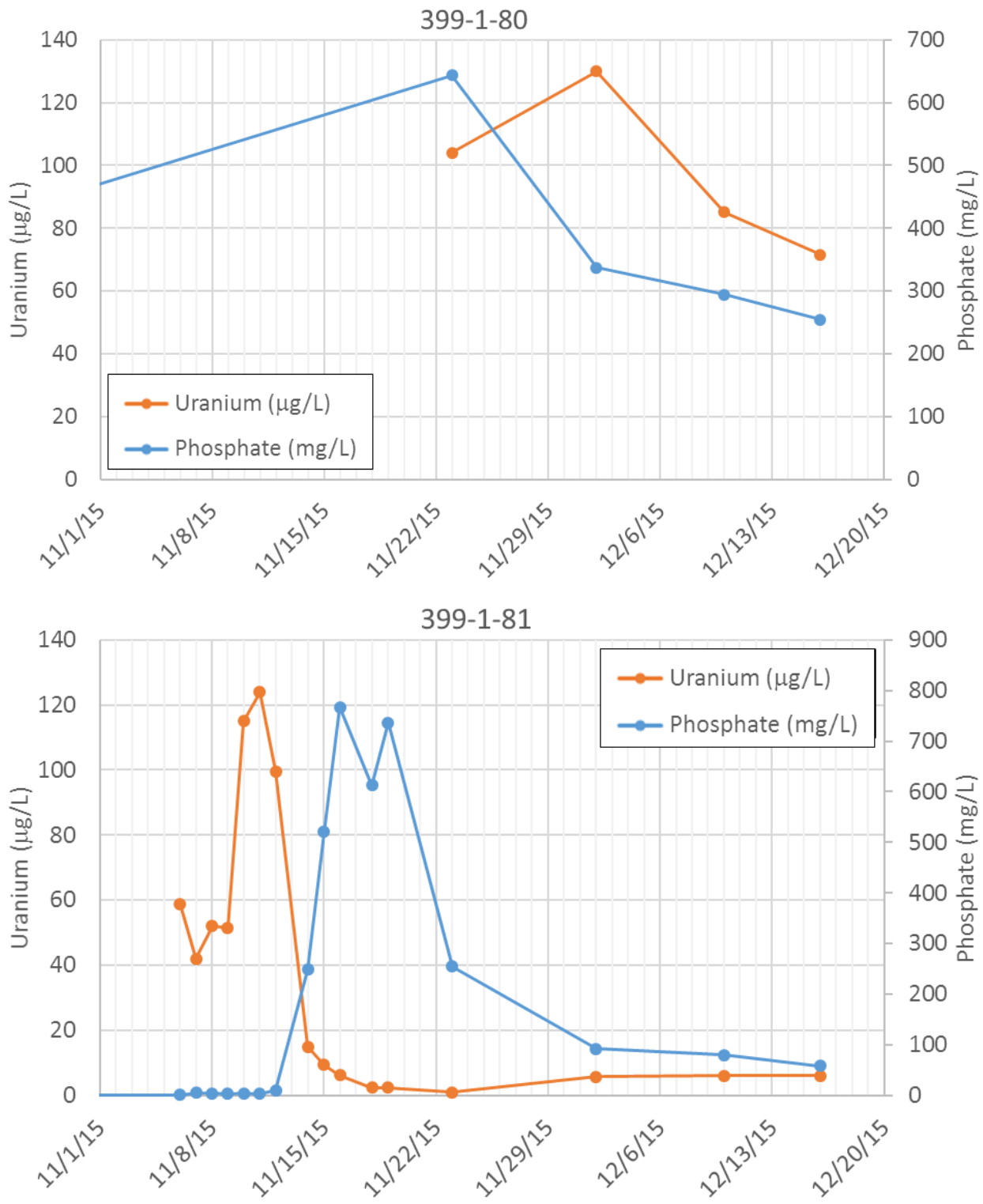

Figure A-12. Comparison of Uranium to Phosphate Concentrations for Wells 399-1-80 and 399-1-81

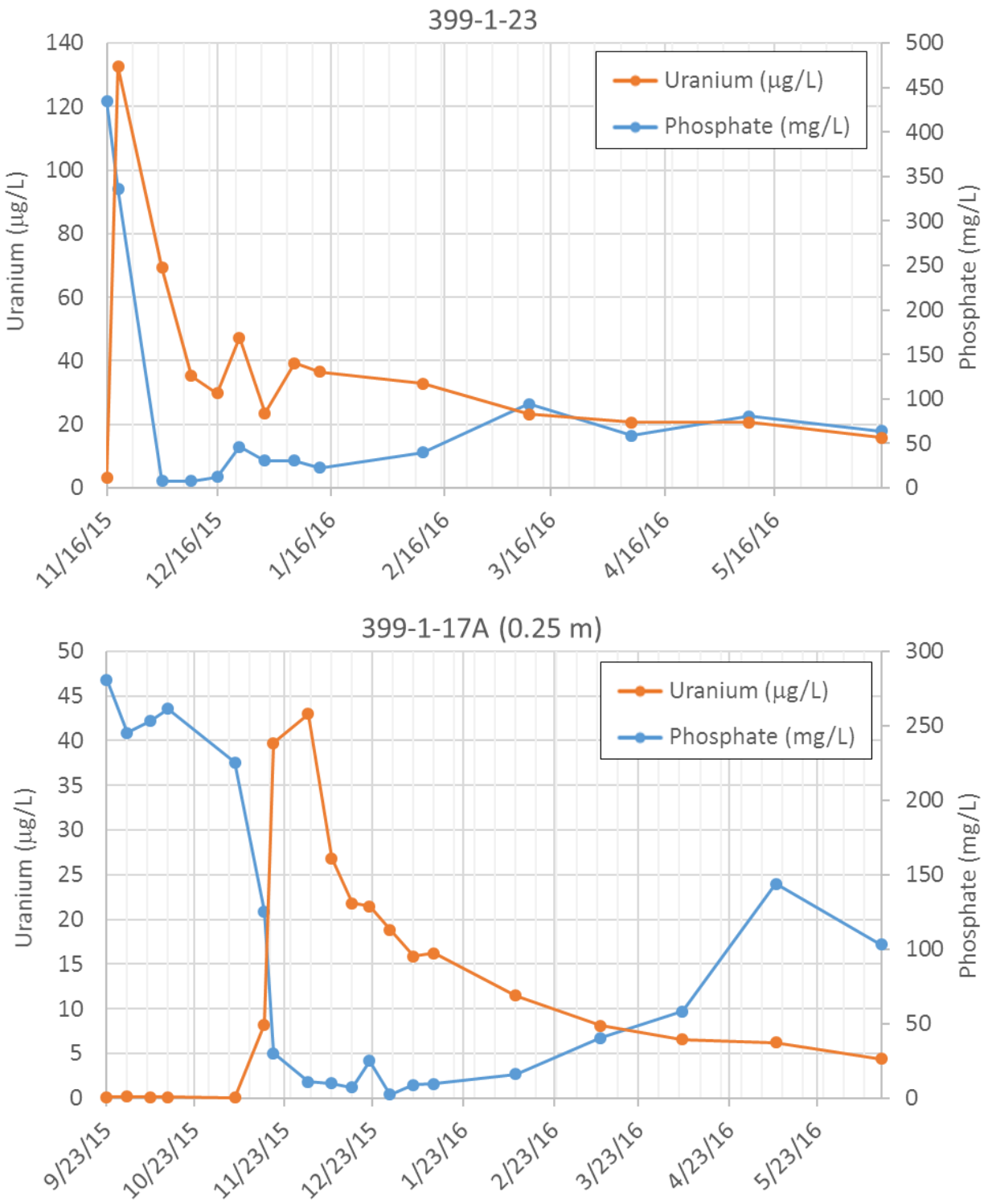

Figure A-13. Comparison of Uranium to Phosphate Concentrations for Wells 399-1-23 and 399-1-17A

A1.4 Calcium Concentration Compared to Phosphate Concentration

Figures A-14 through A-17 show the observed concentrations of calcium and phosphate for the selected wells. Since the goal of the injections/infiltration is to form calcium-uranium-phosphate complex, these results show that calcium was being made available in situ while phosphate was being infiltrated or injected.

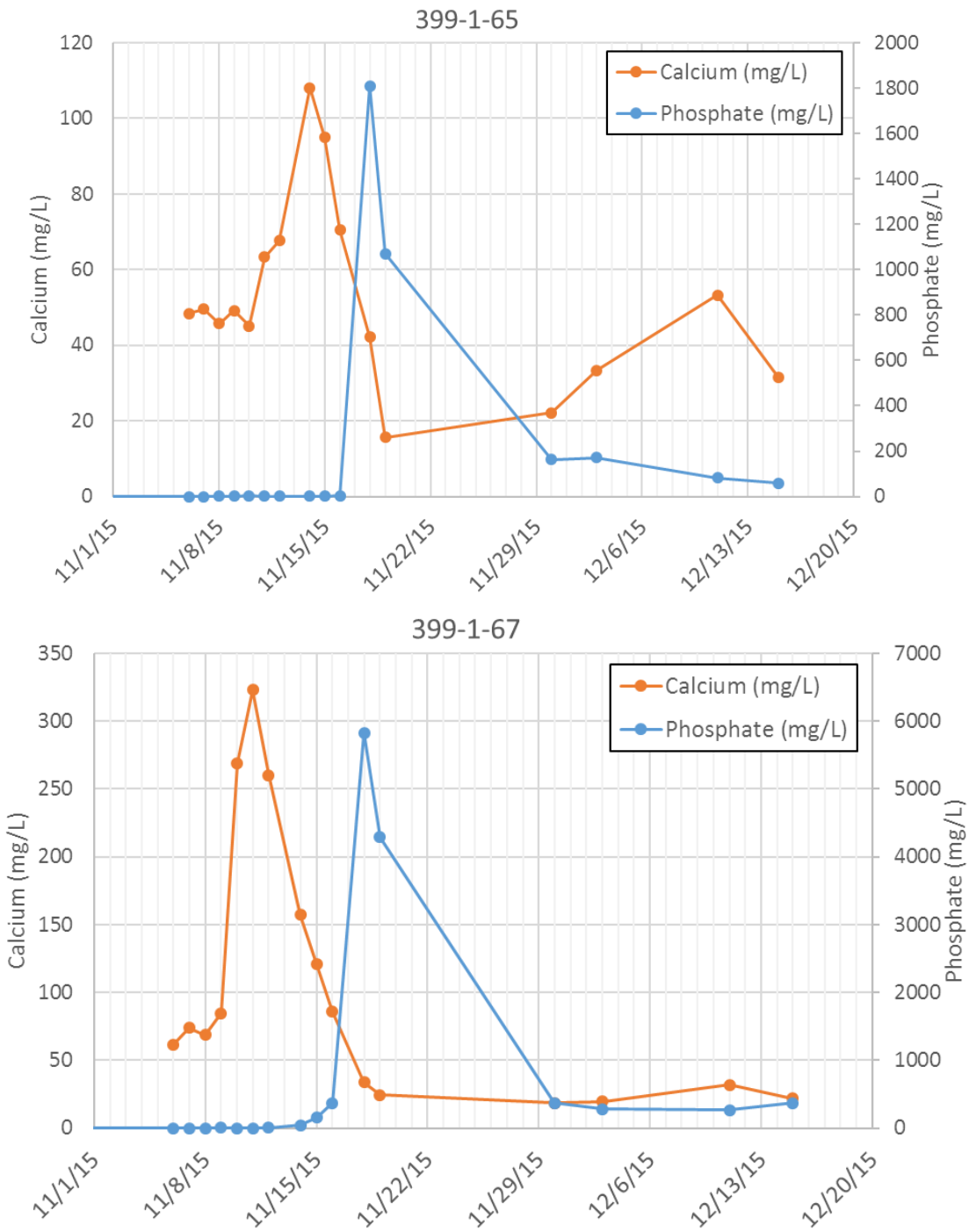

Figure A-14. Comparison of Calcium to Phosphate Concentrations for Wells 399-1-65 and 399-1-67

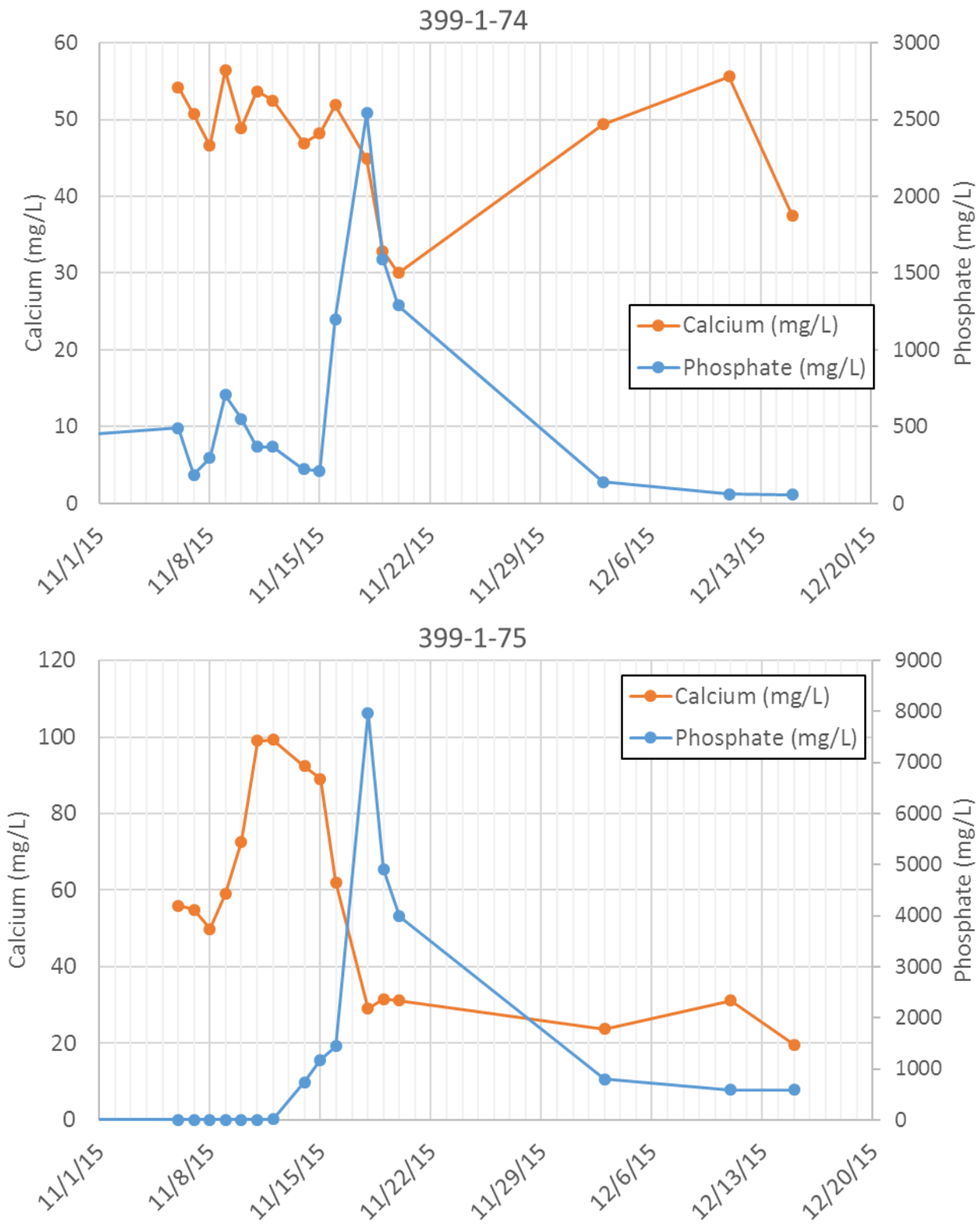

Figure A-15. Comparison of Calcium to Phosphate Concentrations for Wells 399-1-74 and 399-1-75

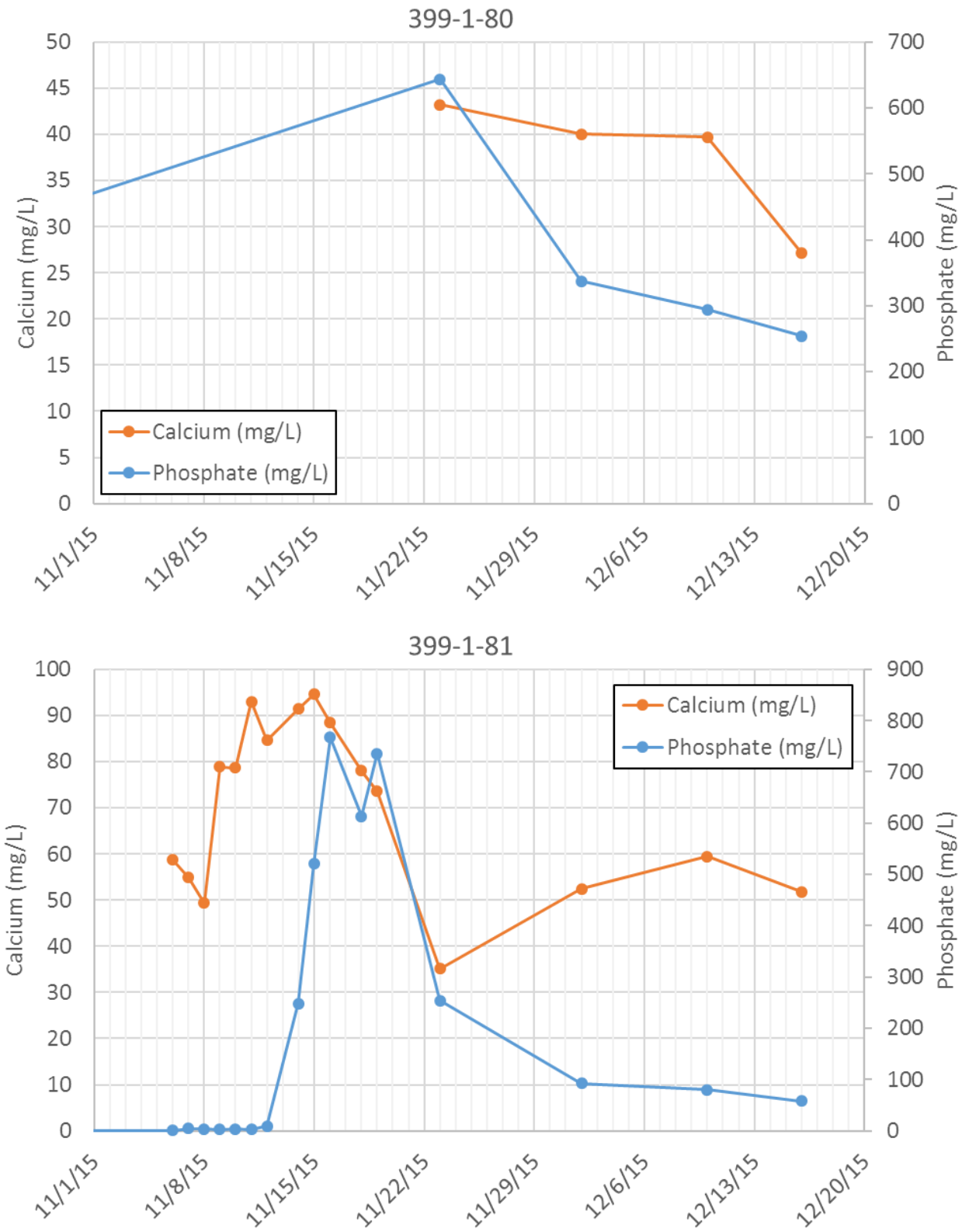

Figure A-16. Comparison of Calcium to Phosphate Concentrations for Wells 399-1-80 and 399-1-81

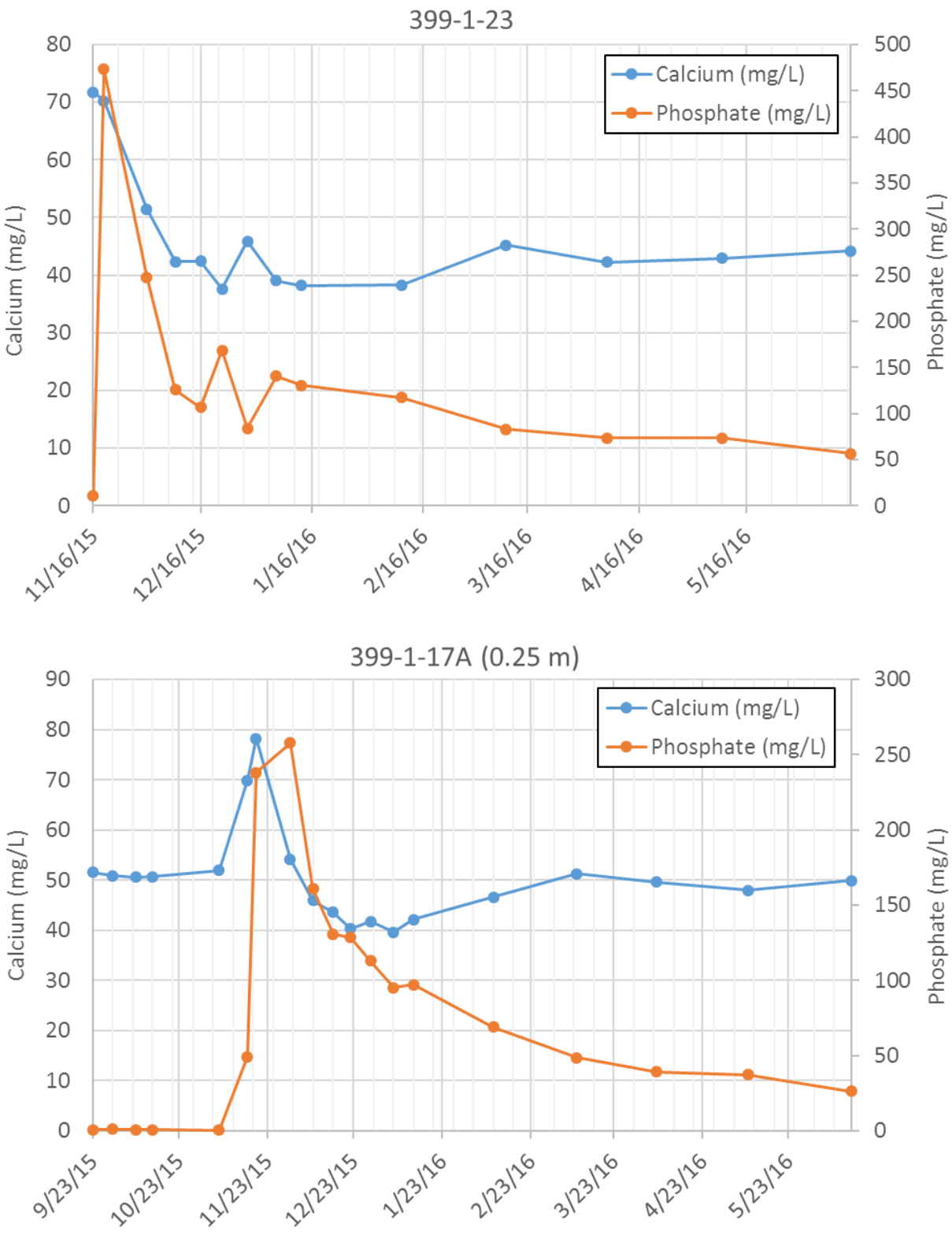

Figure A-17. Comparison of Calcium to Phosphate Concentrations for Wells 399-1-23 and 399-1-17A

A1.5 Calcium to Sodium Ratio Compared to pH

Figures A-18 through A-21 illustrate the Ca:Na ratio (in milliequivalents per liter) along with pH. The Ca:Na ratio changes as the Na rich solutions are infiltrated or injected. Because of concurrent geochemical reactions, pH declines first then gradually increases to pretreatment levels.

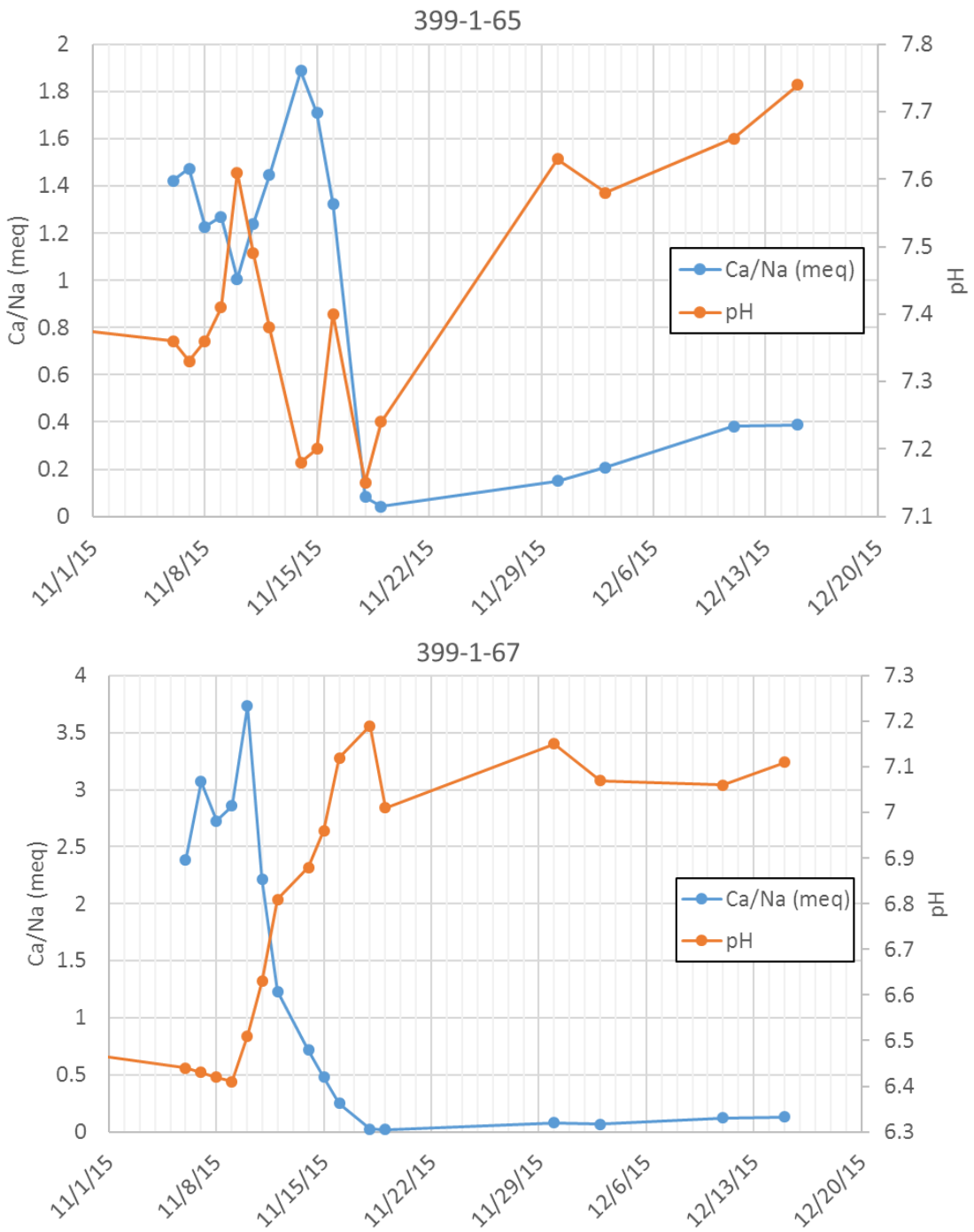

Figure A-18. Comparison of Calcium to Sodium Ratios and pH for Wells 399-1-65 and 399-1-67

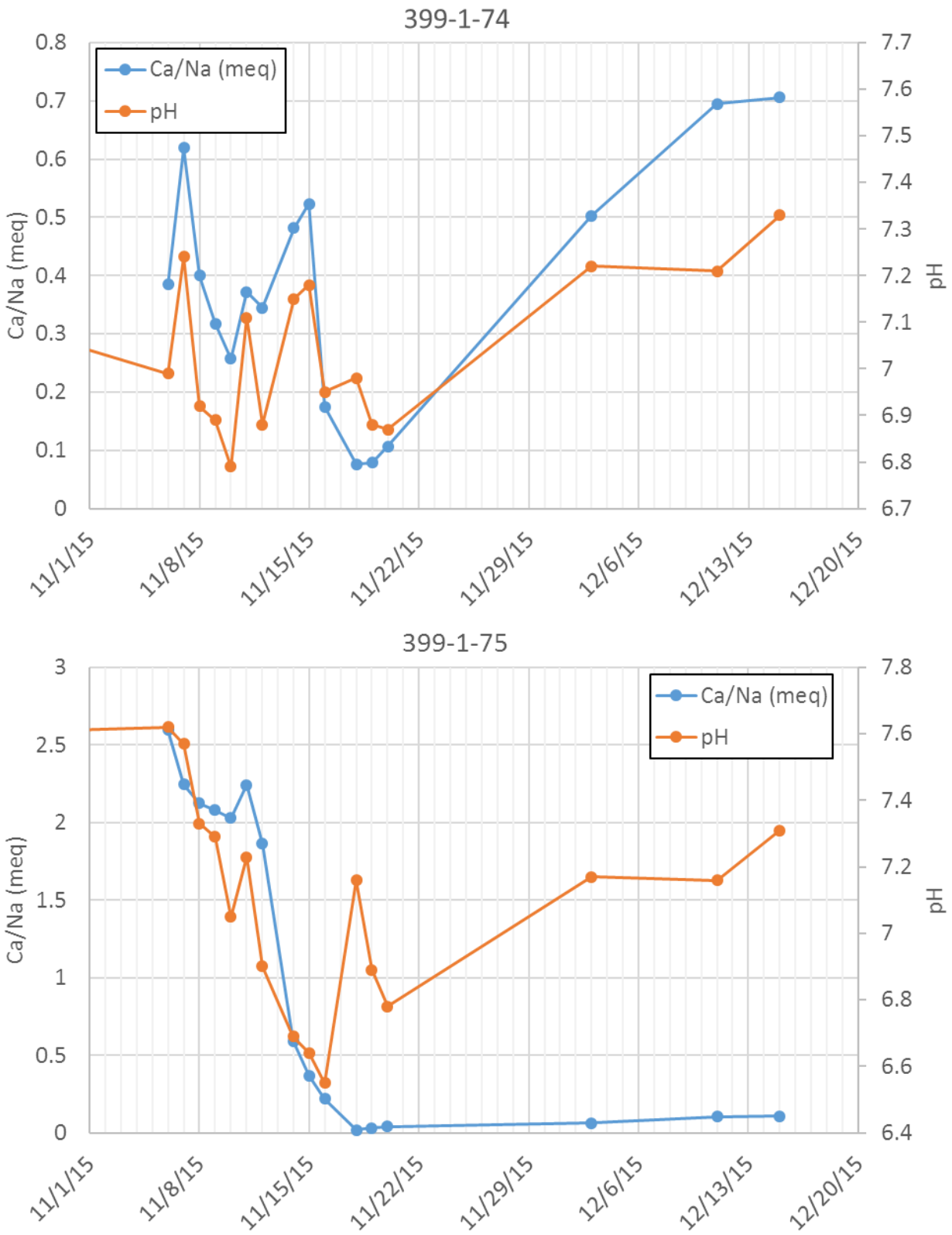

Figure A-19. Comparison of Calcium to Sodium Ratios and pH for Wells 399-1-74 and 399-1-75

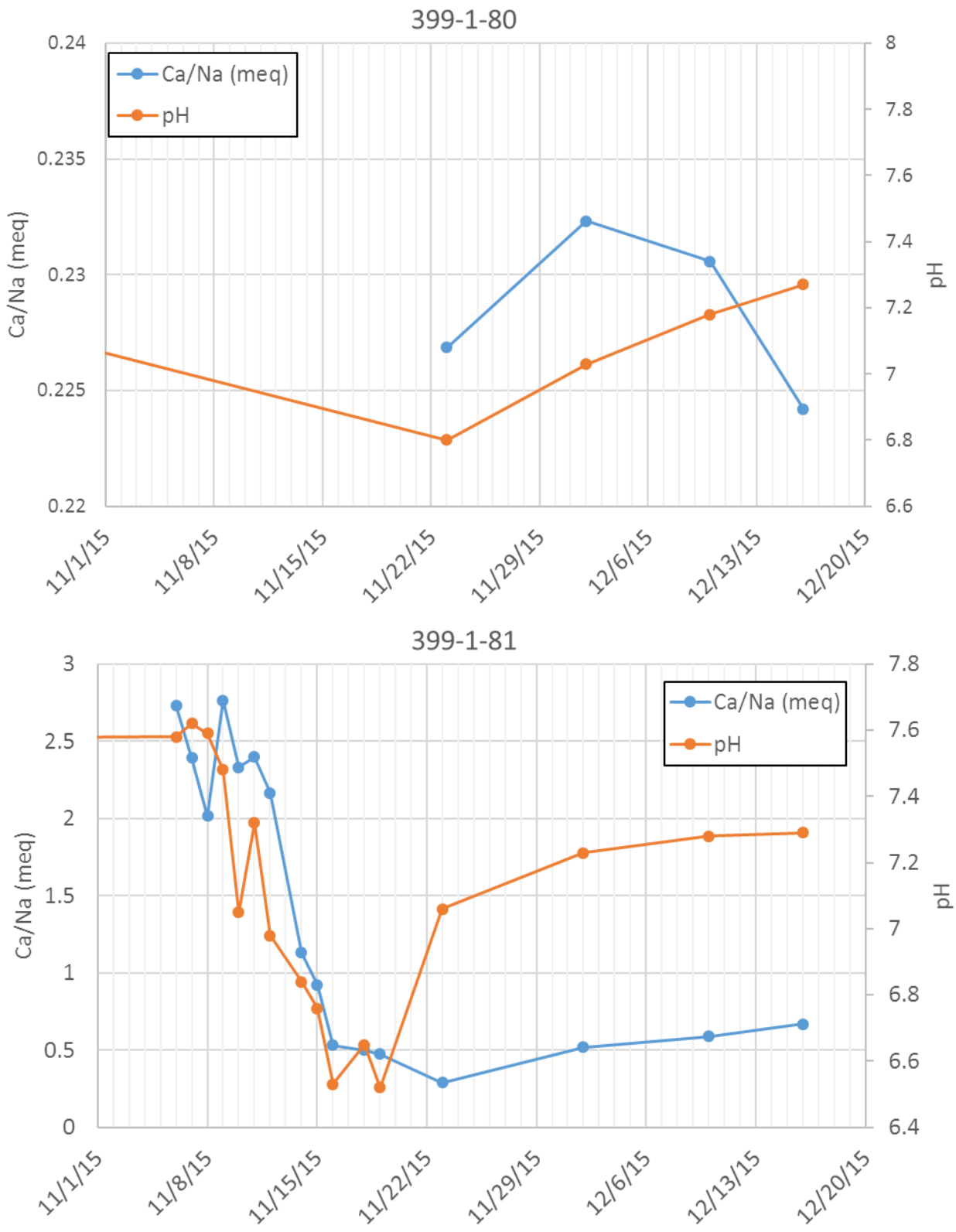

Figure A-20. Comparison of Calcium to Sodium Ratios and pH for Wells 399-1-80 and 399-1-81

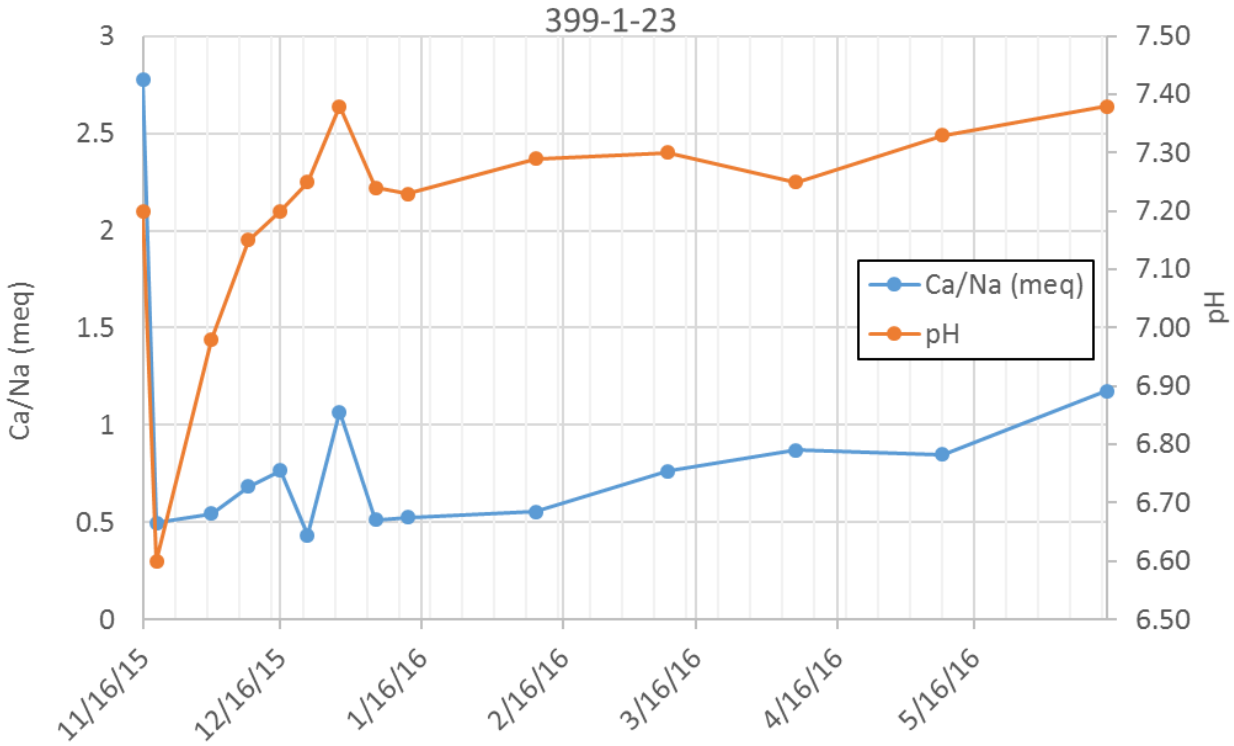

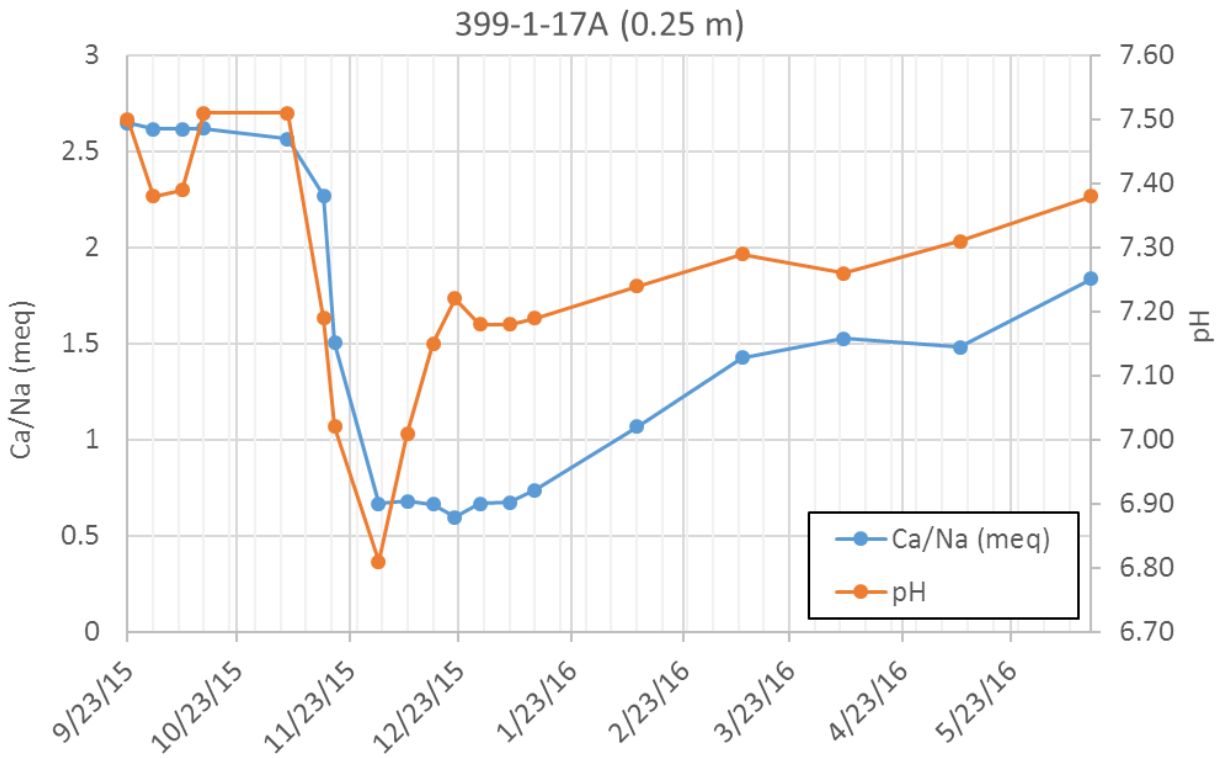

Figure A-21. Comparison of Calcium to Sodium Ratios and pH for Wells 399-1-23 and 399-1-17A

Appendix B

Geochemical Evaluations and Reactive Transport Modeling

This page intentionally left blank.

Terms

1D	one-dimensional
ERT	electrical resistivity tomography
GWB	Geochemist's Workbench
ppm	parts per million
PRZ	periodically rewetted zone

This page intentionally left blank.

B1 Geochemical Evaluations and Reactive Transport Modeling

Complex geochemical reactions occur within the host rock as a result of injecting or infiltrating high concentration of sodium phosphate bearing solutions. Although the ultimate goal is to sequester uranium from leaching to the groundwater, it is important to understand the geochemical processes from a mechanistic point of view that lead to sequestration of uranium. This information gained from this understanding will be used in developing lumped sorption-desorption parameters for predictive modeling using a fate and transport model.

A conceptual model of possible reactions resulting from infiltration of phosphate bearing solutions in the vadose zone is presented in Figure 6-24. The total thickness of the vadose zone (from base of infiltration lines to the water table) is approximately 8 m (26.2 ft). The average vertical velocity of the infiltrated solutions is about 1 m/day based on migration velocities estimated from electrical resistivity tomography (ERT) data (Figure 6-11). In order to gain an understanding of the geochemical reactions from phosphate-sediment interaction, a one-dimensional (1D) reactive transport model is developed using The Geochemist's Workbench (GWB) Version 11.

B1.1 Update of Existing Databases

For the purpose of evaluating geochemical reactions specific to the phosphate interactions, the following updates were made to the underlying databases based on information derived from published literature:

1. Added information about uranyl carbonate and phosphate bearing mineral phases to the thermodynamic database
2. Added reactions to the ion exchange database
3. Added surface species to the surface complexation database

In the default thermodynamic database called thermo.tdat, information regarding 624 minerals is included. However, based on the review of the database, some of the uranium carbonate and uranium phosphate minerals that could form (or dissolve) from reactions with injected/infiltrated solutions were not found. These were added based on review of literature. The following mineral phases were added based on information presented in Gorman-Lewis et al., 2008, "Review of Uranyl Mineral Solubility Measurements," and Gorman-Lewis et al., 2009, "Thermodynamic Properties of Autunite, Uranyl Hydrogen Phosphate, and Uranyl Orthophosphate from Solubility and Calorimetric Measurements":

Mineral Phase	Dissolution Reaction	Log K_{sp} (25°C)
Autunite	$Ca(UO_2)_2(PO_4)_2 \cdot 3H_2O = Ca^{2+} + 2UO_2^{2+} + 2PO_4^{3-} + 3H_2O$	-48.36
Uranyl Hydrogen Phosphate	$UO_2HPO_4 \cdot 3H_2O = UO_2^{2+} + HPO_4^{2-} + 3H_2O$	-13.17
Uranyl Orthophosphate	$(UO_2)_3(PO_4)_2 \cdot 4H_2O = 3UO_2^{2+} + 2PO_4^{3-} + 4H_2O$	-49.36
Andersonite	$Na_2CaUO_2(CO_3)_3(H_2O)_6 = 2Na^{+} + Ca2^{+} + UO_2^{2+} + 3CO_3^{2-} + 6H_2O$	-37.5
Liebigite	$Ca_2UO_2(CO_3)_3(H_2O)_{10} = 2Ca^{2+} + UO_2^{2+} + 3CO_3^{2-} + 10H_2O$	-36.9
Chernikovite	$(UO_2)HPO_4(H_2O)_4 = UO_2^{2+} + HPO_4^{2-} + 4H_2O$	-22.73

The following ion exchange reactions were added to the database called IonEx.sdat in order to model the cation exchange reactions with calcium once sodium and potassium bearing phosphate solutions are added. The ion exchange coefficients relative to Na^+ are presented following the Gaines-Thomas convention (Gaines and Thomas, 1953, "Adsorption Studies on Clay Minerals. II. A Formulation of the Thermodynamics of Exchange Adsorption"). The dataset is taken from Appelo and Postma, 2005, *Geochemistry, Groundwater and Pollution*, based on a compilation by Bruggenwert and Kamphorst, 1982, "Chapter 5: Survey of Experimental Information on Cation Exchange in Soil Systems":

Equation: $Na^+ + 1/i \cdot I\text{-}X_i \longleftrightarrow Na\text{-}X + 1/i \cdot I^+$

Ion Type (*I*)	Ion Exchange Coefficient ($K_{Na\backslash I}$)
Ca^{2+}	0.40
Mg^{2+}	0.50
Fe^{2+}	0.60
K^+	0.20

Two calcium-phosphate surface species were added to the existing database called FeOH+.sdat for modeling surface complexation with hydrous ferric oxide. This dataset contains the Dzombak and Morel, 1990, *Surface Complexation Modeling: Hydrous Ferric Oxide*, compilation, expanded to include surface complexation reactions for which binding constants have only been estimated (Dzombak and Morel, 1990 [Chapter 10, p. 299]). The surface complexation with calcium-phosphate species were missing in the database and was added based on information presented by Spiteri et al., 2008, "Surface complexation effects on phosphate adsorption to ferric iron oxyhydroxides along pH and salinity gradients in estuaries and coastal aquifers" (as modified from Gao and Mucci, 2001, "Acid Base Reactions, Phosphate and Arsenate Complexation, and their Competitive Adsorption at the Surface of Goethite in 0.7 M NaCl Solution"). The stability constants are given as intrinsic constants that are added to the weak surface sorption sites:

$\equiv FeOH(w) + Ca^{2+} + H_2PO_4^- \longleftrightarrow \equiv FeOCaHPO_4^- + 2H^+$ Log K (25°C) = -6.44

$\equiv FeOH(w) + Ca^{2+} + H_2PO_4^- \longleftrightarrow \equiv FeOCaH_2PO_4 + 2H^+$ Log K (25°C) = 0.19

B1.2 Reactive Transport Modeling of Controlled Laboratory Experiment Performed on Contaminated Sediment from 300 Area

Before evaluating the geochemical reactions in the vadose zone, validation of the existing database and adequacy of the current understanding of the possible reactions occurring from mixing of phosphate rich solutions with host sediments was undertaken. This was achieved by comparing the modeling results to the experimental results. Wellman et al., 2007, "Efficacy of soluble sodium tripolyphosphate Amendments for the in-situ immobilisation of uranium," report results of a carefully controlled laboratory experiment where uranium contaminated sediment sample that was taken from the North Process Pond in the 300 Area was flushed with sodium tripolyphosphate solution under both saturated and unsaturated conditions. The experiment conducted under unsaturated conditions is discussed here since it is more relevant to the geochemical reactions in the vadose zone from infiltrated and injected solutions.

As reported by Wellman et al. (2007), the sediment is coarsely textured with ~48 percent gravel, ~40 percent sand, and remaining fraction as silt and clay (~12 percent). The total uranium content within the sediment is 540 mg/kg (or µg/g) and the majority of the uranium is present as carbonates

(~30 percent) and/or associated with amorphous iron and aluminum oxyhydroxides (~55 percent). Unsaturated column experiments were conducted using a pressurized unsaturated flow system where the water content was set to ~20 percent. The experiments were performed on <2 mm size sediments (sand, silt, and clay size) in a cylindrical column of length = 7.62 cm and radius = 0.96 cm. The influent solution containing 1,000 parts per million (ppm) sodium tripolyphosphate ($Na_5P_3O_{10}$) was prepared by mixing with the artificial groundwater (Table 1 of Wellman et al., 2007 shows groundwater composition). The 1,000 mg/L sodium tripolyphosphate ($Na_5P_3O_{10}$) has molecular weight of about 368 g/mole and results in a molar concentration of approximately 2.7×10^{-3} M. The resulting total P in the sodium tripolyphosphate solution is approximately 253 mg/L and sodium concentration is 312.5 mg/L. The pH of sodium tripolyphosphate solution is not mentioned in the report but is probably around 10. The pH of the initial groundwater solution was 8.2.

The flow rate was maintained at 0.08 mL/h. During the experiment, volumetric moisture content was monitored and found to be steady for the first 100 days (~41 pore volumes) at about 20 percent; subsequently, it increased steadily to ~40 percent until the test was terminated.

Considering a steady volumetric flow rate of 0.08 mL/h (or cm^3/h) through the cross-sectional area of 2.9 cm^2 results in a specific discharge of about 0.66 cm/day, and considering a volumetric moisture content of 0.2, the average linear pore water velocity is calculated to be 3.3 cm/day. This corresponds to about 2.4 days of residence time per pore volume.

Results of the experiment are shown in Figure B-1 in terms of effluent concentrations of uranium, phosphorus (P), and calcium as a function of pore volumes. The results are presented for experiments conducted with and without the 1,000 ppm sodium tripolyphosphate amendments. Note that concentration of total P is shown in mg/L while others are presented in µg/L. The results with the phosphate amendment are shown in solid lines and are of interest. The uranium concentrations fluctuate for first 20 pore volumes but remain near the initial concentration of about 5,000 µg/L and then drop rapidly over next 10 pore volumes to about 10 µg/L (similar to background groundwater concentration). This drop coincides with increasing concentration of P, which until then was being consumed in the reactions and/or being retarded due to sorption on the sediments. The P concentrations increase rapidly from 20 to 25 pore volumes but then continue to increase marginally for the remainder of the experiment. Calcium concentrations also show fluctuations between 10 and 20 pore volumes but then decline sharply after 15 pore volumes, reaching a local minimum after 20 pore volumes have passed. The concentrations do not change much past 25 pore volumes.

A 1D reactive transport model was developed using GWB based on the details of the experiment presented in Wellman et al. (2007). The modeling results are then compared to the experimental data. Updated databases (discussed earlier) were used to simulate precipitation and dissolution of phosphate bearing mineral phases, ion exchange reactions, and surface complexation reactions with iron oxyhydroxides. In the model, the ion exchange capacity is set at 0.2 meq/g (20 meq/100 g). This value is deemed reasonable given that the experiments are conducted on <2 mm size sediments with considerable silt and clay fraction (about 23 percent, when considering only <2 mm size). In addition, some minerals were added as reactants with kinetic reactions. These are presented in Table B-1. To match the results, the newly added uranyl carbonate minerals (Andersonite and Liebegite) had to be suppressed.

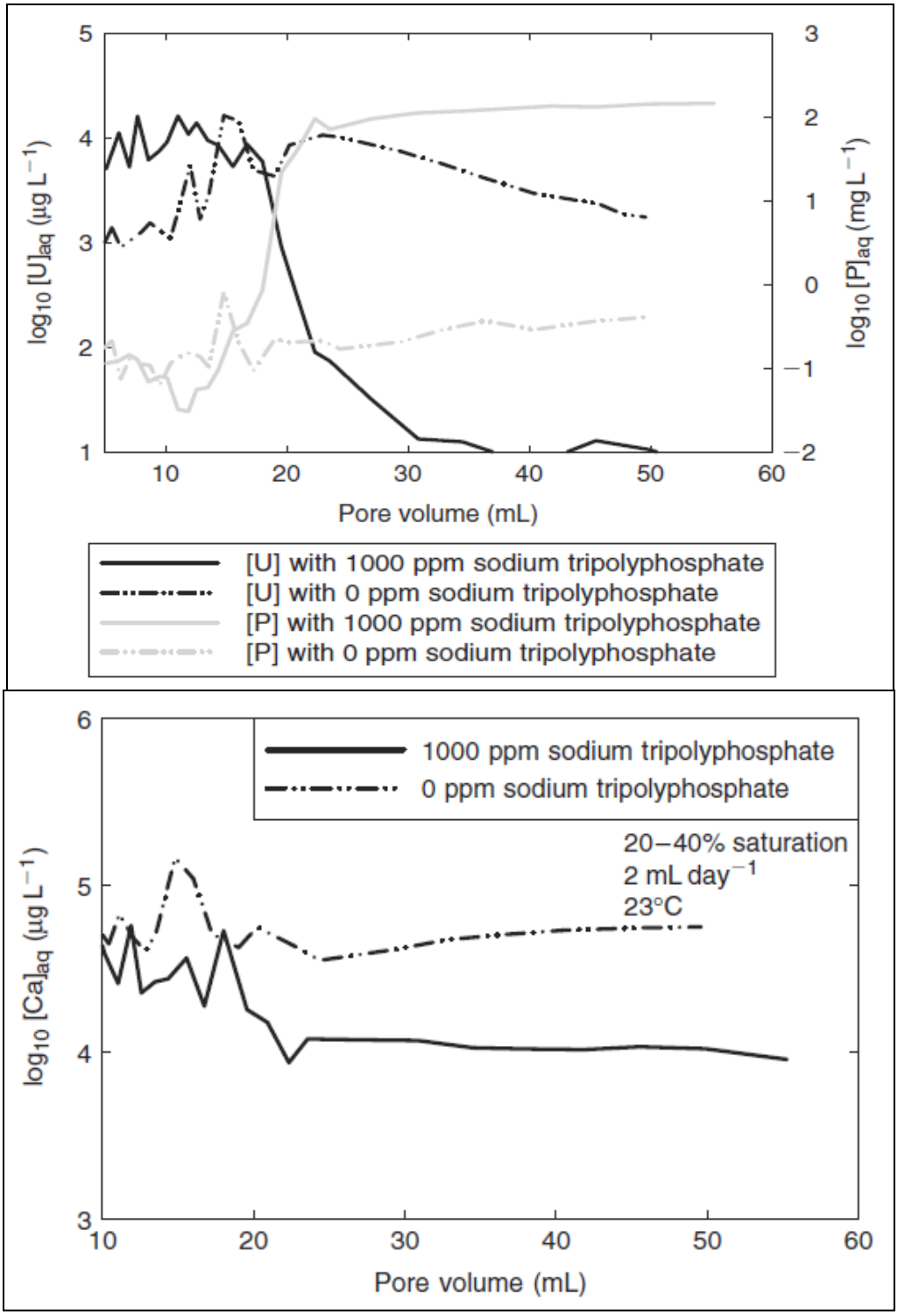

Reference: Wellman et al., 2007, "Efficacy of soluble sodium tripolyphosphate amendments for the in-situ immobilisation of uranium."

Figure B-1. Release of Uranium, Phosphorus, and Calcium from Unsaturated Column Experiments with and without Sodium Tripolyphosphate Amendments at 1,000 ppm Concentration

Table B-1. Mineral Reactants and Associated Parameters Considered for the Column Experiment

Mineral	Amount	Specific Surface Area (cm^2/g)	Dissolution Rate Constant ($mol/cm^2/s$)	Basis for Parameters
Quartz	0.45 (volume fraction in bulk volume)	1,000	4.2×10^{-18}	Volume fraction calculated by assuming 60% quartz content in the solid fraction and 25% porosity; any remaining solid fraction is considered inert. Dissolution rate constant is based on Rimstidt and Barnes, 1980, "The Kinetics of Silica-Water Reactions." Specific surface area is based on typical sand grains from Leamnson et al., 1969, *A Study of the Surface Areas of Particulate Microcrystalline Silica and Silica Sand*.
Calcite	0.0005 (volume fraction in bulk volume)	1,000	7.8×10^{-13}	Volume fraction is estimated based on calcium extracted by weak and strong acetic acid on pretreatment samples. Dissolution rate constant is derived from 1.55×10^{-6} $mol/m^3/s$ rate from Palandri and Kharaka, 2004, *A Compilation of Rate Parameters of Water-Mineral Interaction Kinetics for Application to Geochemical Modeling*. Specific surface area adjusted down based on uranium-calcite value of 3,000 cm^2/g in PNNL-17818, *300 Area Treatability Test: Laboratory Development of Polyphosphate Remediation Technology for In Situ Treatment of Uranium Contamination in the Vadose Zone and Capillary Fringe* (Table 3.3).
Ferrihydrite	0.001 (volume fraction in bulk volume)			The volume fraction is based on estimated amorphous iron oxide content using oxalate extraction on pretreatment samples.
Uranophane	30 mg/kg	10,000	7.8×10^{-13}	Surrogate for uranium bearing mineral phases is composed of carbonates and silicates and for uranium associated with calcite. Solid concentration is derived using 2,000 µg/L observed uranium concentration in water at start of the experiment (without any sodium tripolyphosphate) and considering K_d value of 15 mL/g based on Equation 2 of ECF-300FF5-11-0151, *Groundwater Flow and Uranium Transport Modeling in Support of the 300 Area FF-5 RI/FS*. Dissolution rate constant set is same as that for calcite. Specific surface area is selected from range of 3,000 cm^2/g for uranium calcite and 748,800 cm^2/g for uranophane (Table 3.3 of PNNL-17818).

Results from the 1D reactive transport model using GWB are shown in Figure B-2 based on simulating the experimental conditions. The results match those observed in the experiment. High uranium[3] concentrations are maintained initially at around 1,000 µg/L with fluctuations up to 5,000 µg/L for the first 20 pore volumes and then decline over next 10 pore volumes to a value of 10 µg/L. Higher uranium concentrations can be achieved by introducing minerals with higher specific surface area and kinetic rate constants but due to lack of detailed characterization information have not been modeled. The phosphate concentration (represented in terms of HPO_4^{2-}) remains low for the first 20 pore volumes and then increases sharply from 20 to 25 pore volumes and then continues to increase gradually as in the experiment (Figure B-1). Calcium concentrations also behave in a manner similar to those observed in the experiment. They start in the range of 30,000 to 40,000 µg/L, then show a steady decline, but remain around 10,000 µg/L. The lower figure (in Figure B-2) shows the model predicted concentration time histories for Na^+, HCO_3^-, and pH. The Na^+ and HCO_3^- concentrations do not change much, but pH starts to show a decline with increasing pore volumes. The decline is steeper in first few pore volumes, and pH is about 6.2 after around 10 pore volumes. The pH declines slowly over next 50 pore volumes with a minimum value of about 5.7, indicating that reactions with minerals lead to excess H^+ ions in the solution. The simulated change in pH has not been reported in the experiments but likely occurs given that all other observations are consistent with the simulated results. Effluent uranium concentrations remain much higher over first 10 to 15 pore volumes when treated with sodium polyphosphate solutions, compared to solutions containing no sodium polyphosphate (Figure B-1). This probably results from dissolution of uranium bearing mineral phases due to change in pH.

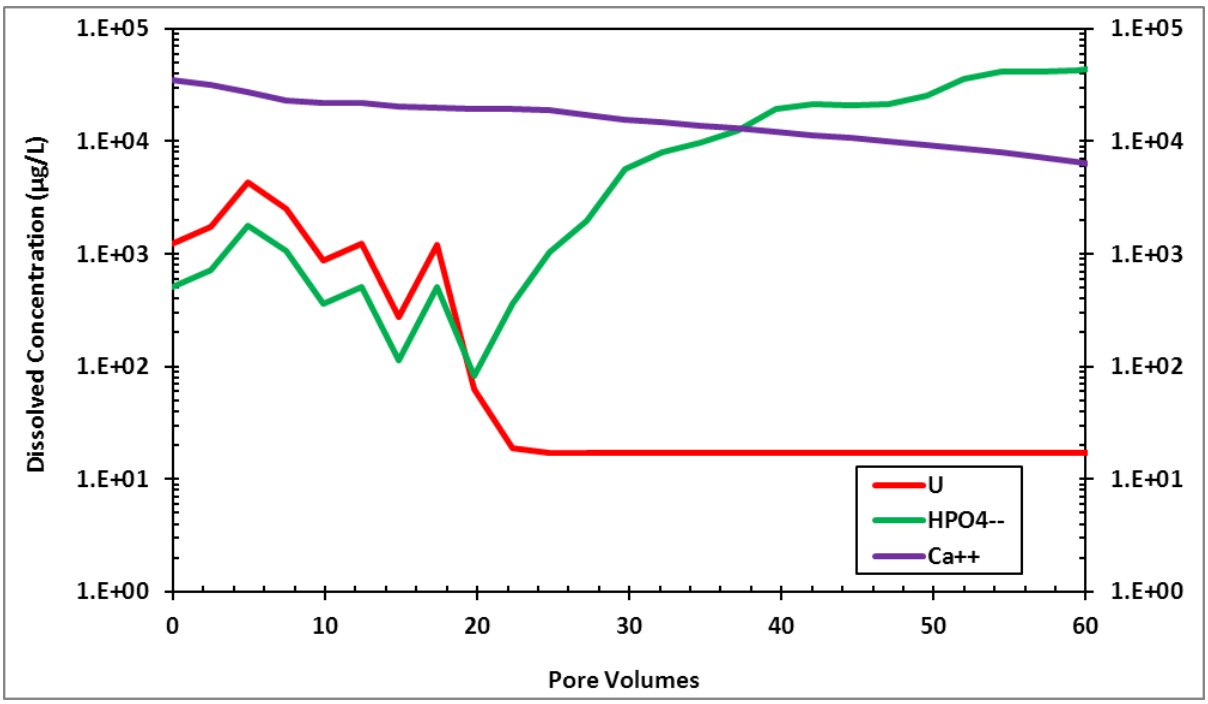

Note: U is reported as $UO_2(H_2PO_4)_2$, the primary species; HPO_4^{2-} is the total concentration of phosphate presented in terms of HPO_4^{2-}.

Figure B-2. Simulated Results from 1D Reactive Transport Model of the Unsaturated Column Experiment Reported by Wellman et al. (2007) with Tripolyphosphate Amendment

[3] Uranium concentration is reported as $UO_2(H_2PO_4)_2$, which is the primary uranium bearing aqueous species. In order to convert this to the U elemental concentration, multiply with 0.51 value.

The calculated saturation indices of selected mineral phases as a function of pore volumes are presented in Figure B-3 to evaluate which mineral phases are thermodynamically favored for dissolution or precipitation. Increasing saturation index (increasing to one or greater) with increasing pore volume indicates conditions favorable for saturation and precipitation of minerals while declining values of saturation index (less than 1) indicates conditions leading to dissolution. Until about 15 pore volumes, the uranium bearing mineral phases were at or above saturation (saturation index >1) and continued to provide uranium to the solution at steady concentrations. However, the saturation index shows a steep decline after 15 pore volumes due to continued dissolution. This also coincides with the decline in uranium concentrations indicating that the mineral phase underwent dissolution due to inflow of phosphate solutions. The saturation indices of calcite (and to some extent quartz) also show steady decline. This results in response to pH buffering primarily by dissolution of uranium bearing mineral phases and carbonates. Uranophane[4] is considered in the model as a surrogate for uranium bearing mineral phases composed of carbonates and silicates and for uranium associated with calcite. Once the uranium bearing mineral phases are exhausted, pH buffering occurs primarily by dissolution of calcite (and perhaps by other carbonate mineral phases). In this process, the dissolution of clay minerals and existing iron oxyhydroxide mineral phases occurring as coatings around the quartz grains is also expected to occur. Following the dissolution of uranium bearing minerals and with increasing availability of Ca^{2+} ions in the solution (due to ion exchange reactions with Na^{+} and from dissolution of calcite), the formation of calcium-phosphate mineral phases such as hydroxyapatite ($Ca_5(PO_4)_3OH$) and whitlockite ($Ca_3(PO_4)_2$) are favored. These show increasing saturation indices after about 20 pore volumes. These results are consistent with the experimental observations where the P concentrations increase from about 15 to 25 pore volumes and then reach a constant concentration indicating continued precipitation of calcium-phosphate bearing mineral phases.

Since phosphate is the primary reactant of interest, an evaluation is undertaken regarding the predominant speciation of HPO_4^{2-} based on the modeling results. The simulated distribution of phosphate species within the column experiment is presented in Figure B-4 at four different pore volumes. The x-axis shows the relative distance along the length of the column (0 is the start of the column and 1 is at the end of the column). After 5 pore volumes had passed through the column, the phosphate concentration distribution within the column is dominated by surface complexation reactions with iron oxyhydroxide (e.g., >(w)FeHPO4- and >(w)FeH2PO4). The concentration front has only moved to the relative distance of 0.6 at this stage. Other species, such as HPO_4^{2-} and $H_2PO_4^{-}$ are further retarded. Only minor concentrations of phosphate species have reached the end of the column (relative distance of 1). After 15 pore volumes, the distribution of phosphate is still dominated by surface complexation, but by now the concentration front has moved through and is near the end of the column indicating that all of the surface sorption sites associated with iron oxyhydroxide are in equilibrium with the solution and almost all sorption sites are filled. These surface reactions occur due to changes in surface charge from introduction of sodium tripolyphosphate solutions that leads to deprotonation and protonation reactions. After 22 pore volumes, concentrations associated with the surface species (e.g., >(w)FeHPO4- and >(w)FeH2PO4) are near maximum throughout the column, indicating that all of the buffering and reactions with available sorption sites have taken place. At this stage, the phosphate concentrations in the effluent show a steep rise, indicating breakthrough (Figure B-2). While >(w)FeHPO4- and >(w)FeH2PO4 concentrations are high within most of the column, they are much lower near the start of the column (relative distance of 0.1). This probably results from competition for surface sorption sites by species, such as >(w)FePO4--, which now occupy most of the sorption sites. Aqueous species HPO_4^{2-} is also

[4] According to PNNL-20004, *Remediation of Uranium in the Hanford Vadose Zone Using Ammonia Gas: FY 2010 Laboratory-Scale Experiments*, uranium bearing silicate (e.g., Na-boltwoodite) is predominantly dissolved (85 percent) in the acetic acid extraction. Therefore, some of the uranium fraction is present as silicate in addition to being associated with carbonates.

dominant up to relative distance of 0.2 but then its concentration drops. After 30 pore volumes have been flushed, the distribution of phosphate species reaches near steady state. The surface complexation of phosphate that results in formation of surface species >(w)FeHPO4-and >(w)FeH2PO4 is a dominant reaction.

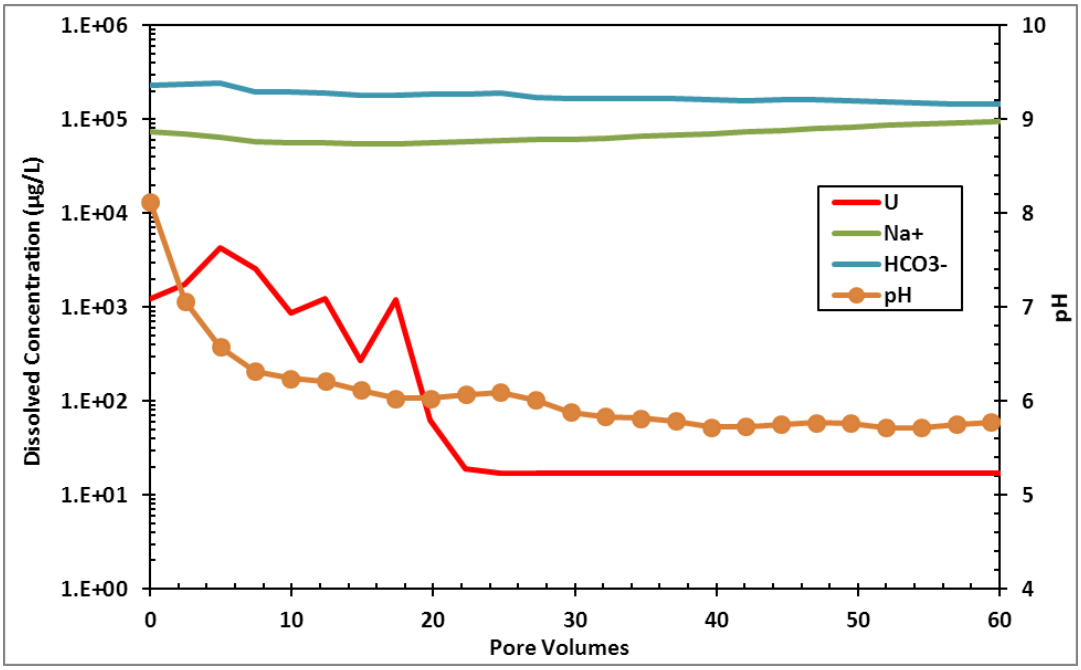

Note: U reported as UO2(H2PO4)2, the primary species.

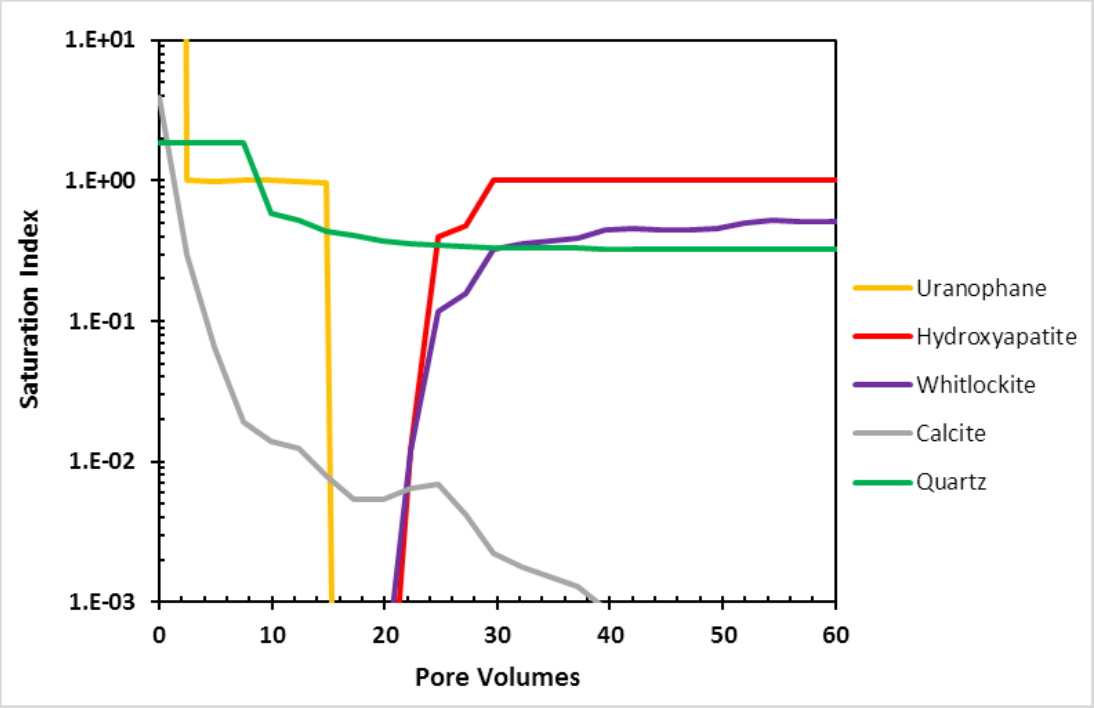

Figure B-3. Mineral Saturation Index as a Function of Pore Volume Using 1D Reactive Transport Model of the Unsaturated Column Experiment Reported by Wellman et al. (2007) with Tripolyphosphate Amendment

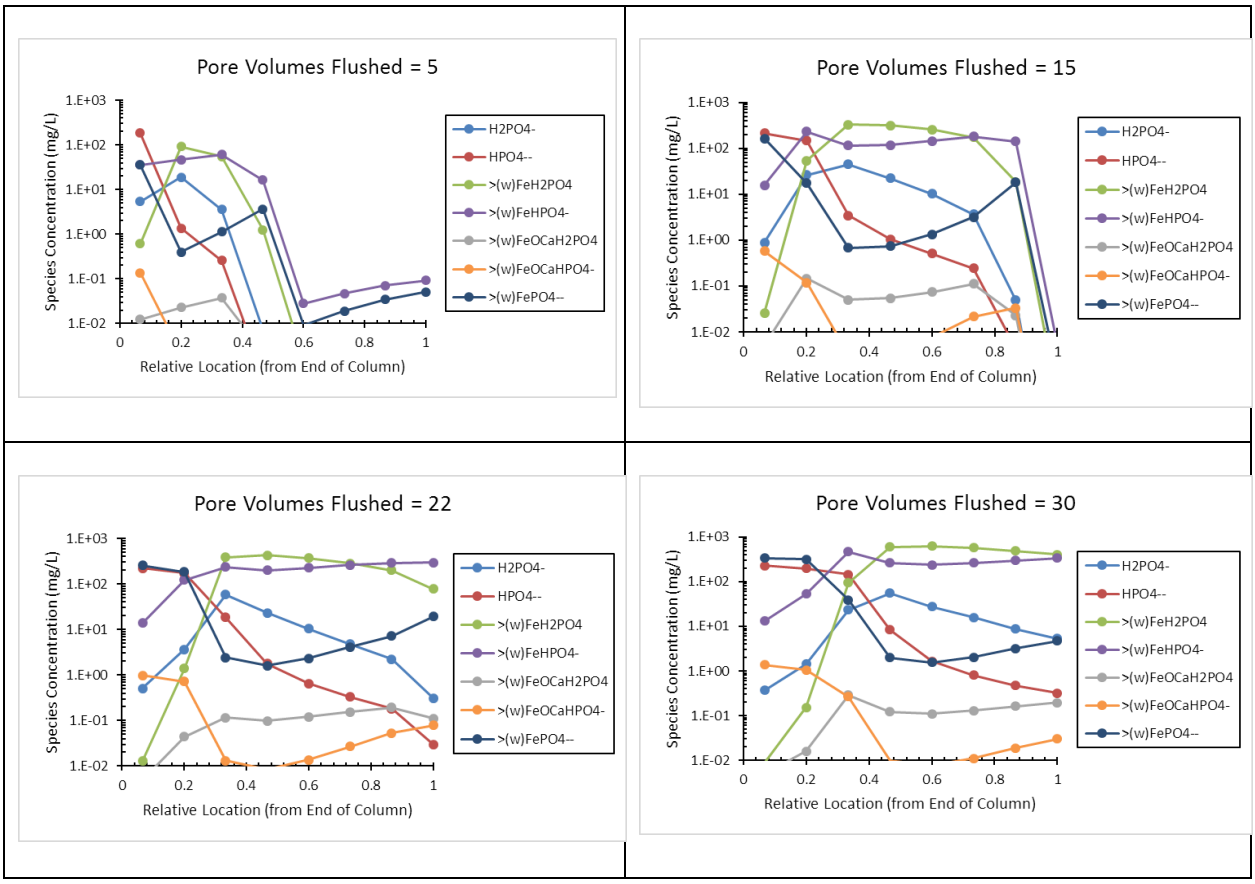

Figure B-4. Simulated Distribution of HPO_4^{2-} Species within the Column at Selected Pore Volumes

Based on modeling and evaluation of a carefully controlled laboratory experiment, where a uranium contaminated sediment sample from the North Process Pond in the 300 Area was flushed with sodium tripolyphosphate solution, the following inferred sequence of primary reactions are summarized:

1. As phosphate amendments are prepared in the pH range of 7 to 10, the predominant phosphate species in the solution will be HPO_4^{2-}.

2. As and when the sodium phosphate bearing solution contacts the sediment, the following reactions get initiated:

   a. Ion exchange reaction with Na^+ ion leads to release of Ca^{2+} in the solution:

   $$Na^+ + 0.5\ Ca\text{-}X_i \leftrightarrow Na\text{-}X + 0.5\ Ca^{2+}$$

   b. Ca^{2+} and HPO_4^{2-} react in the solution to form calcium-phosphate bearing mineral phases and result in deprotonation (release of H^+):

   $$5\ Ca^{2+} + 3\ HPO_4^{2-} + H_2O \rightarrow Ca_5(PO_4)_3OH + 4\ H^+$$

   Hydroxyapatite

   $$3\ Ca^{2+} + 2\ HPO_4^{2-} \rightarrow Ca_3(PO_4)_2 + 2\ H^+$$

   Whitlockite

3. As the pH starts to decline due to continued supply of H^+, buffering reactions start to occur where protons are consumed and pH is buffered. The following reactions consume protons:

   a. Surface complexation based reactions that are sensitive to changes in pH occur on both weak sites (>(w)FeOH) and strong binding sites (>(s)FeOH) that are collectively represented as (≡FeOH):

   $$\equiv FeOH + H_2PO_4^- + H^+ \leftrightarrow \equiv FeH_2PO_4 + H_2O$$
   $$\equiv FeOH + HPO_4^{2-} + H^+ \leftrightarrow \equiv FeHPO_4^- + H_2O$$

   It should be noted that surface complexation reactions with phosphate will occur just from supply of phosphate ions in the solutions even if the calcium and phosphate reactions were not occurring. The pH of the initial solution is around 8, which is near the point of zero net proton charge on the surface of iron oxyhydroxides. As the HPO_4^{2-} ions are introduced, and since the pH of the influent solution is different (~10) than the resident pore water pH, the charge balance in the solution changes and leads to surface complexation reactions due to amphoteric nature of iron oxyhydroxide surfaces.

   b. Mineral reactions that lead to consumption of protons can cause mineral phase dissolution. For uranium bearing mineral phases that are associated with carbonates and silicates (represented by uranophane mineral as shown below) such reactions would lead to dissolution of mineral and release of uranyl ion that could result in increased dissolved concentration of uranium:

   $$Ca(H_3O)_2(UO_2)_2(SiO_4)_2(H_2O)_3 + 6\ H^+ \leftrightarrow Ca^{2+} + 2UO_2^{\ 2+} + 2SiO_2 + 9H_2O$$

   c. Other carbonate bearing mineral phases, predominantly calcite, that are present in the sediments will undergo dissolution in order to consume protons:

   $$CaCO_3 + H^+ \rightarrow Ca^{2+} + HCO_3^-$$

4. While there is continued supply of phosphate, the released Ca^{2+} made available from the above two reactions will continue to bind with HPO_4^{2-} to form calcium-phosphate bearing mineral phases and in turn lead to deprotonation (as shown in Step 2). This cycle of deprotonation followed by consumption of protons will continue as long as supply of both phosphate and reacting iron oxyhydroxide surfaces and minerals (primarily uranium bearing carbonates and silicates and calcite) is maintained. If and when the surface capacity is reached (i.e., all surface sorption sites are at equilibrium with the influent solution) and if the buffering mineral phases (primary buffers) completely dissolve away, then the phosphate concentrations will rise in the effluent. Due to excess supply, the phosphate will start to react with the available calcium (that is still made available from ion exchange reactions) and start forming calcium phosphate bearing mineral phases. In this process any uranium in the solution will adsorb or get bound (forming uranyl orthophosphate or uranyl hydrogen phosphate) and be sequestered.

5. While surface reactions occur quickly and buffer the pH initially, the primary buffering reactions are expected to be controlled by the mineral phase dissolution. As a result, the kinetics of the mineral dissolution along with initial available amount of reactants plays an important role in describing the behavior of the system.

B.1.3 Reactive Transport Modeling to Simulate Stage A Infiltration and Injection

Based on the information learned from the controlled laboratory experiment performed under unsaturated conditions, reactive transport modeling was undertaken to simulate the infiltration of phosphate bearing solutions in Stage A and predict the probable reactions occurring in the subsurface.

A 1D column through the vadose zone was conceptualized, as shown in Figure 6-24. The vertical thickness of the column is set at 8 m (26.24 ft), which is the approximate distance from the point of infiltration to the water table within the Stage A area. The specific discharge through the column is calculated to maintain an average linear pore water velocity of 1 m/day, consistent with the ERT data. The moisture content was set at 0.2 for the duration of the infiltration. The infiltration was simulated for 9 days consistent with the infiltration period (November 7 through 15). The model simulation was run for an additional 6 days under no infiltration conditions to evaluate the effects during and post-infiltration for the total simulated duration of 15 days.

The model domain was discretized into 16 grid blocks of 0.5 m (1.6 ft) length each. Under constant flow conditions simulated, this discretization is deemed adequate. The initial pore water composition was based on the water composition of well 399-1-87 (a periodically rewetted zone [PRZ] well) from November 6, 2015 (prior to start of infiltration). Where major ion data were not available, the concentrations were based on sampling from well 399-1-17A on September 30, 2015. The infiltrated solution composition was based on sampling the mixing skid on Day 3 of infiltration, when influent concentrations were stable. The compositions of the solutions are presented in Table B-2. In addition, mineral reactants were added with kinetic reactions as presented in Table B-3. The cation-exchange capacity was set at 0.01 meq/g (1 meq/100 g), which is a typical value for the 300 Area sediments. PNNL-21733, *Use of Polyphosphate to Decrease Uranium Leaching in Hanford 300 Area Smear Zone Sediment*, reports average cation exchange capacity of 1 to 2 meq/100 g with 77 percent ion exchange sites occupied with calcium and total surface calcium available for exchange is 0.9 to 1.5 mmol/100 g.

Table B-2. Composition of Initial Pore Water and Infiltrated Water for the Reactive Transport Simulations

Analyte	Pore Water Composition[a] (Concentrations in mg/L)	Infiltrated Water Composition[b] (Concentrations in mg/L)
Ca^{2+}	49.7	15.2
Na^{+}	33	1,440
Mg^{2+}	12	4
K^{+}	5.3	1,110
Fe (Total)	0.01	0.01
U (Total)	0.060	10^{-6}
$HCO3^{-}$	128	1,780
$NO3^{-}$	25	2
Cl^{-}	20.6	50
SO_4^{2-}	60.9	63
HPO_4^{2-}	0.01	1,600 (Total Phosphorus)
DO	9	8
pH	7.25	7.01

a. Based on water composition from PRZ well 399-1-87 and groundwater well 399-1-17A.

b. Based on composition from mixing skid on Day 3.

Table B-3. Mineral Reactants and Associated Parameters Considered for Modeling Stage A Infiltration

Mineral	Amount	Specific Surface Area (cm^2/g)	Dissolution Rate Constant ($mol/cm^2/s$)	Basis for Parameters
Quartz	0.45 (volume fraction in bulk volume)	1,000	4.2×10^{-18}	Volume fraction is calculated by assuming 60% quartz content in the solid fraction and 25% porosity. Dissolution rate is constant based on Rimstidt and Barnes, 1980, "The Kinetics of Silica-Water Reactions." Specific surface area is based on typical sand grains from Leamnson et al., 1969, *A Study of the Surface Areas of Particulate Microcrystalline Silica and Silica Sand*.
K-Feldspar	0.26 (volume fraction in bulk volume)	1,000	3×10^{-17}	Volume fraction is calculated by assuming 35% feldspar content in the solid fraction and 25% porosity. Dissolution rate constant is based on Blum and Stillings, 1995, "Feldspar Dissolution Kinetics." Specific surface area is the same as quartz.
Calcite	0.0015 (volume fraction in bulk volume)	1,000	7.8×10^{-13}	Volume fraction is estimated based on calcium extracted by weak and strong acetic acid on pretreatment samples. Dissolution rate constant is derived from 1.55×10^{-6} $mol/m^3/s$ rate from Palandri and Kharaka, 2004, *A Compilation of Rate Parameters of Water-Mineral Interaction Kinetics for Application to Geochemical Modeling*. Specific surface area is adjusted down, based on uranium-calcite value of 3,000 cm^2/g in PNNL-17818 (Table 3.3).
Kaolinite and Illite Clay Minerals	0.022	100,000	1×10^{-17}	Volume fraction is based on 3-6% clay content in the sediments. Dissolution rate constant is taken from Nagy, 1995, "Dissolution and Precipitation Kinetics of Sheet Silicates," and specific surface area is from Carrol and Walther, 1990, "Kaolinite Dissolution at 25°, 60°, and 80°C."
Ferrihydrite	0.002 (volume fraction in bulk volume)			The volume fraction is based on estimate of amorphous iron oxide content using oxalate extraction on pretreatment samples.

Table B-3. Mineral Reactants and Associated Parameters Considered for Modeling Stage A Infiltration

Mineral	Amount	Specific Surface Area (cm^2/g)	Dissolution Rate Constant ($mol/cm^2/s$)	Basis for Parameters
Uranophane	10 mg/kg	10,000	1×10^{-14}	Surrogate for uranium bearing mineral phases is composed of carbonates and silicates and for uranium associated with calcite. Solid concentration is derived using 1,500 µg/L observed uranium concentration in water at start of the column tests and considering K_d value of 15 mL/g based on Equation 2 of ECF-300FF5-11-0151, *Groundwater Flow and Uranium Transport Modeling in Support of the 300 Area FF-5 RI/FS*, and assuming 40% gravel fraction. Dissolution rate constant is rounded up from the value used for calcite. Specific surface area is selected from range of 3,000 cm^2/g for uranium calcite and 748,800 cm^2/g for uranophane (Table 3.3 of PNNL-17818).

Results of the simulation are presented in terms of distribution of selected components in the fluid for selected times across the length of the column (Figure B-5). For each time point, a pair of results are presented with the left side showing the concentration of selected cations and anions of interest.
The HPO42- concentration shown on the left figure is the total concentration of phosphate represented as HPO42- while the right hand figure shows the speciation of HPO42- along with the pH of the solution. The selected time points for display are concentrations at 0, 3.3, 6.3, 7.8, and 10.2 days after start of infiltration. Concentration distribution prior to infiltration is shown in figures related to 0 days.
For purpose of tracking simulated transport of a conservative (nonreactive) species, Br- is added to the infiltrated water at a concentration of 1 mg/L. This is done strictly for the purpose of simulation in order to compare the retardation of species compared to a conservative species (Br-).

After 3.3 days of infiltration of phosphate-rich solutions, the concentration of HPO42- shows a steep decline between 2.5 m and 4 m (8.2 and 13.1 ft) depth. This is indicative of a developing reaction front that leads to retardation of HPO42-. Behind this zone (between 0 and 2 m [0 to 6.5 ft] depth) the Ca2+ concentrations have declined to much lower values while in front of this zone (>4 m [>13.1 ft] depth), the concentrations are near the pre-infiltration levels. The U (elemental uranium) concentration also shows a steep decline at the reaction front just like HPO42- while Fe2+ shows elevated concentration behind the reaction front and slight increase ahead of the front from advective transport. The pH shows a steep decline between 2.5 and 3 m (8.2 and 9.8 ft) depth, with a low value of 5.75 that increases before and after this depth. The primary HPO42- species are surface complexed species >(w)FeH2PO4 and >(w)FeHPO4- and aqueous species HPO42- and H2PO4-. The concentration of these species follow the pH decline. The HPO42- reaction front is a net result of several reactions – as HPO42- is added to the sediments, the resulting deprotonation reactions lead to excess H+ ions (and pH reduction) that in turn leads to buffering reactions through ion exchange, surface complexation, and mineral phase dissolution. The elevated concentration of Fe2+ behind the reaction front indicates reactions between iron oxyhydroxide (and clay minerals) with incoming HPO42-.

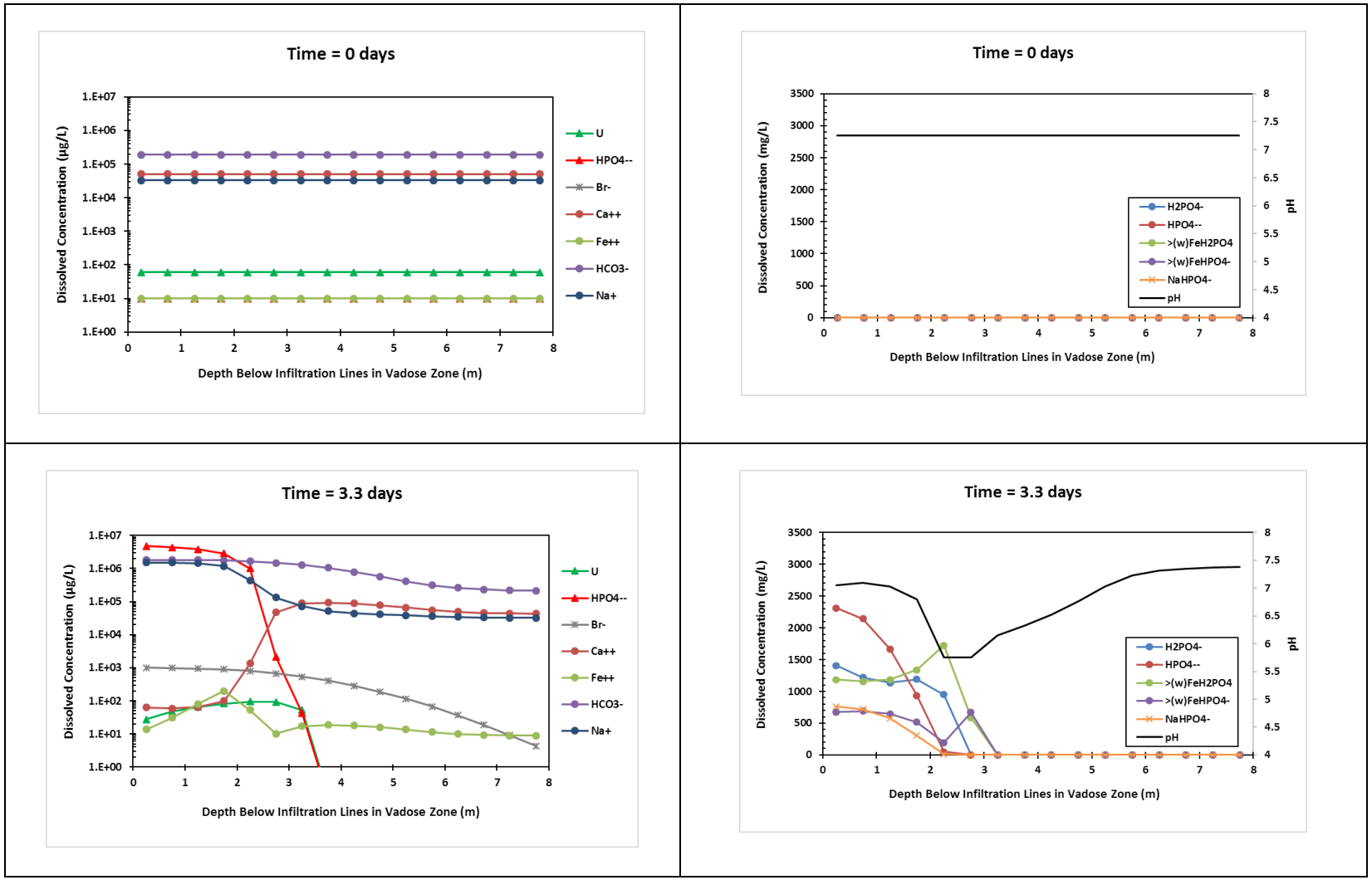

Figure B-5. Simulated Concentrations of Selected Constituents from Infiltration of Phosphate Bearing Solutions for Stage A (page 1 of 3)

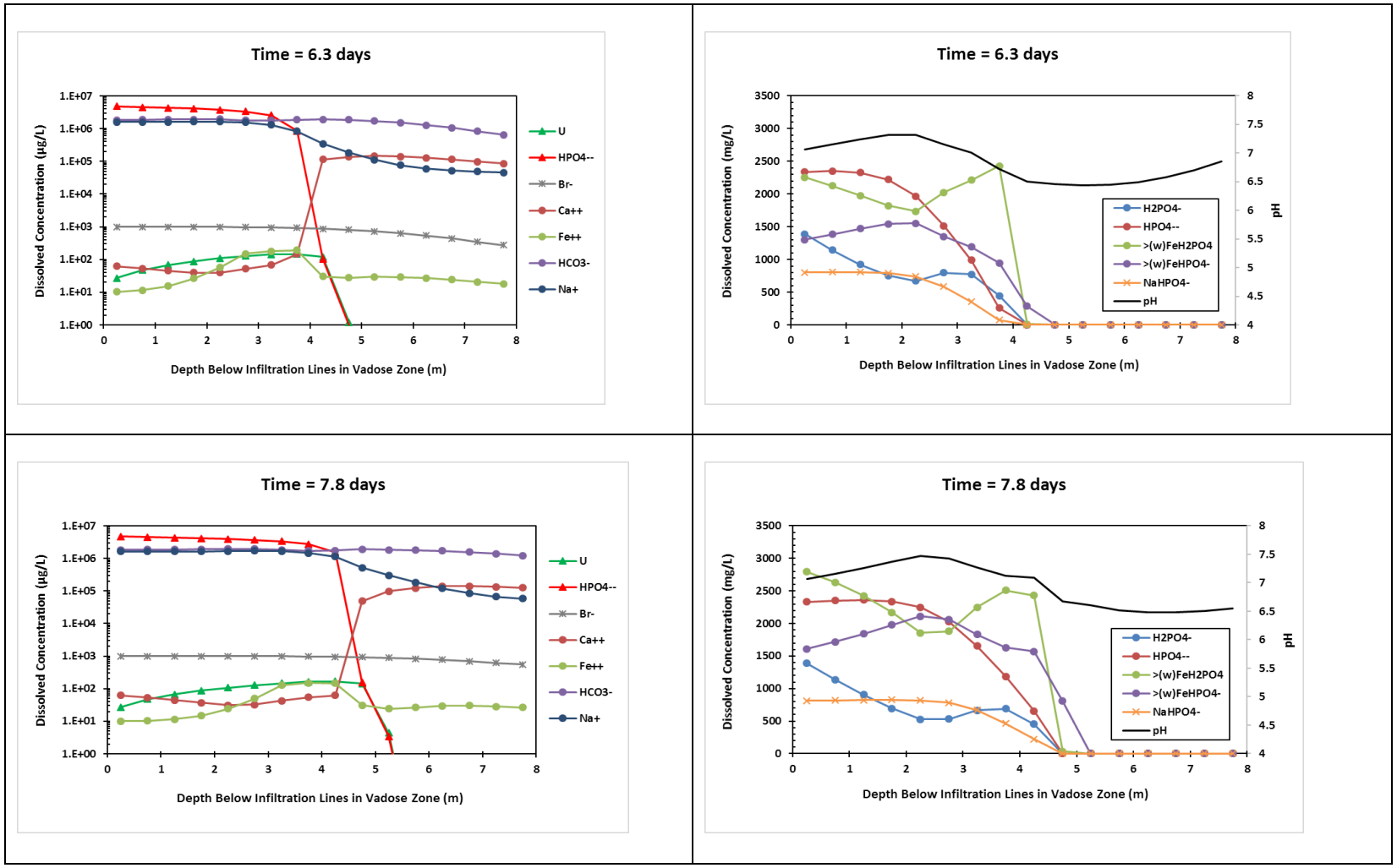

Figure B-5. Simulated Concentrations of Selected Constituents from Infiltration of Phosphate Bearing Solutions for Stage A (page 2 of 3)

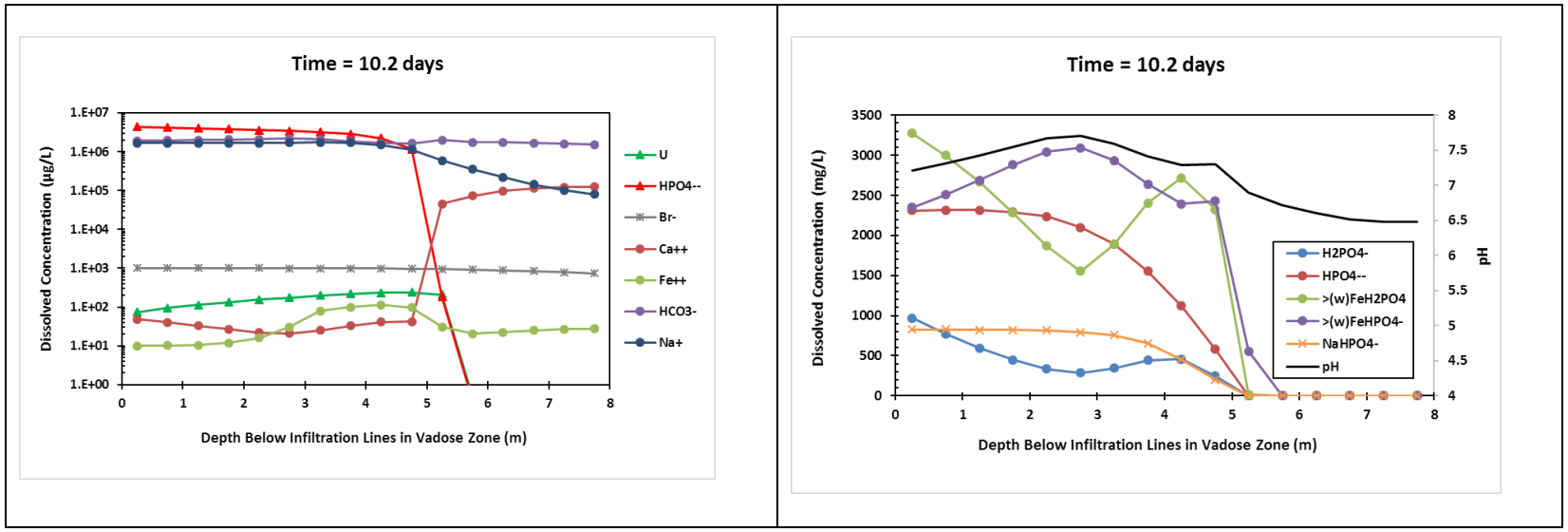

Notes: Uranium concentrations presented here are the uranium elemental concentrations. Left hand side figures show concentrations of selected constituents, while right hand side figures show speciation of HPO_4^{2-} and pH variations.

Figure B-5. Simulated Concentrations of Selected Constituents from Infiltration of Phosphate Bearing Solutions for Stage A (page 3 of 3)

After 6.3 days, the reaction front has moved to about 4 to 5 m (13.1 to 16.4 ft) depth (below infiltration lines). Uranium concentrations shows a steep decline at the reaction front. Other ions, such as Ca^{2+} and Fe^{2+} show a similar behavior as seen for previous time. The dominant HPO_4^{2-} species also remain the same; however, the pH decline is no longer that steep and the lowest pH value is around 6.4 that occurs at depth of about 5 m (16.4 ft). By the end of 7.8 days, the front has moved only a little distance (~0.5 m [1.6 ft]) compared to its location at 6.3 days but the pH profile shows some recovery from ongoing buffering reactions, however, the pH remains lower in the region of 6 to 7 m (19.7 to 22.9 ft) depth. Behind the reaction front the pH shows a gradual increase indicating that the deprotonation reactions have slowed compared to proton consuming reactions, such as formation of surface species of phosphate and mineral dissolution of carbonates. After 10.2 days, the reaction front profile does not show much of a change compared to 7.8 days. This is because the infiltration stopped on the 9th day and, therefore, there is no advective transport in the model. The pH continues to climb gradually behind the reaction front and the surface complexed species of phosphate are the dominant species. The pH at a depth of 8 m (26.2 ft), which is also the end of the vadose zone, is around 6.5, indicating some reaction with leading edge of phosphate ions.

The majority of the phosphate remains within the depth of 0 to 6 m (0 to 19.7 ft) and does not show any breakthrough at the end of the vadose zone. At and beyond the reaction front, the uranium concentration remained low. By end of 8th day, about one pore volume has been flushed. This can be seen by the concentration profile of Br^- that is simulated as a conservative tracer. The breakthrough profile shows that more than half the initial concentration of Br^- reaches the end of the vadose zone by about 8 days.

The simulated results help explain the observations of the post-treatment sequential leach test samples taken at various depths. Dissolution of U, Ca, Fe, and Mn from oxides and clay mineral phases was inferred due to observed reduction in fraction extractable by the strong nitric acid with corresponding increase in the fraction associated with the carbonates (weak and strong acetic acid extraction) indicating re-precipitation. In addition, the simulated results are consistent with the reduction in pH observed during daily monitoring of the PRZ wells. Figure B-6 presents the observations from the two PRZ wells (399-1-81 and 399-1-75) located within the Stage A area. The pH declines during the infiltration period (November 7 through 15) while the Ca/Na concentration ratio (in terms of meq/L concentration) show a continued decline as Na bearing fluids move through the vadose zone. Similar qualitative behavior is seen in the simulated results where the Na concentrations continue to rise. Figure B-7 presents the observations in terms of uranium and phosphate concentrations for the same two PRZ wells. During the infiltration time period (November 7 through 15), the uranium concentrations show an initial increase followed by sharp decline while the phosphate concentrations remain negligibly small. The initial increase in uranium could be partially due to dissolution of mineral phases in order to buffer the pH change. The increase in phosphate observed after November 15 is due to start of PRZ and aquifer injections. Small increase prior to November 15 may be due to either phosphate arriving from prior aquifer injection (November 9) or due to breakthrough of phosphate from infiltration at this time. The initial increase in uranium followed by decline and negligible phosphate in the PRZ along with declining pH and Ca/Na ratio all are consistent with the simulated results.

While the simulated results are qualitatively similar and provide useful understanding of the system behavior, they are not directly comparable to the observations due to various simplifications made for conducting the simulations: the concentration of the infiltrated solution was fixed over the 9-day time period even though considerable variability was observed as shown in Figure 6-3 in terms of phosphate concentrations. In addition, the linear pore water velocity was held constant at 1 m/day even though variability exists due to variable rates of infiltration (Table 6-1) and from field-scale heterogeneities observed from ERT images.

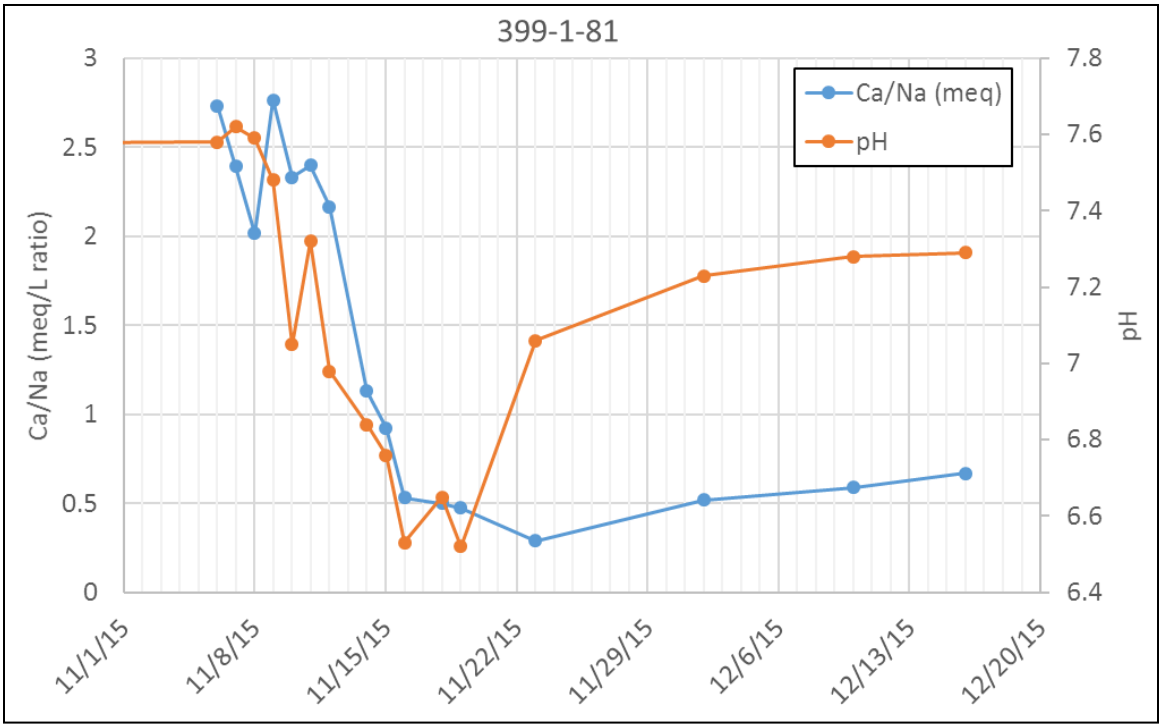

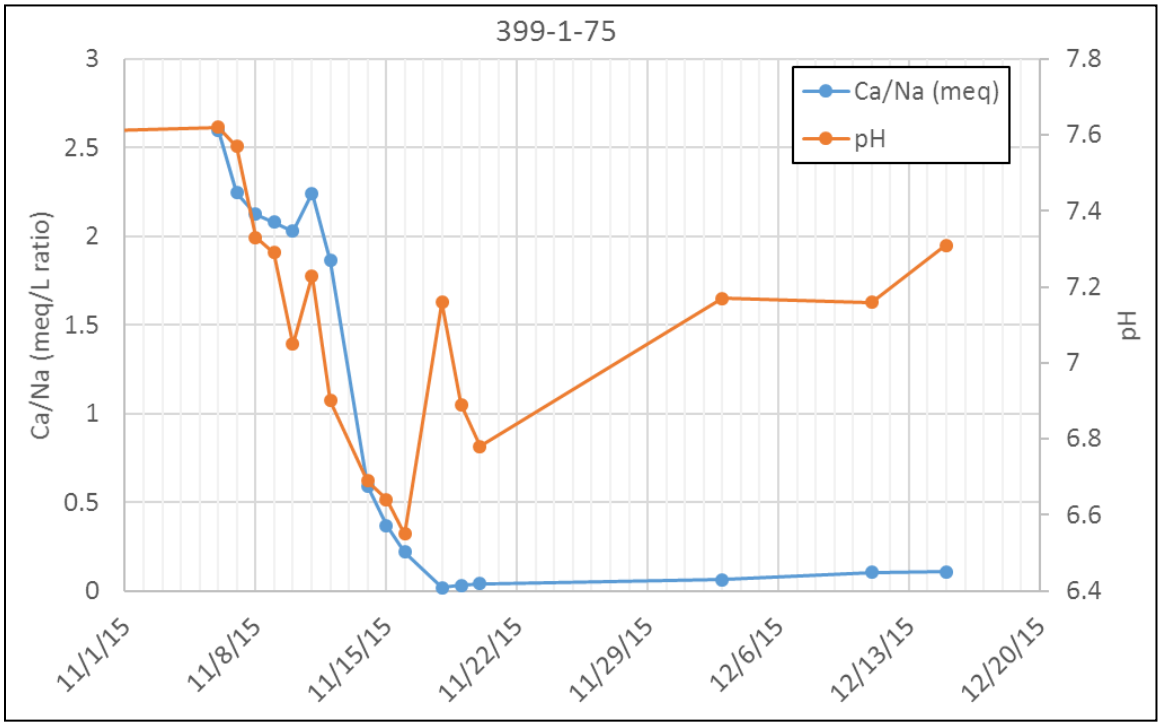

Note: The ratio of Ca/Na concentrations (in terms of meq/L) is shown on the left, while pH is shown on the right side.

Figure B-6. Observations from Daily Monitoring of PRZ Wells 399-1-81 and 399-1-75

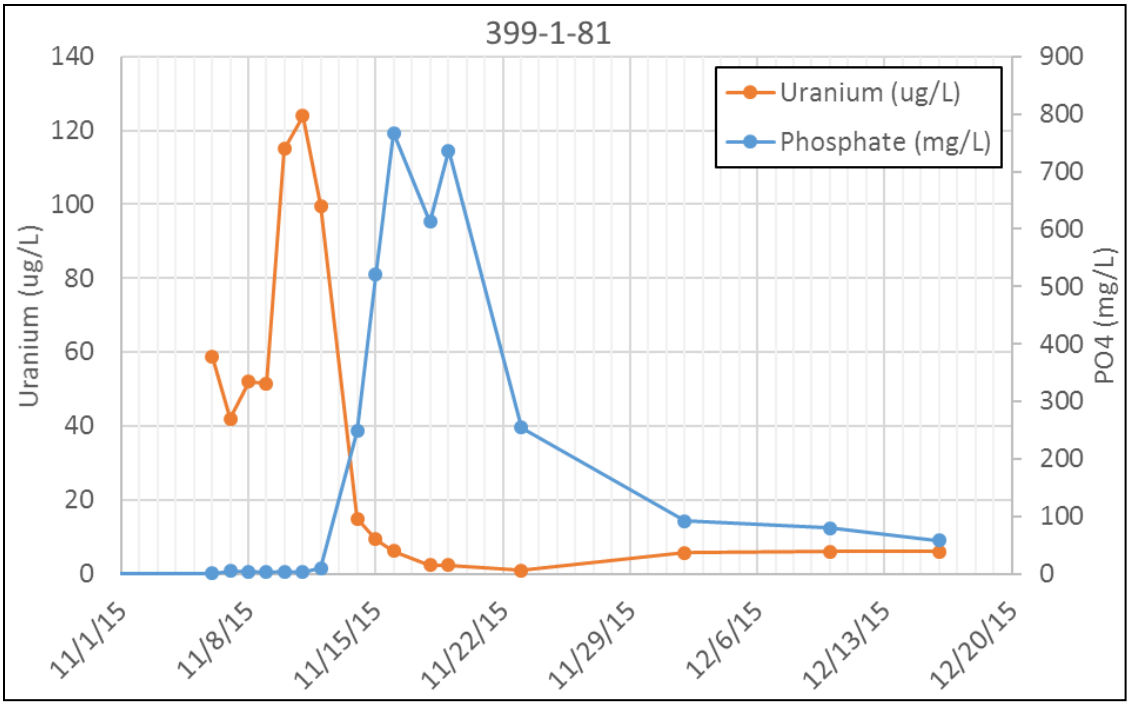

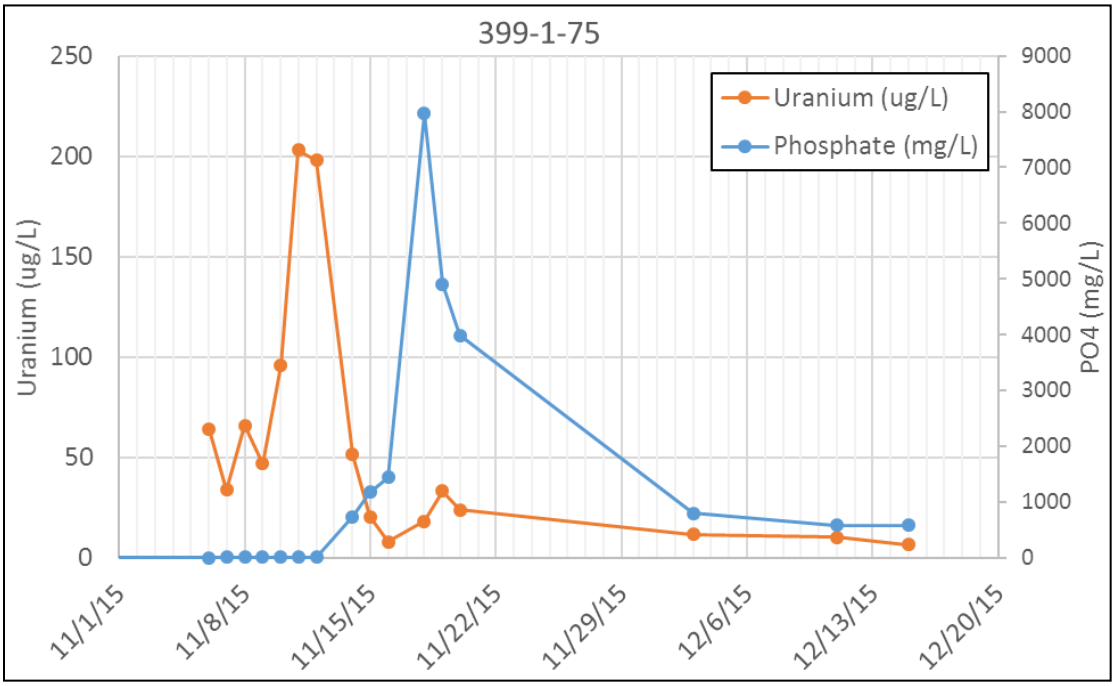

Figure B-7. Observations from Daily Monitoring of PRZ Wells 399-1-81 and 399-1-75 for Uranium and Phosphate Concentrations

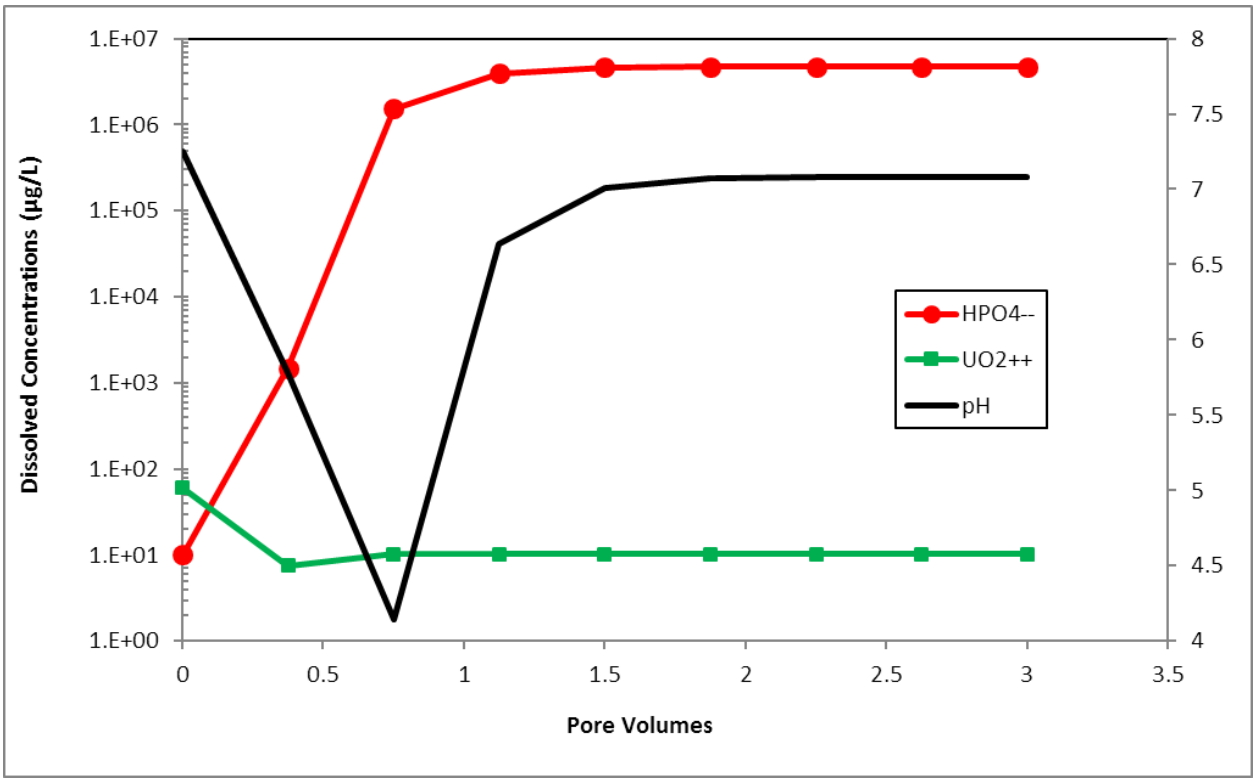

Figure B-8. Simulated Results of Conducting Injection

To simulate the effects of injection, a simplified calculation was made where the model setup for the infiltration (as discussed earlier) was used, but the flow rate was increased by a factor of 10. Results are presented in Figure B-8 for a distance located about 5 m (16.4 ft) from the injection point. The results are shown in terms of pore volumes at that location. HPO_4^{2-} concentrations increase quickly, while uranium concentrations go down and reach the background levels (~10 µg/L). The pH also reduces due to phosphate injection and resulting reactions but quickly recovers and reaches the value of injected solution.

B2 References

Appelo, C.A.J. and D. Postma, 2005, *Geochemistry, Groundwater and Pollution*, 2nd Edition, A.A. Balkema Publishers, Leiden, The Netherlands.

Blum, Alex E. and Lisa L. Stillings, 1995, "Feldspar Dissolution Kinetics," Chapter 7 in *Chemical Weathering Rates of Silicate Minerals*, A.F. White and S.L Brantley (Eds.), Mineralogical Society of America, *Reviews in Mineralogy* 31(1):291-352.

Bruggenwert, M.G.M. and A. Kamphorst, 1982, "Chapter 5: Survey of Experimental Information on Cation Exchange in Soil Systems," in *Soil Chemistry*: *B. Physico-Chemical Models*, *Developments in Soil Science* 5(B):141-203.

Carrol, Susan A. and John V. Walther, 1990, "Kaolinite Dissolution at 25°, 60°, and 80°C," *American Journal of Science* 290:797-810. Available at: http://earth.geology.yale.edu/~ajs/1990/07.1990.02Carroll.pdf.

Dzombak, David A. and François M.M. Morel, 1990, *Surface Complexation Modeling: Hydrous Ferric Oxide*, John Wiley & Sons, Inc., New York.

ECF-300FF5-11-0151, 2012, *Groundwater Flow and Uranium Transport Modeling in Support of the 300 Area FF-5 RI/FS*, Rev. 3, CH2M HILL Plateau Remediation Company, Richland, Washington. Available at: http://pdw.hanford.gov/arpir/index.cfm/viewDoc?accession=0078650H

Gaines, George L. and Henry C. Thomas, 1953, "Adsorption Studies on Clay Minerals. II. A Formulation of the Thermodynamics of Exchange Adsorption," *J. Chem. Phys.* 21:714-718.

Gao, Yan and Alfonso Mucci, 2001, "Acid Base Reactions, Phosphate and Arsenate Complexation, and their Competitive Adsorption at the Surface of Goethite in 0.7 M NaCl Solution," *Geochimica et Cosmochimica Acta* 65(14):2361-2378.

Gorman-Lewis, Drew, Peter C. Burns, and Jeremy B. Fein, 2008, "Review of uranyl mineral solubility measurements," *J. Chem. Thermodynamics* 40:335-352. Available at: http://www3.nd.edu/~fein/Publications/Gorman-Lewis%20JThermo%20(40)335.pdf.

Gorman-Lewis, D., T. Shvareva, K. Kubatko, P.C. Burns, D.M. Wellman, B. McNamara, J.E. Szymanowski, A. Navrotsky, and J.B. Fein, 2009, "Thermodynamic Properties of Autunite, Uranyl Hydrogen Phosphate, and Uranyl Orthophosphate from Solubility and Calorimetric Measurements," *Environ. Sci. Technol*. 43:7416-7422. Available at: http://www3.nd.edu/~fein/Publications/Gorman-Lewis%20EST%20(43)7416.pdf.

Leamnson, R.N., Josephus Thomas, Jr., and H.P. Ehrlinger III, 1969, *A Study of the Surface Areas of Particulate Microcrystalline Silica and Silica Sand*, Circular 444, Illinois State Geological Survey, Urbana, Illinois. Available at: https://www.ideals.illinois.edu/bitstream/handle/2142/44623/studyofsurfacear444leam.pdf?sequence=2.

Nagy, Kathryn L., 1995, "Dissolution and Precipitation Kinetics of Sheet Silicates," Chapter 5 in *Chemical Weathering Rates of Silicate Minerals*, A.F. White and S.L Brantley (Eds.), Mineralogical Society of America, *Reviews in Mineralogy* 31(1):173-234.

Palandri, James L. and Yousif K. Kharaka, 2004, *A Compilation of Rate Parameters of Water-Mineral Interaction Kinetics for Application to Geochemical Modeling*, U.S. Geological Survey Open File Report 2004-1068, U.S. Geological Survey, Menlo Park, California. Available at: https://pubs.usgs.gov/of/2004/1068/pdf/OFR_2004_1068.pdf.

PNNL-17818, 2008, *300 Area Treatability Test: Laboratory Development of Polyphosphate Remediation Technology for In Situ Treatment of Uranium Contamination in the Vadose Zone and Capillary Fringe*, Pacific Northwest National Laboratory, Richland, Washington. Available at: http://www.pnl.gov/main/publications/external/technical_reports/PNNL-17818.pdf.

PNNL-20004, 2010, *Remediation of Uranium in the Hanford Vadose Zone Using Ammonia Gas: FY 2010 Laboratory-Scale Experiments*, Pacific Northwest National Laboratory, Richland, Washington. Available at: http://www.pnl.gov/main/publications/external/technical_reports/PNNL-20004.pdf.

PNNL-21733, 2012, *Use of Polyphosphate to Decrease Uranium Leaching in Hanford 300 Area Smear Zone Sediment*, Pacific Northwest National Laboratory, Richland, Washington. Available at: http://www.pnnl.gov/main/publications/external/technical_reports/PNNL-21733.pdf.

Rimstidt, J.D. and H.L. Barnes, 1980, "The Kinetics of Silica-Water Reactions," *Geochimica et Cosmochimica Acta* 44(11):1683-1699.

Spiteri, Claudette, Philippe Van Cappellen, and Pierre Regnier, 2008, "Surface complexation effects on phosphate adsorption to ferric iron oxyhydroxides along pH and salinity gradients in estuaries and coastal aquifers," *Geochimica et Cosmochimica Acta* 72(14):3431-3445. Available at: http://citeseerx.ist.psu.edu/viewdoc/download?doi=10.1.1.463.9074&rep=rep1&type=pdf.

Wellman, Dawn M., Eric M. Pierce, and Michelle M. Valenta, 2007, "Efficacy of soluble sodium tripolyphosphate amendments for the in-situ immobilisation of uranium," *Environ. Chem.* 4(5):293-300.

Appendix C

Mathematical Model for Estimating Kinetic Sorption-Desorption Parameters

This page intentionally left blank.

C1 Introduction

The flow-through column tests performed to evaluate the leaching behavior of uranium provide useful information for quantifying the desorption rates. A single-site kinetic sorption-desorption model is developed to estimate the kinetic rates. The mathematical model (ECF-300FF5-11-0151, *Groundwater Flow and Uranium Transport Modeling in Support of the 300 Area FF-5 RI/FS*) describes the transport of a solute by dispersion and advection with kinetic sorption between the liquid and solid phases. The kinetic sorption is modeled by both a forward reaction rate from the liquid phase to the solid phase and a reverse reaction rate from solid to liquid. The geometry is represented by a one-dimensional column with length (L). The mathematical model consists of mass balance equations for both the dissolved and solid concentrations. The dissolved mass balance equation is as follows:

$$\theta \frac{\partial C}{\partial t} = \theta D \frac{\partial^2 C}{\partial z^2} - v \frac{\partial C}{\partial z} - \rho_b \frac{\partial q}{\partial t}, \quad 0 < z < L \qquad \textbf{Eq. 1}$$

where the z-axis is oriented along the length of the column. The solid mass balance or sorption kinetic equation is as follows:

$$\rho_b \frac{\partial q}{\partial t} = \alpha_f \theta C - \alpha_r \rho_b q \qquad \textbf{Eq. 2}$$

The forward/reverse reaction rates satisfy the relation:

$$\alpha_f = \alpha_r K_d \left(\frac{\rho_b}{\theta} \right) \qquad \textbf{Eq. 3}$$

where:

C: dissolved concentration [$\mu gm\ of\ U / cm^3\ of\ water$]

q: sorbed concentration, [$\mu gm\ of\ U / gm\ of\ solid$]

θ: water content, water volume/bulk volume [dimensionless]

v: Darcy velocity, water volume/area/time [cm / hr]

D: dispersion coefficient [cm^2 / hr]

ρ_b: bulk density, matrix mass/bulk volume [gm / cm^3]

α_f: forward reaction rate (sorption) [hr^{-1}]

α_r: reverse reaction rate (desorption) [hr^{-1}]

K_d: equilibrium constant, volume water/matrix mass [cm^3 / gm]

The sorption kinetic equation (Eq. 2) can be expressed in terms of only the reverse reaction rate by the reaction rate relation (Eq. 3). The sorption kinetic equation is written as follows:

$$\frac{\partial q}{\partial t} = \alpha_r K_d C - \alpha_r q \qquad \textbf{Eq. 4}$$

If Q_{inj} denotes the water injection rate, then the discharge or Darcy velocity is equal to the water injection rate per unit area normal to flow direction.

The model assumes that there is no dispersion across the upper and lower boundary of the column. The bromide experiments have an initial concentration of zero within the column. At the top boundary, an influent with known bromide concentration is maintained over time. The effluent concentration exiting the bottom of the column represents the experimental measured concentration.

The uranium experiments have zero concentration of influent, while initially the column contains uranium in both dissolved and solid states. The transport and kinetic sorption are in equilibrium initially. This implies that the dissolved and solid concentrations are constant throughout the column. At initial time, the solid concentration in equilibrium with the dissolved concentration requires the following:

$$\frac{\partial q}{\partial t}(z,0) = 0$$

which from Eqs. 2 and 3 implies the initial condition for the solid concentration: $q(z,0) = K_d C(z,0)$

The experimental results are presented as dissolved concentration a function of cumulative water pore volumes. The relation between time and pore volumes during flow periods is as follows:

$$PVs = \frac{Q_{inj} t}{\theta V_{bulk}}$$

where:

$$Q_{inj} = water\ injection\ rate\ [cm^3 / hr]$$

$$t = time\ [hr]$$

$$V_{bulk} = columnbulk\ volume\ [cm^3]$$

C1.1 Numerical Model for Kinetic Sorption-Desorption Parameter Derivation

The mathematical model is approximated by a finite difference scheme. Consider a finite difference discretization of space and time. Let the index I denote the spatial cell index, i = 1, 2, …, N_z, where N_z is the number of grid cells. Let the time discretization be denoted $0 = t_0 < t_1 < t_2 < \ldots < t_{N_t}$, where N_t is the number of time steps. The discretization is fully implicit and uses approximations, which are first order for time derivatives, first order upstream weighting for advective transport, and second order for dispersive transport. The discretization for the ith cell and time step from t_n to t_{n+1} for the sorption kinetics, Eq. 4, is as follows:

$$\rho_b \frac{q_i^{n+1} - q_i^n}{\Delta t} = \alpha_r \rho_b K_d C_i^{n+1} - \alpha_r \rho_b q_i^{n+1} \qquad \textbf{Eq. 5}$$

Solve Eq. 5 for the sorbed concentration yields as follows:

$$q_i^{n+1} = \frac{\alpha_r \Delta t K_d}{1 + \alpha_r \Delta t} C_i^{n+1} + \frac{1}{1 + \alpha_r \Delta t} q_i^n \qquad \textbf{Eq. 6}$$

Now discretize the transport equation (Eq. 1), and substitute for q_i^{n+1} the expression in Eq. 6. Expressing the resulting difference equation in tridiagonal form yields the following:

$$\begin{aligned} -\left(\frac{\theta D}{\Delta z^2} + \frac{v}{\Delta z}\right) C_{i-1}^{n+1} + \left(\frac{2\theta D}{\Delta z^2} + \frac{v}{\Delta z} + \frac{\theta}{\Delta t} + \frac{\alpha_r \rho_b K_d}{1 + \alpha_r \Delta t}\right) C_i^{n+1} - \frac{\theta D}{\Delta z^2} C_{i+1}^{n+1} \\ = \frac{\theta}{\Delta t} C_i^n + \frac{\alpha_r \rho_b}{1 + \alpha_r \Delta t} q_i^n \end{aligned} \qquad \textbf{Eq. 7}$$

This system of equations uses known information at the beginning of the time step, C_i^n and q_i^n, to calculate the water concentrations C_i^{n+1}. Once the dissolved concentrations are computed, Eq. 6 provides the sorbed concentrations q_i^{n+1}. Appropriate boundary conditions are applied at the upper and lower boundary cells. The initial data are as follows:

$$C(z,0) = C_{initial} \text{ and } q(z,0) = K_d C(z,0) = q_{initial}$$

For the uranium leach experiments, a no flow condition at the upper cell (influent) is imposed for both dispersive and advective transport. At the lower boundary, there is no dispersive transport out of the column. The advective mass transport at the lower boundary of the column ($i = N_z$) is computed as follows:

$$Q_{inj} \Delta t C_{Nz}^{n+1}$$

C1.2 Determination of Kinetic Sorption-Desorption Parameters

A MATLAB computer model representing the numerical model was implemented (an example presented in Appendix B). The following information was obtained from the experimental test setup:

- Column length
- Column diameter
- Water content
- Injection rate
- Soil bulk density

These parameters are provided for all samples in Table 6-5. Dispersion coefficient was estimated as $D = 10^{-3} cm^2 / hr$ for all cases.

For the uranium tests, the initial water concentration is estimated from the early time experimental results. The fitting parameters include the partition coefficient, K_d, and the reverse reaction rate, f_r. The forward sorption rate is computed from Eq. 3. At initial time it is assumed that the liquid/solid concentrations are in equilibrium; consequently, the initial solid concentration is $q(z,0) = K_d C(z,0)$. The history match of the experimental data is obtained by manually adjusting the partition coefficient and the reverse reaction rate until a best fit of the experimental data is obtained.

The nonsorbing bromide simulations assume that the initial column concentration is zero, and the influent has a specified dissolved concentration. Since bromide is nonsorbing, the partition coefficient is zero; consequently, both the forward and reverse reaction rates are zero. The bromide transport properties are all known, and the bromide simulations require no history matching process.

C1.3 Simulation Results

Four column experiments were run with a fine grain soil (<2 mm soil) for which the coarse grains were removed. These four fine grain (<2 mm size) soil sample tests were denoted as B347F1F3, B347P5P8, B247R1, and B347T7 (Table 6-5). Three field-textured (bulk) soil tests were denoted as B347P4, B347R0, and B347T6 (Table 6-5). Results for these seven sample cases were obtained for both bromide (nonsorbing) and uranium (sorbing).

A summary for all samples of the history match results for the kinetic reaction parameters is provided in Table C-1. The parameters include the initial dissolved concentration, partition coefficient, and reverse reaction rate determined from the history match of the sample data. The forward reaction rate is computed from Eq. 3.

Table C-1. Kinetic Reaction Parameters Used to History Match Post-Treatment Uranium Leach Experiments

Sample Number	Soil Type	Initial Dissolved Concentration (µg/cm^3)	K_d (cm^3/g)	Reverse Rate (1/hr)	Forward Rate (1/hr)
B347F1F3	Fine Grain (<2 mm)	0.02	9	0.009	0.361
B347P5P8	Fine Grain (<2 mm)	25	0.30	0.07	0.095
B347P4	Field-Textured (Bulk)	2.7	0.40	0.03	0.108

Table C-1. Kinetic Reaction Parameters Used to History Match Post-Treatment Uranium Leach Experiments

Sample Number	Soil Type	Initial Dissolved Concentration (µg/cm^3)	K_d (cm^3/g)	Reverse Rate (1/hr)	Forward Rate (1/hr)
B247R1	Fine Grain (<2 mm)	4.6	1.2	0.06	0.381
B347R0	Field-Textured (Bulk)	4.0	0.3	0.06	0.222
B347T7	Fine Grain (<2 mm)	0.007	5	0.017	0.436
B347T6	Field-Textured (Bulk)	0.016	0.98	0.019	0.288

C1.3.1 Sample B347F1F3 Fine Grain (<2 mm Size) Soil

Input and simulation results for sample B347F1F3 fine grain (<2 mm size) soil with bromide transport are shown in Table C-2 and Figure C-1, respectively. The numerical model results are in good agreement with the experimental results. The dissolved concentration on input have units of µg/cm^3 but are reported in Figure C-1 with µg/L units. This is the case for all subsequent results.

Table C-2. Input Parameters for Sample B347F1F3 Fine Grain (<2 mm Size) Soil with Bromide Transport

Column Length (cm)	15
Column Diameter (cm)	2.5
Number of Spatial Grid Cells	50
Time Step Size (hr)	0.1
Water Content (Dimensionless)	0.37
Dispersion (cm^2/hr)	0.001
Water Injection Rate (cm^3/hr)	5.53
Injection Stream Concentration (µg/cm^3)	0.05
Initial Concentration (µg/cm^3)	0

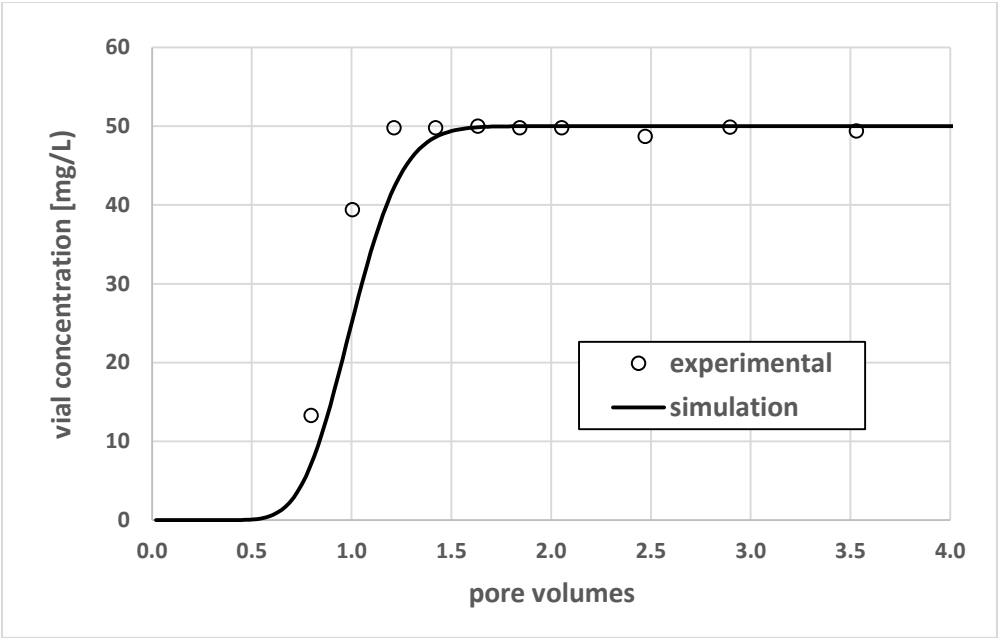

Figure C-1. Sample B347F1F3 Fine Grain (<2 mm Size) Soil with Bromide Transport

Input and simulation results for sample B347F1F3 fine grain (<2 mm size) soil with uranium transport are shown in Table C-3 and Figure C-2, respectively. Table C-3 provides the input data, together with the partition coefficient and reverse sorption rate, which yields the best fit of experimental data.
The simulation results in Figure C-2 show some disparity with the experimental results.
The concentration responses for the first 4 to 5 pore volumes are completely different. The experimental results start at a low concentration and increase, while the numerical simulation concentration decays from the initial concentration.

Table C-3. Input Parameters, Partition Coefficient, and Reverse Sorption Rate for Sample B347F1F3 Fine Grain (<2 mm Size) Soil with Uranium Transport

Column Length (cm)	15
Column Diameter (cm)	2.5
Number of Spatial Cells	50
Time Step (hr)	0.825
Water Content	0.372
Injection Rate (cm^3/hr)	5.53
Diffusion Coefficient (cm^2/hr)	0.001
Soil Bulk Density (g/cm^3)	1.66
K_d (cm^3/g)	9
Initial Water Concentration (µg/cm^3)	0.02
Initial Solid Concentration (µg/g)	0.18
Reverse Sorption Rate (1/hr)	0.0090
Forward Sorption Rate (1/hr)	0.361

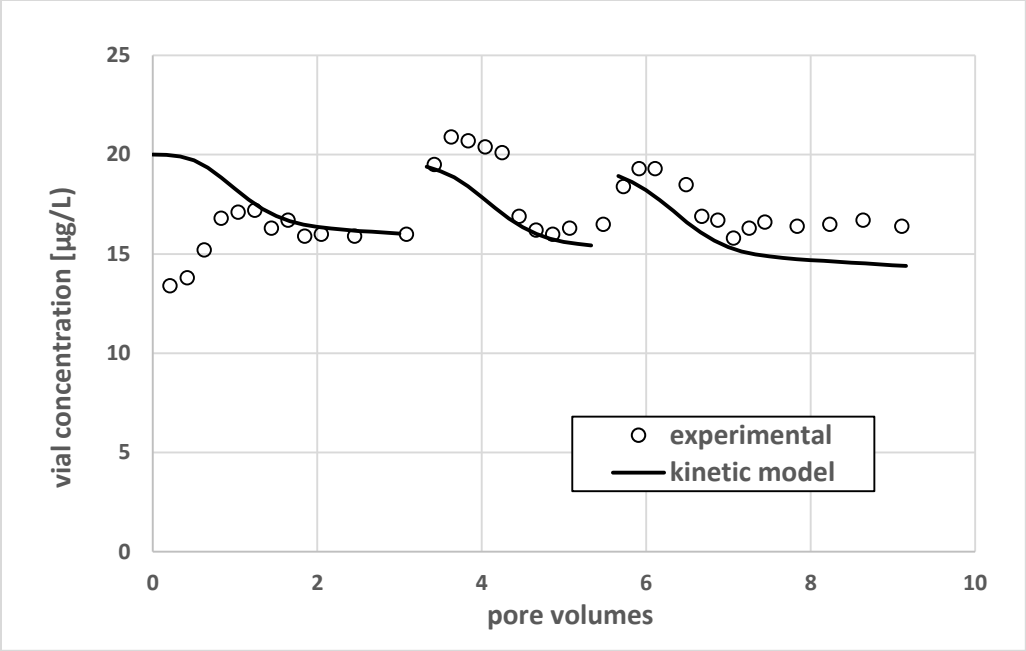

Figure C-2. Sample B347F1F3 Fine Grain (<2 mm size) Soil with Uranium Transport

C1.3.2 Sample B347P5P8 Fine Grain (<2 mm Size) Soil

Input and simulation results for sample B347P5P8 fine grain (<2 mm size) soil with bromide transport are shown in Table C-4 and Figure C-3, respectively. The simulation results are in good agreement with the experimental results.

Table C-4. Input Parameters for Sample B347P5P8 Fine Grain (<2 mm Size) Soil with Bromide Transport

Column Length (cm)	15
Column Diameter (cm)	2.5
Number of Spatial Grid Cells	50
Time Step Size (hr)	0.06
Water Content (Dimensionless)	0.22
Dispersion (cm^2/hr)	0.001
Water Injection Rate (cm^3/hr)	5.53
Injection Stream Concentration (µg/cm^3)	0.05
Initial Concentration (µg/cm^3)	0

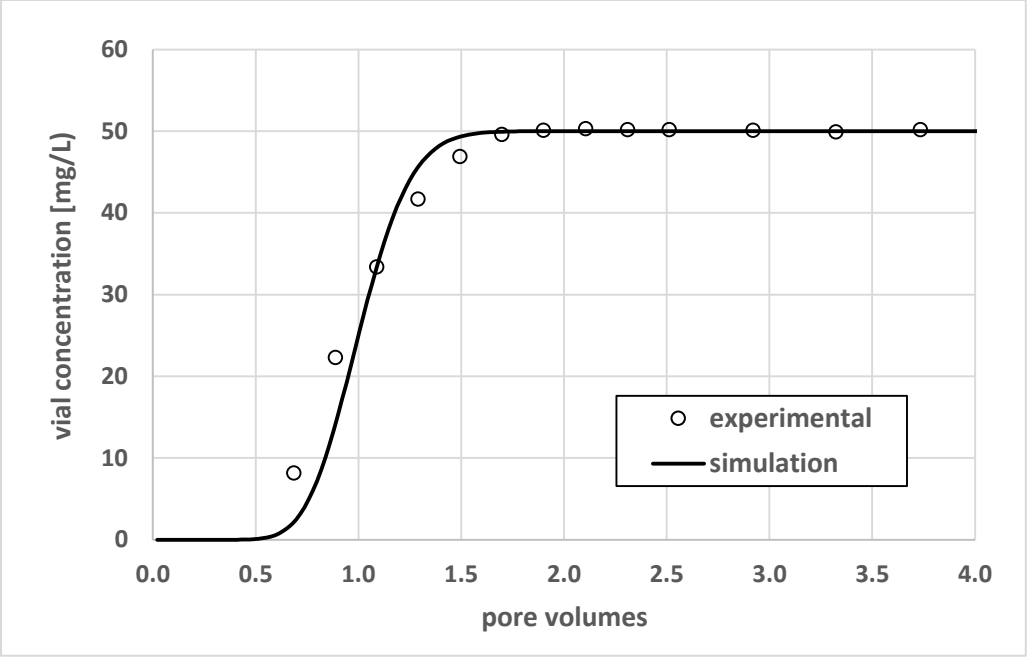

Figure C-3. Sample B347P5P8 Fine Grain (<2 mm Size) Soil with Bromide Transport

Input and simulation results for sample B347P5P8 fine grain (<2 mm size) soil and uranium transport are shown in Table C-5 and Figure C-4, respectively. Table C-4 provides the input data, together with the partition coefficient and reverse sorption rate, which yields the best fit of experimental data.
The simulation is in good agreement with the experimental data.

Table C-5. Input Parameters and Reverse Sorption Rate for Sample B347P5P8 Fine Grain (<2 mm Size) Soil with Uranium Transport

Column Length (cm)	15
Column Diameter (cm)	2.5
Number of Spatial Cells	50
Time Step (hr)	0.85
Water Content	0.380
Injection Rate (cm^3/hr)	5.54
Diffusion Coefficient (cm^2/hr)	0.001
Soil Bulk Density (g/cm^3)	1.72
K_d (cm^3/g)	0.3
Initial Water Concentration (µg/cm^3)	25
Initial Solid Concentration (µg/g)	7.5
Reverse Sorption Rate (1/hr)	0.07
Forward Sorption Rate (1/hr)	0.095

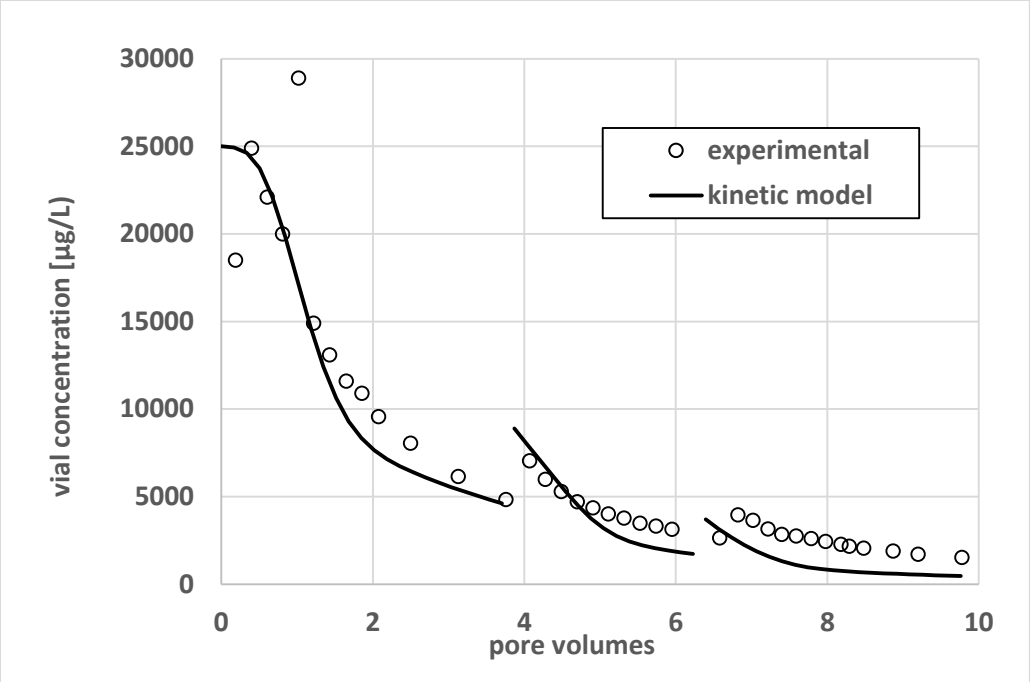

Figure C-4. Sample B345P5P8 Fine Grain (<2 mm Size) Soil with Uranium Transport

C1.3.3 Sample B347P4 Field-Textured (Bulk) Soil

Input and simulation results for sample B347P4 field-textured (bulk) soil with bromide transport are shown in Table C-6 and Figure C-5, respectively. The simulation results and experimental results both approach the injection concentration of 50 µg/L. The simulation concentration results match the observations.

Table C-6. Input Parameters for Sample B347P4 Field-Textured (Bulk) Soil with Bromide Transport

Column Length (cm)	13.2
Column Diameter (cm)	9.53
Number of Spatial Grid Cells	50
Time Step Size (hr)	0.14
Water Content (Dimensionless)	0.22
Dispersion (cm^2/hr)	0.001
Water Injection Rate (cm^3/hr)	74.4
Injection Stream Concentration (µg/cm^3)	0.05
Initial Concentration (µg/cm^3)	0

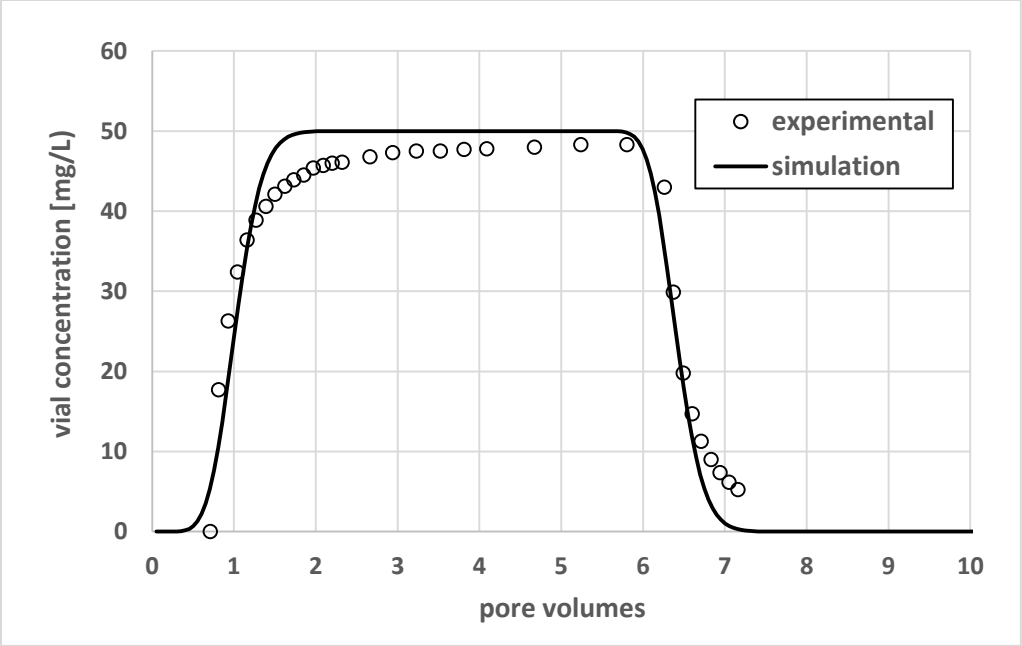

Figure C-5. Sample B347P4 Field-Textured (Bulk) Soil with Bromide Transport

Input and simulation results for sample B347P4 field-textured (bulk) soil with uranium transport are shown in Table C-7 and Figure C-6, respectively. Table C-6 provides the input data, together with the partition coefficient and the reverse sorption rate, which yields the best fit of experimental data. The simulation is in good agreement with the experimental data.

Table C-7. Input Parameters and Reverse Sorption Rate for Sample B347P4 Field-Textured (Bulk) Soil with Uranium Transport

Column Length (cm)	13.2
Column Diameter (cm)	9.53
Number of Spatial Cells	50
Time Step (hr)	0.835
Water Content	0.228
Injection Rate (cm^3/hr)	74.2
Diffusion Coefficient (cm^2/hr)	0.001
Soil Bulk Density (g/cm^3)	2.05
K_d (cm^3/g)	0.40
Initial Water Concentration (µg/cm^3)	2.7
Initial Solid Concentration (µg/g)	1.08
Reverse Sorption Rate (1/hr)	0.030
Forward Sorption Rate (1/hr)	0.108

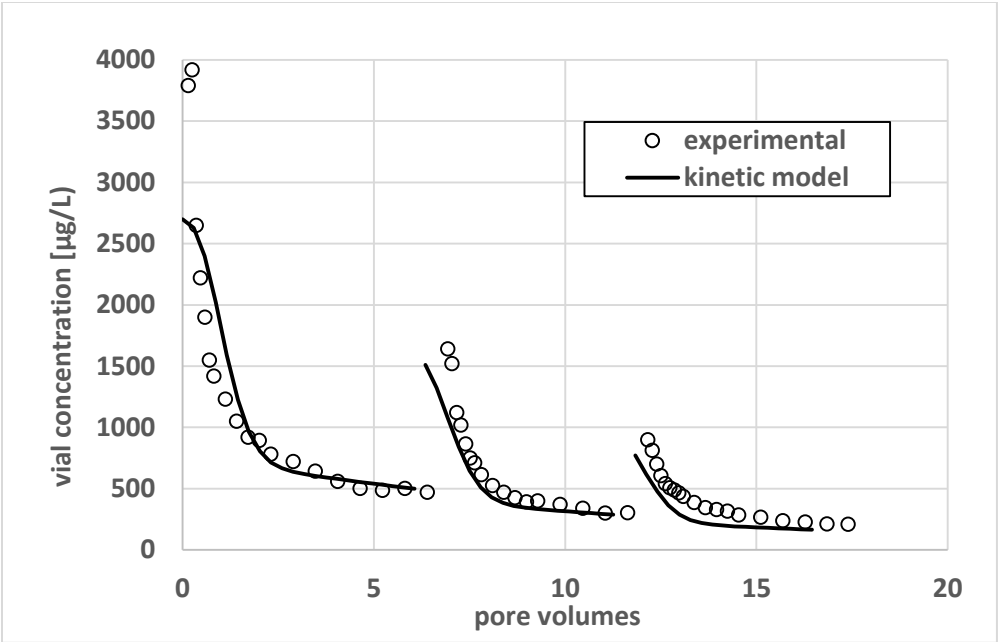

Figure C-6. B347P4 Field-Textured (Bulk) Soil with Uranium Transport

C1.3.4 Sample B347R1 Fine Grain (<2 mm Size) Soil

Input and simulation results for sample B347R1 fine grain (<2 mm size) soil and bromide transport are shown in Table C-8 and Figure C-7, respectively. The simulation results and experimental results both approach the injection concentration of 50 µg/L with very good agreement between the simulation model and the experimental data.

Table C-8. Input Parameters for Sample B347R1 Fine Grain (<2 mm Size) Soil with Bromide Transport

Column Length (cm)	15
Column Diameter (cm)	2.5
Number of Spatial Grid Cells	50
Time Step Size (hr)	0.1
Water Content	0.34
Dispersion (cm^2/hr)	0.001
Water Injection Rate (cm^3/hr)	5.7
Injection Stream Concentration (µg/cm^3)	0.05
Initial Concentration (µg/cm^3)	0

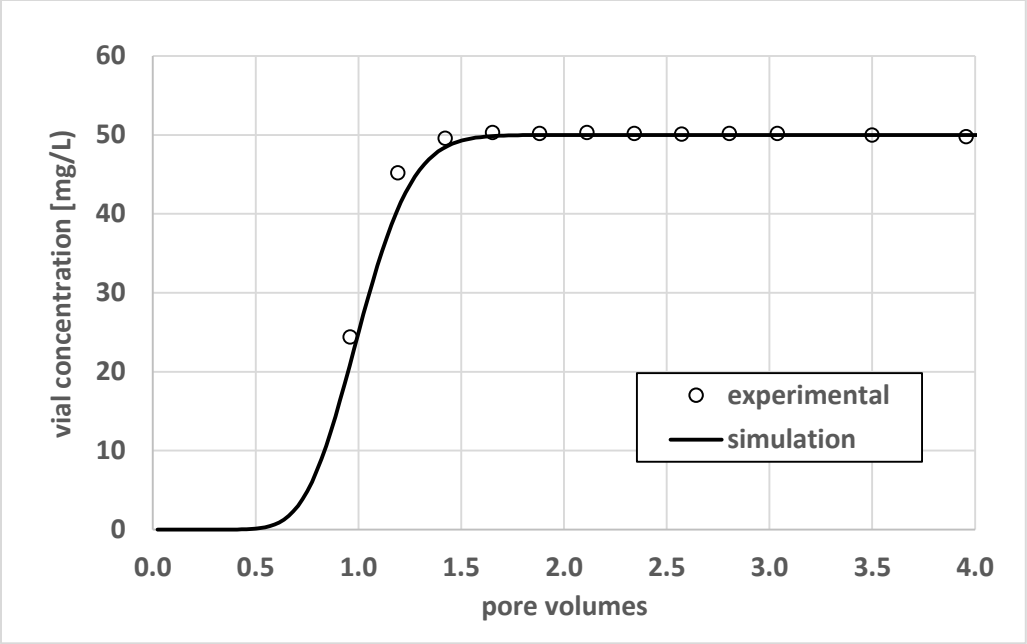

Figure C-7. Sample B347R1 Field-Textured (Bulk) Soil with Bromide Transport

Input and simulation results for sample B347R1 field-textured (bulk) soil and uranium transport are shown in Table C-9 and Figure C-8, respectively. Table C-9 provides the input data, together with the partition coefficient and reverse sorption rate, which yields the best fit of experimental data. The results in Figure C-8 are in good agreement with the observations.

Table C-9. Input Parameters and Reverse Sorption Rate for Sample B347R1 Fine Grain (<2 mm Size) Soil with Uranium Transport

Column Length (cm)	15
Column Diameter (cm)	2.5
Number of Spatial Cells	50
Time Step (hr)	0.825
Water Content	0.338
Injection Rate (cm^3/hr)	5.69
Diffusion Coefficient (cm^2/hr)	0.001
Soil Bulk Density (g/cm^3)	1.79
K_d (cm^3/g)	1.2
Initial Water Concentration (µg/cm^3)	4.6
Initial Solid Concentration (µg/g)	5.52
Reverse Sorption Rate (1/hr)	0.06
Forward Sorption Rate (1/hr)	0.381

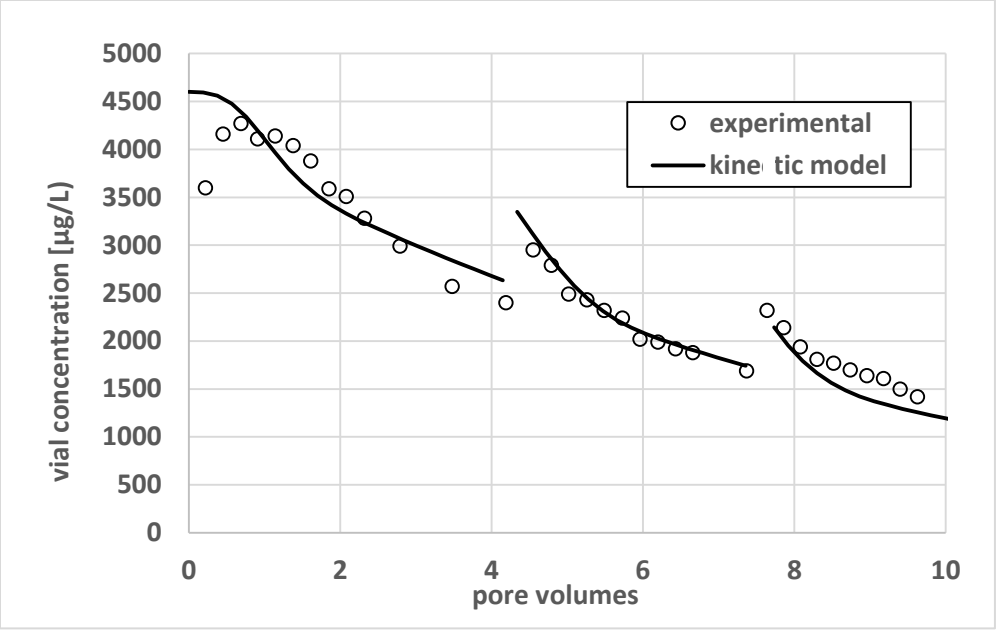

Figure C-8. Input Parameters and Reverse Sorption Rate for Sample B347R1 Fine Grain (<2 mm Size) Soil with Uranium Transport

C1.3.5 Sample B347R0 Field-Textured (Bulk) Soil

Input and simulation results for sample B347R0 are shown in Table C-10 and Figure C-9. The agreement is good between the simulated model results and experimental data.

Table C-10. Input Parameters for B347R0 Field-Textured (Bulk) Soil with Bromide Transport

Column Length (cm)	14
Column Diameter (cm)	9.53
Number of Spatial Grid Cells	50
Time Step Size (hr)	0.115
Water Content	0.17
Dispersion (cm^2/hr)	0.001
Water Injection Rate (cm^3/hr)	74.5
Injection Stream Concentration (µg/cm^3)	0.05
Initial Concentration (µg/cm^3)	0

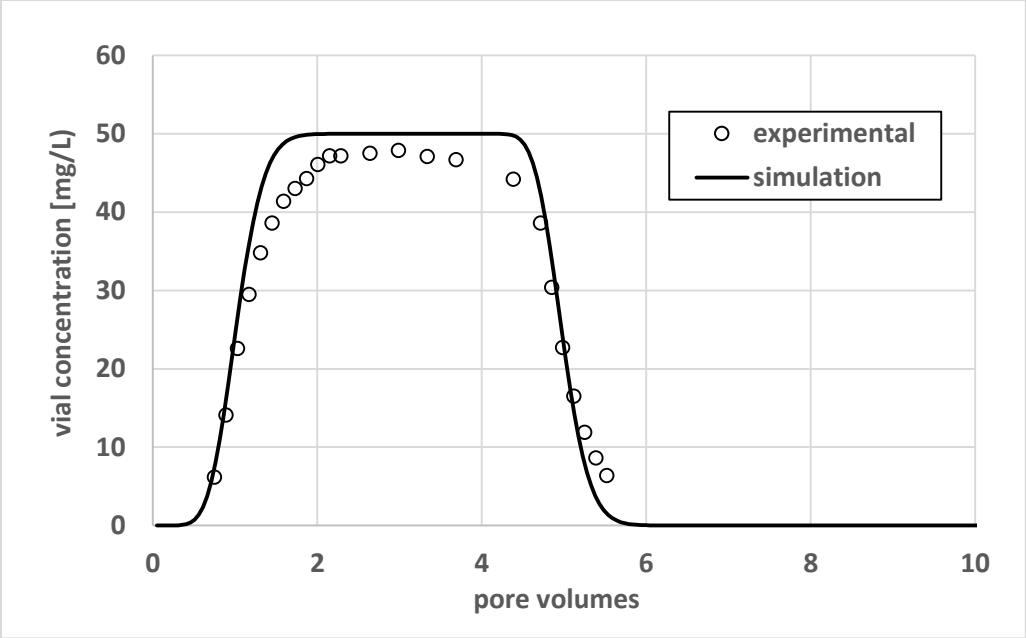

Figure C-9. Sample B347R0 Field-Textured (Bulk) Soil with Bromide Transport

Input and simulation results for sample B347R0 field-textured (bulk) soil with uranium transport are shown in Table C-11 and Figure C-10, respectively. Table C-11 provides the input data, together with the partition coefficient and the reverse sorption rate, which yields the best fit of experimental data.
The results in Figure C-10 are in good agreement over the first 10 pore volumes.

Table C-11. Input Parameters and Reverse Sorption Rate for Sample B347R0 Field-Textured (Bulk) Soil with Uranium Transport

Column Length (cm)	14
Column Diameter (cm)	9.53
Number of Spatial Cells	50
Time Step (hr)	0.75
Water Content	0.177
Injection Rate (cm^3/hr)	74.5
Diffusion Coefficient (cm^2/hr)	0.001
Soil Bulk Density (g/cm^3)	2.18
K_d (cm^3/g)	0.3
Initial Water Concentration (µg/cm^3)	4.0
Initial Solid concentration (µg/g)	1.2
Reverse Rate (1/hr)	0.06
Forward Rate (1/hr)	0.222

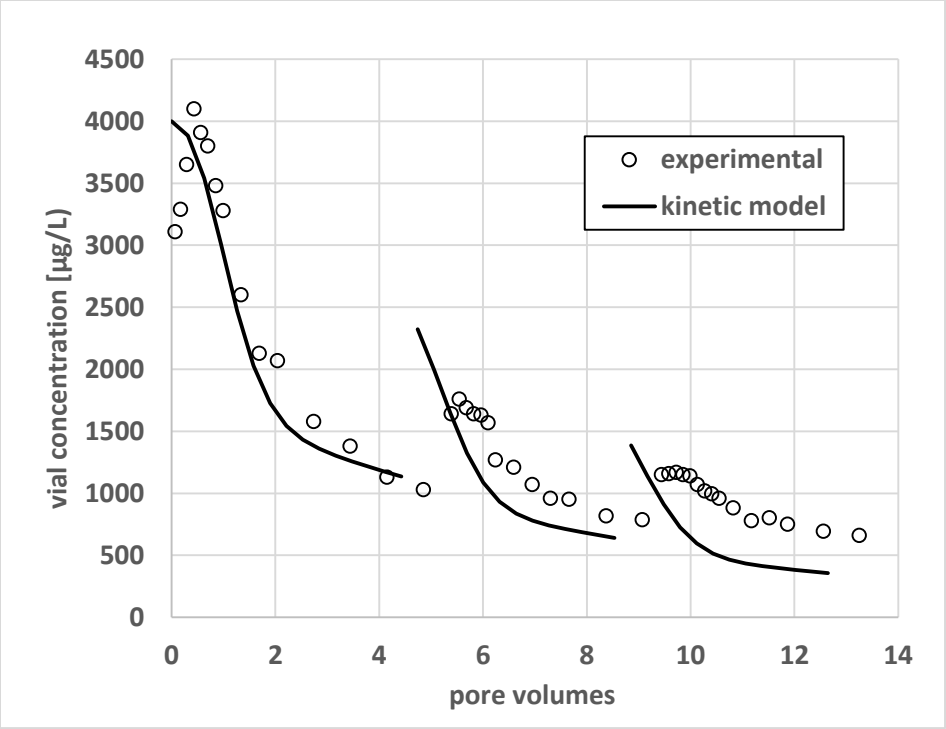

Figure C-10. Sample B347R0 Field-Textured (Bulk) Soil with Uranium Transport

C1.3.6 Sample B347T7 Fine Grain (<2 mm Size) Soil

Input and simulation results for sample B347T7 are shown in Table C-12 and Figure C-11, respectively. The agreement is excellent between the simulation model results and experimental data.

Table C-12. Input Parameters for Sample B347T7 Fine Grain (<2 mm Size) Soil with Bromide Transport

Column Length (cm)	15
Column Diameter (cm)	2.5
Number of Spatial Grid Cells	50
Time Step Size (hr)	0.1
Water Content	0.35
Dispersion (cm^2/hr)	0.001
Water Injection Rate (cm^3/hr)	5.58
Injection Stream Concentration (µg/cm^3)	0.05
Initial Concentration (µg/cm^3)	0

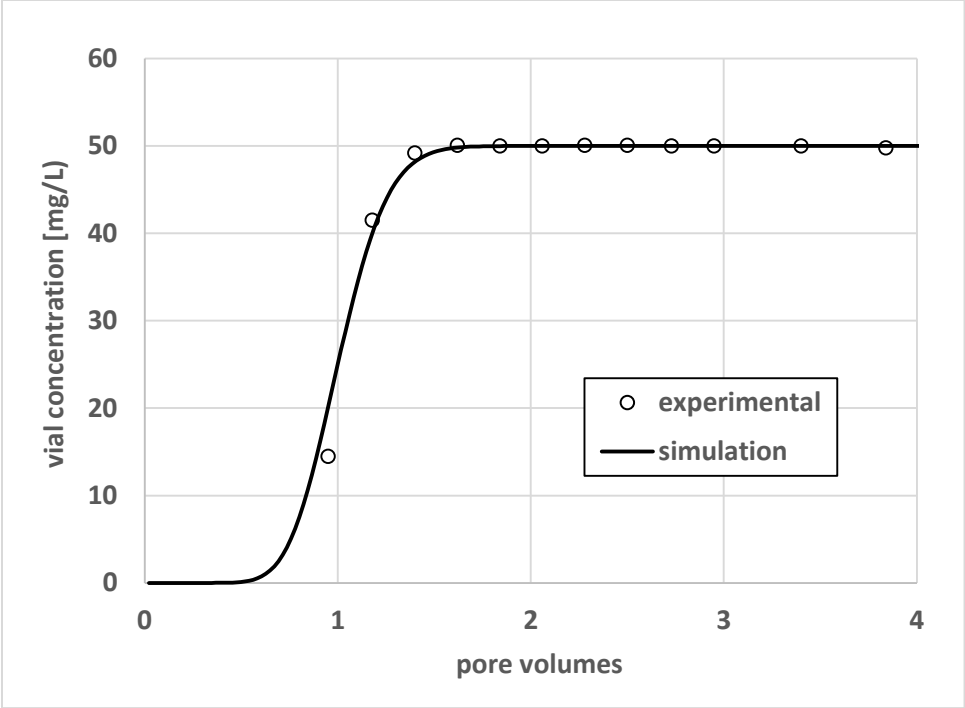

Figure C-11. Sample B347T7 Fine Grain (<2 mm Size) Soil with Bromide Transport

Input and simulation results for sample B347T7 field-textured (bulk) soil with uranium transport are shown in Table C-13 and Figure C-12, respectively. Table C-13 provides the input data, together with the partition coefficient and reverse sorption rate, which yields the best fit of experimental data. The results in Figure C-12 are in good agreement during most of the simulation. Concentrations remain low and vary within a narrow range over multiple pore volumes.

Table C-13. Input Parameters and Sorption Rates for Sample B347T7 Fine Grain (<2 mm Size) Soil with Uranium Transport

Column Length (cm)	15
Column Diameter (cm)	2.5
Number of Spatial Cells	50
Time Step (hr)	0.875
Water Content	0.347
Injection Rate (cm^3/hr)	5.61
Diffusion Coefficient (cm^2/hr)	0.001
Soil Bulk Density (g/cm^3)	1.78
K_d (cm^3/g)	5
Initial Water Concentration (µg/cm^3)	0.007
Initial Solid Concentration (µg/g)	0.035
Reverse Rate (1/hr)	0.017
Forward Rate (1/hr)	0.2

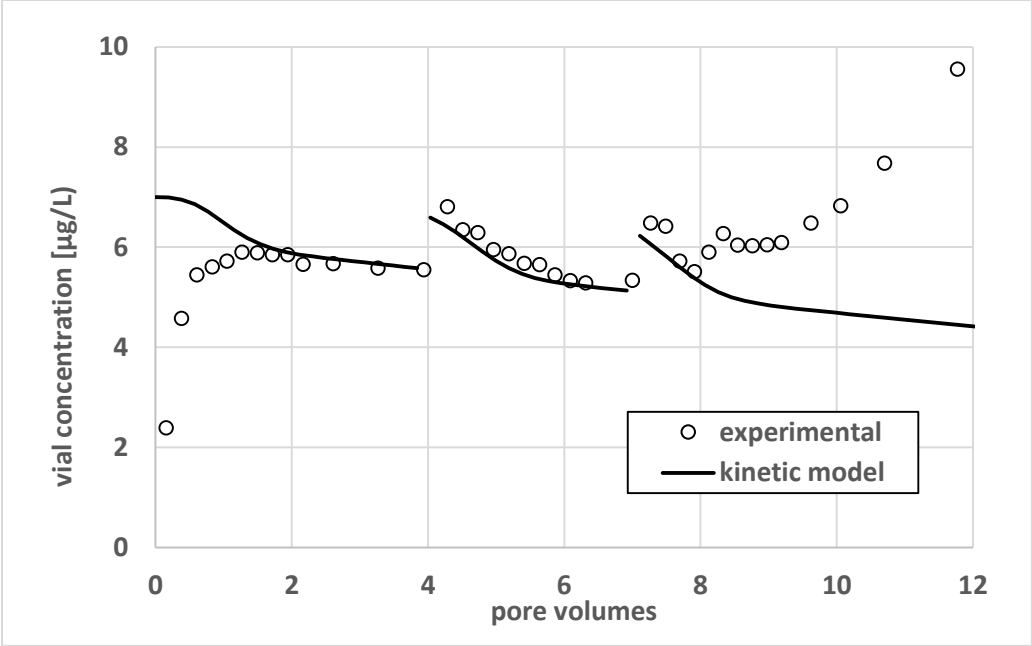

Figure C-12. Sample B347T7 Fine Grain (<2 mm Size) Soil with Uranium Transport

C1.3.7 Sample B347T6 Field-Textured (Bulk) Soil

Input and simulation results for sample B347T6 field-textured (bulk) soil with bromide transport are shown in Table C-14 and Figure C-13, respectively. The results in Figure C-13 show some disparity between the simulation results and experimental data, but qualitatively the behavior is in agreement.

Table C-14. Input Parameters and Sorption Rates for Sample B347T6 Field-Textured (Bulk) Soil with Bromide Transport

Column Length (cm)	13.7
Column Diameter (cm)	9.53
Number of Spatial Grid Cells	50
Time Step Size (hr)	0.065
Water Content	0.14
Dispersion (cm^2/hr)	0.001
Water Injection Rate (cm^3/hr)	72.7
Injection Stream Concentration (µg/cm^3)	0.05
Initial Concentration (µg/cm^3)	0

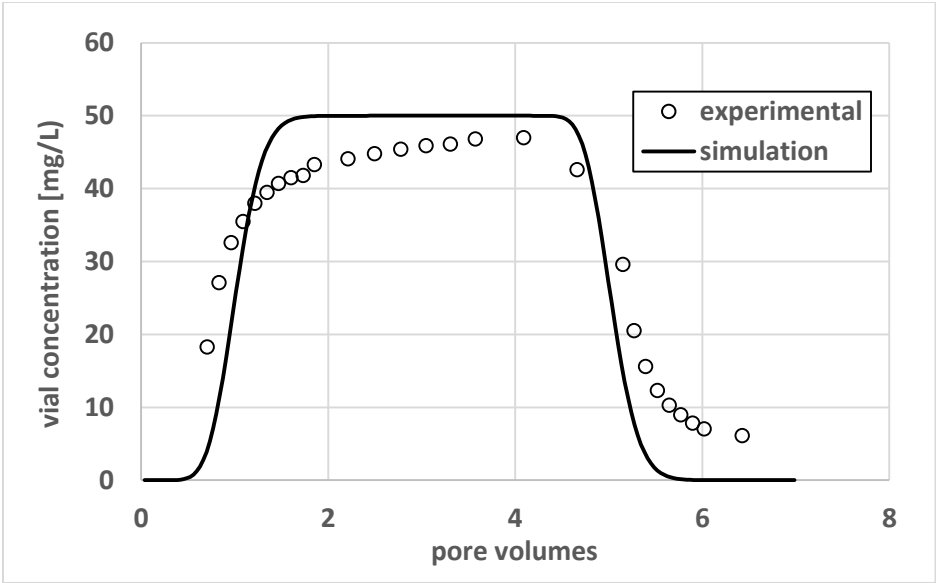

Figure C-13. Sample B347T6 Field-Textured (Bulk) Soil with Bromide Transport

Input and simulation results for sample B347T6 field-textured (bulk) soil with uranium transport are shown in Table C-15 and Figure C-14, respectively. Table C-15 provides the input data, together with the partition coefficient and the reverse sorption rate, which yields the best fit of experimental data.
The results in Figure C-14 are in good agreement over first 10 pore volumes. The increase in concentration observed after 10 pore volumes may be related to dissolution of additional uranium bearing mineral phases.

Table C-15. Input Parameters and Sorption Rates for Sample B347T6 Field-Textured (Bulk) Soil and Uranium Transport

Column Length (cm)	13.7
Column Diameter (cm)	9.53
Number of Spatial Cells	50
Time Step (hr)	0.76
Water Content	0.146
Injection Rate (cm^3/hr)	72.7
Diffusion Coefficient (cm^2/hr)	0.001
Soil Bulk Density (g/cm^3)	2.26
K_d (cm^3/g)	0.98
Initial Water Concentration (µg/cm^3)	0.016
Initial Solid Concentration (µg/g)	0.01568
Reverse Rate (1/hr)	0.019
Forward Rate (1/hr)	0.288

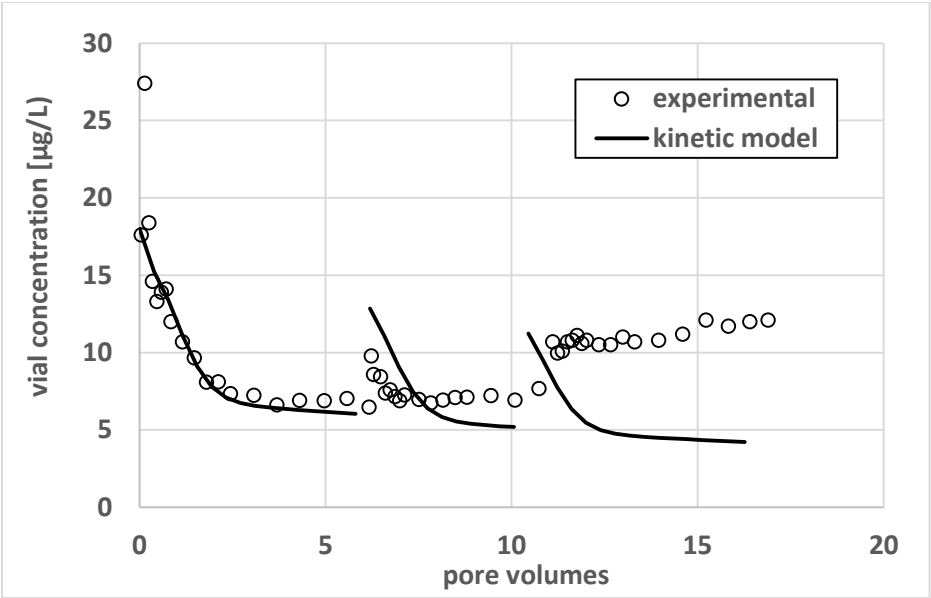

Figure C-14. Sample B347T6 Field-Textured (Bulk) Soil with Uranium Transport

C.2 Alternative Parameter Matching of Experimental Data

An alternative method for determination of kinetic sorption parameters assumes a value for the reverse reaction rate. The experimental data are matched by adjusting the partition coefficient (K_d) to provide the best fit to the data by the numerical model results. The value selected is taken to be representative of the reverse rates provided by Table C-1. An arithmetic average of the reverse rates for the seven samples in Table C-1 yields a value of 0.038/hr. A rounded up value of 0.03/hr is assigned as the reverse reaction rate for all samples. The partition coefficients, together with the reverse and forward reaction rates for the seven samples, are shown in Table C-16. Figures C-15 through C-21 show the model fits to the observed results, indicating reasonable matches. For some samples, the initial dissolved concentration was varied slightly from the Table C-1 values.

In this approach, since the reverse rate is fixed and fit is made by changing the K_d value that also affect the forward rate, comparing the K_d value among different samples provides insight into the variable leaching characteristics. By comparing the fine grain (<2 mm size) sediment results, B347F1F3 and B347T7 have K_d values that are about a factor of 5 to 10 greater than B347P5P8 and B247R1. For the field-textured (bulk) sediment samples, the K_d value for B347T6 is twice that of the other two bulk sediment samples (B347R0 and B347P4). The samples showing higher K_d values are located at periodically rewetted zone (PRZ) depths (Table 6-5) and have higher phosphate concentrations resulting from PRZ injections (and infiltration), as shown in Figure 6-17.

Table C-16. History Match Parameters for the Final Post-Treatment Uranium Leach Results with Reverse Reaction Rate of 0.03/Hr

Sample Number	Soil Type	Initial Dissolved Concentration (µg/cm^3)	K_d (cm^3/G)	Reverse Rate (1/Hr)	Forward Rate (1/Hr)
B347F1F3	Fine Grain (<2 mm size)	0.018	5.0	0.03	0.67
B347P5P8	Fine Grain (<2 mm Size)	27	0.30	0.03	0.041
B347P4	Field-Textured (Bulk)	2.7	0.40	0.03	0.11
B247R1	Fine Grain (<2 mm Size)	4.6	1.4	0.03	0.22
B347R0	Field-Textured (Bulk)	4.0	0.4	0.03	0.15
B347T7	Fine Grain (<2 mm Size)	0.0065	4.0	0.03	0.62
B347T6	Field-Textured (Bulk)	0.016	0.70	0.03	0.33

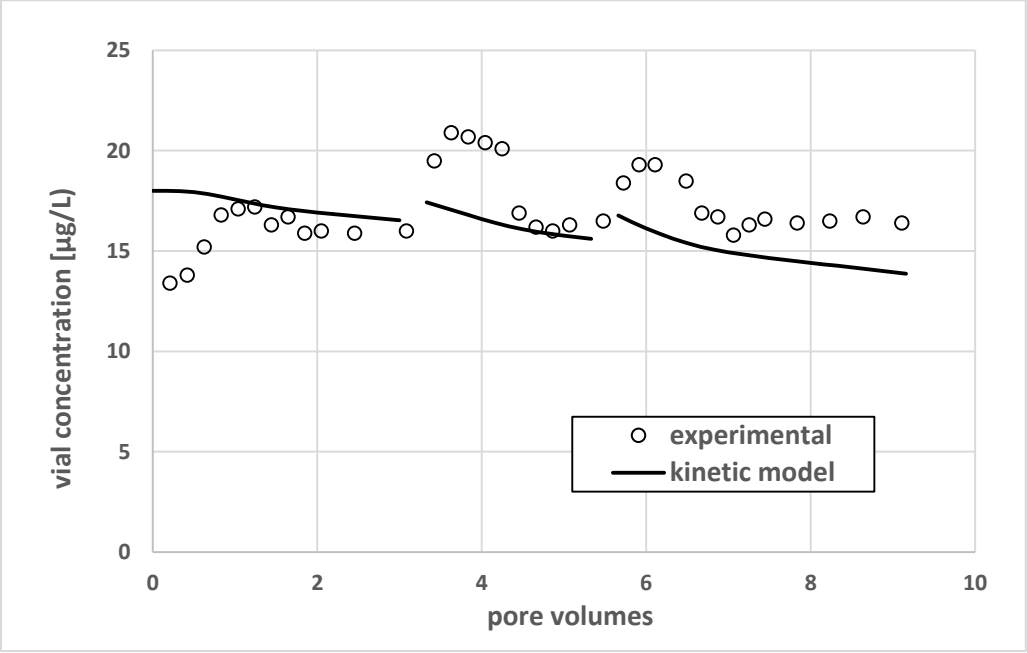

Figure C-15. Sample B347F1F3 Fine Grain (<2 mm Size) Soil with Uranium Transport; Reverse Rate = 0.03/Hr

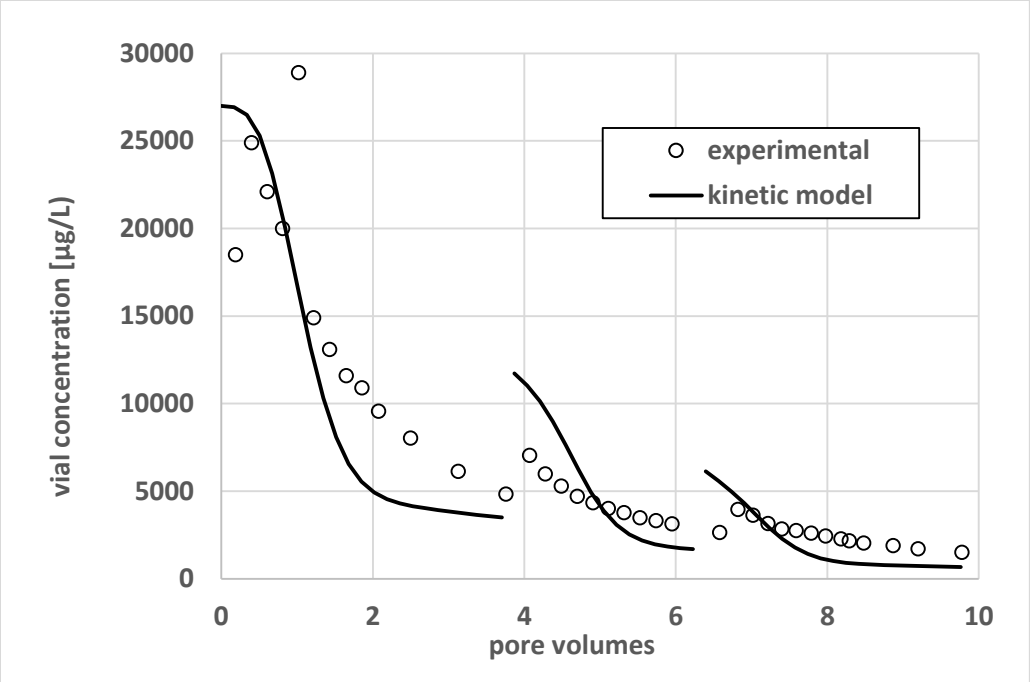

Figure C-16. Sample B345P5P8 Fine Grain (<2 mm Size) Soil with Uranium Transport; Reverse Rate = 0.03/Hr

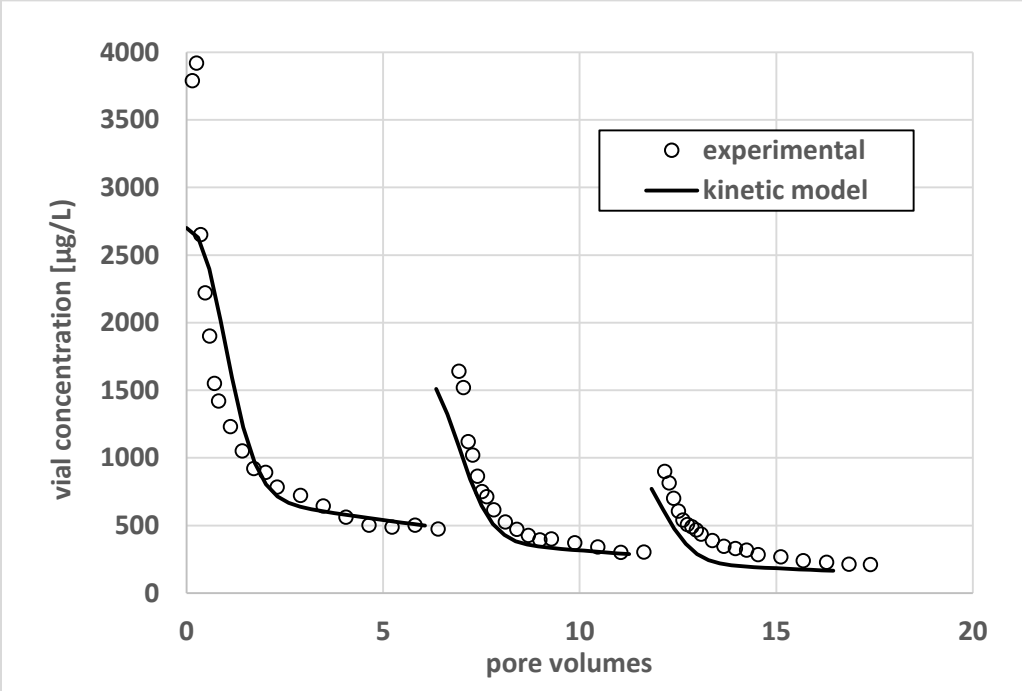

Figure C-17. B347P4 Field-Textured (Bulk) Soil with Uranium Transport; Reverse Rate = 0.03/Hr

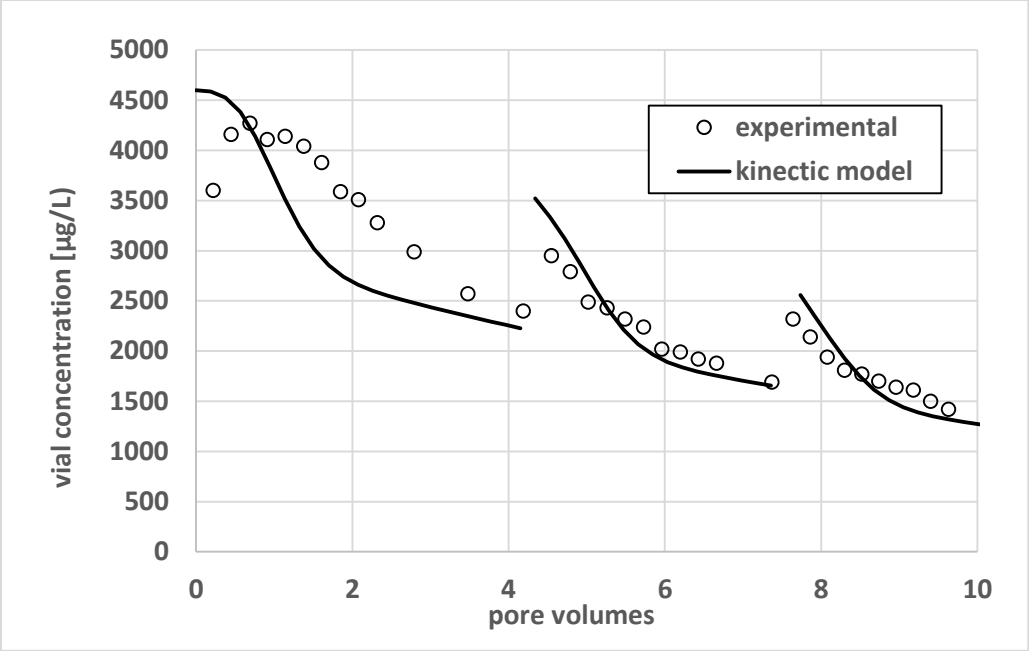

Figure C-18. B347R1 Fine Grain (<2 mm Size) Soil with Uranium Transport; Reverse Rate = 0.03/Hr

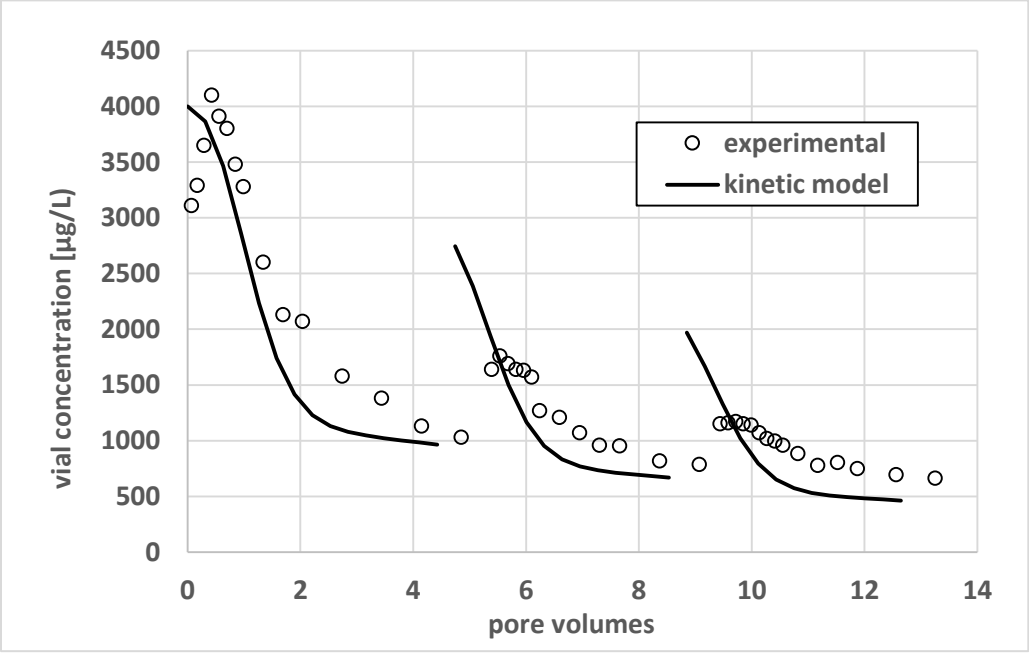

Figure C-19. Sample B347R0 Field-Textured (Bulk) Soil with Uranium Transport; Reverse Rate = 0.03/Hr

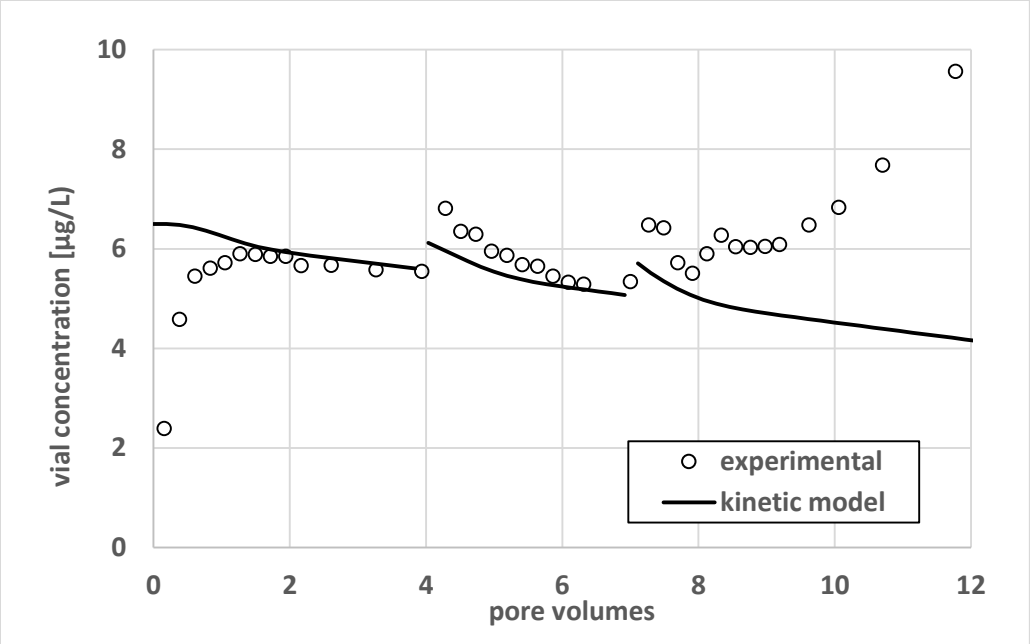

Figure C-20. Sample B347T7 Fine Grain (<2 mm Size) Soil with Uranium Transport; Reverse Rate = 0.03/Hr

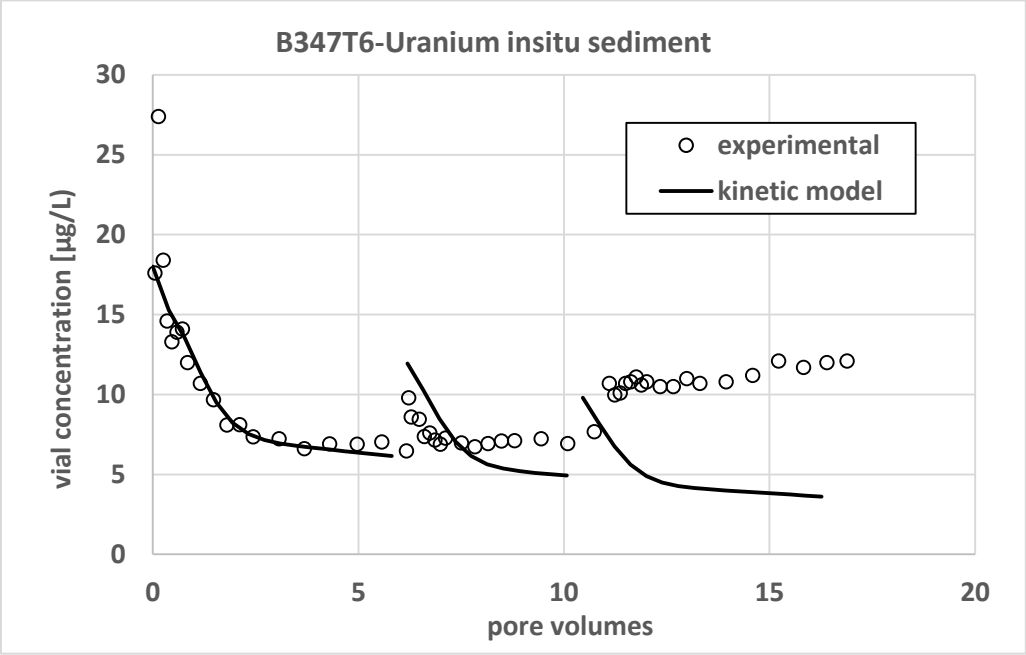

Figure C-21. Sample B347T6 Field-Textured (Bulk) Soil with Uranium Transport; Reverse Rate = 0.03/Hr

This page intentionally left blank.

Appendix D

MATLAB Files for Sample B347P4 Bulk Soil Kinetic Sorption Model Calculation

This page intentionally left blank.

D1 Introduction

The kinetic sorption model calculations were implemented as MATLAB® script using two files. The file "fd_transport.m" (finite difference transport) initially runs the input file "transport_data.m". The input file initiates the necessary model input in MATLAB Workspace (i.e., memory). Inputs include the geometry of the column, soil properties, uranium sorption parameters, initial conditions, one-dimensional spatial discretization, and time step schedule. After execution of the input file, "fd_transport.m" calculates the concentration time history of uranium transport within the column and effluent exiting the column. Each script block is explained further in the comment lines (preceded by the percent [%] sign).

All experimental samples were conducted with two stop flow or shut-in events. The elapsed time during flow is computed by the volume per unit pore volume multiplied by the pore volumes and divided by the injection rate. During a stop flow event, the pore volumes are constant.

Concentrations are known at the beginning of a time step, and the numerical model calculation provides the concentrations at the end of the time step. The time step calculation uses matrix inversion and matrix/vector multiplication utilizing MATLAB built-in matrix functions. The resulting solution for the concentrations satisfies the finite difference equations for the uranium transport within the column subject to the initial concentrations and the boundary conditions at the upper and lower column boundaries. The time iteration continues to update these concentration profiles at all time steps. Within each time step, the evaluated concentrations and designed flows (injected pore volumes) are used to evaluate mass fluxes and check the mass balance. After each time step, the column effluent (exiting) concentration is stored, and a mass balance is calculated. Output is exported to a Microsoft Excel® file (e.g., "B347P4_insitu_U_Kinetic.xlsx"), which includes mass balance results, input parameters, and time history of the effluent concentration.

The Excel output file is designed with a preset graph to compare the simulated result with experimental data. Values for the relevant parameters are set, and the model is run. Model results are compared to experimental results, and model parameters are manually adjusted until a best fit of the experimental data is obtained. This history matching procedure is carried out for all relevant samples.

® MATLAB is a registered trademark of The MathLab, Inc., Natick, Massachusetts.
® Microsoft and Excel are registered trademarks of Microsoft Corporation, Redmond, Washington.

D2 MATLAB Input File Used to Match Uranium Leaching Sample B347P4 Experimental Results Using Single-Site Kinetic Sorption Model

File Name: Transport_Data.m

```
%Input data for Uranium kinetic sorption leaching model
%Reference Data: Rashid, H, Groundwater Flow and Uranium Transport Modeling in %Support
of the 300 Area FF-5 RI/FS Document, CHPRC/EP&SP, Oct. 2012.
%units internal to code:
%length[cm]
%time[hr]
%concentration[mmol/cm^3]
%mass[g]
%
%Input data for Uranium sample B347P4 bulk soil
%Reference Data: Rashid, H, Groundwater Flow and Uranium Transport Modeling
%in Support of the 300 Area FF-5 RI/FS Document, CHPRC/EP&SP, Oct. 2012.
%Reference data includes column geometry, water content, soil bulk density,
%injection rate, and dispersion coefficient.
%The Uranium input data is pre-processed from the reference data.
%units internal to code:
%length[cm]
%time[hr]
%concentration[micro-mol/cm^3]
%mass[g]
%
%column length [cm]
L = 13.2;
%discretization of column
Nz = 50;
delz = L/Nz;
z = zeros(Nz,1);
z(1) = 0.5*delz;
for i = 2:Nz
 z(i) = z(i-1) + delz;
end
%diameter of column [cm] and area normal to tranport [cm^2]
diameter_column = 9.53;
Az = pi()*(diameter_column/2)^2;
%cell bulk volume[cm^3]
Vol_total = Az*L;
%saturated water content (saturated porosity)
wtr_content = 0.228;
%volume water per pore volume
Vwtr_per_PV = wtr_content*Vol_total;
%
%Water injection rate [cm^3/hr]
inj_rate = 74.2;
%Darch velocity [cm/hr]
v = inj_rate/Az;
%Dispersion coefficient [cm^2/hr]
Dispersion = 1.E-3;
%
%bulk density [g/cm^3]
bulk_density = 2.05;
%
```

```
%sorption coefficient [cm^3-water/g-solid]
%if Kd_flag = 0, no sorption (bromide); otherwise sorption (U-238)
Kd_flag = 1;
if Kd_flag == 1;
 analyte = {'U-238'};
%Kd [ml/g = cm^3/g]
 K_d = 0.4;
else
 analyte = {'bromide'};
 K_d = 0;
end
%reverse reaction rate [1/hr]
rate_r = 3.E-2;
%forward reaction rate
rate_f = rate_r*K_d*bulk_density/wtr_content;
%conc_water_initial [micro-g-U/Vwtr]
conc_water_initial = 2.7;
%initial conditions [conc_solid: micro-g-U/g-solid]
conc_solid_initial = K_d*conc_water_initial;
initial_mass_solid = bulk_density*Vol_total*conc_solid_initial;
initial_mass_water = wtr_content*Vol_total*conc_water_initial;
%the *_old are the beginning of time step values. For 1st time step this is
%the initial values
conc_old = zeros(Nz,1);
conc_old_solid = zeros(Nz,1);
conc_old = conc_water_initial*ones(Nz,1);
conc_old_solid = conc_solid_initial*ones(Nz,1);
%initial mass in place
initial_massinplace = initial_mass_water + initial_mass_solid;
%
%time array [hr] and number of time steps
end_time = 167;
NT = 200;
delt = end_time/NT;
t = zeros(NT,1);
t(1) = delt;
%%
for it = 2:NT
 t(it) = t(it-1) + delt;
end
input = zeros(13,1);
%input includes transport parameters, numerical discretization, partition
%coefficient, initial concentrations, reverse and forward kinetic rates.
%input is written to output file B347P4_insitu_U_Kinetic
input = [L,diameter_column,Nz,delt,wtr_content,inj_rate,Dispersion,...
bulk_density,K_d,conc_water_initial,conc_solid_initial,rate_r,rate_f];
'fini transport_initial_data'
```

D3 MATLAB Transport File Used To Match Sample B347P4 Results Using Single-Site Kinetic Sorption Model File name: fd_transport.m

```
%Uranium transport calculation for Sample B347P4
%finite difference solution of advective/dispersive transport with
%kinetic sorption
%
clc
%clf
clear
format long
%read input data
%
transport_data
%
%
%initialize pore volumes
pore_volumes = zeros(NT,1);
vial_conc = zeros(NT,1);
balance_ke = zeros(NT,1);
balance_te = zeros(NT,1);
mass_wtr = zeros(NT,1);
mass_solid = zeros(NT,1);
mass_out = zeros(NT,1);
mass_wtr2 = zeros(NT,1);
mass_solid2 = zeros(NT,1);
%start time step loop
time = 0;
sol_mass = wtr_content*Az*delz*conc_water_initial;
for it = 1:NT
%
 conc = zeros(Nz,1);
 conc_solid = zeros(Nz,1);
 time = time + delt;
%1st shut-in period
 if 17.84 < time && time < 65.84
 v = 0;
 else
 v = inj_rate/Az;
 end
%2nd shut-in period
 if time > 70
 if 80.33 < time && time < 152.33
 v = 0;
 else
 v = inj_rate/Az;
 end
 end
%
%generate coefficient matrix.
 coef = zeros(Nz,Nz);
 A = -(wtr_content*Dispersion/delz/delz + v/delz);
 B = 2*wtr_content*Dispersion/delz/delz + v/delz + wtr_content/delt ...
 + rate_r*bulk_density*K_d/(1+rate_r*delt);
 C = - wtr_content*Dispersion/delz/delz;
 for i = 1:Nz
```

```
 if i == 1
 coef(i,i) = wtr_content*Dispersion/delz/delz + v/delz ...
 + wtr_content/delt + rate_r*bulk_density*K_d/(1+rate_r*delt);
 coef(i,i+1) = C;
 elseif i == Nz
 coef(i,i-1) = A;
 coef(i,i) = wtr_content*Dispersion/delz/delz + v/delz ...
 + wtr_content/delt + rate_r*bulk_density*K_d/(1+rate_r*delt);
 else
 coef(i,i-1) = A;
 coef(i,i) = B;
 coef(i,i+1) = C;
 end
 end
%compute inverse of coefficient matrix
 A_inv = zeros(Nz,Nz);
 A_inv = inv(coef);
%assign rhs vector
 rhs = zeros(Nz,1);
 for i = 1:Nz
 rhs(i) = wtr_content*conc_old(i)/delt ...
 + bulk_density*rate_r*conc_old_solid(i)/(1+rate_r*delt);
 end
%solution for water concentration
 conc = A_inv*rhs;
%solution for solid concentration
 for i = 1:Nz
 conc_solid(i) = (rate_r*delt*K_d*conc(i)/(1+rate_r*delt))...
 + conc_old_solid(i)/(1 + rate_r*delt);
 end
%mass balance kinectic equation and transport equation
 balance_ke(it) = 0;
 balance_te(it) = 0;
 mass_wtr(it) = 0;
 mass_solid(it) = 0;
 for i = 1:Nz;
 mass_ke = bulk_density*(conc_solid(i)-conc_old_solid(i))/delt...
 -rate_r*bulk_density*K_d*conc(i)...
 + rate_r*bulk_density*conc_solid(i);
 if i == 1
 mass_te = (wtr_content/delt)*(conc(i)-conc_old(i))...
 + (wtr_content*Dispersion/delz/delz)*(conc(i)-conc(i+1))...
 + (v/delz)*conc(i)...
 + (rate_r*bulk_density/(1+rate_r*delt))*(K_d*conc(i)-conc_old_solid(i));
 elseif i == Nz
 mass_te = (wtr_content/delt)*(conc(i)-conc_old(i))...
 + (wtr_content*Dispersion/delz/delz)*(conc(i)-conc(i-1))...
 + (v/delz)*(conc(i)-conc(i-1))...
 + (rate_r*bulk_density/(1+rate_r*delt))*(K_d*conc(i)-conc_old_solid(i));
 else
 mass_te = (wtr_content/delt)*(conc(i)-conc_old(i))...
 + (wtr_content*Dispersion/delz/delz)*(-conc(i-1)+2*conc(i)-conc(i+1))...
 + (v/delz)*(conc(i)-conc(i-1))...
 + (rate_r*bulk_density/(1+rate_r*delt))*(K_d*conc(i)-conc_old_solid(i));
 end
 if abs(mass_ke) > balance_ke(it)
 balance_ke(it) = abs(mass_ke);
```

```
 end
 if abs(mass_te) > balance_te(it);
 balance_te(it) = abs(mass_te);
 end
%mass in place
 mass_wtr(it) = mass_wtr(it) + delz*Az*wtr_content*conc(i);
 mass_solid(it) = mass_solid(it)...
 + delz*Az*bulk_density*conc_solid(i);
%
%end loop over grid cells
 end
%cumulative mass out
 if it == 1
 mass_out(it) = v*delt*Az*conc(Nz);
 else
 mass_out(it) = mass_out(it-1) + v*delt*Az*conc(Nz);
 end
%update conc_old
 conc_old = conc;
 conc_old_solid = conc_solid;
%number of cumulative pore volumes at time t(it)
%pore_volumes(it) = inj_rate*delt/Vwtr_per_PV;
 if (it) == 1
 pore_volumes(it) = v*Az*delt/Vwtr_per_PV;
 else
 pore_volumes(it) = pore_volumes(it-1) + v*Az*delt/Vwtr_per_PV;
 end
%vial concentration mg/L
 if v == 0
 vial_conc(it) = vial_conc(it-1);
 else
 vial_conc(it) = 1000*conc(Nz);
 end
%
%end of time step loop
end
%write input
xlswrite('B347P4_insitu_U_Kinetic.xlsx',transpose(input),'Input','B2')
%write time history of pore volumes and concentration
xlswrite('B347P4_insitu_U_Kinetic.xlsx',t,'B347P4_U_Kinetic','C5:C204')
xlswrite('B347P4_insitu_U_Kinetic.xlsx',pore_volumes,'B347P4_U_Kinetic','D5:D
204')
xlswrite('B347P4_insitu_U_Kinetic.xlsx',vial_conc,'B347P4_U_Kinetic','E5:E204
')
%write balance equation results
xlswrite('B347P4_insitu_U_Kinetic.xlsx',t,'balance','B4:B203')
xlswrite('B347P4_insitu_U_Kinetic.xlsx',balance_ke,'balance','C4:C203')
xlswrite('B347P4_insitu_U_Kinetic.xlsx',balance_te,'balance','D4:D203')
%
xlswrite('B347P4_insitu_U_Kinetic.xlsx',initial_mass_water,'balance','F3')
xlswrite('B347P4_insitu_U_Kinetic.xlsx',initial_mass_solid,'balance','G3')
xlswrite('B347P4_insitu_U_Kinetic.xlsx',mass_wtr,'balance','F4:F203')
xlswrite('B347P4_insitu_U_Kinetic.xlsx',mass_solid,'balance','G4:G203')
xlswrite('B347P4_insitu_U_Kinetic.xlsx',mass_out,'balance','H4:H203')
%
delete('*.tmp')
'fini fd_transport'
```

Appendix E

Assessment of Effect of Polyphosphate Injection/Infiltration on Aquifer Properties

This page intentionally left blank.

E1 Assessment of Effect of Polyphosphate Injection/Infiltration on Aquifer Properties

This appendix assesses the effect of polyphosphate injections/infiltration on hydraulic properties of the aquifer (such as porosity or permeability) in the vicinity of the treatment zone. Stage A Enhanced Attenuation Area (EAA) and surrounding wells are shown in Figure E-1.

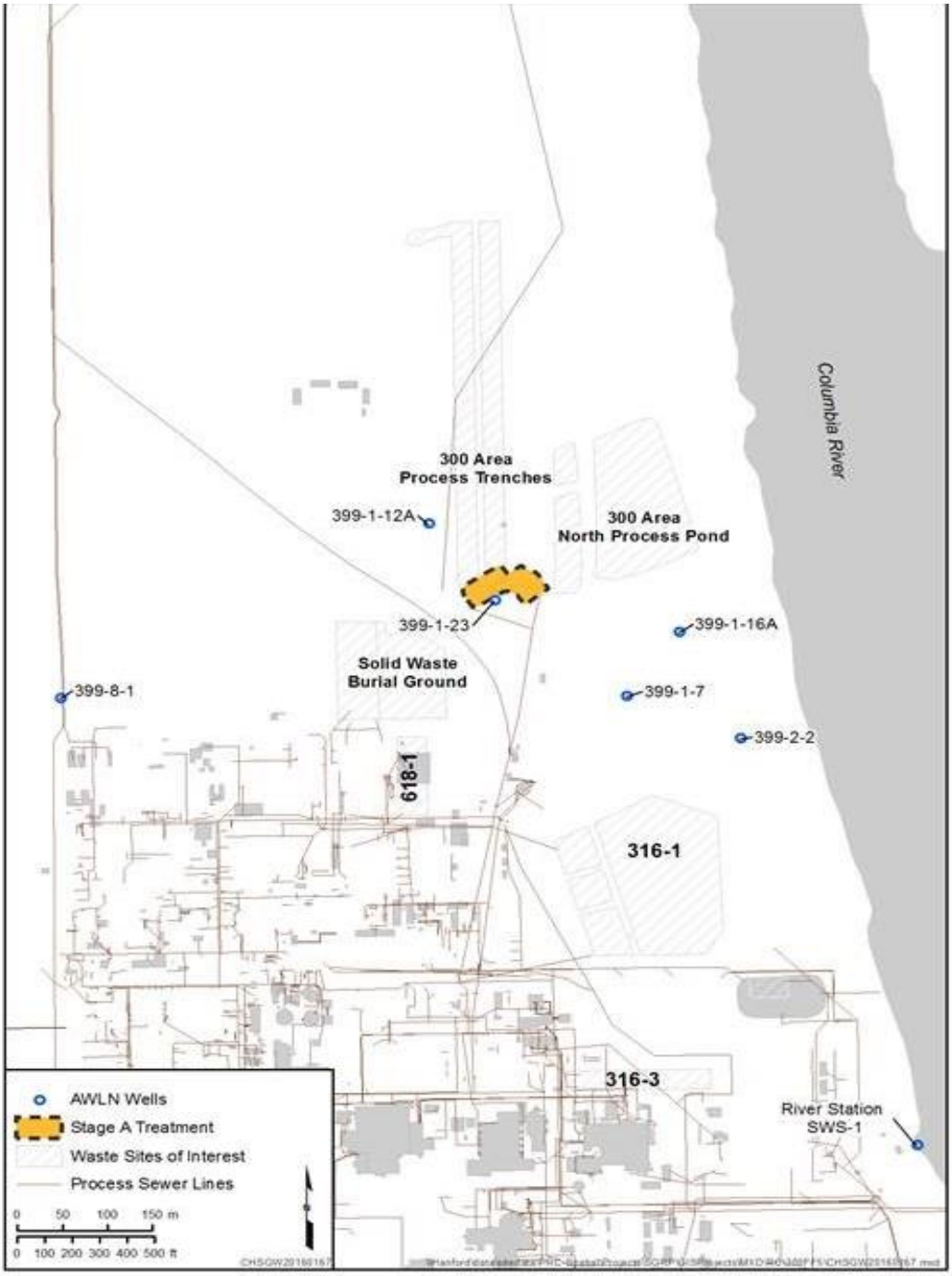

Figure E-1. Stage A EAA and Monitoring Wells

E2 Water Table Elevations

For this analysis, the water level elevations from two monitoring wells were examined: 399-1-23, which is located just outside the Stage A treatment area, and 399-1-12, which is located northwest and upgradient of the study area. Both wells are continuously monitored as part of the automated water level network in 15 to 30 minute intervals and the data records are available for water level elevation in m (above mean sea level).

The assumption for this analysis is that well 399-1-23 water levels could be influenced by injections due to proximity to the injection sites, but well 399-1-12 should not be affected by changes caused by injection due to its up-gradient location and distance from the Stage A treatment area. The water level elevations for both wells are shown in Figure E-2. The plot depicts changes in water levels prior to treatment (injection/infiltration), during treatment (marked as time of interest), and for some time period after treatment.

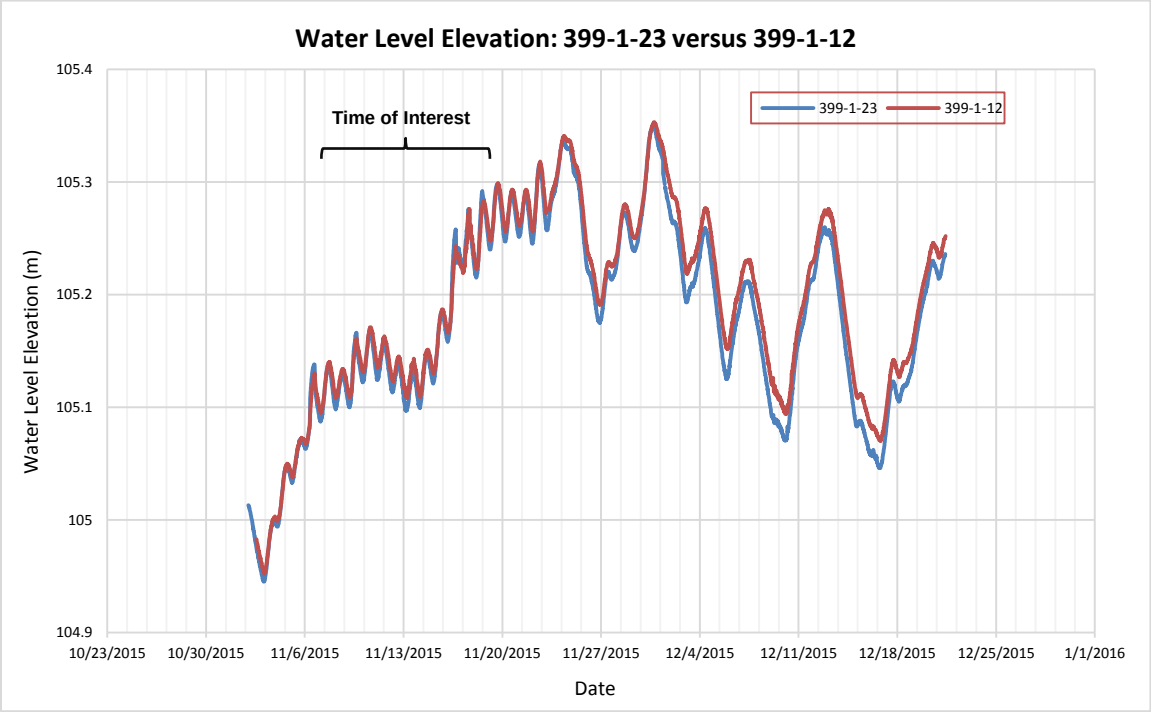

Figure E-2. Water Level Elevation Difference for 399-1-23 and 399-1-12

Throughout the observation time period, both wells showed a similar trend with minor differences resulting from differences in their respective locations. In the pretreatment and during treatment (time of interest), water level fluctuations in both wells remained similar (and virtually overlapping) indicating negligible or no impact of changes in the aquifer properties during treatment. Following the treatment, water levels between the two wells also remained very similar, indicating negligible or no impact on aquifer properties following treatment. During the treatment, the frequency of water level perturbations appeared to be enhanced, but they are likely induced by river stage fluctuations since both wells showed similar changes.

Water levels and specific conductance measurements for well 399-1-23 are 399-1-12 are presented in Figure E-3 and Figure E-4, respectively. Specific conductance for 399-1-23 shows step increases during the time of treatment (November 6 through November 17, 2015), indicating that it was receiving

polyphosphate solutions when they were injected/infiltrated in the Stage A EAA. Specific conductance increased from 0.5 mS/cm to over 1.5 mS/cm. On the other hand, specific conductance in well 399-1-12 remained at background levels, indicating no or negligible influence of polyphosphate solutions during treatment. Given that 399-1-23 showed large increases in specific conductance during injection of polyphosphate solution, it continued to have similar water level trends as 399-1-12, which indicates that no appreciable changes in aquifer properties (porosity or permeability) have occurred.

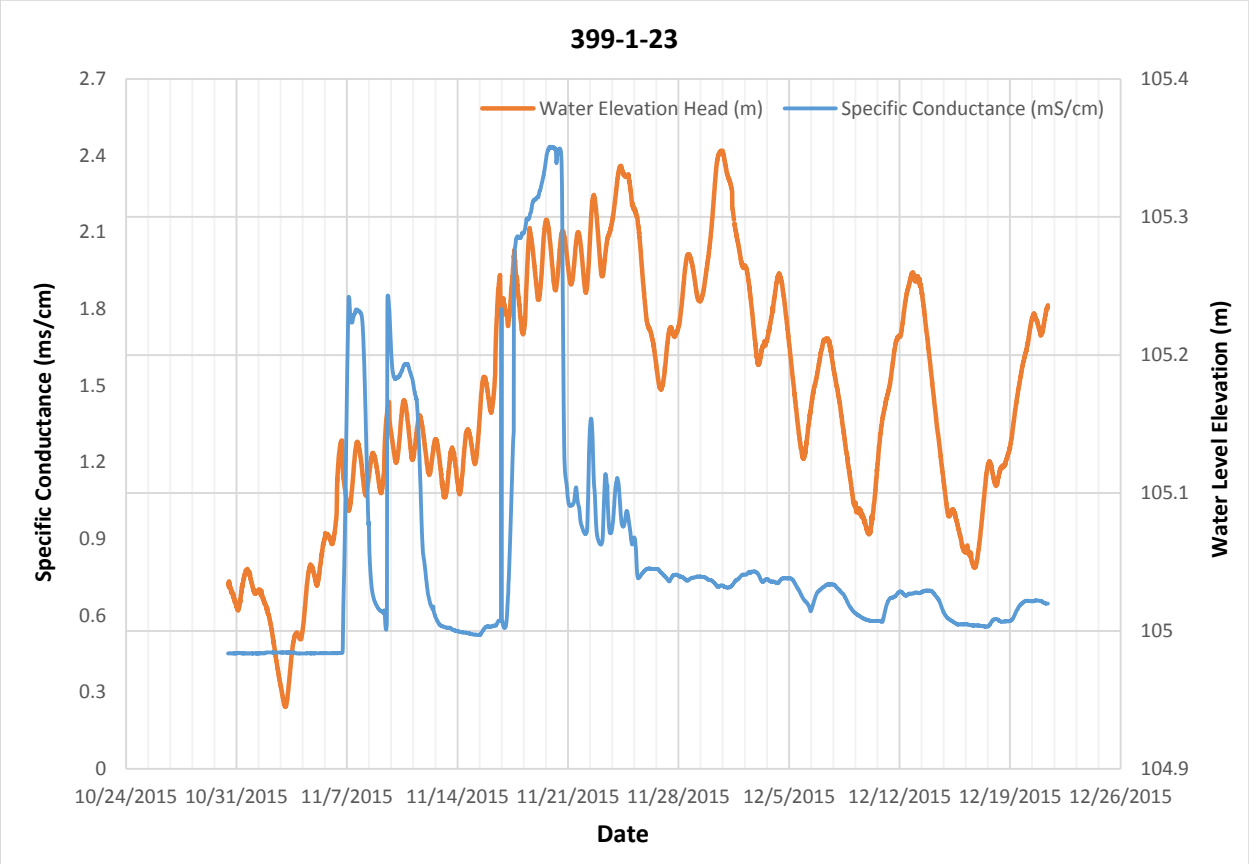

Figure E-3. Specific Conductance and Water Level Elevation Correlation Graph for 399-1-23

Absolute difference in heads between the two wells is presented in Figure E-5 to evaluate any significant changes. Due to location differences, some head differences are expected, and the trend typically varies from a 0.01 to 0.015 m difference. However, some rise in water levels was noticeable in well 399-1-23 during the time of injection (marked as time of interest between November 6 and 18, 2015), indicating influence of the nearby injection well. The larger difference after December 1, 2015 is correlated to the general rise in water level reflecting increasing river stage. This perhaps results in slight increase in vertical gradients within the aquifer; therefore, head differences between the two wells are slightly larger, and part of natural variation is expected with the rise and fall of river stage. Based on these observations, it is concluded that no or negligible change in aquifer properties occurred due to polyphosphate injections.

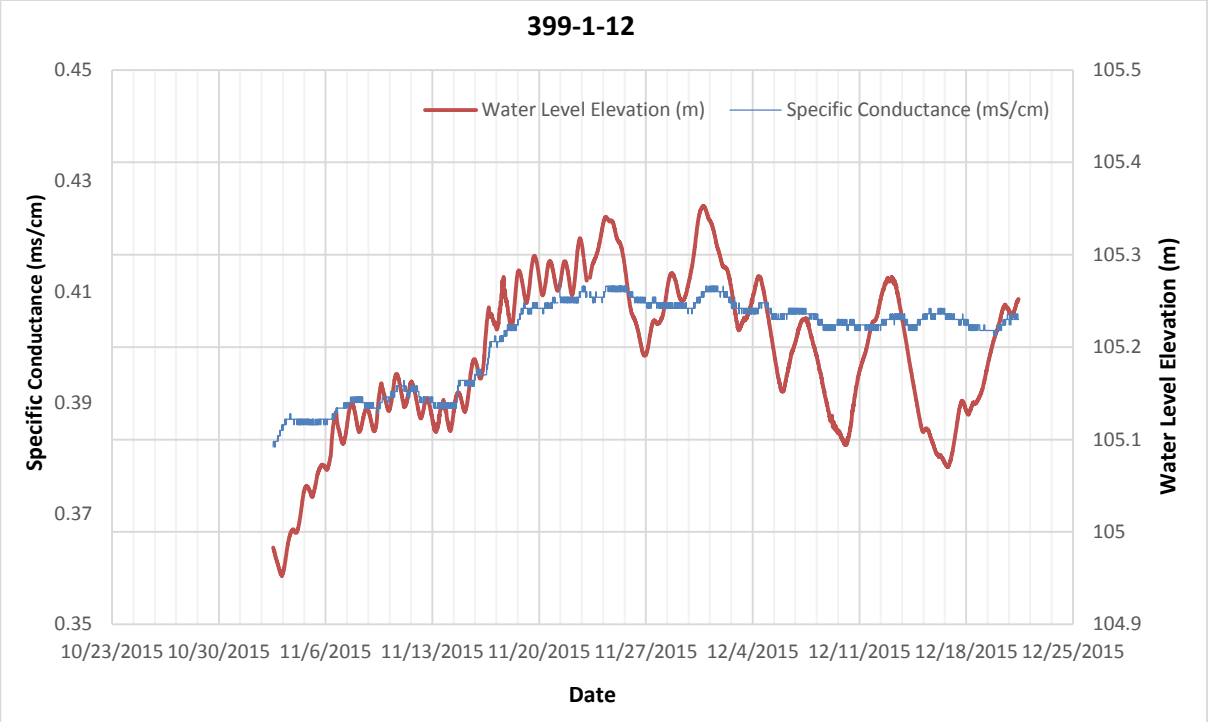

Figure E-4. Specific Conductance and Water Level Elevation for 399-1-12

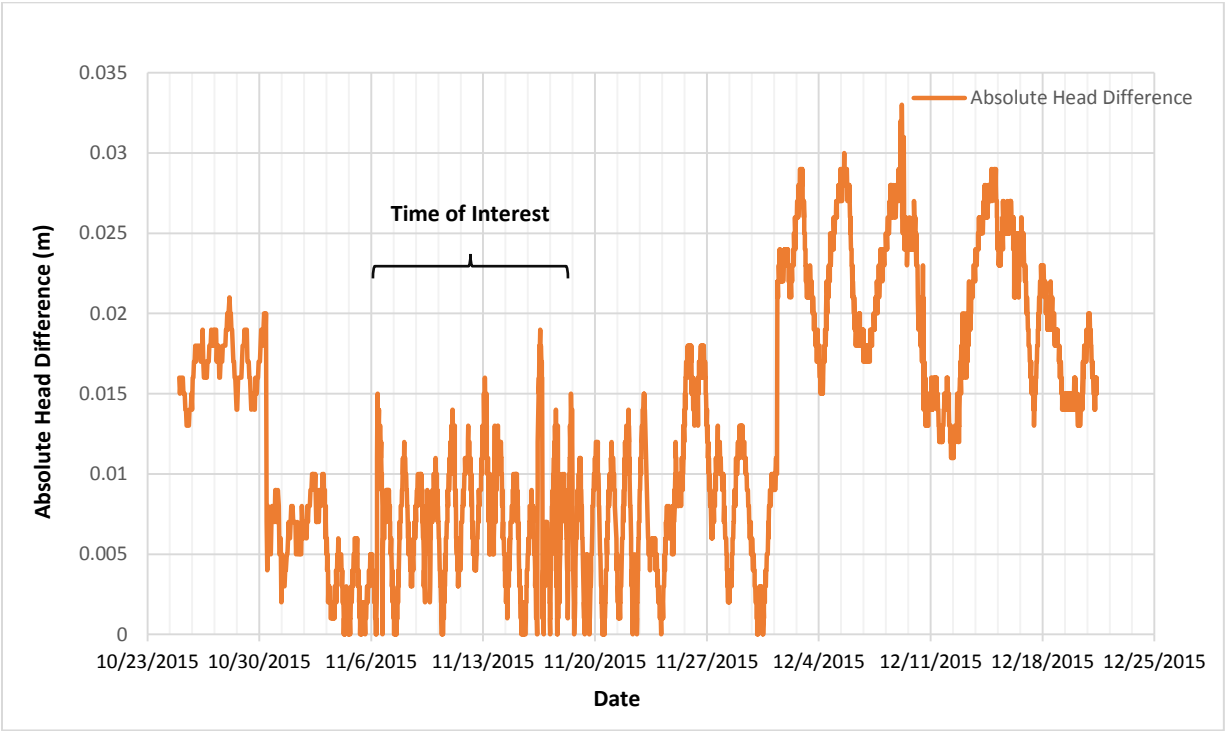

Figure E-5. Absolute Head Difference for 399-1-23 Versus 399-1-12

E3 Time Travel Calculations

This section estimates travel time by calculating how long polyphosphate took to reach downstream monitoring wells. For this analysis, three wells were used: 399-1-23, 399-1-7, and 399-2-2 (Figure E-1). These wells are located along an inferred flow path within the aquifer. Normalized specific conductance values were calculated for all three wells to find the first peak value for each well as shown in Figure E-6.

To calculate the travel time, well 399-1-23 was used as a base point to find the distance between each well using X and Y coordinates, then the date and time of the first peak were determined from the plot. Finally, travel velocity from well 399-1-23 to other wells was calculated for each well, and results are presented in Table E-1. The travel times shown in the table are with respect to well 399-1-23. The peak concentration took approximately 20 days to reach well 399-1-7, leading to an estimated average linear velocity of 9.2 m/day. The peak concentration in well 399-2-2 was observed approximately after 28 days, indicating an average linear velocity of 11.5 m/day. These average linear velocity estimates following injection are similar to the velocity estimated in previous studies (prior to injection) (PNNL-18529, *300 Area Uranium Stabilization Through Polyphosphate Injection: Final Report*; PNNL-22048) indicating that the aquifer properties have not been altered.

Table E-1. Travel Time Calculation Results

Well	Travel Time from Max (Days)	Velocity (m/d)
399-1-7	20.49	9.2
399-2-2	28	11.5
	Average Velocity	10.3

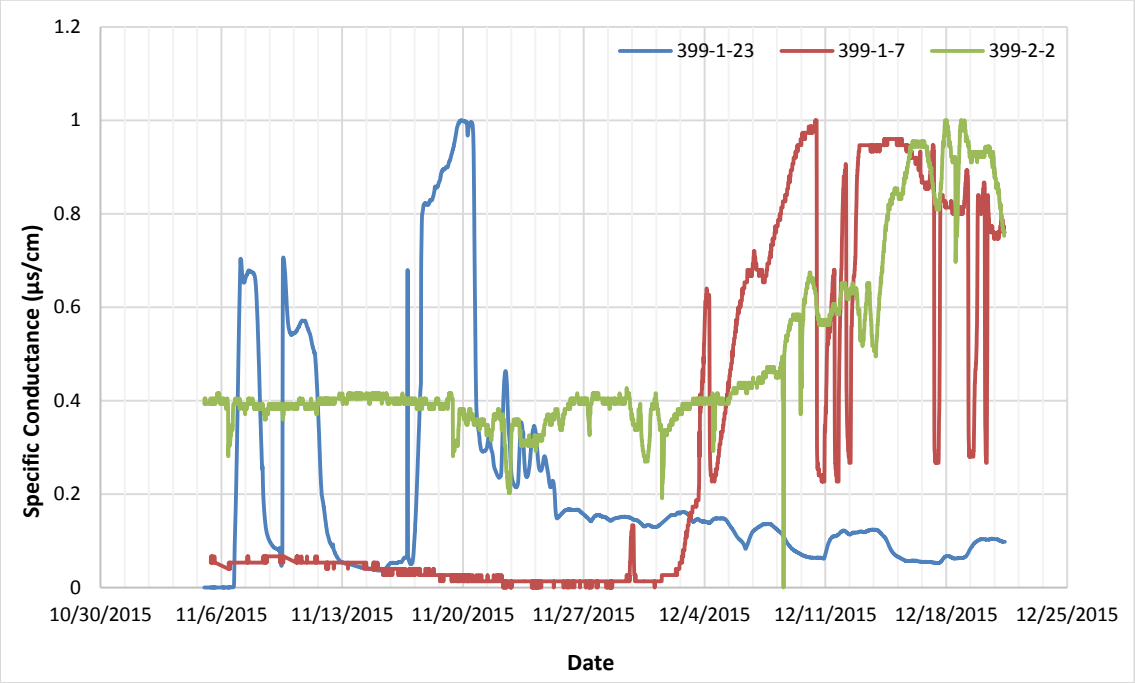

Figure E-6. Observed Specific Conductance as a Function of Time for Groundwater Monitoring Wells 399-1-23, 399-1-7, and 399-2-2

E4 References

PNNL-18529, 2009, *300 Area Uranium Stabilization Through Polyphosphate Injection: Final Report*, Pacific Northwest National Laboratory, Richland, Washington. Available at: http://www.pnl.gov/main/publications/external/technical_reports/PNNL-18529.pdf.

PNNL-22048, 2012, *Updated Conceptual Model for the 300 Area Uranium Groundwater Plume*, Pacific Northwest National Laboratory, Richland, Washington. Available at: http://www.pnnl.gov/main/publications/external/technical_reports/PNNL-22048.pdf.

Appendix F

Software Installation and Checkout Forms

This page intentionally left blank.

CHPRC SOFTWARE INSTALLATION AND CHECKOUT FORM

Software Owner Instructions:

Complete Fields 1-13, then run test cases in Field 14. Compare test case results listed in Field 15 to corresponding Test Report outputs. If results are the same, sign and date Field 19. If not, resolve differences and repeat above steps.

Software Subject Matter Expert Instructions:

Assign test personnel. Approve the installation of the code by signing and dating Field 21, then maintain form as part of the software support documentation.

GENERAL INFORMATION:

1. Software Name: STOMP (Subsurface Transport Over Multiple Phases) Software Version No.: Bld 4

EXECUTABLE INFORMATION:

2. Executable Name (include path):

```
All executable files installed in directory [redacted]/bin
--------------------------------  ---------------------------
MD5 File Signature                Executable File Name
--------------------------------  ---------------------------
6536b8e12d8c5b83dca76f2c947b6153  stomp-wae-bcg-chprc04i.x
e0cdf04bc1a2f6c55c5a1b499939f663  stomp-wae-bcg-chprc04l.x
6e72340bb39f6056e232fe5ff241c4d4  stomp-wae-bd-chprc04i.x
3f837a0fb8d9f47dbcada686f542d7fc  stomp-wae-bd-chprc04l.x
7e5b4cc36a8991b3d5a8ea2ed155ce47  stomp-wae-cgsq-chprc04i.x
00a898c0c3ec06817485781ad1c9ec46  stomp-wae-cgsq-chprc04l.x
f18ff5ab5667065d8ab12657344fb6a0  stomp-wae-cgst-chprc04i.x
061af86cf21ad8435b046d0efabe971b  stomp-wae-cgst-chprc04l.x
3c8111a9855dc0e430bf3c8a7abcf37e  stomp-w-bcg-chprc04i.x
20436d615a94955a2ce8eecdb8cba546  stomp-w-bcg-chprc04l.x
8b3df29df21d040189c3e2a50ef823bb  stomp-w-bd-chprc04i.x
066a289a75aedb933eb2536da5d7d1ff  stomp-w-bd-chprc04l.x
c8e62ad7a0d9b6fca39d8a8952ef5d8e  stomp-w-cgsq-chprc04i.x
28ad16806e1307aca51fd7bf89793e75  stomp-w-cgsq-chprc04l.x
6c25051016db2fe1f883a7caaaab1e97  stomp-w-cgst-chprc04i.x
ff9ff6f29b3469419ffaece87d7e772b  stomp-w-cgst-chprc04l.x
0c3e3fba40f5b93e71bcf9586432fd27  stomp-w-r-bcg-chprc04i.x
78492aee80a8c2d0a4e82aabf4a9c213  stomp-w-r-bcg-chprc04l.x
84b129786aba9c4be884e15e45a67389  stomp-w-r-bd-chprc04i.x
e990f1566c8099a8d54508de3da9cd88  stomp-w-r-bd-chprc04l.x
18a589a2b55aab2db290efea19b39351  stomp-w-r-cgsq-chprc04i.x
6569959476772a137df35ce874821889  stomp-w-r-cgsq-chprc04l.x
```

3. Executable Size (bytes): MD5 signatures above uniquely identify each executable file

COMPILATION INFORMATION:

4. Hardware System (i.e., property number or ID):

Tellus Subsurface Modeling Platform

5. Operating System (include version number):

Linux tellusmgmt.rl.gov 2.6.18-308.4.1.el5 #1 SMP Tue Apr 17 17:08:00 EDT 2012 x86_64 x86_64 x86_64 GNU/Linux

INSTALLATION AND CHECKOUT INFORMATION:

6. Hardware System (i.e., property number or ID):

Green Linux Cluster

7. Operating System (include version number):

Linux green 3.2.0-35-generic #55-Ubuntu SMP Wed Dec 5 17:42:16 UTC 2012 x86_64 x86_64 x86_64 GNU/Linux

Page 1 of 2 A-6005-149 (REV 0)

CHPRC SOFTWARE INSTALLATION AND CHECKOUT FORM (continued)

1. Software Name: STOMP (Subsurface Transport Over Multiple Phases) Software Version No.: Bld 4

8. Open Problem Report? (●) No ( ) Yes PR/CR No.

TEST CASE INFORMATION:

9. Directory/Path:

[redacted]/itc

10. Procedure(s):

CHPRC-00211 Rev 1, STOMP Software Test Plan

11. Libraries:

N/A (static linking)

12. Input Files:

Input files for ITC-STOMP-1, ITC-STOMP-2, and ITC-STOMP-2
(Baseline for comparison are results files from ATC-STOMP-1, ATC-STOMP-2, and ATC-STOMP-3 prepared on Tellus during acceptance testing)

13. Output Files:

plot.* files produced by STOMP in testing

14. Test Cases:

ITC-STOMP-1, ITC-STOMP-2, and ITC-STOMP-3

15. Test Case Results:

Pass for all executable files listed above.

16. Test Performed By: WE Nichols

17. Test Results: (●) Satisfactory, Accepted for Use ( ) Unsatisfactory

18. Disposition (include HISI update):

Accepted; Installation noted in HISI for users TJ Budge, N Hasan, A Mayenna, WJ McMahon, WE Nichols, S Mehta, H Rashid.

Prepared By:

19.	WE Nichols	25 APRIL 2013
Software Owner (Signature)	Print	Date

20. Test Personnel:

	WE Nichols	25 APRIL 2013
Sign	Print	Date
Sign	Print	Date
Sign	Print	Date

Approved By:

21.	N/R (per CHPRC-00211 Rev 1)	
Software SME (Signature)	Print	Date

Page 2 of 2 A-6005-149 (REV 0)

CHPRC SOFTWARE INSTALLATION AND CHECKOUT FORM

Software Owner Instructions:

Complete Fields 1-13, then run test cases in Field 14. Compare test case results listed in Field 15 to corresponding Test Report outputs. If results are the same, sign and date Field 19. If not, resolve differences and repeat above steps.

Software Subject Matter Expert Instructions:

Assign test personnel. Approve the installation of the code by signing and dating Field 21, then maintain form as part of the software support documentation.

GENERAL INFORMATION:

1. Software Name: The Geochemists Workbench Software Version No.: 11.0.3

EXECUTABLE INFORMATION:

2. Executable Name (include path):

[redacted]\Workbench.exe

3. Executable Size (bytes): 9,236,104

COMPILATION INFORMATION:

4. Hardware System (i.e., property number or ID):

Vendor compiled

5. Operating System (include version number):

Windows (vendor compiled)

INSTALLATION AND CHECKOUT INFORMATION:

6. Hardware System (i.e., property number or ID):

INTERA-Blue

7. Operating System (include version number):

Window Server 2008 SP2 (32-bit)

8. Open Problem Report? (•) No ( ) Yes PR/CR No.

TEST CASE INFORMATION:

9. Directory/Path:

[redacted]\rdockter\

10. Procedure(s):

CHPRC-01874 Rev. 2, Geochemists Workbench Integrated Software Management Plan

11. Libraries:

12. Input Files:

Case1_seawater.rea, Case2_Amazon_table 6_7.sp8

13. Output Files:

ATC-1 React output 20July2016.txt, ATC-2 SpecE8 output 20July2016.txt

14. Test Cases:

GWB-ITC-1; GWB-ITC-2

15. Test Case Results:

All tests passed.

16. Test Performed By: Randy Dockter

17. Test Results: (•) Satisfactory, Accepted for Use ( ) Unsatisfactory

18. Disposition (include HISI update):

Installation added to HISI Entry

Page 1 of 2 A-6006-149 (REV 0)

CHPRC SOFTWARE INSTALLATION AND CHECKOUT FORM (continued)

1. Software Name: The Geochemists Workbench Software Version No.: 11.0.3

Prepared By:

19. William E. Nichols — WE Nichols — Software Owner (Signature) / Print / Date

20. Test Personnel:

Sign	Print	Date
Randy Dockter	RANDY DOCKTER	7-20-2016

Approved By:

21. Software SME (Signature) / Print / Date

Page 2 of 2 A-6005-149 (REV 0)